Analysis of a Laminated Composite Panel with Discrete Variable Stiffeners

A Thesis

Submitted to the

Department of Mechanical Engineering

of

Bangladesh University of Engineering and Technology

by

Partha Modak (Student ID: 040810040F)

Under the Supervision of

Professor S. Reaz Ahmed

In Partial Fulfilment of the

Requirements for the Degree

of

Master of Science in Mechanical Engineering

Defense Date: February 13, 2013

RECOMMENDATIONS OF THE BOARD OF EXAMINERS

The thesis titled, *Analysis of a Laminated Composite Panel with Discrete Variable Stiffeners* submitted by Partha Modak, Roll no: 040810040F, session: April, 2008 has been accepted as satisfactory in partial fulfilment of the requirement for the degree of Master of Science in Mechanical Engineering on February 13, 2013.

BOARD OF EXAMINERS

____

Dr. S. Reaz Ahmed (Supervisor)
Professor
Department of Mechanical Engineering, BUET
Dhaka, Bangladesh

Chairman

____

Dr. Md. Ehsan
Professor and Head
Department of Mechanical Engineering, BUET
Dhaka, Bangladesh

Member
Ex-Officio

____

Dr. Md. Mahbubur Razzaque
Professor
Department of Mechanical Engineering, BUET
Dhaka, Bangladesh

Member

Dr. Monon Mahbub
Assistant Professor
Department of Mechanical Engineering, BUET
Dhaka, Bangladesh

Member

Professor Md. Fazli Ilahi
Former-Vice Chancellor
Islamic University of Technology
Board Bazar, Gazipur, Bangladesh

External

DECLARATION

This thesis work does not contain any material extracted from elsewhere or from a work published by any body else. The work of this thesis has not been published elsewhere by the author for any degree or any other University or Institute of learning.

PARTHA MODAK

Roll No. 040810040F

Session: April 2008

DEDICATION

This dissertation is dedicated to my parents.

ACKNOWLEDGEMENTS

I would like to express my deepest gratitude to my supervisor Dr. Reaz Ahmed, Professor, Department of Mechanical Engineering, Bangladesh University of Engineering and Technology, Dhaka for his support, guidance, inspiration, constructive suggestions and close supervision throughout the entire period of my graduate study.

The author acknowledges his gratefulness to Mechanical Engineering Department for providing required facilities. I would like to take the opportunity to thank the members of examination committee for their constructive comments and criticism.

I am deeply indebted to Professor Khan Amanat for his guidance throughout the ANSYS study. His teaching of ”being focused” has remained a guideline for me.

I wanted to express my deepest gratitude to my parents, for their unparallel love, dedication, and encouragement throughout my whole life. Without their effort none of this would have been possible.

Finally, I am extremely grateful to my elder brother, Dr. Sukomal Modak who has supplied me with unlimited encouragement and friendship throughout my years of study. He taught me how to learn, a gift which I appreciate as much as any other. He has all contributed to making me a better researcher as well as a person.

CONTENTS

LIST OF TABLES

LIST OF FIGURES

ABSTRACT

This research addresses a new analysis of the elastic field of laminated composite structures under the influence of discrete stiffeners at the bounding surfaces. In this work, theory of elasticity, a new potential function, constitutive relations for composite materials, special lamination theory and finite-difference computational algorithm are integrated to develop a new computational scheme for stress analysis of laminated composite structures. Specific contribution are follows:

A new mathematical formulation is developed for the analysis of structural components of laminated composites with mixed and changeable boundary conditions. In this formulation, the displacement components of plane elasticity are expressed in terms of a single potential function, which satisfies one of the equilibrium equations automatically. The remaining equilibrium equation is transformed into a fourth order partial differential equation of the unknown potential function. Thus the mixed boundary value plane elasticity problem is reduced to the solution of a single fourth order partial differential equation. The finite difference technique is used to develop an efficient computational algorithm based on the potential function formulation.

A general computer program is developed based on the finite difference computational algorithm, which is capable of dealing with almost all the special cases of composite material, namely orthotropic and anisotropic lamina, angle-ply and cross-ply symmetric laminates, symmetric balanced laminates, etc., with mixed and changeable physical conditions at the surfaces of the structural composites.

The application of the computational scheme is investigated to stress analysis of dis-

cretely stiffened panels of laminated composites. A number of practical problems of interest are solved and results are presented in the form of graphs. The problem includes symmetric and antisymmetric discretely stiffened laminated cantilever under shear loading, a laminated panel with periodic axial stiffeners subjected to eccentric loading and a laminated cantilever panel with discrete variable stiffeners.

Finally, in an attempt to validate the new computational method, the potential function solutions are compared with both analytical and numerical solutions obtained by standard computational method. For this purpose, finite element solutions are obtained using the commercial FEM software, SAP2000. For all the problems, both the numerical solutions are found to be in excellent agreement with each other, which in turn, establishes the suitability and appropriateness of the present potential function computational scheme.

NOMENCLATURE

x, y	Rectangular co-ordinate
a, b, h	Dimensions of the panel
σ	Stress
σ_{xx}	Normal stresses in x direction
σ_{yy}	Normal stresses in y direction
σ_{zz}	Normal stresses in z direction
σ_{xy}	Shear stresses in xy planes
σ_{yz}	Shear stresses in yz planes
σ_{zx}	Shear stresses in zx planes
σ_0	Maximum intensity of applied shear loading
u_x	Displacement component along x direction
u_y	Displacement component along y direction
ε	Strain
ε_{xx}	Normal strains in x direction
ε_{yy}	Normal strains in y direction
ε_{zz}	Normal strains in z direction
ε_{xy}	Shear strains in xy plane
ε_{yz}	Shear strains in yz plane
ε_{zx}	Shear strains in zx plane

E	Elastic modulus of material
E_1	Elastic modulus of material in direction 1
E_2	Elastic modulus of material in direction 2
ν	Poisson ratio
ν_{12}	Major Poisson ratio
ν_{21}	Minor Poisson ratio
h_x	Mesh length along $x-$direction
k_y	Mesh length along $y-$direction
ψ	Displacement potential function
ϕ	Airy's stress function
ξ	Effectiveness of stiffener

CHAPTER
1

INTRODUCTION

1.1 Introduction

A composite is a structural material that consists of two or more constituents that are combined at a microscopic level and are not soluble in each other. One constituent is called the reinforcing phase and the one in which it is embedded is called the matrix. The reinforcing phase material may be in the form of fibers, particles or flakes. The matrix phase material are generally continuous. Advanced composites are composite materials that are traditionally used in the aerospace industries. The composites have high performance reinforcements of thin diameter in a matrix material such as epoxy and aluminium. Examples are graphite/epoxy, boron/epoxy, kelver/epoxy, boron/aluminum composites.

The analysis of composite structures has now become a key subject in the field of solid mechanics. The use of fiber-reinforced composites as the structural material is found to increase extensively in almost all areas of structural applications mainly because of their specific characteristics of light weight, high strength, etc., compared to those of conventional materials. In order to realize the improved characteristics of fiber-reinforced composite laminae in a more effective manner, in most of the practical applications they are found to use as a laminate consisting of more than one lamina bonded together through their thickness

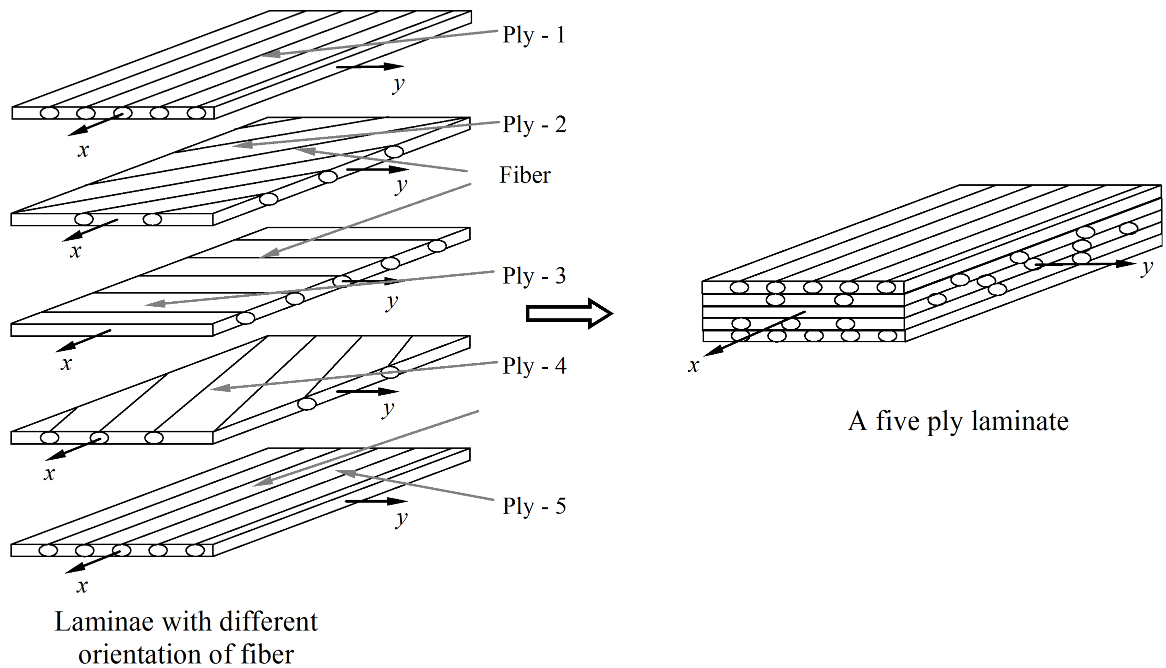

Figure 1.1: Mechanism of laminate formation.

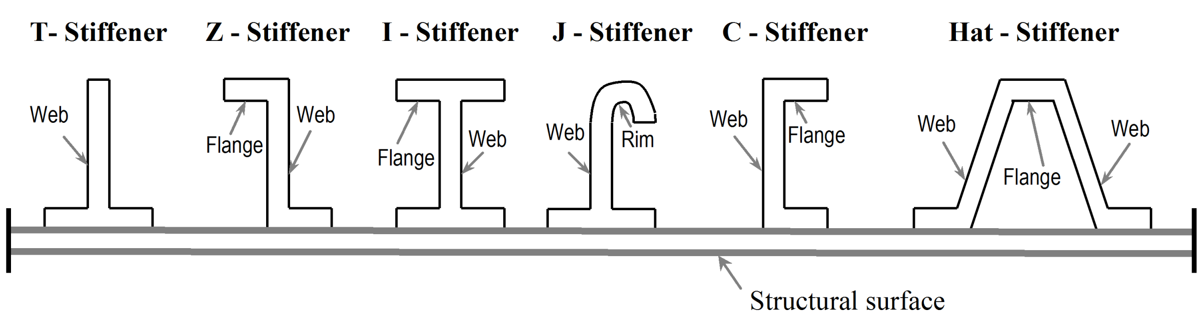

Figure 1.2: Different types of stiffener as encountered in practical structures.

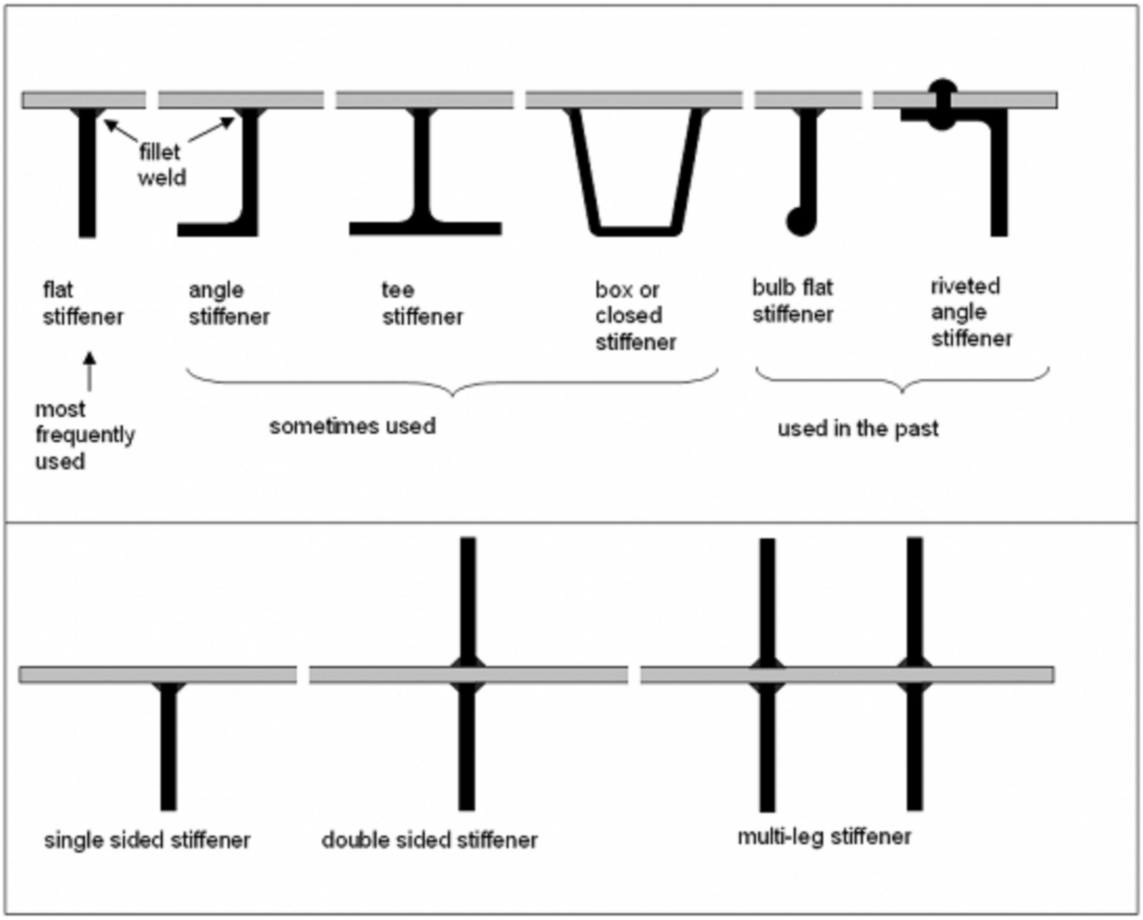

Figure 1.3: Different types of stiffener as encountered in practical structures.

as shown in Figure 1.1. Furthermore, the use of stiffeners especially in the construction of aerospace structures is quite extensive. The stiffeners are basically designed to meet the strength or stiffness requirements of a particular situation as shown in Figures 1.2 to 1.5. In the analysis of stiffened structures, the physical conditions of stiffeners are usually mathematically simulated in terms of a mixed mode of boundary conditions, that is, there will be no strain for the boundary segment at which the stiffener is deployed, while the same will be free for normal loading. A comprehensive and accurate stress analysis of these structures is of great interest, since only it can lead a designer to an appropriate selection of the structural parameter and the stiffener dimensions.

In case of engineering problems, the elementary methods of strength of materials are

Figure 1.4: Transverse web stiffeners.

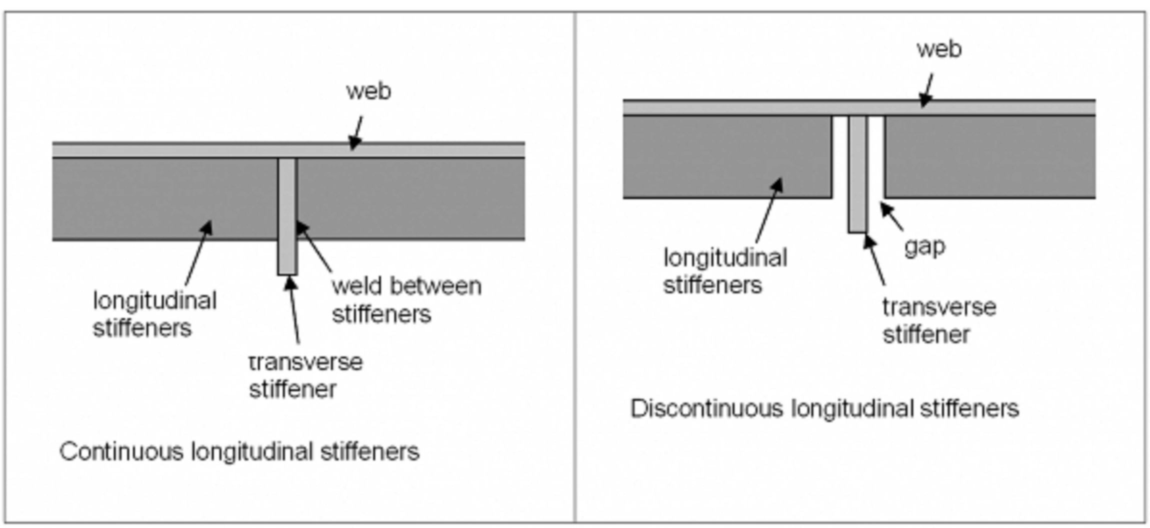

Figure 1.5: Continuous and discontinuous longitudinal stiffeners.

not adequate to provide sufficient and accurate information regarding the elastic field of the corresponding body. So, some more powerful methods are needed in the study of elastic field. Structural analysis comprises the set of physical laws and mathematics required to study and predict the behavior of structures. It is such an engineering artifact whose integrity is judged largely based upon the ability to withstand loads on building, bridge, ship, submarine, aircraft, etc. From theoretical perspective, the primary goal of structural analysis is the computation of deformations, internal forces and stresses. In practice, structural analysis can be viewed more abstractly as a method to derive the engineering design process or to prove the soundness of a design without dependance on directly testing it. Engineering subjects which deal the matter are namely the mechanics of materials (also known as strength of materials) and the theory of elasticity. Again for the cases where the the stress distribution in bodies, with all dimension of same order, has to be investigated, these methods are incapable of furnishing satisfactory information. For example, the stress in rollers and in balls of bearings can be found only by using the methods of the theory of elasticity. So, to obtain satisfactory and reliable information of elastic fields in engineering structures of practical applications, it is mandatory to adopt the theory of elasticity.

The equations of theory of elasticity are basically a system of partial differential equations. Due to the nature of mathematics involved in solving such equations, manual solutions have been only produced for relatively simple geometries. For complex geometries, computation using a modern computer is considered more suitable for better solution.

1.2 Literature Review

The foundation of the classical theory of elastic beam was laid down in 18th century (1705-1750) by leonard paul Euler and Daniel Bernoulli. It was then Claude-Louis Navier, who gave the details of the relation between the cross-section and the bending stiffness parameter in 1819. This theory has remained as an exact solution of the equations of three-dimensional elasticity in the case of homogenous bending, i.e. for a beam with constant bending moment. Then the elementary methods of strength of materials were the primary tools of the practicing engineers for handling the engineering problems of structural elements for long time. However these methods are often inadequate to furnish satisfactory information regarding local stresses near the load and near the supports of the structures. The elementary theory give, no means of investigating stresses in region of sharp variation in cross section of beams or shafts. Stresses in screw threads, around various shapes of holes in structures, bear contact point on gear teeth, rollers and balls of bearing, have all remained beyond the scope of elementary theories. It is thus obvious that, for the designer of modern machines, recourse to more powerful methods of the theory of elasticity is necessary.

Considerable progress have been made in solving important practical problems of stress analysis using the methods of theory of elasticity. In case where the rigorous solution could not be obtained, approximate methods have been developed. In other cases, where even approximate methods could not be developed, solutions have been obtained by using experimental methods. Photoelastic methods, soap-film methods, application of strain gages, moire fringe etc are some of these experimental methods applied in the study of stress concentration at points of sharp variation of cross-sectional dimension and at sharp fillets of re-entrant corners. These results have considerably influenced the modern design of machine parts and helped in many cases to improve the construction by eliminating weak spots through which crack may initiate and thereby propagate. The field of elasticity deals mainly with deformation parameters and stress parameters for the solution of two dimensional problems since most of the three dimensional problems may be resolved through a two dimensional one. If it still remains beyond the extent of analytical studies, the problem has to be handled experimentally as a particular case.

Although the theories of elasticity had been established long before, the solutions of practical problems started mainly after the introduction of a stress function by George Biddell Airy [2], a British astrologer and mathematician. The Airy's stress function is governed by a fourth order partial differential equation and stress components are related to it through its various second order derivatives. The stress function solutions were initially sought taking polynomial expressions of various degrees and suitably adjusting their coefficients. A number of practically important problems of long rectangular strips have been solved Timoshenko and Goodier [3]. But the success of this approach was very limited. Using these polynomial expressions, an elementary derivation of the effect of the shearing force on the curvature of the deflection curve of beams were made by Ranking in England [4] and by Grashof [5] in Germany. The problem of stresses in masonry dams is of great practical interest and has been attempted for solution using polynomial expressions for the stress functions by Levy [6], Scewald [7]. But the solutions obtained do not satisfy the conditions at the bottom of the dam where it is connected with the foundation. A number of works are found with the stress function Conway, Chow, and Morgan [8], Chapel and Smith [9] in this regard. Even though the stress analysis problems are bearing enumerable shortcomings to be addressed yet. The stumbling block of obtaining exact solution using stress function is the inability of managing the physical conditions imposed on them. i.e., management of boundary conditions of practical problems. Boundary restraints specified in terms of the displacement components cannot be satisfactorily imposed on the stress function. Since most of the practical problems in elasticity are of mixed boundary conditions, the approach fails to provide any explicit understanding of the state of stresses at the critical regions of supports and loadings. Moreover, the famous Saint Venant's principle is still applied and its merit is evaluated in solving problems of solid mechanics in which full boundary effects could not be taken into account in the process of solution Parker [10], Horgan and Knowels [11], Horgan and Simmonds [12]. Even now, photoelastic studies are being carried out for classical problems like uniformly loaded beams on two supports mainly because the boundary effects could not be taken into account fully in the analytical method of solutions. Successful application of the stress function formulation in conjunction with finite-difference technique has been reported for the solution of plane elastic problems, where all the conditions on the boundary are prescribed in terms of stresses only Chow, Conway, and Winter [13]. Further, Conway and Ithaca [14] extended the stress function formulation in the form of Fourier integrals to the case where the material is orthotropic and obtained analytical solutions for a number of ideal problems. As most of the practical problems of elasticity are of mixed boundary conditions, the approach fails to provide any explicit understanding of the state of stresses at the critical regions of supports. The displacement formulation, on the other hand, involves finding two displacement functions simultaneously from the two second-order elliptic partial differential equations of equilibrium, which is extremely difficult and this problem becomes more serious when the boundary conditions are mixed [15].

Mixed-boundary-value problems are those in which the boundary conditions are specified as a mixture of boundary restraints and boundary loadings. Observing the drawback of Airy's stress function and the difficulties of experimental works lead to work out for finding way to solve the engineering problems where boundary conditions have been in terms of displacements. Thus the displacement formulation was induced for those problems where boundary restraints are there Uddin [16], Ahmed, Khan, Islam, and Uddin [17]. This process involves finding of two displacement functions simultaneously from the two second-order elliptic partial differential equations of equilibrium. It is noted that the recent research and developments in using the displacement potential boundary modeling approach Idris, Ahmed, and Uddin [18],Ahmed, Idris, and Uddin [19], Ahmed, Khan, Islam, and Uddin [20] have generated renewed interest in the field of numerical solutions of stress problems.

Composites are relatively new candidates in the field of engineering and structural materials. They are nonhomogeneous and anisotropic materials. Therefore, elasticity problems of these materials become more complex in order to obtain analytical solutions. So far, various elasticity problems of different composites have been solved. An experimental study of the nonlinear response and failure characteristics of internally pressurized 4 to 16 ply thick Graphite/Epoxy cylindrical panels is carried out by Richard and Eric [21]. However, Stress analysis of actual structures of composite materials is mainly handled by numerical methods, especially, the finite element method. This method has received widespread application in all aspect of structural analysis especially with the advent of high powered computing machines. Han and Hoa [22] have developed a three-dimensional multilayered composite finite element method on a composite variational functions for the analysis of stress in composite laminates. Leoni and Brandford [23] present a comparison of available numerical structural analysis formulations for composite beams with partial shear interaction. Jarmai and Frkas [24] have investigated the optimum design of an orthogonally stiffened cylindrical shell member of an offshore fixed platform truss, loaded by axial compression and external pressure. A comparison of the computed optimum costs of the stiffened and the un-stiffened assemblies shows that significant cost savings can be achieved by orthogonal stiffening since the later allows for considerable reduction of the shell thickness, which results in large material and manufacturing cost savings. Armero and Ehrlish [25] have proposed new finite elements for thin Euler-Bernoulli beams that incorporate the softening hinges observed at failure. A large number of studies on bending, buckling and vibration of composite panels by finite element method are available in the literature Mallela and Upadhyay [26], Zhang and Yang [27]. **?**] has been found the optimum stacking sequence design of composite materials for constant stiffness deign and variable stiffness design. The author has not found any article related to the variable stiffening on the boundary. Studies on bending, buckling and design of the variable stiffness composite panels are available by the researchers Shahriar, Zafer, and Layne [28], Grdal and Wu [29], Tatting [30].

The uncertainties associated with the prediction of surface stresses by the standard FEM have been pointed out by several researches, for examples, Richards [31], Smart [32], Dow and Harwood [33]. On the other hand, the accuracy of finite-difference method (FDM) in reproducing the state of stresses along the bounding surfaces has been repeatedly verified to be much higher than that of FE analysis (Dow and Harwood [33], Nath and Ahmed [34]). In the research of Ranzi [35], the FDM has also been identified to be an adequate numerical tool for describing the composite behavior of beams, and the corresponding FD solutions are shown to be more accurate when compared with the usual eight-dof-FEM solutions, even with finer discretization for the latter one. Recently, a general potential-function formulation has been proposed for the analysis of anisotropic composite structures by Ahmed, Hossain, and Uddin [36]. Further, Nath and Ahmed [34], Nath, Afsar, and Ahmed [37] have extended the use of the formulation to the problems of orthotropic laminae, and obtained analytical as well as numerical solutions for a number of composite structures. Using a layer-wise shell theory, a modeling approach of discretely stiffened laminated composite plates and cylindrical shells has been reported by Kassegne and Reddy [38] for the analysis of stress, vibration and buckling. The existing layer-wise displacement theory of laminated plates is also applied to analyze laminated beams, and analytical solutions are obtained for static bending and free vibration of the beam by Tahani [39]. A short stiffened composite flat bar was first analyzed by Nath, Ahmed, and Afsar [40] under uniform axial tension where the fibers were oriented perpendicular to the direction of loading. The method is then extended by Nath and Afsar [41] to the solution of a stiffened panel of orthotropic material under uniaxial tensile load, in which the fibers were directed along the longitudinal axis of the panel .

Accurate and reliable prediction of stresses at and around the discrete stiffeners of composite structures is of great concern, as we are constantly aware of the lack of sophistication and doubtful quality of the finite element solutions, especially for critical stresses at the surfaces as well as regions of singularities. No serious attempt has been reported so far in the literature that can provide a reliable analysis of stresses in laminated panels with discrete variable stiffeners. A new investigation of stresses in a laminated panel under the influence of discrete stiffeners is the subject matter of the present thesis. The displacement-potential formulation is first extended for the problems of symmetric laminated composites, wherein the potential of a new variable reduction scheme originally proposed by Ahmed et al. [36] is used to develop the formulation. Therefore, attempt is made to consider a new numerical study of stresses has been considered here which is entirely different from conventional approaches both in terms of mathematical modeling and computational algorithm.

A finite-difference based computational scheme is developed to obtain the numerical solution of the corresponding elastic field. Some of the practical issues of interest, like, ply stresses, stacking sequence, stiffening length, etc. are also discussed in context of the laminated panel. Finally, in order to check the appropriateness as well as accuracy of the present displacement-potential method (DPM), results are compared with the corresponding solutions obtained by analytical as well as standard computational methods.

1.3 Objectives

The present study is an attempt to extend the capability of a new displacement potential in order to address stress analysis of laminated composite panels subjected to different arrangement and effectiveness of discrete stiffeners at the bounding surfaces. The specific objectives of the present research work are as follows:

1. Development of a new mathematical model for the stress problems of laminated composite materials with mixed and changeable boundary conditions in terms of a single potential function.

2. Development of an efficient computational scheme for numerical solution of stress problems of laminated composites with mixed and variable physical conditions prescribed along the boundary segments.

3. Analysis of symmetric and anti-symmetric discretely stiffened symmetric laminated composite panels subjected to uniform shear loading.

4. Application of the computational scheme developed for the analysis of a laminated composite panel under discrete periodic stiffeners subjected to an eccentric loading.

5. Analysis of the resulting stress field of a laminated composite panel subjected to discrete variable stiffeners.

6. Establishment of credibility of the present computational scheme for the analysis of discretely stiffened laminated structures by comparing the present results with those

of standard computational techniques.

1.4 Outline of the Methodology

In the proposed research work, the potential function based mathematical formulation of general anisotropic materials Ahmed et al. [36] is extended to obtain a suitable mathematical model for analyzing the stress problems of laminated composite materials in terms of a single variable. A new variable reduction scheme has been used to develop the formulation. Based on the mathematical model, an efficient computational scheme has been developed for analyzing the stress field of a discretely stiffened laminated composite panel subjected to axial and shear loading. The finite-difference method is used to discretize the governing partial differential equation of equilibrium as well as the partial differential equations associated with the boundary conditions. An imaginary boundary, exterior to the physical boundary of the panel, has been realized for the sake of discretization of the domain using a central differencing scheme of the governing equation. The discrete values of the function at the mesh points of the panel are obtained by solving the system of algebraic equations resulting from the discretization of the domain into mesh-points. All the parameters of interest associated with the composite panel are then obtained from the nodal values of the potential function as they are expressed as the summation of different derivatives of the potential function.

1.5 Significance of the Present Study

The present study describes the details of development and application of a new computational approach i.e., displacement potential method (DPM) for the analysis of stress and displacement in structural components of laminated composites with mixed and changeable physical conditions at the bounding surfaces. It is expected that the present study would encourage academicians and researchers to explore the concept further and eliminate the lack of a suitable method for dealing with mixed boundary value problems of laminated composites. In this study, a number of problems of discretely stiffened laminated composites are solved by using the present numerical method and results are presented mainly in the form of graphs. The results may be used as a database, which would be helpful to the designers working especially in the industries of aerospace, shipbuilding and automobile, where numerous composite structures are used. This study also throws challenges to Finite Element Method, especially in context of managing the boundary conditions and singularity points where the boundary conditions change from one type to the other.

1.6 The reason for Finite-Difference Solution

The analysis of stresses and displacements of structural components can be performed either theoretically or by experimental means. Experimental investigation of stresses and displacement could not gain that much popularity in the field of solid mechanics because of their limited flexibility and applications. For every change of geometry, loading and support, it needs separate investigation, involving separate experimental requirement/arrangement, which, in turn, makes it unattractive, especially, for the time involved as well as economical point of views.

The theoretical investigation, on the other hand, can be carried out either by analytical approach or by numerical approach. The analytical methods of solution are not of much help in solving the practical problems, especially of three-dimensional bodies. This is mainly due to the very involvement of a large number of variables, complex boundary conditions and nonuniform boundary shapes. General closed form solutions can be obtained only for very ideal cases and the results obtained for a particular problem, usually with uniform boundary conditions, are invariably approximate and thus away from the actual solution, as they include various idealizations. For two-dimensional elastic problems, existing mathematical models either involve finding three stress components or two displacement components simultaneously. The shortcoming of the stress formulation is that, three partial differential equations are required to be solved simultaneously for three stress components and also this formulation accepts boundary conditions only in terms of boundary loading. Boundary restraints specified in terms of the displacement components cannot be imposed satisfactorily. The displacement formulation, on the other hand, involves finding the two displacement functions simultaneously from the two second order partial differential equations. But solving for two functions satisfying two simultaneous elliptic partial differential equations and variously mixed conditions on the bounding surfaces is impossible. Therefore, there are no alternatives except the numerical methods for the solution of two-dimensional stress problems of practical interest. In the field of numerical analysis, the major numerical methods in use are the method of finite-difference and the method of finite-element.

Finite difference method is an ideal numerical approach for solving partial differential equations. The difference equations that model the governing equations are simple to code and the global coefficient matrix possesses a banded structure that is amenable to efficient solution. Despite these ideal characteristics, the finite-element method dominates in most of the solid mechanics applications as well as composite materials in engineering mainly because of its flexibility in managing the odd shapes of the boundary. The present research is an attempt to bring the finite-difference technique again into light through a novel formulation of two-dimensional analysis of *composite structures*. As the new formulation establishes a priority of finite-difference technique over the finite-element method, the philosophy and approach of the two methods are recapitulated here in brief.

In the application of finite-element method, the body is divided into a number of elements. On the other hand, the finite-difference method relies on the philosophy that the body is in one single piece but the parameters are evaluated only at some selected points within the body, satisfying the governing differential equations approximately. For a comprehensive evaluation, let us list the relative advantages and disadvantages of the two methods.

1.6.1 Finite-Element Method

Advantages

1. It works when all other methods fail.
2. It is very good in managing complex boundary shapes.
3. There are many commercial packages such as ANSYS for analyzing engineering problems.

Disadvantages

1. The body is not in one piece but it is an assemblage of elements connected only at the nodes.
2. Values of parameters across element boundary are usually discontinuous.
3. Variations of parameters over individual elements are assumed to be simple like polynomials of limited order
4. Finite element solution is highly dependent on the element type. Selection of any arbitrary element type may lead to erroneous or no solution at all.
5. FEM cannot handle singularity.

1.6.2 Finite-Difference Method

Advantages

1. The body remains one piece and thus there is no approximation on this account.
2. It permits reduction of parameters to be evaluated at the nodal points to one

3. Total number of unknowns to be solved is much less than that in finite-element and hence, solution is more accurate and the computational time is short.

4. It is simple to use and easy to understand.

5. It produces direct solution, unlike to the case of finite element method.

Disadvantages

1. Derivatives in the governing equations are replaced by their corresponding finite-differences, resulting in some approximation.

2. Complicated boundary shapes and conditions are very difficult, almost impossible to handle.

3. Usual finite-difference method cannot handle singularity well.

Accurate and reliable prediction of critical stresses is of great importance to meet the severe demand of greater reliability as well as economic challenges in design. It is noted that these critical stresses occur most frequently at the surfaces of structural components. But we are constantly aware of the lack of sophistication and doubtful quality of the finite element solutions, especially for stresses at the surfaces, which have however been pointed out by Smart [32]. The investigation of Doe and Harwood [42] verified that the accuracy of finite-difference method in reproducing the state of stresses along the boundary surfaces was much higher than that of FEM analysis. However, the computational effort in their finite-difference boundary-modeling scheme was somewhat greater than that of finite-element method Ranzi [35].

The present displacement potential function formulation in conjunction with the finite-difference technique permits the reduction of variables to be evaluated at each nodal point of the domain, from three components of stress to scalar function. This reduction of unknowns at each nodal point ultimately reduces the total number of algebraic equations to be solved.

Hence, the present approach not only provides more accurate results than those obtained by the usual computational methods, but also the computational work is reduced drastically Ahmed et al. [36]. That is why the present thesis emphasizes the use of finite-difference technique to solve the plane problems using the displacement potential function.

CHAPTER 2

Mathematical Background

2.1 Introduction

Structural analysis necessitates the requirements to investigate the state of stresses, strain and displacements at any point due to given body forces and given conditions at the boundary of the body. Most of the cases the requirement is to find the stress distribution of the body. In some cases, it is also required to find the strain distribution of the body. The state of stress, strains and displacement are termed as the elastic field. A complete description of the elastic fields requires specification of forces acting on the elementary body.

2.2 Stress at a Point

Let us take an infinitesimal cubic element as shown in Figure 2.1, which is cut off from an elastic body with sides parallel to the coordinate axes. The six forces acting on a face may be resolved into two components - one perpendicular to the plane of the face and the other parallel to the face. The stress component acting perpendicular to the plane of the face is called the normal stress and usually denoted by σ with a subscript (Example$-\sigma_{xx}, \sigma_{yy}, \sigma_{zz}$) to indicate its direction of action. According to general convention, these normal are taken positive when producing tension and negative when producing compression. In the same way, the two stress components acting parallel to the face are known as shearing stresses and indicated by the same notation with double subscript - the first indicating the direction of the normal to the face and indicating of the normal of the face and the second indicating the direction of the components of the stress. On any side, the direction of positive shearing stress coincides with the positive direction of the axis if the outward normal on this side has the positive direction of the corresponding axis. If the outward normal has a direction positive to positive axis, the positive shearing stress will also have the opposite direction of the corresponding axis.

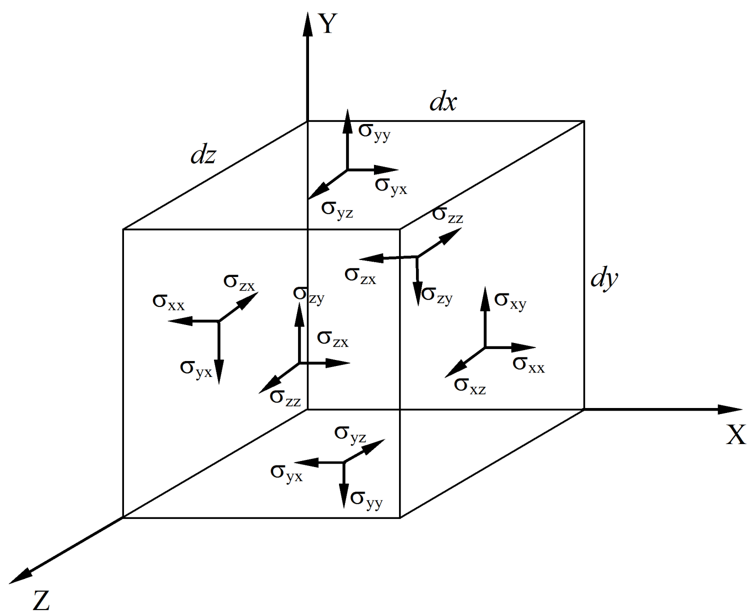

Figure 2.1: Conventions of stress components of the elementary cubic body

Though the cubic element has six different faces, basically, it has three mutually perpendicular faces and the rest of the faces are parallel to these mutually perpendicular faces respectively. Thus, corresponding a cubic element with edges parallel to the three axis of a cartesian co-ordinate system, the state of stress of the six sides of the element are described by three symbols $\sigma_{xx}, \sigma_{yy}, \sigma_{zz}$ for normal stress and six symbols $\sigma_{xy}, \sigma_{yz}, \sigma_{zx}, \sigma_{yx}, \sigma_{zy}, \sigma_{xz}$

for shearing stress.

A consideration of the equilibrium of the cubic element shows that, for two perpendicular sides of the cubic element, the components of shearing stress perpendicular to the line of intersection of these sides are equal. Mathematically stated, from consideration of equilibrium of moments about three mutually perpendicular axes, it can be shown that

$$\sigma_{xy} = \sigma_{yx}$$

$$\sigma_{yz} = \sigma_{zy}$$

$$\sigma_{zx} = \sigma_{xz}$$

Thus the nine components of the stress are reduced to six. Theses six quantities σ_{xx}, σ_{yy}, σ_{zz}, σ_{xy}, σ_{yz}, σ_{zx} are therefore sufficient to describe the stresses acting on the co-ordinate planes through a point and these will be called the components of stresses at the point.

2.3 Stress-Strain Relations

When a body is subjected to external forces, not only are internal stresses generated, but also the body itself is deformed. These deformations of the body can be uniquely specified by assigning three elongations in three perpendicular directions and three shear strains related to the same direction. These directions are taken as the direction of the coordinate axis and the symbol ε is used to denote the strain components with the same subscripts to this symbol as for the stress components. If the components of displacements of particle in the body are specified by u_x, u_y and u_z parallel to the co-ordinate axes x, y and z respectively, then the relations between the components of strain and the components of displacement are given by Timoshenko and Goodier [3]

$$\varepsilon_{xx} = \frac{\partial u_x}{\partial x} \tag{2.1a}$$
$$\varepsilon_{yy} = \frac{\partial u_y}{\partial y} \tag{2.1b}$$
$$\varepsilon_{zz} = \frac{\partial u_z}{\partial z} \tag{2.1c}$$
$$\varepsilon_{xy} = \frac{\partial u_x}{\partial y} + \frac{\partial u_y}{\partial x} \tag{2.1d}$$
$$\varepsilon_{yz} = \frac{\partial u_y}{\partial z} + \frac{\partial u_z}{\partial y} \tag{2.1e}$$
$$\varepsilon_{zx} = \frac{\partial u_x}{\partial z} + \frac{\partial u_z}{\partial x} \tag{2.1f}$$

It is also observed that, $\varepsilon_{xy} = \varepsilon_{yx}, \varepsilon_{yz} = \varepsilon_{zy}$ and $\varepsilon_{zx} = \varepsilon_{xz}$

The equations (2.1) are called the strain-displacement relations, since they define the strain components in terms of the displacement components.

By the application of Hooke's Law, that is, the linear relation between the stress and strain components and the principle of superposition, which are both based on experimental observation, the relation between the components of stress and the components of strain are given by Timoshenko and Goodier [3]

$$\varepsilon_{xx} = \frac{1}{E}\left[\sigma_{xx} - \nu\left(\sigma_{yy} + \sigma_{zz}\right)\right] \tag{2.2a}$$
$$\varepsilon_{yy} = \frac{1}{E}\left[\sigma_{yy} - \nu\left(\sigma_{zz} + \sigma_{xx}\right)\right] \tag{2.2b}$$
$$\varepsilon_{zz} = \frac{1}{E}\left[\sigma_{zz} - \nu\left(\sigma_{xx} + \sigma_{yy}\right)\right] \tag{2.2c}$$
$$\varepsilon_{xy} = \frac{2(1+\nu)}{E}\sigma_{xy} \tag{2.2d}$$
$$\varepsilon_{yz} = \frac{2(1+\nu)}{E}\sigma_{yz} \tag{2.2e}$$
$$\varepsilon_{zx} = \frac{2(1+\nu)}{E}\sigma_{zx} \tag{2.2f}$$

where , E is the modulus of elasticity or young's modulus, and ν is Poisson's ratio.

2.4 Differential Equations of Equilibrium

In section 2.2, the stress at a point of an elastic body has been considered. Let variation of the stress as we change the position of the point. Let us consider the conditions of equilibrium of a small rectangular parallelepiped with the sides $\partial x, \partial y, \partial z$, (Figure (2.1)). The components of the stresses acting on the sides of this small element and their positive directions are indicated in the Figure 2.1. It has taken into account the small changes of the components of the stress due to small increase $\partial x, \partial y, \partial z$ of the coordinates. The subscript of σ denotes the value of stress component at the point in x, y, z directions.

If F_x, F_y, F_z denote the components of body force per unit volume of the element, then the three equations of equilibrium are obtained by summing all the forces acting on the element in x, y, z direction. So, the three equilibrium equations are

$$\frac{\partial \sigma_{xx}}{\partial x} + \frac{\partial \sigma_{xy}}{\partial y} + \frac{\partial \sigma_{xz}}{\partial z} + F_x = 0 \tag{2.3a}$$

$$\frac{\partial \sigma_{yy}}{\partial y} + \frac{\partial \sigma_{yx}}{\partial x} + \frac{\partial \sigma_{yz}}{\partial z} + F_y = 0 \tag{2.3b}$$

$$\frac{\partial \sigma_{zz}}{\partial z} + \frac{\partial \sigma_{zx}}{\partial x} + \frac{\partial \sigma_{zy}}{\partial y} + F_z = 0 \tag{2.3c}$$

Equation (2.3) must be satisfied at all points throughout the volume of the body and when arrive surface that they must be such as to be in equilibrium with the external forces on the surfaces of the body.

2.5 Conditions of Compatibility

It should be noted that the six components of strain at each point are completely determined by the three functions u_x, u_y, u_z representing the components of displacement. Hence the components of strain cannot be taken arbitrary as a function of x, y and z. Now Equations (2.1) are differentiated twice and after simple manipulation, the following set of differential equations are obtained.

$$\frac{\partial^2 \varepsilon_{xx}}{\partial y^2} + \frac{\partial^2 \varepsilon_{yy}}{\partial x^2} = \frac{\partial^2 \varepsilon_{xy}}{\partial x \partial y}; \qquad 2\frac{\partial^2 \varepsilon_{xx}}{\partial y \partial z} = \frac{\partial}{\partial x}\left(-\frac{\partial \varepsilon_{yz}}{\partial x} + \frac{\partial \varepsilon_{zx}}{\partial y} + \frac{\partial \varepsilon_{xy}}{\partial z}\right) \tag{2.4a}$$

$$\frac{\partial^2 \varepsilon_{yy}}{\partial z^2} + \frac{\partial^2 \varepsilon_{zz}}{\partial y^2} = \frac{\partial^2 \varepsilon_{yz}}{\partial y \partial z}; \qquad 2\frac{\partial^2 \varepsilon_{yy}}{\partial z \partial x} = \frac{\partial}{\partial y}\left(\frac{\partial \varepsilon_{yz}}{\partial x} - \frac{\partial \varepsilon_{zx}}{\partial y} + \frac{\partial \varepsilon_{xy}}{\partial z}\right) \tag{2.4b}$$

$$\frac{\partial^2 \varepsilon_{zz}}{\partial x^2} + \frac{\partial^2 \varepsilon_{xx}}{\partial z^2} = \frac{\partial^2 \varepsilon_{zx}}{\partial z \partial x}; \qquad 2\frac{\partial^2 \varepsilon_{zz}}{\partial x \partial y} = \frac{\partial}{\partial z}\left(\frac{\partial \varepsilon_{yz}}{\partial x} + \frac{\partial \varepsilon_{zx}}{\partial y} - \frac{\partial \varepsilon_{xy}}{\partial z}\right) \tag{2.4c}$$

These differential relations are called the *Conditions of Compatibility*. If there are no body forces or if the body forces are constant, another form of the compatibility conditions can be rewritten as

$$(1+\nu)\nabla^2\sigma_{xx} + \frac{\partial^2\Theta}{\partial x^2} = 0; \qquad (1+\nu)\nabla^2\sigma_{yz} + \frac{\partial^2\Theta}{\partial y \partial z} = 0 \tag{2.5a}$$

$$(1+\nu)\nabla^2\sigma_{yy} + \frac{\partial^2\Theta}{\partial y^2} = 0; \qquad (1+\nu)\nabla^2\sigma_{xz} + \frac{\partial^2\Theta}{\partial x \partial z} = 0 \tag{2.5b}$$

$$(1+\nu)\nabla^2\sigma_{zz} + \frac{\partial^2\Theta}{\partial z^2} = 0; \qquad (1+\nu)\nabla^2\sigma_{xy} + \frac{\partial^2\Theta}{\partial x \partial y} = 0 \tag{2.5c}$$

where

$$\nabla^2 = \frac{\partial^2}{\partial x^2} + \frac{\partial^2}{\partial y^2} + \frac{\partial^2}{\partial z^2}$$

$$\Theta = \sigma_{xx} + \sigma_{yy} + \sigma_{zz}$$

The solution of an elasticity problem must satisfy the equilibrium equations (2.3) and the compatibility conditions (2.4) along with the boundary conditions.

2.6 Governing Equations of Plane Elasticity

Although the elastic analysis in general form is of three dimensional can be analyzed using two dimensions on the consideration of symmetry of planes. For such simplification there two options.

(a) Plane stress condition and

(b) Plane strain condition

2.6.1 Plane Stress Problems

The plane stress condition is considered to be a state of stress in which the normal stress σ_{zz} and the shear stresses σ_{zx} and σ_{yz} directed perpendicular to the plane are assumed to be zero. Generally, members that are thin (those with a small z dimension compared to in-plane x and y directions) and whose loads act only in the $x-y$ plane can be considered to be under plane stress. Thus a state of plane stress exists in a thin object loaded in the plane of its largest dimensions. The non-zero stresses σ_{xx}, σ_{yy} and σ_{xy} have been shown in Figure 2.2 lie in the $x-y$ plane and are independent of z and hence the functions of x and y only. A thin beam loaded in its plane and a spur gear tooth are good examples of plane stress problem. Thus, for plane stress conditions,

$$\sigma_{zz} = 0 \qquad \sigma_{zx} = 0 \qquad \sigma_{yz} = 0 \tag{2.7}$$

The stress-strain relations in case of plane stress condition are

$$\varepsilon_{xx} = \frac{1}{E}\left[\sigma_{xx} - \nu\sigma_{yy}\right] \tag{2.8a}$$

$$\varepsilon_{yy} = \frac{1}{E}\left[\sigma_{yy} - \nu\sigma_{xx}\right] \tag{2.8b}$$

$$\varepsilon_{xy} = \frac{2(1+\nu)}{E}\sigma_{xy} \tag{2.8c}$$

2.6.2 Plane Strain Problems

Plain strain condition is said to be a state of strain in which the strain normal to the $x-y$ plane, ε_{zz} and the shear strains ε_{zx} and ε_{yz} are assumed to be zero. The assumptions of the plane strain condition are realistic for long bodies (saying in the z direction) with constant

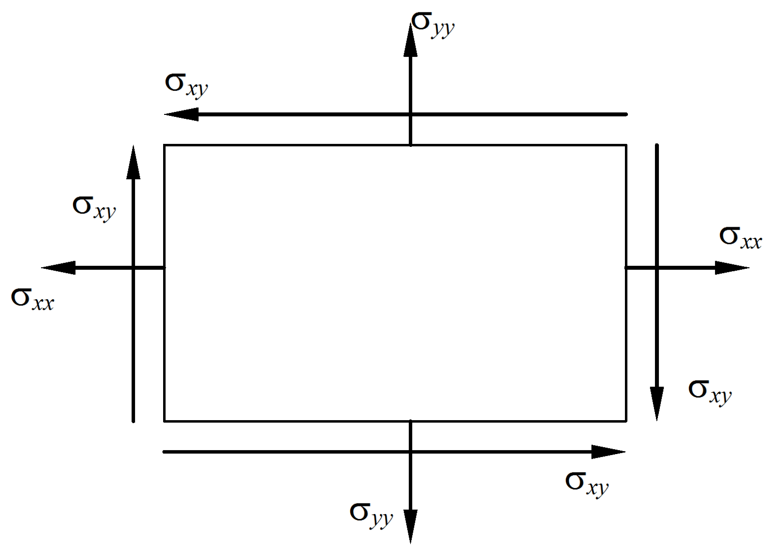

Figure 2.2: Stress components under plane stress on a plane.

cross-sectional area subjected to loads that act only in the x and/or y directions and do not vary in the z direction. Also the other component of displacement u_z is zero all over the body. These condition can be stated mathematically, from equations (2.1) as

$$\varepsilon_{zz} = \frac{\partial u_z}{\partial z} = 0 \tag{2.9a}$$

$$\varepsilon_{zy} = \frac{\partial u_y}{\partial z} + \frac{\partial u_z}{\partial y} = 0 \tag{2.9b}$$

$$\varepsilon_{zx} = \frac{\partial u_x}{\partial z} + \frac{\partial u_z}{\partial x} = 0 \tag{2.9c}$$

The above equations (2.9), in combinations with (2.2c), (2.2e) and (2.2f), show that the stress components $\sigma_{zx} = \sigma_{zy} = 0$ and stress components can be determined from the knowledge of σ_{xx} and σ_{yy} by the relation

$$\sigma_{zz} = \nu\left(\sigma_{xx} + \sigma_{yy}\right) \tag{2.10}$$

Therefore, for both the circumstances, the problem ultimately reduces to the determination of σ_{xx}, σ_{yy} and σ_{xy} as a function of x and y only.

The relations are in case of plane strain condition

$$\varepsilon_{xx} = \frac{1}{E}\left[\left(1-\nu^2\right)\sigma_{xx} - \nu(1+\nu)\sigma_{yy}\right] \tag{2.11a}$$

$$\varepsilon_{yy} = \frac{1}{E}\left[\left(1-\nu^2\right)\sigma_{yy} - \nu(1+\nu)\sigma_{xx}\right] \tag{2.11b}$$

$$\varepsilon_{xy} = \frac{2(1+\nu)}{E}\sigma_{xy} \tag{2.11c}$$

2.6.3 Conditions of Compatibility for Plane Stress and Plane Strain Problems

For the case of plane stress problems, the equilibrium equation (2.3) reduces to

$$\frac{\partial \sigma_{xx}}{\partial x} + \frac{\partial \sigma_{xy}}{\partial y} + F_x = 0 \tag{2.12a}$$

$$\frac{\partial \sigma_{yy}}{\partial y} + \frac{\partial \sigma_{xy}}{\partial x} + F_y = 0 \tag{2.12b}$$

In these equations of equilibrium (2.12) of plane stress problem, the body force are assumed, as they will be throughout this work, to be absent, then the equations (2.12) becomes

$$\frac{\partial \sigma_{xx}}{\partial x} + \frac{\partial \sigma_{xy}}{\partial y} = 0 \tag{2.13a}$$

$$\frac{\partial \sigma_{yy}}{\partial y} + \frac{\partial \sigma_{xy}}{\partial x} = 0 \tag{2.13b}$$

These equilibrium equations (2.12) are required to be solve for the case of a two dimensional problem. These two equations containing three stress components σ_{xx}, σ_{yy}, and σ_{xy} are not sufficient for the determination of these components. Thus, to evaluate these three dependent variables a third equation is necessary. This third equation comes from the consideration of the elastic deformation of the body. This additional equation ensures continuity of deformation in the body which is known as compatibility equation. In fact, it ensures compatibility of displacement u_x and u_y. The mathematical formulation of this condition can be obtained from the strain displacement relation. For two dimensional cases, these relations are

$$\varepsilon_{xx} = \frac{\partial u_x}{\partial x} \tag{2.14a}$$

$$\varepsilon_{yy} = \frac{\partial u_y}{\partial y} \tag{2.14b}$$

$$\varepsilon_{xy} = \frac{\partial u_x}{\partial y} + \frac{\partial u_y}{\partial x} \tag{2.14c}$$

Differentiating the equation (2.14a) twice with respect to y, the equation (2.14b) twice with respect to x and the equation 2.14c once with respect to x and once with respect to y, the expression for condition of compatibility in term of strain as follows

$$\frac{\partial^2 \varepsilon_x}{\partial y^2} + \frac{\partial^2 \varepsilon_y}{\partial x^2} = \frac{\partial^2 \sigma_{xy}}{\partial x \partial y} \tag{2.15}$$

This equation is known as the condition of compatibility and the strain component have to satisfy this equation to ensure the existence of continuous displacement functions u_x and u_y. To express this compatibility equation in terms of stress components, the strain components present in equation (2.15) have to eliminated by their relations with the stress components. This relations can be obtained from the equations (2.2a), (2.2b) and (2.2d) by considering $\sigma_z = 0$ in case of plane stress and $\sigma_z = \nu(\sigma_x + \sigma_y)$ in case of plane strain. For the general case of body forces $(X$ and $Y)$, we can obtain the compatibility equation in the following form:

$$(\frac{\partial^2}{\partial x^2} + \frac{\partial^2}{\partial y^2})(\sigma_{xx} + \sigma_{yy}) = -\frac{1}{(1-\nu)} \left(\frac{\partial X}{\partial x} + \frac{\partial Y}{\partial y} \right) \tag{2.16}$$

2.7 Hooke's Law for Different Types of Materials

The stress-strain relationship for a general material that is not linearly elastic is more complicated. In the simplest approximation the relation between stress and strain is taken to be linear. The generalized Hooke's law relating stresses to strains can be written in concentrated notation as Jones [43]

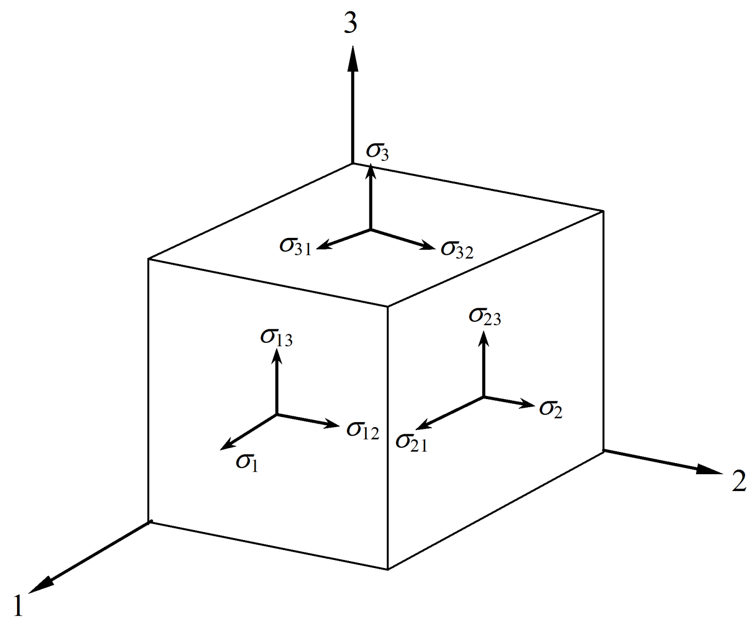

Figure 2.3: Stresses on cubic element

$$\sigma_i = C_{ij}\varepsilon_j \qquad i,j = 1, ..., 6 \tag{2.17}$$

where σ_i are the stress components shown on a three-dimensional cube in $1, 2, 3$ coordinates in Figure (2.3). C_{ij} is the stiffness matrix and ε_j are the strain components. The concentrated notation for three dimensional stresses and strains is defined in comparison to the usual tensor notation in table 2.1 and equation (2.17) can be rewritten as Kaw [1]

Table 2.1: Tensor versus concentrated notation for Stresses and Strain

Stresses		Strains	
Tensor Notation	Notation	Tensor Notation	Notation
σ_{11}	σ_1	ε_{11}	ε_1
σ_{22}	σ_2	ε_{22}	ε_2
σ_{33}	σ_3	ε_{33}	ε_3
σ_{23}	σ_4	ε_{23}	ε_4
σ_{31}	σ_5	ε_{31}	ε_5
σ_{12}	σ_6	ε_{12}	ε_6

$$\begin{bmatrix} \sigma_1 \\ \sigma_2 \\ \sigma_3 \\ \sigma_{23} \\ \sigma_{31} \\ \sigma_{12} \end{bmatrix} = \begin{bmatrix} C_{11} & C_{12} & C_{13} & C_{14} & C_{15} & C_{16} \\ C_{21} & C_{22} & C_{23} & C_{24} & C_{25} & C_{26} \\ C_{31} & C_{32} & C_{33} & C_{34} & C_{35} & C_{36} \\ C_{41} & C_{42} & C_{43} & C_{44} & C_{45} & C_{46} \\ C_{51} & C_{52} & C_{53} & C_{54} & C_{55} & C_{56} \\ C_{61} & C_{62} & C_{63} & C_{64} & C_{65} & C_{66} \end{bmatrix} \begin{bmatrix} \varepsilon_1 \\ \varepsilon_2 \\ \varepsilon_3 \\ \varepsilon_{23} \\ \varepsilon_{31} \\ \varepsilon_{12} \end{bmatrix} \tag{2.18}$$

Inverting equation (2.18), the general strain-stress relationship for a three dimensional body in a $1-2-3$ orthogonal Cartesian coordinate system is

$$\begin{bmatrix} \varepsilon_1 \\ \varepsilon_2 \\ \varepsilon_3 \\ \varepsilon_{23} \\ \varepsilon_{31} \\ \varepsilon_{12} \end{bmatrix} = \begin{bmatrix} S_{11} & S_{12} & S_{13} & S_{14} & S_{15} & S_{16} \\ S_{21} & S_{22} & S_{23} & S_{24} & S_{25} & S_{26} \\ S_{31} & S_{32} & S_{33} & S_{34} & S_{35} & S_{36} \\ S_{41} & S_{42} & S_{43} & S_{44} & S_{45} & S_{46} \\ S_{51} & S_{52} & S_{53} & S_{54} & S_{55} & S_{56} \\ S_{61} & S_{62} & S_{63} & S_{64} & S_{65} & S_{66} \end{bmatrix} \begin{bmatrix} \sigma_1 \\ \sigma_2 \\ \sigma_3 \\ \sigma_{23} \\ \sigma_{31} \\ \sigma_{12} \end{bmatrix} \tag{2.19}$$

where, $[S]_{ij}\left(=\frac{1}{[C]}\right)$ is called compliance matrix and

$$[S]_{ij} = \begin{bmatrix} S_{11} & S_{12} & S_{13} & S_{14} & S_{15} & S_{16} \\ S_{21} & S_{22} & S_{23} & S_{24} & S_{25} & S_{26} \\ S_{31} & S_{32} & S_{33} & S_{34} & S_{35} & S_{36} \\ S_{41} & S_{42} & S_{43} & S_{44} & S_{45} & S_{46} \\ S_{51} & S_{52} & S_{53} & S_{54} & S_{55} & S_{56} \\ S_{61} & S_{62} & S_{63} & S_{64} & S_{65} & S_{66} \end{bmatrix} \tag{2.20}$$

2.7.1 Anisotropic Material

The material that has 21 independent elastic constants at a point is called an anisotropic material. Once these constants are found for a particular point, the stress and strain relationship can be developed at that point. The stiffness matrix, C_{ij} has 36 constants in equation (2.18). However less than 36 of the constants can be shown to actually be independent for elastic material when important characteristics of the strain energy are considered. From the consideration of strain energy density, it can be shown that $C_{ij} = C_{ji}$. Thus 36 constants of the stiffness matrix come down to independent 21 and the stiffness matrix turns to a symmetric matrix as follows

$$\left[\ C_{ij}\ \right] = \begin{bmatrix} C_{11} & C_{12} & C_{13} & C_{14} & C_{15} & C_{16} \\ C_{12} & C_{22} & C_{23} & C_{24} & C_{25} & C_{26} \\ C_{13} & C_{23} & C_{33} & C_{34} & C_{35} & C_{36} \\ C_{14} & C_{24} & C_{34} & C_{44} & C_{45} & C_{46} \\ C_{15} & C_{25} & C_{35} & C_{45} & C_{55} & C_{56} \\ C_{16} & C_{26} & C_{36} & C_{46} & C_{56} & C_{66} \end{bmatrix} \tag{2.21}$$

2.7.2 Monoclinic Material

Material having symmetry with respect to one plane is referred to as monoclinic materials. For such case of material, transformation of axis can be done and found that $C_{14} = C_{15} = C_{24} = C_{25} = C_{34} = C_{35} = C_{46} = C_{56} = 0$ and then the number of independent elastic constant becomes 13 only. So the stiffness matrix of equation (2.21) reduces to

$$\begin{bmatrix} C_{ij} \end{bmatrix} = \begin{bmatrix} C_{11} & C_{12} & C_{13} & 0 & 0 & C_{16} \\ C_{12} & C_{22} & C_{23} & 0 & 0 & C_{26} \\ C_{13} & C_{23} & C_{33} & 0 & 0 & C_{36} \\ 0 & 0 & 0 & C_{44} & C_{45} & 0 \\ 0 & 0 & 0 & C_{45} & C_{55} & 0 \\ C_{16} & C_{26} & C_{36} & 0 & 0 & C_{66} \end{bmatrix} \tag{2.22}$$

2.7.3 Orthotropic Material (Orthogonally Anisotropic)/ Specially Orthotropic

If a material has three mutually perpendicular planes of material symmetry, then the stiffness matrix is given by

$$\begin{bmatrix} C_{ij} \end{bmatrix} = \begin{bmatrix} C_{11} & C_{12} & C_{13} & 0 & 0 & 0 \\ C_{12} & C_{22} & C_{23} & 0 & 0 & 0 \\ C_{13} & C_{23} & C_{33} & 0 & 0 & 0 \\ 0 & 0 & 0 & C_{44} & 0 & 0 \\ 0 & 0 & 0 & 0 & C_{55} & 0 \\ 0 & 0 & 0 & 0 & 0 & C_{66} \end{bmatrix} \tag{2.23}$$

The preceding stiffness matrix can be derived by starting from the stiffness matrix $[C_{ij}]$ of monoclinic material. With two more planes of symmetry, it gives

$C_{16} = 0, C_{26} = 0, C_{36} = 0, C_{45} = 0$

Three mutually perpendicular planes of material symmetry also imply three mutually perpendicular planes of elastic symmetry. Again an orthotropic material has at least two orthogonal planes of symmetry, where material properties are independent of directions within each plane. Example of an orthotropic material include a single lamina of continuous fiber composite arranged in rectangular array, a wooden bar and rolled steel. The compliance matrix (inverse of stiffness matrix) of orthotropic materials reduces to

$$\left[\ S_{ij}\ \right] = \begin{bmatrix} S_{11} & S_{12} & S_{13} & 0 & 0 & 0 \\ S_{12} & S_{22} & S_{23} & 0 & 0 & 0 \\ S_{13} & S_{23} & S_{33} & 0 & 0 & 0 \\ 0 & 0 & 0 & S_{44} & 0 & 0 \\ 0 & 0 & 0 & 0 & S_{55} & 0 \\ 0 & 0 & 0 & 0 & 0 & S_{66} \end{bmatrix} \tag{2.24}$$

2.7.4 Isotropic Material

If all planes in an orthotropic body are identical, it is an isotropic material, then the stiffness matrix is given by

$$\left[\ C_{ij}\ \right] = \begin{bmatrix} C_{11} & C_{12} & C_{12} & 0 & 0 & 0 \\ C_{12} & C_{11} & C_{12} & 0 & 0 & 0 \\ C_{12} & C_{12} & C_{11} & 0 & 0 & 0 \\ 0 & 0 & 0 & \frac{C_{11}-C_{12}}{2} & 0 & 0 \\ 0 & 0 & 0 & 0 & \frac{C_{11}-C_{12}}{2} & 0 \\ 0 & 0 & 0 & 0 & 0 & \frac{C_{11}-C_{12}}{2} \end{bmatrix} \tag{2.25}$$

For a linear isotropic material in the three-dimensional stress state, stress-strain relationships at a point in an $x - y - z$ orthogonal system in matrix from are

$$\begin{bmatrix} \varepsilon_1 \\ \varepsilon_2 \\ \varepsilon_3 \\ \varepsilon_{23} \\ \varepsilon_{31} \\ \varepsilon_{12} \end{bmatrix} = \begin{bmatrix} \frac{1}{E} & -\frac{\nu}{E} & -\frac{\nu}{E} & 0 & 0 & 0 \\ -\frac{\nu}{E} & \frac{1}{E} & -\frac{\nu}{E} & 0 & 0 & 0 \\ -\frac{\nu}{E} & -\frac{\nu}{E} & \frac{1}{E} & 0 & 0 & 0 \\ 0 & 0 & 0 & \frac{1}{G} & 0 & 0 \\ 0 & 0 & 0 & 0 & \frac{1}{G} & 0 \\ 0 & 0 & 0 & 0 & 0 & \frac{1}{G} \end{bmatrix} \begin{bmatrix} \sigma_1 \\ \sigma_2 \\ \sigma_3 \\ \sigma_{23} \\ \sigma_{31} \\ \sigma_{12} \end{bmatrix} \tag{2.26}$$

$$\begin{bmatrix} \sigma_1 \\ \sigma_2 \\ \sigma_3 \\ \sigma_{23} \\ \sigma_{31} \\ \sigma_{12} \end{bmatrix} = \begin{bmatrix} \frac{E(1-\nu)}{(1-2\nu)(1+\nu)} & \frac{\nu E}{(1-2\nu)(1+\nu)} & \frac{\nu E}{(1-2\nu)(1+\nu)} & 0 & 0 & 0 \\ \frac{\nu E}{(1-2\nu)(1+\nu)} & \frac{E(1-\nu)}{(1-2\nu)(1+\nu)} & \frac{\nu E}{(1-2\nu)(1+\nu)} & 0 & 0 & 0 \\ \frac{\nu E}{(1-2\nu)(1+\nu)} & \frac{\nu E}{(1-2\nu)(1+\nu)} & \frac{E(1-\nu)}{(1-2\nu)(1+\nu)} & 0 & 0 & 0 \\ 0 & 0 & 0 & G & 0 & 0 \\ 0 & 0 & 0 & 0 & G & 0 \\ 0 & 0 & 0 & 0 & 0 & G \end{bmatrix} \begin{bmatrix} \varepsilon_1 \\ \varepsilon_2 \\ \varepsilon_3 \\ \varepsilon_{23} \\ \varepsilon_{31} \\ \varepsilon_{12} \end{bmatrix} \tag{2.27}$$

where, ν is the poison's ratio. The shear modulus G is a function of two elastic constant, E and ν, as

$$G = \frac{E}{2(1+\nu)}$$

Relating equations (2.25) and (2.27), that gives

$$C_{11} = \frac{E(1-\nu)}{(1-2\nu)(1+\nu)} \tag{2.28a}$$

$$C_{12} = \frac{\nu E}{(1-2\nu)(1+\nu)} \tag{2.28b}$$

$$\frac{C_{11} - C_{12}}{2} = \frac{E}{2(1+\nu)} = G \tag{2.28c}$$

2.8 Hooke's Law for a Composite Lamina

2.8.1 Unidirectional Composite Lamina

A unidirectional lamina falls under the orthotropic material category. If the lamina is thin and does not carry any out-of-plane loads, one can assume plane stress conditions for the lamina. Therefore, taking Equation (2.19) and (2.24) and assuming $\sigma_3 = 0, \sigma_{23} = 0$ and $\sigma_{31} = 0$, then Hooke's law for an orthotropic plane stress problem Kaw [1], Jones [43] can be written as

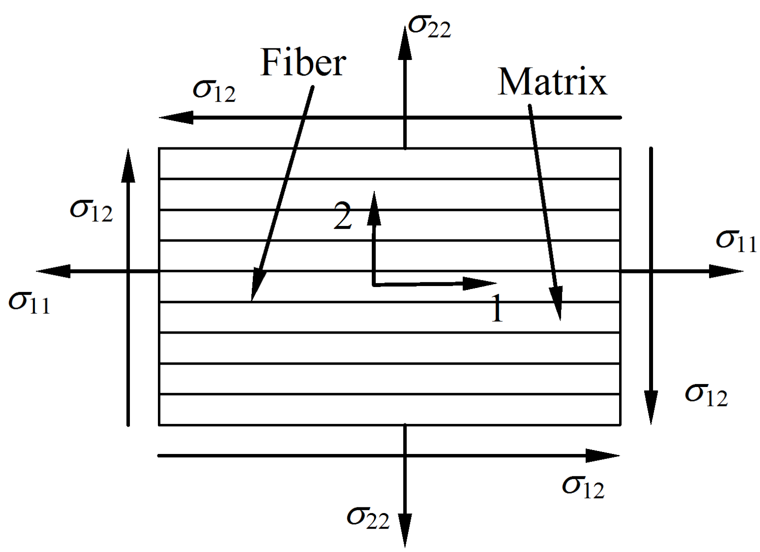

Figure 2.4: Stress components on a plane of unidirectional lamina

$$\begin{bmatrix} \varepsilon_1 \\ \varepsilon_2 \\ \varepsilon_{12} \end{bmatrix} = \begin{bmatrix} S_{11} & S_{12} & 0 \\ S_{12} & S_{22} & 0 \\ 0 & 0 & S_{66} \end{bmatrix} \begin{bmatrix} \sigma_1 \\ \sigma_2 \\ \sigma_{12} \end{bmatrix} \tag{2.29}$$

Inverting Eq. (2.29), gives stress-strain relationship as Kaw [1], Jones [43]

$$\begin{bmatrix} \sigma_1 \\ \sigma_2 \\ \sigma_{12} \end{bmatrix} = \begin{bmatrix} Q_{11} & Q_{12} & 0 \\ Q_{12} & Q_{22} & 0 \\ 0 & 0 & Q_{66} \end{bmatrix} \begin{bmatrix} \varepsilon_1 \\ \varepsilon_2 \\ \varepsilon_{12} \end{bmatrix} \tag{2.30}$$

Where, $[Q_{ij}]$ are called reduced stiffness coefficients, which are related to the engineering constants as follows:

$$Q_{11} = \frac{E_1}{1-\nu_{12}\nu_{21}} \qquad Q_{12} = \frac{\nu_{12}E_2}{1-\nu_{12}\nu_{21}}$$
$$Q_{22} = \frac{E_2}{1-\nu_{12}\nu_{21}} \qquad Q_{66} = G_{12}$$

Again for elastic constant Q_{ij} of equation (2.31) the reciprocal relations can be reduced as:

$$\frac{\nu_{12}}{E_1} = \frac{\nu_{21}}{E_2} \tag{2.32}$$

where,

E_1 = longitudinal Young's modulus (in direction 1)

E_2 = longitudinal Young's modulus (in direction 2)

ν_{12} = major Poisson's ratio, where, the general Poisson's ratio, ν_{ij} is defined as the ratio of the negative of the normal strain in direction j to the normal strain in indirection i, when the only normal load is applied in direction i

G_{12} = in-plane shear modulus (in plane $1-2$)

The unidirectional lamina is a specially orthotropic lamina because normal stress applied in the $1-2$ direction do not result in an shearing strains in the 1-2 plane because Q_{16} = Q_{26} = S_{16} = S_{26} = 0.

2.8.2 Composite Angle Lamina

The coordinate system used for showing an angle lamina is given in Figure (2.5). The axes in the $1-2$ coordinate system are called the local axes or the material axes. The direction 1 is parallel to the fibers and the direction 2 is perpendicular to the fibers.

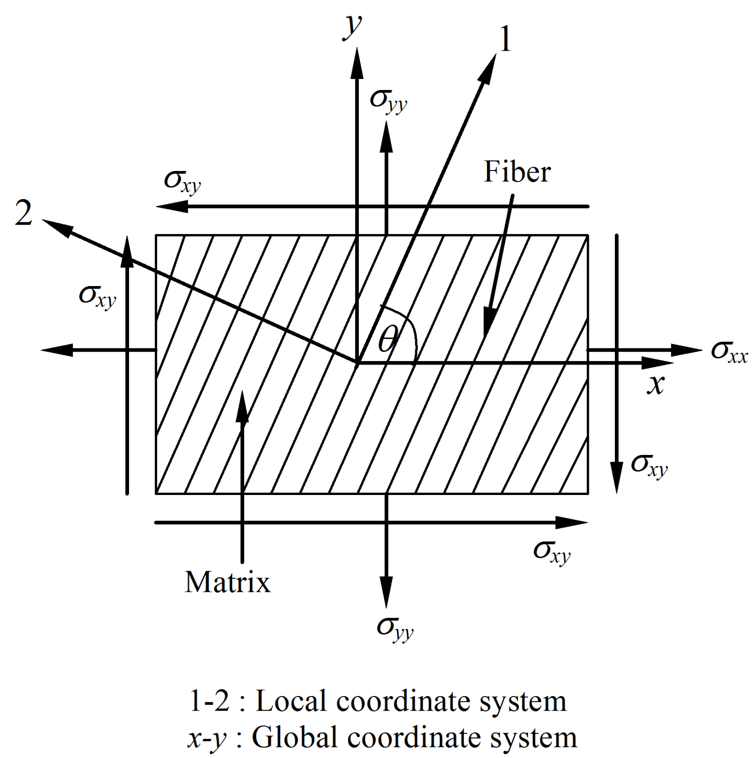

Figure 2.5: Stress components on a plane of angle ply lamina

In some literature, direction 1 is also called the longitudinal direction L and the direction 2 is called the transverse direction T. The axes in the $x-y$ coordinate system are called the global axes or the off-axes. The angle between the two axes is denoted by an angle θ. The stress-strain relationship for two dimensional angle lamina is given by Kaw [1], Jones [43]

$$\begin{bmatrix} \sigma_{xx} \\ \sigma_{yy} \\ \sigma_{xy} \end{bmatrix} = \begin{bmatrix} \overline{Q}_{11} & \overline{Q}_{12} & \overline{Q}_{16} \\ \overline{Q}_{12} & \overline{Q}_{22} & \overline{Q}_{26} \\ \overline{Q}_{16} & \overline{Q}_{26} & \overline{Q}_{66} \end{bmatrix} \begin{bmatrix} \varepsilon_{xx} \\ \varepsilon_{yy} \\ \varepsilon_{xy} \end{bmatrix} \tag{2.33}$$

Where, $\overline{Q}_{ij}$ are called the elements of the transformed reduced stiffness matrix $[\bar{Q}]$ are given by

$$\overline{Q}_{11} = Q_{11}\cos^4\theta + 2(Q_{12} + 2Q_{66})\sin^2\theta\cos^2\theta + Q_{22}\sin^4\theta \tag{2.34}$$

$$\overline{Q}_{12} = (Q_{11} + Q_{22} - 4Q_{66})\sin^2\theta\cos^2\theta + Q_{12}\left(\sin^4\theta + \cos^4\theta\right) \tag{2.35}$$

$$\overline{Q}_{22} = Q_{11}\sin^4\theta + 2(Q_{12} + 2Q_{66})\sin^2\theta\cos^2\theta + Q_{22}\cos^4\theta \tag{2.36}$$

$$\overline{Q}_{16} = (Q_{11} - Q_{12} - 2Q_{66})\cos^3\theta\sin\theta - (Q_{22} - Q_{12} - 2Q_{66})\sin^3\theta\cos\theta \tag{2.37}$$

$$\overline{Q}_{26} = (Q_{11} - Q_{12} - 2Q_{66})\sin^3\theta\cos\theta - (Q_{22} - Q_{12} - 2Q_{66})\cos^3\theta\sin\theta \tag{2.38}$$

$$\overline{Q}_{66} = (Q_{11} + Q_{22} - 2Q_{12} - 2Q_{66})\sin^2\theta\cos^2\theta + Q_{66}\left(\sin^4\theta + \cos^4\theta\right) \tag{2.39}$$

$$\tag{2.40}$$

Note that there are six elements are in the $[\bar{Q}]$ matrix and it can be seen that they are just function of the four stiffness elements, Q_{11}, Q_{12}, Q_{22}, Q_{66} and the angle of the fiber in lamina, θ. Therefore, equation (2.33) are stress-strain equations for a *general orthotropic lamina*.

2.9 Laminated Composite Material

Laminated composite materials consists of a number of layers (more than one lamina/ ply) of at least two different materials that are bonded together. Lamination is used to combine the best aspects of the constituent layers and bonding material in order to achieve a more useful material. The properties that can be emphasized by lamination are strength, stiffness, low weight, corrosion resistance, wear resistance, beauty or attractiveness, thermal insulation, acoustical insulation, etc.

2.9.1 Strain-Displacement Relations

Knowledge of the variation of stress and strain through the laminate thickness is essential to the definition of the extensional and bending stiffness of a laminate. The classical lamination theory is used to develop these relationships. The following assumptions are made in the classical lamination theory Kaw [1].

(a) Each lamina is orthotropic.

(b) Each lamina is homogenous.

(c) A line straight and perpendicular to the middle surface remains straight and perpendicular to the middle surface during deformation.

(d) The laminate is thin and is loaded only in its plane.

(e) Each lamina is elastic.

(f) No slip occurs between the lamina interfaces.

According to the classical lamination theory, the strain-displacement relations are

$$\begin{bmatrix} \varepsilon_{xx} \\ \varepsilon_{yy} \\ \varepsilon_{xy} \end{bmatrix} = \begin{bmatrix} \varepsilon^o_{xx} \\ \varepsilon^o_{yy} \\ \varepsilon^o_{xy} \end{bmatrix} + z \begin{bmatrix} \kappa_{xx} \\ \kappa_{yy} \\ \kappa_{xy} \end{bmatrix} \tag{2.41}$$

where, $\begin{bmatrix} \varepsilon^o_{xx} \\ \varepsilon^o_{yy} \\ \varepsilon^o_{xy} \end{bmatrix}$ and $\begin{bmatrix} \kappa_{xx} \\ \kappa_{yy} \\ \kappa_{xy} \end{bmatrix}$ are the mid-plane strain and the mid-plane curvature and z is distance from the midplane to different layers in laminate through thickness in Z-

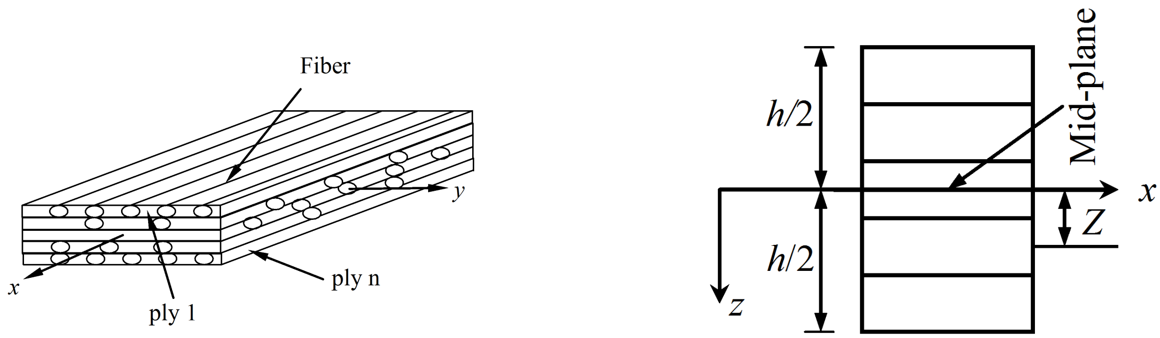

(a) A five ply laminate.

(b) Cross-section and midplane of laminate.

Figure 2.6: Relationship between displacements through the thickness of a plate to mid-plane displacements and curvatures.

direction.

2.9.2 Resultant Laminate Forces and Moments

The midplane strains and plate curvature in equation (2.41) are the unknowns for finding the lamina strains and stresses. The stresses of individual lamina can be integrated through the laminate thickness to give resultant forces and moments. The forces and moment applied to a laminate will be known, so the midplane strain and plate curvatures can then be found. The relationship between applied loads and strain and plate curvatures can be written as [1, 43]

$$\begin{bmatrix} N_{xx} \\ N_{yy} \\ N_{xy} \end{bmatrix} = \begin{bmatrix} A_{11} & A_{12} & A_{16} \\ A_{12} & A_{22} & A_{26} \\ A_{16} & A_{26} & A_{66} \end{bmatrix} \begin{bmatrix} \varepsilon^o_{xx} \\ \varepsilon^o_{yy} \\ \varepsilon^o_{xy} \end{bmatrix} + \begin{bmatrix} B_{11} & B_{12} & B_{16} \\ B_{12} & B_{22} & B_{26} \\ B_{16} & B_{26} & B_{66} \end{bmatrix} \begin{bmatrix} \kappa_{xx} \\ \kappa_{yy} \\ \kappa_{xy} \end{bmatrix} \tag{2.42a}$$

$$\begin{bmatrix} M_{xx} \\ M_{yy} \\ M_{xy} \end{bmatrix} = \begin{bmatrix} B_{11} & B_{12} & B_{16} \\ B_{12} & B_{22} & B_{26} \\ B_{16} & B_{26} & B_{66} \end{bmatrix} \begin{bmatrix} \varepsilon^o_{xx} \\ \varepsilon^o_{yy} \\ \varepsilon^o_{xy} \end{bmatrix} + \begin{bmatrix} D_{11} & D_{12} & D_{16} \\ D_{12} & D_{22} & D_{26} \\ D_{16} & D_{26} & D_{66} \end{bmatrix} \begin{bmatrix} \kappa_{xx} \\ \kappa_{yy} \\ \kappa_{xy} \end{bmatrix} \tag{2.42b}$$

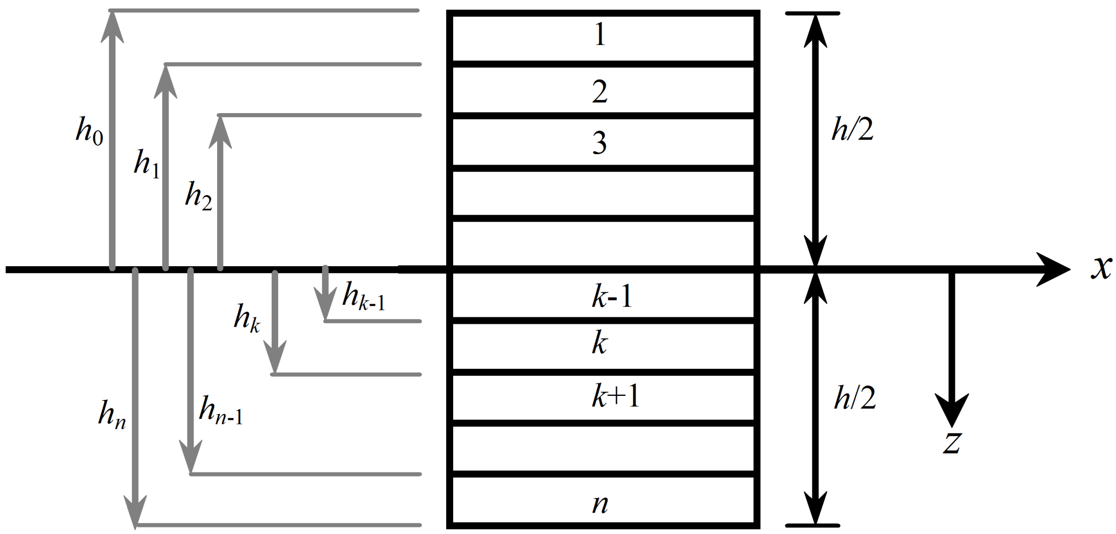

Figure 2.7: Coordinates location of plies in a laminate.

$$A_{ij} = \sum_{k=1}^{n} \left[\left(\overline{Q}_{ij}\right)\right]_k (h_k - h_{k-1}) \qquad i,j = 1,2,6 \tag{2.43a}$$

$$B_{ij} = \frac{1}{2}\sum_{k=1}^{n} \left[\left(\overline{Q}_{ij}\right)\right]_k \left(h_k^2 - h_{k-1}^2\right) \qquad i,j = 1,2,6 \tag{2.43b}$$

$$D_{ij} = \frac{1}{3}\sum_{k=1}^{n} \left[\left(\overline{Q}_{ij}\right)\right]_k \left(h_k^3 - h_{k-1}^3\right) \qquad i,j = 1,2,6 \tag{2.43c}$$

where,

N_x, N_y = normal force per unit length.

N_{xy} = shear force per unit length.

M_x, M_y = bending moments per unit length.

M_{xy} = twisting moments per unit length.

h_k and h_{k-1} is coordinate location of plies as shown in figure 2.7 and n is the total number of ply. The [A], [B] and [D] matrices are called the extensional, coupling, and bending stiffness matrices respectively. The extensional stiffness matrix [A] relates the resultant in-plane forces to the in-plane strains and the bending stiffness matrix [D] relates the resultant bending moments to the plate curvatures. The coupling stiffness matrix [B] couples the force and moment terms to the midplane strains and midplane curvature.

2.10 Special Cases of Laminates

Based on angle, material and thickness of plies, the symmetry or antisymmetry of a laminate may zero out some elements of the three stiffness matrices [A], [B], [D]. There are important to study because they may result in reducing or zeroing out the coupling of forces and bending moments, normal and shear forces, or bending and twisting moments.

2.10.1 Symmetric Laminates

A laminate is called symmetric if the material, angle and thickness of plies are same above and below the midplane. For symmetric laminates from the definition of [B] matrix, it can be proved that [B] = 0. Thus equation (2.42) can be rewritten as

$$\begin{bmatrix} N_{xx} \\ N_{yy} \\ N_{xy} \end{bmatrix} = \begin{bmatrix} A_{11} & A_{12} & A_{16} \\ A_{12} & A_{22} & A_{26} \\ A_{16} & A_{26} & A_{66} \end{bmatrix} \begin{bmatrix} \varepsilon^o_{xx} \\ \varepsilon^o_{yy} \\ \gamma^o_{xy} \end{bmatrix} \tag{2.44a}$$

$$\begin{bmatrix} M_{xx} \\ M_{yy} \\ M_{xy} \end{bmatrix} = \begin{bmatrix} D_{11} & D_{12} & D_{16} \\ D_{12} & D_{22} & D_{26} \\ D_{16} & D_{26} & D_{66} \end{bmatrix} \begin{bmatrix} \kappa_{xx} \\ \kappa_{yy} \\ \kappa_{xy} \end{bmatrix} \tag{2.44b}$$

This shows that the force and moment terms are uncoupled. Thus, if a laminate is subjected only to force, it will have zero midplane curvatures. Similarly, if it is subjected only to moments, it will have zero midplane strains.

For symmetric laminated composite, the effect of curvature of the laminate under in plane loading is usually neglected. So, $\begin{bmatrix} \kappa_{xx} \\ \kappa_{yy} \\ \kappa_{xy} \end{bmatrix} = 0$ and Eq. 2.41 can be rewritten as

$$\begin{bmatrix} \varepsilon_{xx} \\ \varepsilon_{yy} \\ \varepsilon_{xy} \end{bmatrix} = \begin{bmatrix} \varepsilon_{xx}^{o} \\ \varepsilon_{yy}^{o} \\ \varepsilon_{xy}^{o} \end{bmatrix} \tag{2.45}$$

2.10.2 Antisymmetric Laminates

A laminate is called antisymmetric if the material and thickness of the plies are the same above and below the midplane, but the ply orientations at the same distance above and below the midplane are negative of each other. The coupling terms of the stiffness matrix, $A_{16} = A_{26} = 0$ and terms of the bending stiffness matrix, $D_{16} = D_{26} = 0$.

$$\begin{bmatrix} N_{xx} \\ N_{yy} \\ N_{xy} \end{bmatrix} = \begin{bmatrix} A_{11} & A_{12} & 0 \\ A_{12} & A_{22} & 0 \\ 0 & 0 & A_{66} \end{bmatrix} \begin{bmatrix} \varepsilon_{xx}^{o} \\ \varepsilon_{yy}^{o} \\ \varepsilon_{xy}^{o} \end{bmatrix} + \begin{bmatrix} B_{11} & B_{12} & B_{16} \\ B_{12} & B_{22} & B_{26} \\ B_{16} & B_{26} & B_{66} \end{bmatrix} \begin{bmatrix} \kappa_{xx} \\ \kappa_{yy} \\ \kappa_{xy} \end{bmatrix} \tag{2.46a}$$

$$\begin{bmatrix} M_{xx} \\ M_{yy} \\ M_{xy} \end{bmatrix} = \begin{bmatrix} B_{11} & B_{12} & B_{16} \\ B_{12} & B_{22} & B_{26} \\ B_{16} & B_{26} & B_{66} \end{bmatrix} \begin{bmatrix} \varepsilon_{xx}^{o} \\ \varepsilon_{yy}^{o} \\ \varepsilon_{xy}^{o} \end{bmatrix} + \begin{bmatrix} D_{11} & D_{12} & 0 \\ D_{12} & D_{22} & 0 \\ 0 & 0 & D_{66} \end{bmatrix} \begin{bmatrix} \kappa_{xx} \\ \kappa_{yy} \\ \kappa_{xy} \end{bmatrix} \tag{2.46b}$$

2.10.3 Cross-ply Laminates

A laminate is called a cross-ply laminate (also called laminates with *specially orthotropic* layers) if only 0^o and 90^o plies are used to make a laminate. For cross-ply laminates, $A_{16} = A_{26} = 0, B_{16} = B_{26} = 0, D_{16} = D_{26} = 0$; Equation (2.42) can be written as

$$\begin{bmatrix} N_{xx} \\ N_{yy} \\ N_{xy} \end{bmatrix} = \begin{bmatrix} A_{11} & A_{12} & 0 \\ A_{12} & A_{22} & 0 \\ 0 & 0 & A_{66} \end{bmatrix} \begin{bmatrix} \varepsilon^o_{xx} \\ \varepsilon^o_{yy} \\ \varepsilon^o_{xy} \end{bmatrix} + \begin{bmatrix} B_{11} & B_{12} & 0 \\ B_{12} & B_{22} & 0 \\ 0 & 0 & B_{66} \end{bmatrix} \begin{bmatrix} \kappa_{xx} \\ \kappa_{yy} \\ \kappa_{xy} \end{bmatrix} \tag{2.47a}$$

$$\begin{bmatrix} M_{xx} \\ M_{yy} \\ M_{xy} \end{bmatrix} = \begin{bmatrix} B_{11} & B_{12} & 0 \\ B_{12} & B_{22} & 0 \\ 0 & 0 & B_{66} \end{bmatrix} \begin{bmatrix} \varepsilon^o_{xx} \\ \varepsilon^o_{yy} \\ \varepsilon^o_{xy} \end{bmatrix} + \begin{bmatrix} D_{11} & D_{12} & 0 \\ D_{12} & D_{22} & 0 \\ 0 & 0 & D_{66} \end{bmatrix} \begin{bmatrix} \kappa_{xx} \\ \kappa_{yy} \\ \kappa_{xy} \end{bmatrix} \tag{2.47b}$$

In this case, uncoupling occurs between the normal and shear forces, as well as between the bending and twisting moments.

If a cross-ply laminate is symmetric, then in addition to the preceding uncoupling, the coupling matrix [B] = 0 and no coupling takes place between the force and moment terms. Thus, equation (2.47) can be expressed for *Symmetric Cross-Ply Laminate* as

$$\begin{bmatrix} N_{xx} \\ N_{yy} \\ N_{xy} \end{bmatrix} = \begin{bmatrix} A_{11} & A_{12} & 0 \\ A_{12} & A_{22} & 0 \\ 0 & 0 & A_{66} \end{bmatrix} \begin{bmatrix} \varepsilon^o_{xx} \\ \varepsilon^o_{yy} \\ \gamma^o_{xy} \end{bmatrix} \tag{2.48a}$$

$$\begin{bmatrix} M_{xx} \\ M_{yy} \\ M_{xy} \end{bmatrix} = \begin{bmatrix} D_{11} & D_{12} & 0 \\ D_{12} & D_{22} & 0 \\ 0 & 0 & D_{66} \end{bmatrix} \begin{bmatrix} \kappa_{xx} \\ \kappa_{yy} \\ \kappa_{xy} \end{bmatrix} \tag{2.48b}$$

Equation (2.48a) and (2.48b) is called the force and moment equations for *Symmetric Cross-ply Laminate*. Substituting the value of equation (2.45), equation (2.48) becomes

$$\begin{bmatrix} N_{xx} \\ N_{yy} \\ N_{xy} \end{bmatrix} = \begin{bmatrix} A_{11} & A_{12} & 0 \\ A_{12} & A_{22} & 0 \\ 0 & 0 & A_{66} \end{bmatrix} \begin{bmatrix} \varepsilon_{xx} \\ \varepsilon_{yy} \\ \varepsilon_{xy} \end{bmatrix} \tag{2.49}$$

Eq. 2.49 is called the Force equation of *Symmetric Cross-Ply Laminate* under in plane loading.

2.10.4 Angle Ply Laminates

A laminate is called an angle ply laminate if it has the plies of the same material and thickness and only oriented at $+\theta$ and $-\theta$ directions. If a laminate has an even number of plies, then $A_{16} = A_{26} = 0$. However, if the number of plies is odd and it consists of alternating $+\theta$ and $-\theta$ plies, then it is symmetric, given [B] = 0 and A_{16}, A_{26}, D_{16} and D_{26} are also become small as the number of layers increases for same laminate thickness. This behavior is similar to the symmetric cross-ply laminates. If an angle ply consists of even number of ply, force equation (2.42) of the angle ply laminates can be written as

$$\begin{bmatrix} N_{xx} \\ N_{yy} \\ N_{xy} \end{bmatrix} = \begin{bmatrix} A_{11} & A_{12} & 0 \\ A_{12} & A_{22} & 0 \\ 0 & 0 & A_{66} \end{bmatrix} \begin{bmatrix} \varepsilon^o_{xx} \\ \varepsilon^o_{yy} \\ \varepsilon^o_{xy} \end{bmatrix} + \begin{bmatrix} B_{11} & B_{12} & B_{16} \\ B_{12} & B_{22} & B_{26} \\ B_{16} & B_{26} & B_{66} \end{bmatrix} \begin{bmatrix} \kappa_{xx} \\ \kappa_{yy} \\ \kappa_{xy} \end{bmatrix} \tag{2.50a}$$

$$\begin{bmatrix} M_{xx} \\ M_{yy} \\ M_{xy} \end{bmatrix} = \begin{bmatrix} B_{11} & B_{12} & B_{16} \\ B_{12} & B_{22} & B_{26} \\ B_{16} & B_{26} & B_{66} \end{bmatrix} \begin{bmatrix} \varepsilon^o_{xx} \\ \varepsilon^o_{yy} \\ \varepsilon^o_{xy} \end{bmatrix} + \begin{bmatrix} D_{11} & D_{12} & D_{16} \\ D_{12} & D_{22} & D_{26} \\ D_{16} & D_{26} & D_{66} \end{bmatrix} \begin{bmatrix} \kappa_{xx} \\ \kappa_{yy} \\ \kappa_{xy} \end{bmatrix} \tag{2.50b}$$

If an angle ply laminate is symmetric, the coupling matrix [B] = 0 and no coupling takes place between the force and moment terms. Thus, equation (2.50) can be expressed for *Symmetric Angle Ply Laminates* as

$$\begin{bmatrix} N_{xx} \\ N_{yy} \\ N_{xy} \end{bmatrix} = \begin{bmatrix} A_{11} & A_{12} & 0 \\ A_{12} & A_{22} & 0 \\ 0 & 0 & A_{66} \end{bmatrix} \begin{bmatrix} \varepsilon^o_{xx} \\ \varepsilon^o_{yy} \\ \varepsilon^o_{xy} \end{bmatrix} \tag{2.51a}$$

$$\begin{bmatrix} M_{xx} \\ M_{yy} \\ M_{xy} \end{bmatrix} = \begin{bmatrix} D_{11} & D_{12} & D_{16} \\ D_{12} & D_{22} & D_{26} \\ D_{16} & D_{26} & D_{66} \end{bmatrix} \begin{bmatrix} \kappa_{xx} \\ \kappa_{yy} \\ \kappa_{xy} \end{bmatrix} \tag{2.51b}$$

Since laminate is symmetric, equation (2.45) is also valid for symmetric angle ply laminates. Equation (2.51a) can be rewritten as

$$\begin{bmatrix} N_{xx} \\ N_{yy} \\ N_{xy} \end{bmatrix} = \begin{bmatrix} A_{11} & A_{12} & 0 \\ A_{12} & A_{22} & 0 \\ 0 & 0 & A_{66} \end{bmatrix} \begin{bmatrix} \varepsilon_{xx} \\ \varepsilon_{yy} \\ \varepsilon_{xy} \end{bmatrix} \tag{2.52}$$

Above (2.52) is called force equation of the angle ply laminates under in plane loading. It is not only applicable for even number angle plies but also for large number odd plies of symmetric laminates. Above force equation (2.52) of angle ply laminate is exactly the same as that of symmetric cross-ply laminate.

2.10.5 Balanced Laminates

A laminate is balanced if layers at angles other than 0^o and 90^o occur only as plus and minus pairs of $+\theta$ and $-\theta$. The plus and minus pairs do not need to be adjacent to each other, but the thickness and material of the plus and minus pairs need to be the same. Here, the terms $A_{16} = A_{16} = 0$. An example of a balanced laminate is $[30/40/-30/30/-30/-40]$. Equation (2.42) can be written as

$$\begin{bmatrix} N_{xx} \\ N_{yy} \\ N_{xy} \end{bmatrix} = \begin{bmatrix} A_{11} & A_{12} & 0 \\ A_{12} & A_{22} & 0 \\ 0 & 0 & A_{66} \end{bmatrix} \begin{bmatrix} \varepsilon^o_{xx} \\ \varepsilon^o_{yy} \\ \varepsilon^o_{xy} \end{bmatrix} + \begin{bmatrix} B_{11} & B_{12} & B_{16} \\ B_{12} & B_{22} & B_{26} \\ B_{16} & B_{26} & B_{66} \end{bmatrix} \begin{bmatrix} \kappa_{xx} \\ \kappa_{yy} \\ \kappa_{xy} \end{bmatrix} \tag{2.53a}$$

$$\begin{bmatrix} M_{xx} \\ M_{yy} \\ M_{xy} \end{bmatrix} = \begin{bmatrix} B_{11} & B_{12} & B_{16} \\ B_{12} & B_{22} & B_{26} \\ B_{16} & B_{26} & B_{66} \end{bmatrix} \begin{bmatrix} \varepsilon^o_{xx} \\ \varepsilon^o_{yy} \\ \varepsilon^o_{xy} \end{bmatrix} + \begin{bmatrix} D_{11} & D_{12} & D_{16} \\ D_{12} & D_{22} & D_{26} \\ D_{16} & D_{26} & D_{66} \end{bmatrix} \begin{bmatrix} \kappa_{xx} \\ \kappa_{yy} \\ \kappa_{xy} \end{bmatrix} \tag{2.53b}$$

If a balanced laminate is symmetric, the coupling matrix [B] = 0 and no coupling takes place between the force and moment terms. Thus, equation (2.53) can be expressed for

Symmetric Balanced Laminates as

$$\begin{bmatrix} N_{xx} \\ N_{yy} \\ N_{xy} \end{bmatrix} = \begin{bmatrix} A_{11} & A_{12} & 0 \\ A_{12} & A_{22} & 0 \\ 0 & 0 & A_{66} \end{bmatrix} \begin{bmatrix} \varepsilon^o_{xx} \\ \varepsilon^o_{yy} \\ \varepsilon^o_{xy} \end{bmatrix} \tag{2.54a}$$

$$\begin{bmatrix} M_{xx} \\ M_{yy} \\ M_{xy} \end{bmatrix} = \begin{bmatrix} D_{11} & D_{12} & 0 \\ D_{12} & D_{22} & 0 \\ 0 & 0 & D_{66} \end{bmatrix} \begin{bmatrix} \kappa_{xx} \\ \kappa_{yy} \\ \kappa_{xy} \end{bmatrix} \tag{2.54b}$$

Since the laminate is symmetric, equation (2.45) is also valid for symmetric balanced laminate. Equation (2.54a) can then be rewritten as

$$\begin{bmatrix} N_{xx} \\ N_{yy} \\ N_{xy} \end{bmatrix} = \begin{bmatrix} A_{11} & A_{12} & 0 \\ A_{12} & A_{22} & 0 \\ 0 & 0 & A_{66} \end{bmatrix} \begin{bmatrix} \varepsilon_{xx} \\ \varepsilon_{yy} \\ \varepsilon_{xy} \end{bmatrix} \tag{2.55}$$

Above force equation (2.55) of balanced laminate is exactly the same as symmetric cross-ply laminate.

CHAPTER

3

Displacement Potential Formulation for Laminated Composites

3.1 Introduction

In the existing mathematical models of elasticity, the two-dimensional problems are formulated either in terms of three stress components or in terms of two-displacement components. However, neither of the approaches is suitable for solving the practical problems of elasticity. This is mainly because of the inability to deal with a large number of variables in their numerical computation and also of the involvement of mixed boundary conditions. In fact, serious attempts have been started towards the solution of two-dimensional practical problems of elasticity after the introduction of the finite-element method of solution. It is noted that in the finite element method of solution, at least two variables are used at each node of an element for solving two dimensional problems. The corresponding computational work remains similar to that of the displacement formulation of the problems. In this thesis, a new approach to solution of boundary-value plane problems of laminated composites is introduced by which the problems can be formulated in terms of a single potential function, defined by the two displacement components. The computational work required to obtain the solution of a problem is thus reduced drastically through the use of the present displacement potential function.

3.2 Available Mathematical Models for Solution of Laminated Structures

3.2.1 Stress Function Formulation

The usual solution procedure of the two-dimensional elastic problems is to introduce a function $\phi(x, y)$, known as the stress function or Airy's stress function Timoshenko and Goodier [3], defined by

$$\sigma_{xx} = \frac{\partial^2 \phi}{\partial y^2} \tag{3.1a}$$

$$\sigma_{yy} = \frac{\partial^2 \phi}{\partial x^2} \tag{3.1b}$$

$$\sigma_{xy} = -\frac{\partial^2 \phi}{\partial x \partial y} \tag{3.1c}$$

The compatibility condition from equation (2.15) is

$$\frac{\partial^2 \varepsilon_{xx}}{\partial y^2} + \frac{\partial^2 \varepsilon_{yy}}{\partial x^2} = \frac{\partial^2 \varepsilon_{xy}}{\partial x \partial y} \tag{3.2}$$

By inverse operation, equation (2.49) can be written as

$$\begin{bmatrix} \varepsilon_{xx} \\ \varepsilon_{yy} \\ \varepsilon_{xy} \end{bmatrix} = \begin{bmatrix} I_{11} & I_{12} & 0 \\ I_{12} & I_{22} & 0 \\ 0 & 0 & I_{66} \end{bmatrix} \begin{bmatrix} \sigma_{xx} \\ \sigma_{yy} \\ \sigma_{xy} \end{bmatrix} h \tag{3.3}$$

The inverse operation of the compliance matrix I and the stiffness matrix A have a relation of $[I] = [A]^{-1}$.

The function $\phi(x, y)$ is defined by the equations (3.1) satisfy the equilibrium equations (2.13) and must satisfy the compatibility equation (3.2). By making use of equations (2.13), (3.1) and (3.3), one can obtain

$$I_{22}\frac{\partial^4\phi}{\partial x^4} + 2\left(I_{12} + \frac{I_{66}}{2}\right)\frac{\partial^4\phi}{\partial x^2\partial y^2} + I_{11}\frac{\partial^4\phi}{\partial y^4} = 0 \tag{3.4}$$

Combining the equations (2.13), (3.1) and (3.3), expression of the strain components in terms of stress function ϕ can be written as

$$\varepsilon_{xx} = \frac{\partial u}{\partial x} = \left(I_{11}\frac{\partial^2\phi}{\partial y^2} + I_{12}\frac{\partial^2\phi}{\partial y^2}\right)h \tag{3.5a}$$

$$\varepsilon_{yy} = \frac{\partial v}{\partial y} = \left(I_{22}\frac{\partial^2\phi}{\partial x^2} + I_{12}\frac{\partial^2\phi}{\partial y^2}\right)h \tag{3.5b}$$

$$\varepsilon_{xy} = \frac{\partial u}{\partial y} + \frac{\partial v}{\partial x} = -I_{66}\frac{\partial^2\phi}{\partial x\partial y}h \tag{3.5c}$$

The solution of elasticity problems following the Airy stress function approach requires the solution of equation (3.4). However, this approach appears to be efficient only for stress boundary conditions as one can readily apply the stress boundary conditions by using equation (3.1). When boundary conditions are prescribed in terms of displacement/constrains, it is quite difficult to directly apply the boundary conditions as one requires integration of equation (3.5) before applying the boundary conditions. Thus, this approach seems to be inconvenient for displacement and mixed boundary conditions.

3.2.2 Displacement Parameter Approach

Making use of equilibrium equations (2.12) (neglecting body forces), strain–displacement relations (2.14) and (2.44a), the differential equation of equilibrium for laminated composites in terms of displacement parameters, u_x and u_y are

$$A_{11}\frac{\partial^2 u_x}{\partial x^2} + 2A_{16}\frac{\partial^2 u_x}{\partial x \partial y} + A_{66}\frac{\partial^2 u_x}{\partial y^2} + A_{16}\frac{\partial^2 u_y}{\partial x^2} + (A_{12} + A_{66})\frac{\partial^2 u_y}{\partial x \partial y}$$
$$+ A_{26}\frac{\partial^2 u_y}{\partial y^2} = 0 \tag{3.6a}$$
$$A_{16}\frac{\partial^2 u_x}{\partial x^2} + (A_{12} + A_{66})\frac{\partial^2 u_x}{\partial x \partial y} + A_{26}\frac{\partial^2 u_x}{\partial y^2} + A_{66}\frac{\partial^2 u_y}{\partial x^2} + 2A_{26}\frac{\partial^2 u_y}{\partial x \partial y}$$
$$+ A_{22}\frac{\partial^2 u_y}{\partial y^2} = 0 \tag{3.6b}$$

Putting the strain values from equation (2.14), the three stress-displacement relations for the plane stress problems, obtained from equation (2.44a) and (2.45) are as follows:

$$\sigma_{xx} = \frac{1}{h}\left[A_{11}\frac{\partial u_x}{\partial x} + A_{16}\frac{\partial u_y}{\partial x} + A_{16}\frac{\partial u_x}{\partial y} + A_{12}\frac{\partial u_y}{\partial y}\right] \tag{3.7a}$$
$$\sigma_{yy} = \frac{1}{h}\left[A_{12}\frac{\partial u_x}{\partial x} + A_{26}\frac{\partial u_y}{\partial x} + A_{26}\frac{\partial u_x}{\partial y} + A_{22}\frac{\partial u_y}{\partial y}\right] \tag{3.7b}$$
$$\sigma_{xy} = \frac{1}{h}\left[A_{16}\frac{\partial u_x}{\partial x} + A_{66}\frac{\partial u_y}{\partial x} + A_{66}\frac{\partial u_x}{\partial y} + A_{26}\frac{\partial u_y}{\partial y}\right] \tag{3.7c}$$

Equation (3.6) represents two coupled second order elliptic partial differential equations of equilibrium. It is quite difficult to obtain the solution satisfying these two partial differential equations simultaneously especially with mixed conditions on the boundaries. Although this is suitable for applying displacement boundary conditions. Further, equations (3.7) is the corresponding stress equation for displacement parameter approach. This stress equation is directly related with displacement parameters.

3.2.3 Displacement Potential Approach

As discussed above, both the airy stress function approach and the displacement parameter approach are not adequate to obtain numerical solution of elasticity problems, particularly the mixed boundary value problems. Thus, the present study is aimed at developing a method for the solution of elasticity problems of structural elements of composite materials under any boundary conditions prescribed in terms of either stress or displacement or any combination of these, i.e., mixed boundary conditions. To realize this, a new function, called displacement potential function $\psi(x, y)$, has been introduced for different materials like isotropic [17, 18], orthotropic [40, 41] and anisotropic [36].

Isotropic Materials

For the case of isotropic material, the two displacement parameter u_x and u_y are expressed in terms of the displacement potential function $\psi(x, y)$ as

$$u_x = \frac{\partial^2 \psi}{\partial x \partial y} \tag{3.8a}$$

$$u_y = -\frac{1}{2(1+\nu)}\left[2\frac{\partial^2 \psi}{\partial x^2} + (1-\nu)\frac{\partial^2 \psi}{\partial y^2}\right] \tag{3.8b}$$

With the definition of potential function $\psi(x, y)$, governing differential equation for isotropic materials is

$$\frac{\partial^4 \psi}{\partial x^4} + 2\frac{\partial^4 \psi}{\partial x^2 \partial y^2} + \frac{\partial^4 \psi}{\partial y^4} = 0 \tag{3.9}$$

and stress and displacement components in term's of potential function ψ for isotropic materials can be expressed as

$$u_x = \frac{\partial^2 \psi}{\partial x \partial y} \tag{3.10a}$$

$$u_y = -\frac{1}{2(1+\nu)}\left[2\frac{\partial^2 \psi}{\partial x^2} + (1-\nu)\frac{\partial^2 \psi}{\partial y^2}\right] \tag{3.10b}$$

$$\sigma_{xx} = \frac{E}{(1+\nu)^2}\left[\frac{\partial^3 \psi}{\partial x^2 \partial y} - \nu\frac{\partial^3 \psi}{\partial y^3}\right] \tag{3.10c}$$

$$\sigma_{yy} = -\frac{E}{(1+\nu)^2}\left[(2+\nu)\frac{\partial^3 \psi}{\partial x^2 \partial y} + \frac{\partial^3 \psi}{\partial y^3}\right] \tag{3.10d}$$

$$\sigma_{xy} = \frac{E}{(1+\nu)^2}\left[-\frac{\partial^3 \psi}{\partial x^3} + \nu\frac{\partial^3 \psi}{\partial x \partial y^2}\right] \tag{3.10e}$$

Orthotropic Materials

Again, for the general unidirectional Lamina, the two displacement parameter u_x and u_y are expressed in terms of the displacement potential function $\psi(x, y)$ as

$$u_x = \frac{\partial^2 \psi}{\partial x \partial y} \tag{3.11a}$$

$$u_y = -\frac{1}{\nu_{xy} E_x E_y + G_{xy}(E_x - \nu_{xy}^2 E_y)} \left[E_x^2 \frac{\partial^2 \psi}{\partial x^2} + G_{xy} \left(E_x - \nu_{xy}^2 E_y \right) \frac{\partial^2 \psi}{\partial y^2} \right] \tag{3.11b}$$

With the definition of potential function $\psi(x, y)$, governing differential equation of equilibrium for general unidirectional lamina is

$$E_x G_{xy} \frac{\partial^4 \psi}{\partial x^4} + E_y (E_x - 2\nu_{xy} G_{xy}) \frac{\partial^4 \psi}{\partial x^2 \partial y^2} + E_y G_{xy} \frac{\partial^4 \psi}{\partial y^4} \tag{3.12}$$

and stress and displacement components in term's of ψ can be expressed as

$$u_x = \frac{\partial^2 \psi}{\partial x \partial y} \tag{3.13a}$$

$$u_y = -\frac{1}{\nu_{xy} E_x E_y + G_{xy}(E_x - \nu_{xy}^2 E_y)} \left[E_x^2 \frac{\partial^2 \psi}{\partial x^2} + G_{xy} \left(E_x - \nu_{xy}^2 E_y \right) \frac{\partial^2 \psi}{\partial y^2} \right] \tag{3.13b}$$

$$\sigma_{xx} = \frac{E_x G_{xy}}{\nu_{xy} E_x E_y + G_{xy}(E_x - \nu_{xy}^2 E_y)} \left[E_x \frac{\partial^3 \psi}{\partial x^2 \partial y} - \nu_{xy} E_y \frac{\partial^3 \psi}{\partial y^3} \right] \tag{3.13c}$$

$$\sigma_{yy} = \frac{E_x E_y}{\nu_{xy} E_x E_y + G_{xy}(E_x - \nu_{xy}^2 E_y)} \left[(\nu_{xy} G_{xy} - E_x) \frac{\partial^3 \psi}{\partial x^2 \partial y} - G_{xy} \frac{\partial^3 \psi}{\partial y^3} \right] \tag{3.13d}$$

$$\sigma_{xy} = -\frac{E_x G_{xy}}{\nu_{xy} E_x E_y + G_{xy}(E_x - \nu_{xy}^2 E_y)} \left[E_x \frac{\partial^3 \psi}{\partial x^3} - \nu_{xy} E_y \frac{\partial^3 \psi}{\partial x \partial y^2} \right] \tag{3.13e}$$

Another explicit expression of the general governing differential equation for the case of orthotropic materials is

$$\frac{\partial^4 \psi}{\partial x^4} + \left(\frac{\overline{Q}_{22}}{\overline{Q}_{66}} - \frac{\overline{Q}_{12}^2}{\overline{Q}_{11} \overline{Q}_{66}} - \frac{2\overline{Q}_{12}}{\overline{Q}_{11}} \right) \frac{\partial^4 \psi}{\partial x^2 \partial y^2} + \frac{\overline{Q}_{22}}{\overline{Q}_{11}} \frac{\partial^4 \psi}{\partial y^4} = 0 \tag{3.14}$$

General unidirectional lamina can be replaced by the case of 0^o fiber angle (with x-axis) lamina or 90^o fiber angle (with x-axis) lamina shown in Fig. (2.5). For the case of 0^o fiber angle (with x-axis) lamina, E_x, E_y and ν_{xy} can be replaced by E_1, E_2 and ν_{12} in equation (3.12) where they are used to denote the young's modulus in fiber direction in the perpendicular to fiber direction respectively or substituting the value of $\overline{Q}$'s (from equation (2.34)) into equation (3.14) and putting $\theta = 0$ the expression of the governing differential equation for the case of orthotropic materials with 0^0 fiber angle

$$E_1 G_{12}\frac{\partial^4\psi}{\partial x^4} + E_2(E_1 - 2\nu_{12}G_{12})\frac{\partial^4\psi}{\partial x^2\partial y^2} + E_2 G_{12}\frac{\partial^4\psi}{\partial y^4} \tag{3.15}$$

Explicit expressions for the body parameters in terms of the function ψ are obtained from the general equations (3.13) when the respective conditions of orthotropic material are substituted on them. When $\theta = 0^o$, the conditions are,

$$u_x = \frac{\partial^2\psi}{\partial x\partial y} \tag{3.16a}$$

$$u_y = -\frac{1}{D_n}\left[E_1^2\frac{\partial^2\psi}{\partial x^2} + G_{12}\left(E_1 - \nu_{12}^2 E_2\right)\frac{\partial^2\psi}{\partial y^2}\right] \tag{3.16b}$$

$$\sigma_{xx} = \frac{E_1 G_{12}}{D_n}\left[E_1\frac{\partial^3\psi}{\partial x^2\partial y} - \nu_{12}E_2\frac{\partial^3\psi}{\partial y^3}\right] \tag{3.16c}$$

$$\sigma_{yy} = \frac{E_1 E_2}{D_n}\left[(\nu_{12}G_{12} - E_1)\frac{\partial^3\psi}{\partial x^2\partial y} - G_{12}\frac{\partial^3\psi}{\partial y^3}\right] \tag{3.16d}$$

$$\sigma_{xy} = -\frac{E_1 G_{12}}{D_n}\left[E_1\frac{\partial^3\psi}{\partial x^3} - \nu_{12}E_2\frac{\partial^3\psi}{\partial x\partial y^2}\right] \tag{3.16e}$$

where, $D_n = \nu_{12}E_1E_2 + G_{12}(E_1 - \nu_{12}^2 E_2)$

For the case of 90^o fiber angle (with x-axis) lamina, E_x, E_y and ν_{xy} can be replaced by E_2, E_1 and ν_{21} where they are used to denote the young's modulus in fiber direction in the perpendicular to fiber direction respectively or substituting the value of $\overline{Q}$'s (from equation (2.34)) into equation (3.14) and putting $\theta = 90$ the expression of the governing differential equation for the case of orthotropic materials with 90^0 fiber angle

$$E_2G_{12}\frac{\partial^4\psi}{\partial x^4} + E_2(E_1 - 2\nu_{12}G_{12})\frac{\partial^4\psi}{\partial x^2\partial y^2} + E_1G_{12}\frac{\partial^4\psi}{\partial y^4} \tag{3.17}$$

Similar way, Orthotropic material with $(\theta = 90^o)$ fiber angle with the x-axis, the explicit expression of body parameters are

$$u_x = \frac{\partial^2\psi}{\partial x\partial y} \tag{3.18a}$$

$$u_y = -\frac{1}{D_n}\left[E_1E_2\frac{\partial^2\psi}{\partial x^2} + G_{12}\left(E_1 - \nu_{12}^2E_2\right)\frac{\partial^2\psi}{\partial y^2}\right] \tag{3.18b}$$

$$\sigma_{xx} = \frac{E_1E_2G_{12}}{D_n}\left[\frac{\partial^3\psi}{\partial x^2\partial y} - \nu_{12}\frac{\partial^3\psi}{\partial y^3}\right] \tag{3.18c}$$

$$\sigma_{yy} = \frac{E_1}{D_n}\left[E_2(\nu_{12}G_{12} - E_1)\frac{\partial^3\psi}{\partial x^2\partial y} - E_1G_{12}\frac{\partial^3\psi}{\partial y^3}\right] \tag{3.18d}$$

$$\sigma_{xy} = -\frac{E_1E_2G_{12}}{D_n}\left[-\frac{\partial^3\psi}{\partial x^3} + \nu_{12}\frac{\partial^3\psi}{\partial x\partial y^2}\right] \tag{3.18e}$$

where, $D_n = \nu_{12}E_1E_2 + G_{12}(E_1 - \nu_{12}^2E_2)$

Further G_{xy} is replaced by G_{12} for both two cases to denote the shear modulus for on-axis orientation.

Anisotropic Materials

The governing equation of *anisotropic material* can be written as

$$\beta_1\frac{\partial^4\psi}{\partial x^4} + \beta_2\frac{\partial^4\psi}{\partial x^3\partial y} + \beta_3\frac{\partial^4\psi}{\partial x^2\partial y^2} + \beta_4\frac{\partial^4\psi}{\partial x\partial y^3} + \beta_5\frac{\partial^4\psi}{\partial y^4} = 0 \tag{3.19}$$

where

$$\beta_1 = \left(\alpha_1\overline{Q}_{11} + \alpha_4\overline{Q}_{16}\right)$$
$$\beta_2 = \left(\alpha_1\left(\overline{Q}_{12} + \overline{Q}_{66}\right) + \alpha_2\overline{Q}_{16} + 2\alpha_4\overline{Q}_{26} + \alpha_5\overline{Q}_{66}\right)$$
$$\beta_3 = \left(\alpha_1\overline{Q}_{26} + \alpha_2\left(\overline{Q}_{12} + \overline{Q}_{66}\right) + \alpha_3\overline{Q}_{16} + \alpha_4\overline{Q}_{22} + 2\alpha_5\overline{Q}_{26} + \alpha_6\overline{Q}_{66}\right)$$
$$\beta_4 = \left(\alpha_2\overline{Q}_{26} + \alpha_3\left(\overline{Q}_{12} + \overline{Q}_{66}\right) + \alpha_5\overline{Q}_{22} + 2\alpha_6 + \overline{Q}_{26}\right)$$
$$\beta_5 = \left(\alpha_3\overline{Q}_{26} + \alpha_6\overline{Q}_{22}\right)$$

The general expressions for the body parameters in terms of the function ψ of anisotropic material

$$u_x = \alpha_1\frac{\partial^2\psi}{\partial x^2} + \alpha_2\frac{\partial^2\psi}{\partial x\partial y} + \alpha_3\frac{\partial^2\psi}{\partial y^2} \tag{3.20a}$$
$$u_y = \alpha_4\frac{\partial^2\psi}{\partial x^2} + \alpha_5\frac{\partial^2\psi}{\partial x\partial y} + \alpha_6\frac{\partial^2\psi}{\partial y^2} \tag{3.20b}$$
$$\begin{aligned}\sigma_{xx} = \frac{1}{bh}\Bigg[&(\alpha_1\overline{Q}_{11} + \alpha_4\overline{Q}_{16})\frac{\partial^3\psi}{\partial x^3} + (\alpha_1\overline{Q}_{16} + \alpha_2\overline{Q}_{11} + \alpha_4\overline{Q}_{12} + \alpha_5\overline{Q}_{16})\\ &\frac{\partial^3\psi}{\partial x^2\partial y} + (\alpha_2\overline{Q}_{16} + \alpha_3\overline{Q}_{11} + \alpha_5\overline{Q}_{12} + \alpha_6\overline{Q}_{16})\frac{\partial^3\psi}{\partial x\partial y^2} + \big(\alpha_3\overline{Q}_{16}\\ &+\alpha_6\overline{Q}_{12}\big)\frac{\partial^3\psi}{\partial x^3}\Bigg]\end{aligned} \tag{3.20c}$$
$$\begin{aligned}\sigma_{yy} = \frac{1}{bh}\Bigg[&(\alpha_1\overline{Q}_{12} + \alpha_4\overline{Q}_{26})\frac{\partial^3\psi}{\partial x^3} + (\alpha_1\overline{Q}_{26} + \alpha_2\overline{Q}_{12} + \alpha_4\overline{Q}_{22} + \alpha_5\overline{Q}_{26})\\ &\frac{\partial^3\psi}{\partial x^2\partial y} + (\alpha_2\overline{Q}_{26} + \alpha_3\overline{Q}_{12} + \alpha_5\overline{Q}_{22} + \alpha_6\overline{Q}_{26})\frac{\partial^3\psi}{\partial x\partial y^2} + \big(\alpha_3\overline{Q}_{26}\\ &+\alpha_6\overline{Q}_{22}\big)\frac{\partial^3\psi}{\partial x^3}\Bigg]\end{aligned} \tag{3.20d}$$
$$\begin{aligned}\sigma_{xy} = \frac{1}{bh}\Bigg[&(\alpha_1\overline{Q}_{16} + \alpha_4\overline{Q}_{66})\frac{\partial^3\psi}{\partial x^3} + (\alpha_1\overline{Q}_{66} + \alpha_2\overline{Q}_{16} + \alpha_4\overline{Q}_{26} + \alpha_5\overline{Q}_{66})\\ &\frac{\partial^3\psi}{\partial x^2\partial y} + (\alpha_2\overline{Q}_{66} + \alpha_3\overline{Q}_{16} + \alpha_5\overline{Q}_{26} + \alpha_6\overline{Q}_{66})\frac{\partial^3\psi}{\partial x\partial y^2} + \big(\alpha_3\overline{Q}_{66}\\ &+\alpha_6\overline{Q}_{26}\big)\frac{\partial^3\psi}{\partial x^3}\Bigg]\end{aligned} \tag{3.20e}$$

where

$$\alpha_1 = -\frac{\overline{Q}_{16}}{PC.\overline{Q}_{11}}\left(\overline{Q}_{11} + \overline{Q}_{16}.\alpha_5\right) \tag{3.21a}$$

$$\alpha_2 = 1 \tag{3.21b}$$

$$\alpha_3 = -\frac{\overline{Q}_{26}}{QC.\overline{Q}_{66}}\left(\overline{Q}_{66} + \overline{Q}_{26}.\alpha_5\right) \tag{3.21c}$$

$$\alpha_4 = \frac{1}{PC}\left(\overline{Q}_{11} + \overline{Q}_{16}.\alpha_5\right) \tag{3.21d}$$

$$\alpha_5 = -\frac{\left(2.\overline{Q}_{16} + \frac{RC}{PC}\overline{Q}_{11} + \frac{SC}{QC}\overline{Q}_{66}\right)}{\left(\frac{RC}{PC}\overline{Q}_{16} + \frac{SC}{QC}\overline{Q}_{26} + \overline{Q}_{12} + \overline{Q}_{66}\right)} \tag{3.21e}$$

$$\alpha_6 = \frac{1}{QC}\left(\overline{Q}_{66} + \overline{Q}_{26}.\alpha_5\right) \tag{3.21f}$$

$$PC = 2\frac{\overline{Q}_{16}^2}{\overline{Q}_{11}} - \overline{Q}_{12} - \overline{Q}_{66} \qquad QC = 2\frac{\overline{Q}_{16}.\overline{Q}_{26}}{\overline{Q}_{66}} - \overline{Q}_{12} - \overline{Q}_{66}$$

$$RC = -\frac{\overline{Q}_{16}.\overline{Q}_{66}}{\overline{Q}_{11}} + \overline{Q}_{26} \qquad SC = -\frac{\overline{Q}_{11}.\overline{Q}_{26}}{\overline{Q}_{66}} + \overline{Q}_{16}$$

The above governing equations and boundary conditions is derived for isotropic materials as well as single composite lamina. The general governing equations and boundary conditions of the symmetric laminated composites has been discussed in section 3.3. The details application of the potential function ψ of a composite material has been also discussed in section 3.3.

It is interesting to note that all components of stress and displacement have been expressed in terms of the displacement potential function $\psi(x, y)$. Thus, this approach is suitable for any boundary conditions wheatear they prescribed in terms of either stress or displacement or any combination of them.

3.3 Development of Governing Equation For General Symmetric Laminates

This section describes the development of the displacement-potential formulation for the solution of stress problems of laminated composite materials. The formulation derived earlier for the case of general anisotropic material [36] has been extended here for laminated composites by incorporating necessary modifications. From equation (2.13), for general anisotropic material in absence of body forces, the governing equations of equilibrium for the plane problems of elastic bodies of Hookean materials, in terms of stress components, are as follows [3]

$$\frac{\partial \sigma_{xx}}{\partial x} + \frac{\partial \sigma_{xy}}{\partial y} = 0 \tag{3.22a}$$

$$\frac{\partial \sigma_{yy}}{\partial y} + \frac{\partial \sigma_{xy}}{\partial x} = 0 \tag{3.22b}$$

for symmetric laminates subjected to in-plane loadings only, one can neglect the effect of curvature, i.e, $[\kappa] = 0$. Thus equation 2.41 can be reduced as

$$\begin{bmatrix} \varepsilon_{xx} \\ \varepsilon_{yy} \\ \varepsilon_{xy} \end{bmatrix} = \begin{bmatrix} \varepsilon^o_{xx} \\ \varepsilon^o_{yy} \\ \varepsilon^o_{xy} \end{bmatrix} \tag{3.23}$$

If curvature effect is not present, then variation of strain is equal to the variation of mid-plane strain. The stress–strain relations for the *symmetric laminated composite materials* are expressed through the transformed material stiffness matrix from equation 2.44a as follows

$$\begin{Bmatrix} \sigma_{xx} \\ \sigma_{yy} \\ \sigma_{xy} \end{Bmatrix} = \frac{1}{h} \begin{bmatrix} A_{11} & A_{12} & A_{16} \\ A_{12} & A_{22} & A_{26} \\ A_{16} & A_{26} & A_{66} \end{bmatrix} \begin{Bmatrix} \varepsilon_{x} \\ \varepsilon_{y} \\ \varepsilon_{xy} \end{Bmatrix} \tag{3.24}$$

Where

$$A_{ij} = \sum_{k=1}^{n} [(\bar{Q})_{ij}]_k \left(h_k - h_{k-1}\right) \qquad i = 1, 2, 6; \qquad j = 1, 2, 6 \tag{3.25}$$

$$Q_{11} = \frac{E_1}{1 - \nu_{12}\nu_{21}} \qquad Q_{12} = \frac{\nu_{12}E_1}{1 - \nu_{12}\nu_{21}}$$
$$Q_{22} = \frac{E_2}{1 - \nu_{12}\nu_{21}} \qquad Q_{66} = G_{12}$$

θ is the fiber orientation of individual ply with respect to x-axis, $(h_k - h_{k-1})$ is the thickness of each ply, k is the ply number $(k = 1, 2, 3, ..., n)$, h is the total thickness of the laminated panel. E_1 and E_2 are the young's modulus in lateral and axial direction of each ply, respectively, ν_{12} and ν_{21} are the major and minor Poison's ratio respectively; G_{12} is the in-plane shear modulus.

For the Potential function formulation, the stresses are required to be express in terms of displacement components. Putting the strain values from equation (2.14) the three stress-displacement relations for the plane problems of anisotropic materials, obtained from equation (3.24) are as follows:

$$\sigma_{xx} = \frac{1}{h}\left[A_{11}\frac{\partial u_x}{\partial x} + A_{16}\frac{\partial u_y}{\partial x} + A_{16}\frac{\partial u_x}{\partial y} + A_{12}\frac{\partial u_y}{\partial y}\right] \tag{3.26a}$$
$$\sigma_{yy} = \frac{1}{h}\left[A_{12}\frac{\partial u_x}{\partial x} + A_{26}\frac{\partial u_y}{\partial x} + A_{26}\frac{\partial u_x}{\partial y} + A_{22}\frac{\partial u_y}{\partial y}\right] \tag{3.26b}$$
$$\sigma_{xy} = \frac{1}{h}\left[A_{16}\frac{\partial u_x}{\partial x} + A_{66}\frac{\partial u_y}{\partial x} + A_{66}\frac{\partial u_x}{\partial y} + A_{26}\frac{\partial u_y}{\partial y}\right] \tag{3.26c}$$

Combining equation (3.22) and (3.26) and equilibrium equations can be expressed in terms of displacement components as follows

$$A_{11}\frac{\partial^2 u_x}{\partial x^2} + A_{16}\frac{\partial^2 u_y}{\partial x^2} + 2A_{16}\frac{\partial^2 u_x}{\partial x \partial y} + (A_{12} + A_{66})\frac{\partial^2 u_y}{\partial x \partial y} + A_{66}\frac{\partial^2 u_x}{\partial y^2} + A_{26}\frac{\partial^2 u_y}{\partial y^2} = 0 \tag{3.27a}$$

$$A_{16}\frac{\partial^2 u_x}{\partial x^2} + A_{66}\frac{\partial^2 u_y}{\partial x^2} + (A_{12} + A_{66})\frac{\partial^2 u_x}{\partial x \partial y} + 2A_{26}\frac{\partial^2 u_y}{\partial x \partial y} + A_{26}\frac{\partial^2 u_x}{\partial y^2} + A_{22}\frac{\partial^2 u_y}{\partial y^2} = 0 \tag{3.27b}$$

In the present approach, the two-dimensional problem of elasticity is reduced to the determination of a single function by introducing a scheme of reduction of unknowns. In order to attain that, the displacement components are expressed in terms of a potential function ψ of space variables as follows:

$$u_x(x,y) = \alpha_1\frac{\partial^2 \psi}{\partial x^2} + \alpha_2\frac{\partial^2 \psi}{\partial x \partial y} + \alpha_3\frac{\partial^2 \psi}{\partial y^2} \tag{3.28a}$$

$$u_y(x,y) = \alpha_4\frac{\partial^2 \psi}{\partial x^2} + \alpha_5\frac{\partial^2 \psi}{\partial x \partial y} + \alpha_6\frac{\partial^2 \psi}{\partial y^2} \tag{3.28b}$$

where, α_i are unknown material constants. Combining (3.27), and (3.28), we obtain the equilibrium equations in terms of the function ψ, which are

$$\begin{aligned}
&(\alpha_1 A_{11} + \alpha_4 A_{16})\frac{\partial^4 \psi}{\partial x^4} \\
&+ \{2\alpha_1 A_{16} + \alpha_2 A_{11} + \alpha_4 (A_{12} + A_{66}) + \alpha_5 A_{16}\}\frac{\partial^4 \psi}{\partial x^3 \partial y} \\
&+ \{\alpha_1 A_{66} + 2\alpha_2 A_{16} + \alpha_3 A_{11} + \alpha_4 A_{26} + \alpha_5 (A_{12} + A_{66}) + \alpha_6 A_{16}\}\frac{\partial^4 \psi}{\partial x^2 \partial y^2} \\
&+ \{\alpha_2 A_{66} + 2\alpha_3 A_{16} + \alpha_5 A_{26} + \alpha_6 (A_{12} + A_{66})\}\frac{\partial^4 \psi}{\partial x \partial y^3} \\
&+ (\alpha_3 A_{66} + \alpha_6 A_{26})\frac{\partial^4 \psi}{\partial y^4} = 0
\end{aligned} \tag{3.29a}$$

$$
\begin{aligned}
&(\alpha_1 A_{11} + \alpha_4 A_{16}) \frac{\partial^4 \psi}{\partial x^4} \\
&+ \{\alpha_1 (A_{12} + A_{66}) + \alpha_2 A_{16} + 2\alpha_4 A_{26} + \alpha_5 A_{66}\} \frac{\partial^4 \psi}{\partial x^3 \partial y} \\
&+ \{\alpha_1 A_{26} + \alpha_2 (A_{12} + A_{66}) + \alpha_3 A_{16} + \alpha_4 A_{22} + 2\alpha_5 A_{26} + \alpha_6 A_{66}\} \frac{\partial^4 \psi}{\partial x^2 \partial y^2} \\
&+ \{\alpha_2 A_{26} + \alpha_3 (A_{12} + A_{66}) + \alpha_5 A_{22} + 2\alpha_6 + A_{26}\} \frac{\partial^4 \psi}{\partial x \partial y^3} \\
&+ (\alpha_3 A_{26} + \alpha_6 A_{22}) \frac{\partial^4 \psi}{\partial y^4} = 0
\end{aligned}
\tag{3.29b}
$$

Let us now choose α in such a way that Eq. (3.29b) is automatically satisfied under all the circumstances. This will happen when coefficients of all the derivatives present in Eq. (3.29a) are individually zero. That is, when

$$\alpha_1 A_{11} + \alpha_4 A_{16} = 0 \tag{3.30a}$$

$$2\alpha_1 A_{16} + \alpha_2 A_{11} + \alpha_4 (A_{12} + A_{66}) + \alpha_5 A_{16} = 0 \tag{3.30b}$$

$$\alpha_1 A_{66} + 2\alpha_2 A_{16} + \alpha_3 A_{11} + \alpha_4 A_{26} + \alpha_5 (A_{12} + A_{66}) + \alpha_6 A_{16} = 0 \tag{3.30c}$$

$$\alpha_2 A_{66} + 2\alpha_3 A_{16} + \alpha_5 A_{26} + \alpha_6 (A_{12} + A_{66}) = 0 \tag{3.30d}$$

$$\alpha_3 A_{66} + \alpha_6 A_{26} = 0 \tag{3.30e}$$

Thus, for ψ to be a solution of the stress problem, it has to satisfy Eq. (3.29b) only. However, the value of α_i must be known in advance. Here, there are five equations in Eq. (3.30) for obtaining six unknown α. One can thus assign an arbitrary value to one of these six unknowns and solve for the remaining unknowns from Eq. (3.29b). Let us assume $\alpha_2 = 1$ and, writing Eq. (3.30) in matrix form, we get

$$
\begin{bmatrix}
A_{11} & 0 & A_{16} & 0 & 0 \\
A_{66} & A_{11} & A_{26} & (A_{12} + A_{66}) & A_{16} \\
2A_{16} & 0 & (A_{12} + A_{66}) & A_{16} & 0 \\
0 & 2A_{16} & 0 & A_{26} & (A_{12} + A_{66}) \\
0 & A_{66} & 0 & 0 & A_{26}
\end{bmatrix}
\begin{Bmatrix} \alpha_1 \\ \alpha_3 \\ \alpha_4 \\ \alpha_5 \\ \alpha_6 \end{Bmatrix}
=
\begin{Bmatrix} 0 \\ -2A_{16} \\ -A_{11} \\ -A_{66} \\ 0 \end{Bmatrix}
\tag{3.31}
$$

After solving the matrix equation (3.31), α values are

$$\alpha_1 = -\frac{A_{16}}{Z1.A_{11}}\left(A_{11} + A_{16}.\alpha_5\right) \tag{3.32a}$$

$$\alpha_2 = 1 \tag{3.32b}$$

$$\alpha_3 = -\frac{A_{26}}{Z2.A_{66}}\left(A_{66} + A_{26}.\alpha_5\right) \tag{3.32c}$$

$$\alpha_4 = \frac{1}{Z1}\left(A_{11} + A_{16}.\alpha_5\right) \tag{3.32d}$$

$$\alpha_5 = -\frac{\left(2.A_{16} + \frac{Z3}{Z1}A_{11} + \frac{Z4}{Z2}A_{66}\right)}{\left(\frac{Z3}{Z1}A_{16} + \frac{Z4}{Z2}A_{26} + A_{12} + A_{66}\right)} \tag{3.32e}$$

$$\alpha_6 = \frac{1}{Z2}\left(A_{66} + A_{26}.\alpha_5\right) \tag{3.32f}$$

where,

$$Z1 = 2\frac{A_{16}^2}{A_{11}} - A_{12} - A_{66} \qquad Z2 = 2\frac{A_{16}.A_{26}}{A_{66}} - A_{12} - A_{66}$$

$$Z3 = -\frac{A_{16}.A_{66}}{A_{11}} + A_{26} \qquad Z4 = -\frac{A_{11}.A_{26}}{A_{66}} + A_{16}$$

It is noted that, any other values of α_2 could have been chosen leaving aside the homogeneous solutions. Different values of α_2 will make the coefficients of the unknowns ψ different. $\alpha_2 = 1$ leads to most simplified differential equations and hence more well-conditioned algebraic equations.

The problem has now been reduced to the solution of a single function ψ from a single equation Eq. (3.29b) . Let the equation be written as

$$D_1\frac{\partial^4\psi}{\partial x^4} + D_2\frac{\partial^4\psi}{\partial x^3\partial y} + D_3\frac{\partial^4\psi}{\partial x^2\partial y^2} + D_4\frac{\partial^4\psi}{\partial x\partial y^3} + D_5\frac{\partial^4\psi}{\partial y^4} = 0 \tag{3.33}$$

where

$$D_1 = (\alpha_1 A_{11} + \alpha_4 A_{16})$$
$$D_2 = (\alpha_1 (A_{12} + A_{66}) + \alpha_2 A_{16} + 2\alpha_4 A_{26} + \alpha_5 A_{66})$$
$$D_3 = (\alpha_1 A_{26} + \alpha_2 (A_{12} + A_{66}) + \alpha_3 A_{16} + \alpha_4 A_{22} + 2\alpha_5 A_{26} + \alpha_6 A_{66})$$
$$D_4 = (\alpha_2 A_{26} + \alpha_3 (A_{12} + A_{66}) + \alpha_5 A_{22} + 2\alpha_6 + A_{26})$$
$$D_5 = (\alpha_3 A_{26} + \alpha_6 A_{22})$$

Now combining equations (3.26) and (3.28), the expressions of stress components can be expressed in terms of ψ as

$$\begin{aligned}\sigma_{xx} = \frac{1}{h}\Bigg[&(\alpha_1 A_{11} + \alpha_4 A_{16})\frac{\partial^3\psi}{\partial x^3}\\ &+(\alpha_1 A_{16} + \alpha_2 A_{11} + \alpha_4 A_{12} + \alpha_5 A_{16})\frac{\partial^3\psi}{\partial x^2\partial y}\\ &+(\alpha_2 A_{16} + \alpha_3 A_{11} + \alpha_5 A_{12} + \alpha_6 A_{16})\frac{\partial^3\psi}{\partial x\partial y^2}\\ &+(\alpha_3 A_{16} + \alpha_6 A_{12})\frac{\partial^3\psi}{\partial x^3}\Bigg]\end{aligned} \tag{3.34a}$$

$$\begin{aligned}\sigma_{yy} = \frac{1}{h}\Bigg[&(\alpha_1 A_{12} + \alpha_4 A_{26})\frac{\partial^3\psi}{\partial x^3}\\ &+(\alpha_1 A_{26} + \alpha_2 A_{12} + \alpha_4 A_{22} + \alpha_5 A_{26})\frac{\partial^3\psi}{\partial x^2\partial y}\\ &+(\alpha_2 A_{26} + \alpha_3 A_{12} + \alpha_5 A_{22} + \alpha_6 A_{26})\frac{\partial^3\psi}{\partial x\partial y^2}\\ &+(\alpha_3 A_{26} + \alpha_6 A_{22})\frac{\partial^3\psi}{\partial x^3}\Bigg]\end{aligned} \tag{3.34b}$$

$$\begin{aligned}\sigma_{xy} = \frac{1}{h}\Bigg[&(\alpha_1 A_{16} + \alpha_4 A_{66})\frac{\partial^3\psi}{\partial x^3}\\ &+(\alpha_1 A_{66} + \alpha_2 A_{16} + \alpha_4 A_{26} + \alpha_5 A_{66})\frac{\partial^3\psi}{\partial x^2\partial y}\\ &+(\alpha_2 A_{66} + \alpha_3 A_{16} + \alpha_5 A_{26} + \alpha_6 A_{66})\frac{\partial^3\psi}{\partial x\partial y^2}\\ &+(\alpha_3 A_{66} + \alpha_6 A_{26})\frac{\partial^3\psi}{\partial x^3}\Bigg]\end{aligned} \tag{3.34c}$$

3.4 Boundary Conditions

When a body, under external loads, is in equilibrium, it is known that the stress components must satisfy the differential equations of equilibrium at all points throughout the body. These stress component vary over the volume of the body and at the outer surface, or the boundary of the body, they must be in equilibrium with the given external forces there. The external forces may therefore be considered as a continuation of the internal stress distribution.

3.4.1 General Consideration of the Boundary Conditions

The practical situations which may exist along the edge or boundary of a laminated composite body are visualized in two different ways, namely,

- displacement or strain
- loading, that is, stresses

Both the displacements/strain and stresses are defined by their respective components. These components are

1. normal displacement/ normal strain
2. tangential displacement / tangential strain
3. normal stress
4. tangential stress

3.4.2 Displacement, Stress and Strain Components in Terms of the Potential Function, ψ

In order to solve the problem by solving the function ψ of the governing equation (3.27), defined by the relations (3.28). The boundary parameters of displacement components are

$$u_x(x, y) = \alpha_1 \frac{\partial^2 \psi}{\partial x^2} + \alpha_2 \frac{\partial^2 \psi}{\partial x \partial y} + \alpha_3 \frac{\partial^2 \psi}{\partial y^2} \tag{3.35a}$$

$$u_y(x, y) = \alpha_4 \frac{\partial^2 \psi}{\partial x^2} + \alpha_5 \frac{\partial^2 \psi}{\partial x \partial y} + \alpha_6 \frac{\partial^2 \psi}{\partial y^2} \tag{3.35b}$$

So, boundary parameters of stress components should be expressed in terms of ψ. These conditions are given by

$$\sigma_{xx}(x,y) = \frac{1}{h}\left[(\alpha_1 A_{11} + \alpha_4 A_{16})\frac{\partial^3\psi}{\partial x^3}\right.$$
$$+(\alpha_1 A_{16} + \alpha_2 A_{11} + \alpha_4 A_{12} + \alpha_5 A_{16})\frac{\partial^3\psi}{\partial x^2\partial y}$$
$$+(\alpha_2 A_{16} + \alpha_3 A_{11} + \alpha_5 A_{12} + \alpha_6 A_{16})\frac{\partial^3\psi}{\partial x\partial y^2}$$
$$\left.+(\alpha_3 A_{16} + \alpha_6 A_{12})\frac{\partial^3\psi}{\partial x^3}\right] \tag{3.36a}$$

$$\sigma_{yy}(x,y) = \frac{1}{h}\left[(\alpha_1 A_{12} + \alpha_4 A_{26})\frac{\partial^3\psi}{\partial x^3}\right.$$
$$+(\alpha_1 A_{26} + \alpha_2 A_{12} + \alpha_4 A_{22} + \alpha_5 A_{26})\frac{\partial^3\psi}{\partial x^2\partial y}$$
$$+(\alpha_2 A_{26} + \alpha_3 A_{12} + \alpha_5 A_{22} + \alpha_6 A_{26})\frac{\partial^3\psi}{\partial x\partial y^2}$$
$$\left.+(\alpha_3 A_{26} + \alpha_6 A_{22})\frac{\partial^3\psi}{\partial x^3}\right] \tag{3.36b}$$

$$\sigma_{xy}(x,y) = \frac{1}{h}\left[(\alpha_1 A_{16} + \alpha_4 A_{66})\frac{\partial^3\psi}{\partial x^3}\right.$$
$$+(\alpha_1 A_{66} + \alpha_2 A_{16} + \alpha_4 A_{26} + \alpha_5 A_{66})\frac{\partial^3\psi}{\partial x^2\partial y}$$
$$+(\alpha_2 A_{66} + \alpha_3 A_{16} + \alpha_5 A_{26} + \alpha_6 A_{66})\frac{\partial^3\psi}{\partial x\partial y^2}$$
$$\left.+(\alpha_3 A_{66} + \alpha_6 A_{26})\frac{\partial^3\psi}{\partial x^3}\right] \tag{3.36c}$$

The corresponding expressions for the components of strain for Symmetric Laminates are

$$\varepsilon_{xx}(x,y) = \frac{\partial u_x}{\partial x} = \alpha_1\frac{\partial^3\psi}{\partial x^3} + \alpha_2\frac{\partial^3\psi}{\partial x^2\partial y} + \alpha_3\frac{\partial^3\psi}{\partial x\partial y^2} \tag{3.37a}$$
$$\varepsilon_{yy}(x,y) = \frac{\partial u_y}{\partial y} = \alpha_4\frac{\partial^3\psi}{\partial x^2\partial y} + \alpha_5\frac{\partial^3\psi}{\partial x\partial y^2} + \alpha_6\frac{\partial^3\psi}{\partial x^3} \tag{3.37b}$$
$$\varepsilon_{xy}(x,y) = \frac{\partial u_x}{\partial y} + \frac{\partial u_y}{\partial x} = \alpha_4\frac{\partial^3\psi}{\partial x^3} + (\alpha_1+\alpha_5)\frac{\partial^3\psi}{\partial x^2\partial y} + (\alpha_2+\alpha_6)\frac{\partial^3\psi}{\partial x\partial y^2} + \alpha_3\frac{\partial^3\psi}{\partial y^3} \tag{3.37c}$$

Where, the values of α has shown in equation (3.32)

From these expression it is found that, as far as the boundary conditions are concerned, there is no technical difficulty in this approach. No knowledge of the displacement, strain and stress components away from the boundary is needed to evaluate the function ψ at the boundary. Moreover, this approach has the additional advantage over the method of solving the problem in terms of displacement components, that the evaluation of a single function at a time is performed.

3.5 Special Cases of the General Governing Equations and Boundary Conditions

3.5.1 Symmetric Cross-ply Laminates

3.5.1.1 Governing Equation

In this section, the differential equation governing the potential function ψ is deduced for the symmetric cross-ply laminates, where the fiber axes of the alternate plies are 0^o and 90^o with respect to $x-$axis. i.e., the value of θ of plies is 0^o or 90^o in figure 2.5. All the relations are obtained here as a special case of the general formulation for the case of symmetric laminate by substituting the value of $\theta = 0^o$ and 90^o. From the definition of the cross–ply laminate, $A_{16} = A_{26} = 0$. From the equation (3.24) the stress-strain relations for *symmetric cross-ply laminates* are expressed through the stiffness matrix as follows:

$$\left\{\begin{array}{c}\sigma_{xx}\\ \sigma_{yy}\\ \sigma_{xy}\end{array}\right\} = \frac{1}{h}\left[\begin{array}{ccc}A_{11} & A_{12} & 0\\ A_{12} & A_{22} & 0\\ 0 & 0 & A_{66}\end{array}\right]\left\{\begin{array}{c}\varepsilon_{x}\\ \varepsilon_{y}\\ \varepsilon_{xy}\end{array}\right\} \tag{3.38}$$

The two equilibrium equations, for the problems of symmetric cross-ply laminates in terms of the displacement components, u_x and u_y, obtained from equation (3.27), are

$$A_{11}\frac{\partial^2 u_x}{\partial x^2} + (A_{12} + A_{66})\frac{\partial^2 u_y}{\partial x \partial y} + A_{66}\frac{\partial^2 u_x}{\partial y^2} = 0 \tag{3.39a}$$

$$A_{66}\frac{\partial^2 u_y}{\partial x^2} + (A_{12} + A_{66})\frac{\partial^2 u_x}{\partial x \partial y} + A_{22}\frac{\partial^2 u_y}{\partial y^2} = 0 \tag{3.39b}$$

The corresponding two equilibrium equations in terms of the function ψ, as obtained directly from equation (3.29), are

$$\begin{aligned}&\alpha_1 A_{11}\frac{\partial^4\psi}{\partial x^4} + (\alpha_2 A_{11} + \alpha_4(A_{12} + A_{66}))\frac{\partial^4\psi}{\partial x^3 \partial y}\\&+ (\alpha_1 A_{66} + \alpha_3 A_{11} + \alpha_5(A_{12} + A_{66}))\frac{\partial^4\psi}{\partial x^2 \partial y^2}\\&+ (\alpha_2 A_{66} + \alpha_6(A_{12} + A_{66}))\frac{\partial^4\psi}{\partial x \partial y^3} + \alpha_3 A_{66}\frac{\partial^4\psi}{\partial y^4} = 0\end{aligned} \tag{3.40a}$$

$$\begin{aligned}&\alpha_1 A_{11}\frac{\partial^4\psi}{\partial x^4} + (\alpha_1(A_{12} + A_{66}) + \alpha_5 A_{66})\frac{\partial^4\psi}{\partial x^3 \partial y}\\&+ (\alpha_2(A_{12} + A_{66}) + \alpha_4 A_{22}\alpha_6 A_{66})\frac{\partial^4\psi}{\partial x^2 \partial y^2}\\&+ (\alpha_3(A_{12} + A_{66}) + \alpha_5 A_{22})\frac{\partial^4\psi}{\partial x \partial y^3} + \alpha_6 A_{22}\frac{\partial^4\psi}{\partial y^4} = 0\end{aligned} \tag{3.40b}$$

Likewise the case of general symmetric laminates, assuming $\alpha_2 = 1$, the solutions for the remaining α's are obtained from equation (3.32) by interesting respective conditions. The values of α's thus obtained, are as follows:

$$\alpha_1 = \alpha_3 = \alpha_5 = 0 \tag{3.41a}$$

$$\alpha_2 = 1 \tag{3.41b}$$

$$\alpha_4 = -\frac{A_{11}}{(A_{12} + A_{66})} \tag{3.41c}$$

$$\alpha_6 = -\frac{A_{66}}{(A_{12} + A_{66})} \tag{3.41d}$$

Knowing the values of α's for the cross-ply laminated composites, the coefficients of different derivatives of equation (3.40b), i.e., D's (used in equation (3.33)) are obtained as follows:

$$\begin{aligned}
D_1 &= -\frac{A_{11}A_{66}}{A_{12}+A_{66}} \\
D_2 &= D_4 = 0 \\
D_3 &= A_{12}+A_{66}-\frac{A_{11}A_{22}}{A_{12}+A_{66}}-\frac{A_{66}^2}{A_{12}+A_{66}} \\
D_5 &= -\frac{A_{22}A_{66}}{A_{12}+A_{66}}
\end{aligned}$$

Substituting the value of D's in equation (3.33) the explicit expression of the governing differential equation for the case of symmetric cross-ply laminate becomes

$$\frac{\partial^4\psi}{\partial x^4}+\left(\frac{A_{22}}{A_{66}}-\frac{A_{12}^2}{A_{11}A_{66}}-\frac{2A_{12}}{A_{11}}\right)\frac{\partial^4\psi}{\partial x^2\partial y^2}+\frac{A_{22}}{A_{11}}\frac{\partial^4\psi}{\partial y^4}=0 \tag{3.42}$$

3.5.1.2 Boundary Conditions for Symmetric Cross-Ply Laminates

The general expressions for the body parameters in terms of the function ψ after substituting the respective conditions of the symmetric cross-ply laminates into equation (3.35) and (3.36), are given by

Displacement components

$$u_x(x,y)=\frac{\partial^2\psi}{\partial x\partial y} \tag{3.43a}$$

$$u_y(x,y)=-\frac{1}{A_{12}+A_{66}}\left[A_{11}\frac{\partial^2\psi}{\partial x^2}+A_{66}\frac{\partial^2\psi}{\partial y^2}\right] \tag{3.43b}$$

Stress components

$$\sigma_{xx}(x,y) = \frac{A_{66}}{h(A_{12}+A_{66})}\left[A_{11}\frac{\partial^3\psi}{\partial x^2\partial y} - A_{12}\frac{\partial^3\psi}{\partial y^3}\right] \tag{3.44a}$$

$$\sigma_{yy}(x,y) = \frac{1}{h(A_{12}+A_{66})}\left[(A_{12}^2 + A_{12}A_{16} - A_{11}A_{22})\frac{\partial^3\psi}{\partial x^2\partial y} - A_{22}A_{66}\frac{\partial^3\psi}{\partial y^3}\right] \tag{3.44b}$$

$$\sigma_{xy}(x,y) = \frac{A_{66}}{h(A_{12}+A_{66})}\left[-A_{11}\frac{\partial^3\psi}{\partial x^3} + A_{12}\frac{\partial^3\psi}{\partial x\partial y^2}\right] \tag{3.44c}$$

The corresponding expressions for the components of strain for symmetric cross-ply Laminates are obtained from (3.37), which are

$$\varepsilon_{xx}(x,y) = \frac{\partial^3\psi}{\partial x^2\partial y} \tag{3.45a}$$

$$\varepsilon_{yy}(x,y) = -\frac{1}{A_{12}+A_{66}}\left[A_{11}\frac{\partial^3\psi}{\partial x^2\partial y} + A_{66}\frac{\partial^3\psi}{\partial y^3}\right] \tag{3.45b}$$

$$\varepsilon_{xy}(x,y) = -\frac{1}{A_{12}+A_{66}}\left[A_{11}\frac{\partial^3\psi}{\partial x^3} - A_{12}\frac{\partial^3\psi}{\partial x\partial y^2}\right] \tag{3.45c}$$

3.5.1.3 Applicability of Formulation

The above governing equation and boundary conditions of the symmetric cross-ply laminates can readily be applied to the following cases of laminated composites:

Cross-ply laminates

The above governing equation (3.42) and boundary conditions (3.43), (3.44) and (3.45) are derived for the case of symmetric cross-ply laminates. It is applicable for symmetric cross-ply laminates with any even or odd number of piles.

Angle ply laminates

If a laminate has an even number of plies, then the elements of the stiffness matrix $A_{16} = A_{26} = 0$ Again, when the laminate is symmetric, it is know that given $[B] = 0$. This behavior is similar to the symmetric cross-ply laminates. So, the above governing equation (3.42) and boundary conditions (3.43), (3.44) and (3.45) are also applicable for symmetric angle ply laminates with even number of piles. Further, when the number of plies is odd and the laminate consists of alternating $+\theta$ and $-\theta$ plies, then it is symmetric, for which $[B] = 0$. In addition, elements A_{16} and A_{26} are also become very small as the number of layers increases for the same laminate thickness. This behavior is very similar to the symmetric cross-ply laminates. So, the governing equation (3.42) and boundary conditions (3.43), (3.44) and (3.45) are also applicable for symmetric angle ply laminates when the number of plies are odd. If the laminate consists of a few number of piles, which is also odd, the governing equation and boundary conditions derived for the symmetric cross-ply laminates will not be applicable for that particular type of angle ply laminates. For this case, the equations derived for general symmetric laminates will be suitable.

Balanced ply laminates

A laminate is balanced if layers at angles other than 0^o and 90^o occur only as plus and minus pairs of $+\theta$ and $-\theta$. The plus and minus pairs do not need to be adjacent to each other, but the thickness and material of the plus and minus pairs need to be the same. Here, the terms $A_{16} = A_{16} = 0$ and if it is symmetric, given $[B] = 0$. The governing equation (3.42), boundary conditions (3.43), (3.44) and (3.45) are applicable for symmetric Balanced ply laminates

3.5.2 Evaluation of Stress Components for Individual Lamina

In previous section, stress components have been evaluated for overall laminate by solving stiffness matrix. Stress and displacement for lamina of the composite has been solved by the help of strain distribution. Strain distributions for overall laminate or global strain distribution has evaluated from the ψ values of the mesh point by using equation in tabulated form.

Since the laminated panel are symmetric, the distributions of strain components are similar for all plies of the laminated panel. Similarly, the expressions for the components of stresses for points of the each entire plies are

$$\left\{ \begin{array}{c} \sigma_{xx} \\ \sigma_{yy} \\ \sigma_{xy} \end{array} \right\}_{k_i} = \frac{1}{h} \begin{bmatrix} \overline{Q}_{11} & \overline{Q}_{12} & \overline{Q}_{16} \\ \overline{Q}_{12} & \overline{Q}_{22} & \overline{Q}_{26} \\ \overline{Q}_{16} & \overline{Q}_{26} & \overline{Q}_{66} \end{bmatrix}_{k_i} \left\{ \begin{array}{c} \varepsilon_{xx} \\ \varepsilon_{yy} \\ \varepsilon_{xy} \end{array} \right\} \tag{3.46}$$

where, k_i represents the number of ply of the laminate.

CHAPTER 4

Numerical Solution

4.1 Introduction

The method of finite difference is an *approximate numerical technique* which yields a simplified solution form in which the differential equations of equilibrium and the boundary conditions are replaced by a set of algebraic equations. The general approach of finite difference solution assumes that the function can be represented in a prescribed range with a sufficient degree of accuracy either by Taylor's series with origin at the successive pivotal points of the range or the polynomial which passes through a certain number of pivotal points. The values of functions at the nodal points are required to satisfy difference equations obtained by replacing the partial derivatives by their difference formulae. All finite difference formulae are approximations to infinite series of differences. Therefore, it is necessary that the series should coverage, or that error should caused by truncation after a certain no. of terms should be sufficiently small. In this problem the pivotal points are taken as the regular net points of the domains of dependence of the functions obtained by dividing the domain by lines parallel to the co-ordinate axes.

In finite difference method, the region occupied by structure under consideration is divided into meshes to give nodal points as shown in figure (4.1(c)). The solid line represents the physical boundary of the cantilever. The discretized form of governing differential equation is applied at each of the nodal points (i, j) inside the physical boundary. This gives a set of algebraic equations for the determination of nodal unknowns. However, the number of unknowns is greater than the number of equation, which make the problem intractable. This is because the application of the governing equation to the interior points also involves the points on and outside the boundary. The line formed by connecting the nodal points outside the physical boundary is called imaginary boundary, as shown in figure (4.1(c)). The number of unknowns is equal to the number of nodal points including boundary and exterior points. To make the problem tractable, it is necessary to generate more equations. The requirement is met up by applying the descretized boundary conditions at the nodal points on the boundary and this gives the complete set of simultaneous algebraic equations which is solved by a suitable numerical technique.

4.2 Solution Procedure

4.2.1 Finite Difference Discretization of the Governing Equation of Symmetric Cross-ply Laminate

The governing differential equation (3.42) for the cross-ply laminates used to evaluate the function ψ at the interior mesh points, can be expressed in its corresponding difference form when all the derivatives are replaced by corresponding central difference expressions. The central difference expressions of the individual fourth order derivatives of ψ are as follows:

$$\left(\frac{\partial^4 \psi}{\partial x^4}\right)_{i,j} = \frac{1}{h_x^4}\{\psi(i+2,j) - 4\psi(i+1,j) + 6\psi(i,j) - 4\psi(i-1,j)\}$$
$$+ \psi(i-2,j) \quad + \mathrm{O}(h_x^2) \tag{4.1}$$

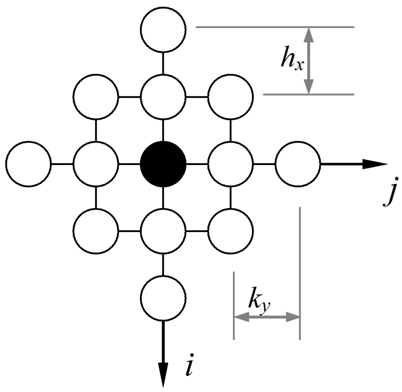

(a) Stencil for symmetric cross ply laminates.

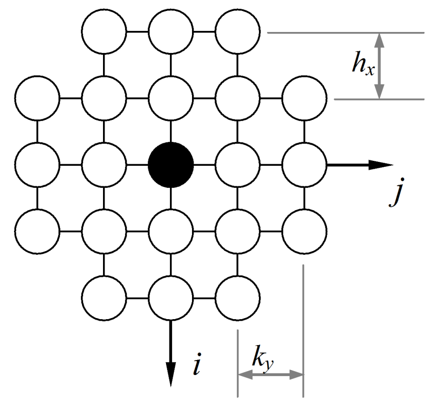

(b) Stencil for general symmetric laminates.

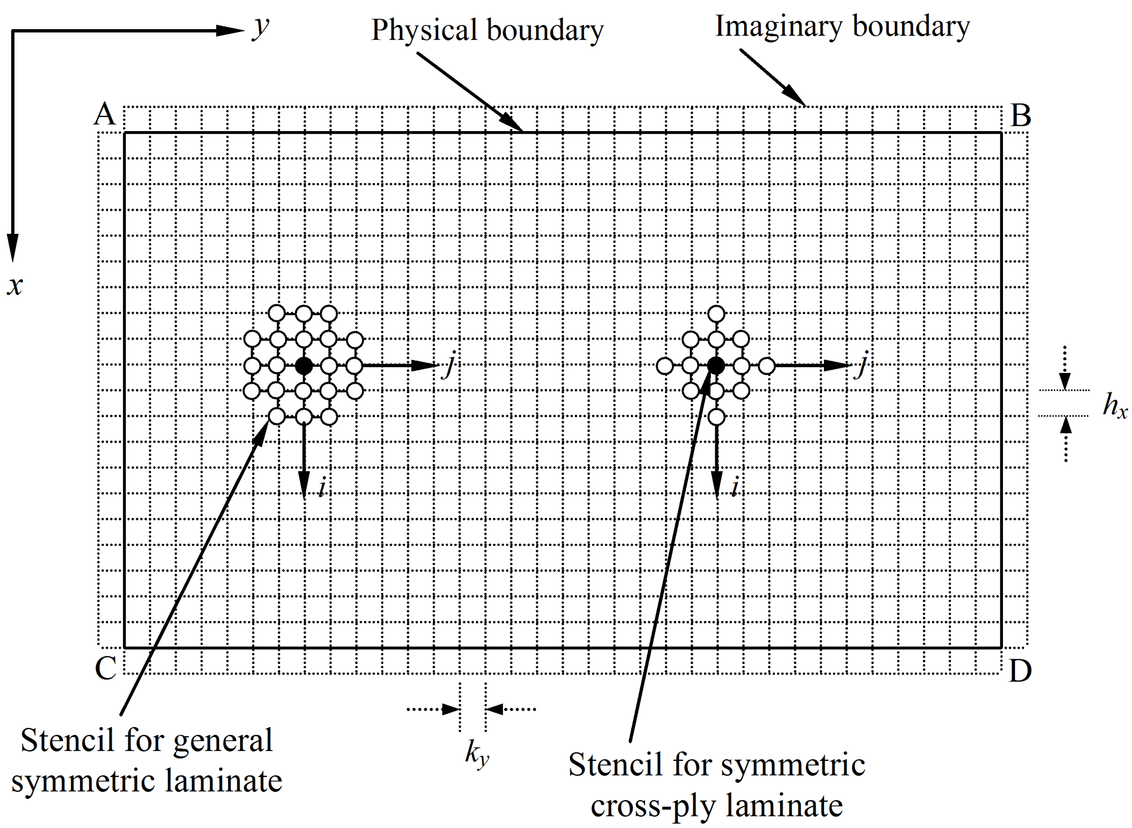

(c) Application of governing equation stencils.

Figure 4.1: Governing equation stencils for (a) symmetric cross ply laminates (b) general symmetric laminates and their application.

$$\left(\frac{\partial^4\psi}{\partial y^4}\right)_{i,j} = \frac{1}{k_y^4}\{\psi(i,j+2) - 4\psi(i,j+1) + 6\psi(i,j) - 4\psi(i,j-1) + \psi(i,j-2)\} \quad + \mathrm{O}(h_x^2) \tag{4.2}$$

$$\left(\frac{\partial^4\psi}{\partial x^2 \partial y^2}\right)_{i,j} = \frac{1}{h_x^2 k_y^2}[\psi(i+1,j+1) + \psi(i+1,j-1) + \psi(i-1,j+1) + \psi(i-1,j-1) + 4\psi(i,j) - 2\{\psi(i+1,j) + \psi(i,j+1) + \psi(i,j-1) + \psi(i-1,j)\}] \quad + \mathrm{O}(h_x^2) \tag{4.3}$$

at a general mesh point (i,j) can be obtained by replacing the derivatives with their difference formulae as given by equation (4.1), (4.2) and (4.3). Assuming ψ to be the continuous function at different mesh points, the equation in its finite difference form becomes

$$\begin{aligned} &pk1[\psi(i+2,j) + \psi(i-2,j)] - (4pk1 + 2pk2)\{\psi(i+1,j) \\ &+ \psi(i-1,j)\} - (2pk2 + 4pk3)[\psi(i,j+1) + \psi(i,j-1)] + (6pk1 \\ &+ 4pk2 + 6pk3)\psi(i,j) + pk2[\psi(i+1,j+1) + \psi(i+1,j-1) \\ &+ \psi(i-1,j+1) + \psi(i-1,j1)] + pk3[\psi(i,j+2) + \psi(i,j-2)] = 0 \end{aligned} \tag{4.4}$$

where

$$pk1 = \frac{1}{h_x^4}$$
$$pk2 = \left(\frac{A_{22}}{A_{66}} - \frac{{A_{22}}^2}{A_{11}A_{66}} - \frac{2A_{12}}{A_{11}}\right)\frac{1}{h_x^2 k_y^2}$$
$$pk3 = \frac{A_{22}}{A_{11}}\frac{1}{k_y^4}$$

where, h_x, k_y is the nodal distance between two nodal points in x and y direction respectively as shown in Figure 4.1. Therefore equation (4.4) is the difference approximation to the governing equation (3.42) of the symmetric cross-ply laminates and valid for all internal mesh points except for that on boundaries. Figure (4.1(a)) illustrates the corresponding FD stencil of equation (4.4) for an arbitrary interior nodal point (i, j) on the body. The FD stencil of the governing differential equation (3.33) for a general symmetric laminated composite is illustrated in Figure 4.1(b).

4.2.2 Finite Difference Expressions for Boundary Conditions

The boundary conditions are given by equations (3.43) and (3.44) in chapter 3. When the boundary conditions are given either in terms of displacement/ strain or stress components expressed as a function of independent variables on the boundary, the values of these components at any point on the boundary can be determined as numbers. With this assumption the four possible conditions at any point on the boundaries parallel to $y-$axis become

1. (a)

$$u_x(x, y) = \frac{\partial^2 \psi}{\partial x \partial y}$$

or

$$\varepsilon_{xx}(x, y) = \frac{\partial^3 \psi}{\partial x^2 \partial y}$$

(b)

$$u_y(x, y) = -\frac{1}{A_{12} + A_{66}} \left[A_{11} \frac{\partial^2 \psi}{\partial x^2} + A_{66} \frac{\partial^2 \psi}{\partial y^2} \right]$$

or

$$\varepsilon_{yy}(x, y) = -\frac{1}{A_{12} + A_{66}} \left[A_{11} \frac{\partial^3 \psi}{\partial x^2 \partial y} + A_{66} \frac{\partial^3 \psi}{\partial y^3} \right]$$

2. (a)

$$u_x(x,y) = \frac{\partial^2 \psi}{\partial x \partial y}$$

or

$$\varepsilon_{xx}(x,y) = \frac{\partial^3 \psi}{\partial x^2 \partial y}$$

(b)

$$\sigma_{xy}(x,y) = \frac{A_{66}}{h(A_{12}+A_{66})}\left[-A_{11}\frac{\partial^3 \psi}{\partial x^3} + A_{12}\frac{\partial^3 \psi}{\partial x \partial y^2}\right]$$

3. (a)

$$u_y(x,y) = -\frac{1}{A_{12}+A_{66}}\left[A_{11}\frac{\partial^2 \psi}{\partial x^2} + A_{66}\frac{\partial^2 \psi}{\partial y^2}\right]$$

or

$$\varepsilon_{yy}(x,y) = -\frac{1}{A_{12}+A_{66}}\left[A_{11}\frac{\partial^3 \psi}{\partial x^2 \partial y} + A_{66}\frac{\partial^3 \psi}{\partial y^3}\right]$$

(b)

$$\sigma_{xx}(x,y) = \frac{A_{66}}{h(A_{12}+A_{66})}\left[A_{11}\frac{\partial^3 \psi}{\partial x^2 \partial y} - A_{12}\frac{\partial^3 \psi}{\partial y^3}\right]$$

4. (a)

$$\sigma_{xx}(x,y) = \frac{A_{66}}{h(A_{12}+A_{66})}\left[A_{11}\frac{\partial^3 \psi}{\partial x^2 \partial y} - A_{12}\frac{\partial^3 \psi}{\partial y^3}\right]$$

(b)

$$\sigma_{xy}(x,y) = \frac{A_{66}}{h(A_{12}+A_{66})}\left[-A_{11}\frac{\partial^3 \psi}{\partial x^3} + A_{12}\frac{\partial^3 \psi}{\partial x \partial y^2}\right]$$

The two displacement, two strain and the three stress components have to be expressed in finite difference form. Out of these four conditions one has to be satisfied by a single boundary mesh point at a time and thus two difference equations will be written for a single point on the boundary.

From the equations (3.43) and (3.44), the finite difference expressions for the displacement and stress components at any point closer to A (including A) can be obtained by substituting the appropriate difference formulae of the derivatives present in the differential equations. Therefore the general difference expressions for the displacement, strain and stress components at points on boundaries AB, closer to point A (applicable at AE region), are given by

$$\begin{aligned} u_x &= \frac{\partial^2 \psi}{\partial x \partial y} \\ &= C_1[9\psi(i,j) - 12\{\psi(i,j+1) + \psi(i+1,j)\} + 16\psi(i+1,j+1) \\ &\quad + 3\{\psi(i,j+2) + \psi(i+2,j)\} - 4\{\psi(i+1,j+2) + \psi(i+2,j+1)\} \\ &\quad + \psi(i+2,j+2)] \end{aligned} \tag{4.5}$$

$$\begin{aligned} u_y &= -\frac{1}{A_{12} + A_{66}} \left[A_{11} \frac{\partial^2 \psi}{\partial x^2} + A_{66} \frac{\partial^2 \psi}{\partial y^2} \right] \\ &= C_2\{\psi(i+1,j) + \psi(i-1,j)\} + C_3\{\psi(i,j+1) + \psi(i,j-1)\} \\ &\quad - 2(C_2 + C_3)\psi(i,j) \end{aligned} \tag{4.6}$$

$$\begin{aligned} \varepsilon_{xx} &= \frac{\partial^3 \psi}{\partial x^2 \partial y} \\ &= L_1[-3\{\psi(i-1,j) + \psi(i+1,j)\} + 4\{\psi(i-1,j+1) \\ &\quad + \psi(i+1,j+1)\} + 6\psi(i,j) - 8\psi(i,j+1) + 2\psi(i,j+2) \\ &\quad - \{\psi(i-1,j+2) + \psi(i+1,j+2)\}] \end{aligned} \tag{4.7}$$

$$
\begin{aligned}
\varepsilon_{yy} = & -\frac{1}{A_{12}+A_{66}}\left[A_{11}\frac{\partial^3\psi}{\partial x^2\partial y}+A_{66}\frac{\partial^3\psi}{\partial y^3}\right] \\
= & (6L_2+10L_3)\psi(i,j)-(8L_2+12L_3)+\psi(i,j+1)+(2L_2+6L_3) \\
& \psi(i,j+2)-L_3\psi(i,j+3)-3L_3\psi(i,j-1)+L_2[-3\psi(i-1,j) \\
& -3\psi(i+1,j)+4\psi(i-1,j+1)+4\psi(i+1,j+1) \\
& -\psi(i-1,j+2)-\psi(i+1,j+2)]
\end{aligned}
\tag{4.8}
$$

$$
\begin{aligned}
\sigma_{xx} = & \frac{A_{66}}{h(A_{12}+A_{66})}\left[A_{11}\frac{\partial^3\psi}{\partial x^2\partial y}-A_{12}\frac{\partial^3\psi}{\partial y^3}\right] \\
= & (6C_4+10C_5)\psi(i,j)-(8C_4+12C_5)\psi(i,j+1)+(2C_4+6C_5) \\
& \psi(i,j+2)-C_5\psi(i,j+3)-3C_5\psi(i,j-1)+C_4[-3\psi(i-1,j) \\
& -3\psi(i+1,j)+4\psi(i-1,j+1)+4\psi(i+1,j+1)-\psi(i-1, \\
& j+2)-\psi(i+1,j+2)]
\end{aligned}
\tag{4.9}
$$

$$
\begin{aligned}
\sigma_{xy} = & \frac{A_{66}}{h(A_{12}+A_{66})}\left[A_{12}\frac{\partial^3\psi}{\partial x\partial y^2}-A_{11}\frac{\partial^3\psi}{\partial x^3}\right] \\
= & (6C_8+10C_9)\psi(i,j)-(8C_8+12C_9)\psi(i+1,j)+(2C_8+6C_9) \\
& \psi(i+2,j)+C_8[-3\psi(i,j-1)-3\psi(i,j+1)+4\psi(i+1,j-1) \\
& +4\psi(i+1,j+1)-\psi(i+2,j-1)-\psi(i+2,j+1)] \\
& -C_9[3\psi(i-1,j)+\psi(i+3,j)]
\end{aligned}
\tag{4.10}
$$

Corresponding stencils of above equations (4.5) to (4.10) has been shown in Figures 4.2 -4.8. The above difference equations have been obtained by adopting i-forward, j-forward central-difference schemes for individual derivatives of the function ψ. In order to apply the above boundary conditions for points closer to B on the same boundary AB , it requires separate versions of difference equations for most of the conditions. The difference equations on AB closer to B (including point B, applicable at region BE) are given by

$$u_x = C_1[-9\psi(i,j) + 12\{\psi(i,j-1) + \psi(i+1,j)\} - 16\psi(i+1,$$
$$j-1) - 3\{\psi(i,j-2) + \psi(i+2,j)\} + 4\{\psi(i+1,j-2)$$
$$+ \psi(i+2,j-1)\} - \psi(i+2,j-2)] \tag{4.11}$$

$$u_y = C_2\{\psi(i+1,j) + \psi(i-1,j)\} + C_3\{\psi(i,j+1) + \psi(i,j-1)\}$$
$$- 2(C_2 + C_3)\psi(i,j) \tag{4.12}$$

$$\varepsilon_{xx} = L_1[3\{\psi(i-1,j) + \psi(i+1,j)\} - 4\{\psi(i-1,j-1) + \psi(i+1,$$
$$j-1)\} + 6\psi(i,j) + 8\psi(i,j-1) - 2\psi(i,j-2) - \{\psi(i-1,j-2)$$
$$+ \psi(i+1,j-2)\}] \tag{4.13}$$

$$\varepsilon_{yy} = -(6L_2 + 10L_3)\psi(i,j) + (8L_2 + 12L_3)\psi(i,j-1) - (2L_2 + 6L_3)$$
$$\psi(i,j-2) + L_3\psi(i,j-3) + 3L_3\psi(i,j+1) + L_2[3\psi(i-1,j)$$
$$+ 3\psi(i+1,j) - 4\psi(i-1,j-1) - 4\psi(i+1,j-1)$$
$$+ \psi(i-1,j-2) + \psi(i+1,j-2)] \tag{4.14}$$

$$\sigma_{xx} = -(6C_4 + 10C_5)\psi(i,j) + (8C_4 + 12C_5)\psi(i,j-1) - (2C_4 + 6C_5)$$
$$\psi(i,j-2) + C_5\psi(i,j-3) + 3C_5\psi(i,j+1) + C_4[3\psi(i-1,j)$$
$$+ 3\psi(i+1,j) - 4\psi(i-1,j-1) - 4\psi(i+1,j-1) + \psi(i-1$$
$$,j-2) - \psi(i+1,j-2)] \tag{4.15}$$

$$\sigma_{xy} = (6C_8 + 10C_9)\psi(i,j) - (8C_8 + 12C_9)\psi(i+1,j) + (2C_8 + 6C_9)$$
$$\psi(i+2,j) + C_8[-3\psi(i,j-1) - 3\psi(i,j+1) + 4\psi(i+1,j-1)$$
$$+ 4\psi(i+1,j+1) - \psi(i+2,j-1) - \psi(i+2,j+1)]$$
$$- C_9[3\psi(i-1,j) + \psi(i+3,j)] \tag{4.16}$$

Corresponding stencils of above equations (4.11) to (4.16) has been shown in Figures 4.2 -4.8. The above difference equations have been obtained by adopting i-forward, j-backward-difference schemes for individual derivatives of the function ψ. The discretization scheme for shear stress, σ_{xy} of equation (4.10) closer to A and equation (4.16) closer to B are exactly same as shown in Figure 4.8. Similar discretization of shear stress has been used for both corner points A and B, and It is applicable at AEB region. because it is symmetric with respect to $i-$ direction.

If it is assumed that the plate is divided into m number of mesh points in the x-direction and n number of mesh points in the y-direction, then the indexing in the mesh points on the edge AB and CD will be as shown in figure 4.1(c). With this indexing and preceding as before, the difference equations of the on CD closer to C (including point C, applicable at region CF), are given by

$$u_x = C_1[-9\psi(i,j) + 12\{\psi(i,j+1) + \psi(i-1,j)\} - 16\psi(i-1,$$
$$j+1) - 3\{\psi(i,j+2) + \psi(i-2,j)\} + 4\{\psi(i-1,j+2)\}$$
$$+ \psi(i-2,j+1) - \psi(i-2,j+2)] \tag{4.17}$$

$$u_y = C_2\{\psi(i+1,j) + \psi(i-1,j)\} + C_3\{\psi(i,j+1) + \psi(i,j-1)\}$$
$$- 2(C_2 + C_3)\psi(i,j) \tag{4.18}$$

$$\begin{aligned}\varepsilon_{xx} = L_1[&-3\{\psi(i-1,j)+\psi(i+1,j)\}+4\{\psi(i-1,j+1)+\psi(i+1,\\&j+1)\}+6\psi(i,j)-8\psi(i,j+1)+2\psi(i,j+2)-\{\psi(i-1,j+2)\\&+\psi(i+1,j+2)\}]\end{aligned} \tag{4.19}$$

$$\begin{aligned}\varepsilon_{yy} = &(6L_2+10L_3)\psi(i,j)-(8L_2+12L_3)\psi(i,j+1)+(2L_2+6L_3)\\&\psi(i,j+2)-L_3\psi(i,j+3)-3L_3\psi(i,j-1)+L_2[-3\psi(i-1,j)\\&-3\psi(i+1,j)+4\psi(i-1,j+1)+4\psi(i+1,j+1)\\&-\psi(i-1,j+2)-\psi(i+1,j+2)]\end{aligned} \tag{4.20}$$

$$\begin{aligned}\sigma_{xx} = &(6C_4+10C_5)\psi(i,j)-(8C_4+12C_5)\psi(i,j+1)+(2C_4+6C_5)\\&\psi(i,j+2)-C_5\psi(i,j+3)-3C_5\psi(i,j-1)+C_4[-3\psi(i-1,j)\\&-3\psi(i+1,j)+4\psi(i-1,j+1)+4\psi(i+1,j+1)-\psi(i-1,\\&j+2)-\psi(i+1,j+2)]\end{aligned} \tag{4.21}$$

$$\begin{aligned}\sigma_{xy} = &-(6C_8+10C_9)\psi(i,j)+(8C_8+12C_9)\psi(i-1,j)-(2C_8+6C_9)\\&\psi(i-2,j)+C_8[3\psi(i,j-1)3\psi(i,j+1)-4\psi(i-1,j-1)\\&-4\psi(i-1,j+1)+\psi(i-2,j+1)+\psi(i-2,j-1)]\\&+C_9[3\psi(i+1,j)+\psi(i-3,j)]\end{aligned} \tag{4.22}$$

Corresponding stencils of above equations (4.17) to (4.22) has been shown in Figures 4.2 -4.8. The above difference equations have been obtained by adopting i-backward, j-forward-difference schemes for individual derivatives of the function ψ. Another version of descritization of equations (3.43) and (3.44) on the boundary CD, closer to point D (including point D, applicable at region DF), can be written as

$$\begin{aligned}u_x = C_1[9\psi(i,j) - 12\{\psi(i,j-1) + \psi(i-1,j)\} + 16\psi(i-1,\\ j-1) + 3\{\psi(i,j-2) + \psi(i-2,j)\} - 4\{\psi(i-1,j-2)\\ + \psi(i-2,j-1)\} + \psi(i-2,j-2)]\end{aligned} \tag{4.23}$$

$$\begin{aligned}u_y = C_2\{\psi(i+1,j) + \psi(i-1,j)\} + C_3\{\psi(i,j+1) + \psi(i,j-1)\}\\ - 2(C_2 + C_3)\psi(i,j)\end{aligned} \tag{4.24}$$

$$\begin{aligned}\varepsilon_{xx} = L_1[3\{\psi(i-1,j) + \psi(i+1,j)\} - 4\{\psi(i-1,j-1) + \psi(i+1,\\ j-1)\} + 6\psi(i,j) + 8\psi(i,j-1) - 2\psi(i,j-2) - \{\psi(i-1,j-2)\\ + \psi(i+1,j-2)\}]\end{aligned} \tag{4.25}$$

$$\begin{aligned}\varepsilon_{yy} = & -(6L_2 + 10L_3)\psi(i,j) + (8L_2 + 12L_3)\psi(i,j-1) - (2L_2 + 6L_3)\\ & \psi(i,j-2) + L_3\psi(i,j-3) + 3L_3\psi(i,j+1) + L_2[3\psi(i-1,j)\\ & + 3\psi(i+1,j) - 4\psi(i-1,j-1) - 4\psi(i+1,j-1)\\ & + \psi(i-1,j-2) + \psi(i+1,j-2)]\end{aligned} \tag{4.26}$$

$$\begin{aligned}\sigma_{xx} = & -(6C_4 + 10C_5)\psi(i,j) + (8C_4 + 12C_5)\psi(i,j-1) - (2C_4 + 6C_5)\\ & \psi(i,j-2) + C_5\psi(i,j-3) + 3C_5\psi(i,j+1) + C_4[3\psi(i-1,j)\\ & + 3\psi(i+1,j) - 4\psi(i-1,j-1) - 4\psi(i+1,j-1)\\ & + \psi(i-1,j-2) - \psi(i+1,j-2)]\end{aligned} \tag{4.27}$$

$$
\begin{aligned}
\sigma_{xy} = & -(6C_8 + 10C_9)\psi(i,j) + (8C_8 + 12C_9)\psi(i-1,j) - (2C_8 + 6C_9) \\
& \psi(i-2,j) + C_8[3\psi(i,j-1)3\psi(i,j+1) - 4\psi(i-1,j-1) \\
& -4\psi(i-1,j+1) + \psi(i-2,j+1) + \psi(i-2,j-1)] \\
& + C_9[3\psi(i+1,j) + \psi(i-3,j)]
\end{aligned} \tag{4.28}
$$

Corresponding stencils of above equations (4.23) to (4.28) has been shown in Figures 4.2 -4.8. The above difference equations have been obtained by adopting i-backward, j-backward central-difference schemes for individual derivatives of the function ψ.The discretization scheme for shear stress, σ_{xy} of equation (4.21) closer to C and equation (4.27) closer to D are exactly same as shown in Figure 4.8. Similar discretization of shear stress has been used for both corner points C and D and applicable in CFD region, because it is symmetric with respect to $i-$ direction.

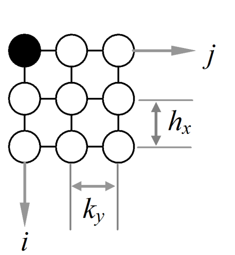

(a) Closer to point A.

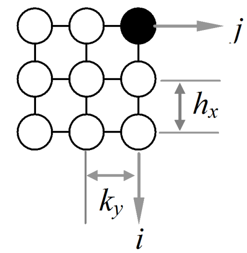

(b) Closer to point B.

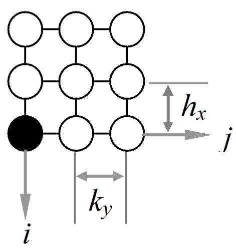

(c) Closer to point C.

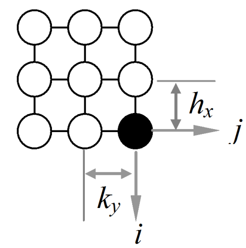

(d) Closer to point D.

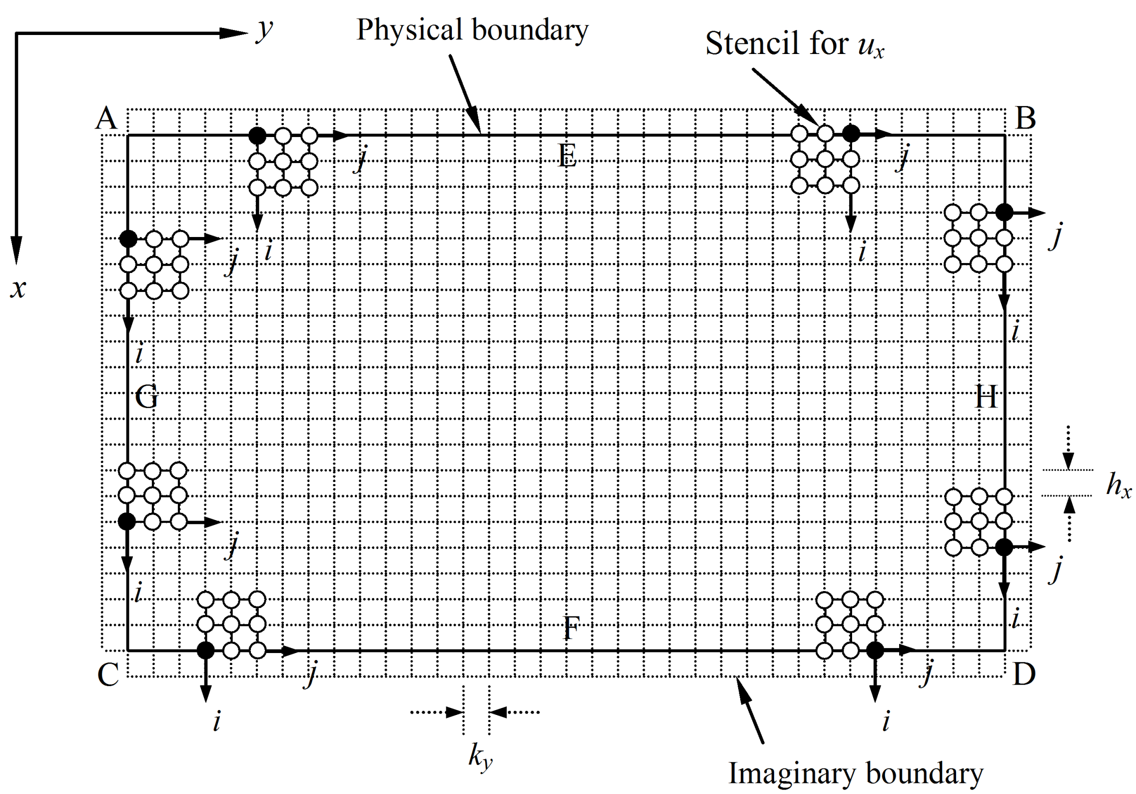

(e) Application of u_x stencils on the boundaries.

Figure 4.2: Different stencils for u_x at (a) top left (b) top right (c) bottom left and (d) bottom right corner and (e) their application on the boundaries.

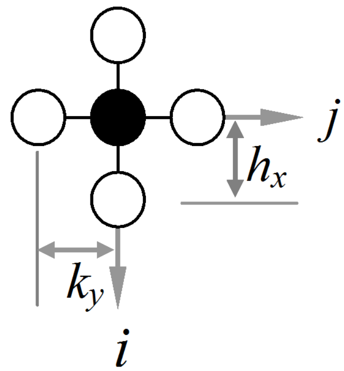

(a) Stencils of u_y on the entire boundaries.

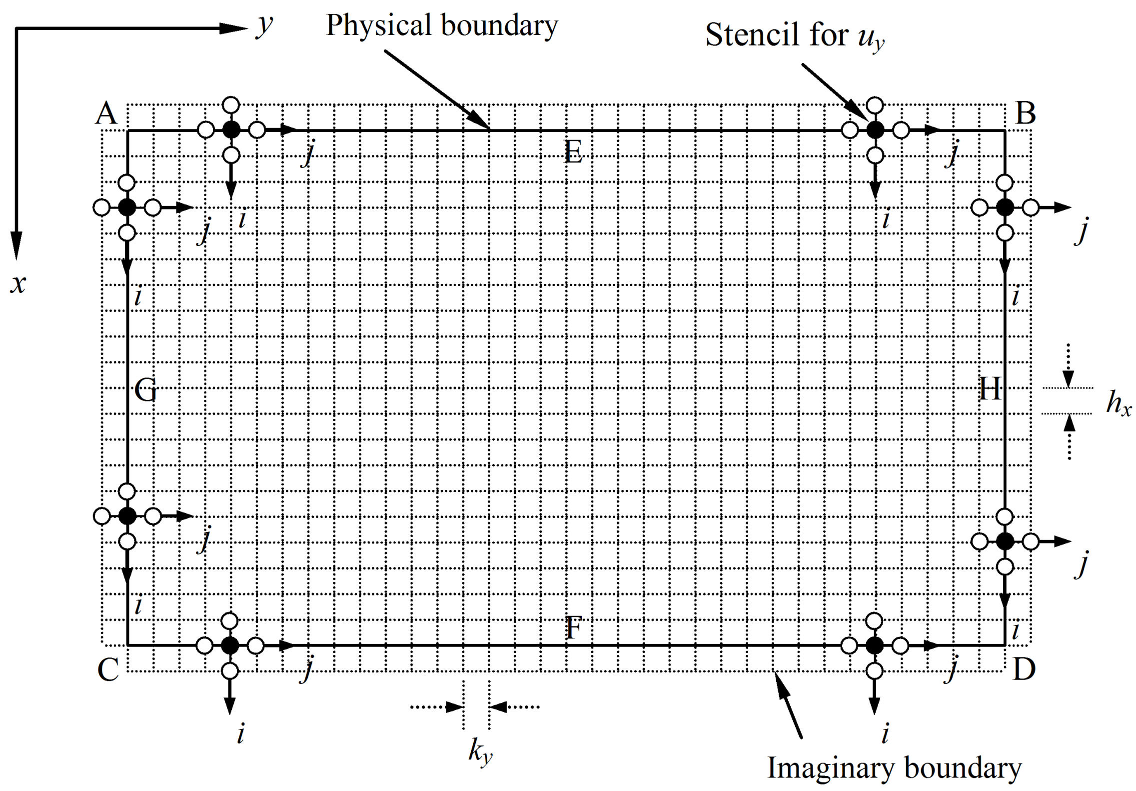

(b) Application of u_y stencils on the boundaries.

Figure 4.3: Displacement (u_y) stencils and its application on the boundaries.

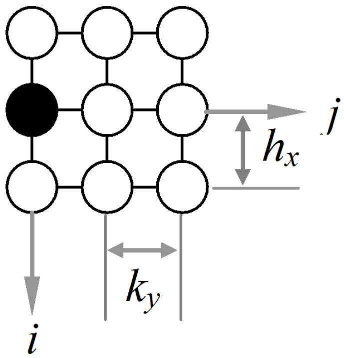

(a) Closer to point A and C.

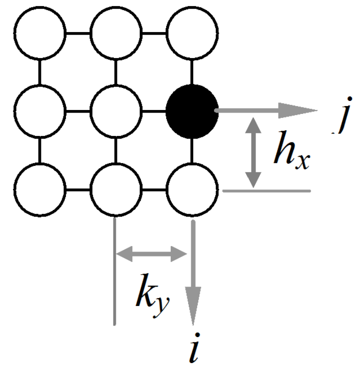

(b) Closer to point B and D.

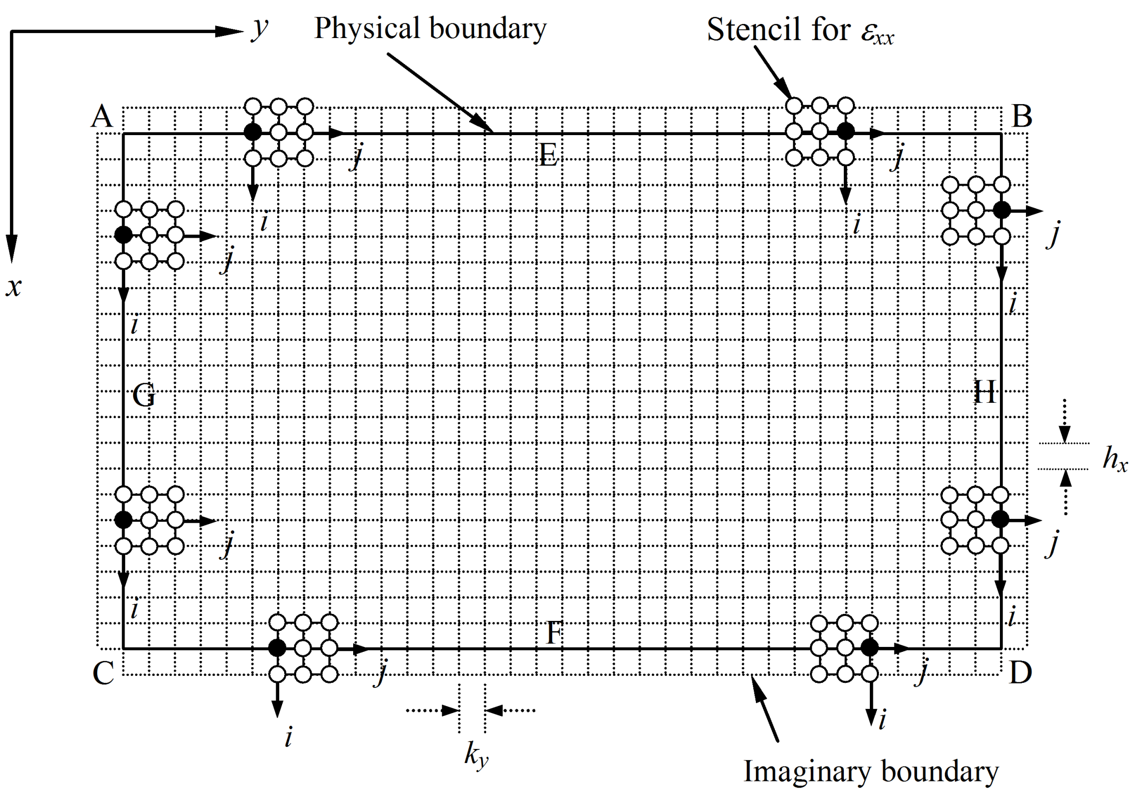

(c) Application of normal component of strain, ε_{xx} stencils on the boundaries.

Figure 4.4: Different stencils for ε_{xx} at (a) top left and bottom left corner (b) top right and bottom right corner and (c) their application on the boundaries.

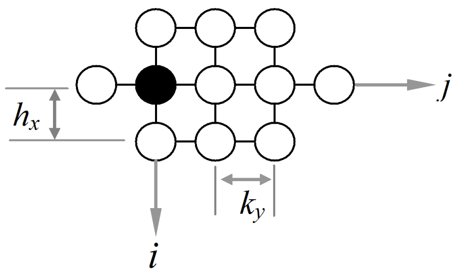

(a) Closer to point A and C.

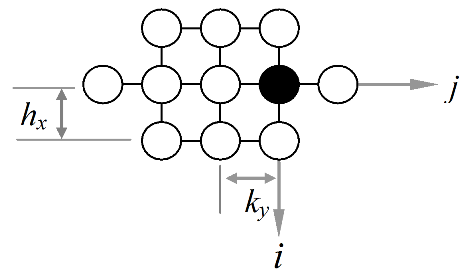

(b) Closer to point B and D.

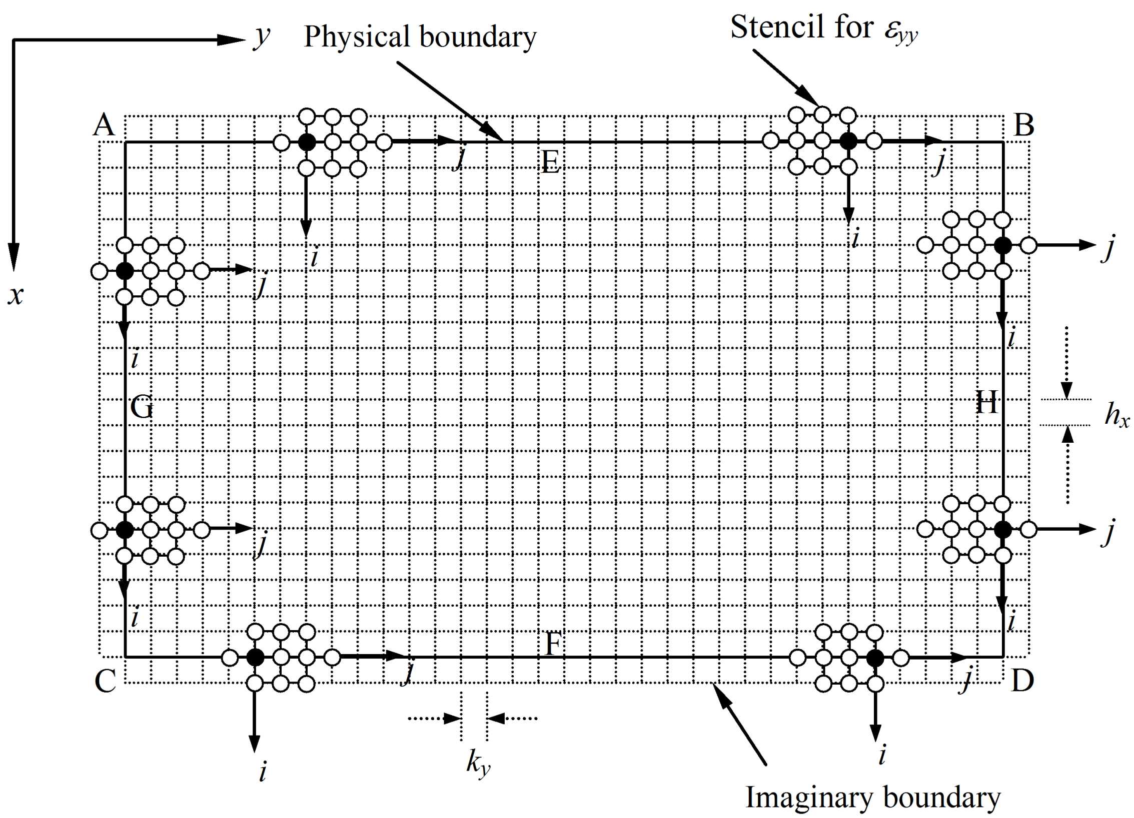

(c) Application of normal component of strain, ε_{yy} stencils on the boundaries.

Figure 4.5: Different stencils for ε_{yy} at (a) top left and bottom left corner (b) top right and bottom right corner and (c) their application on the boundaries.

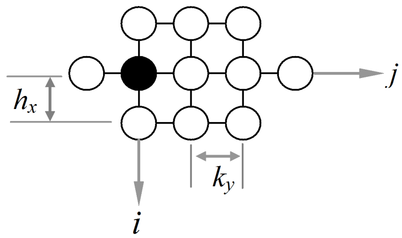

(a) Closer to point A and C.

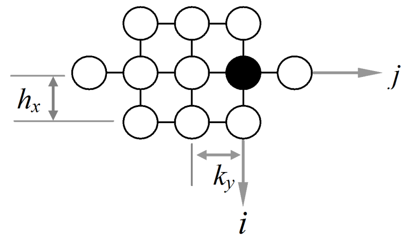

(b) Closer to point B and D.

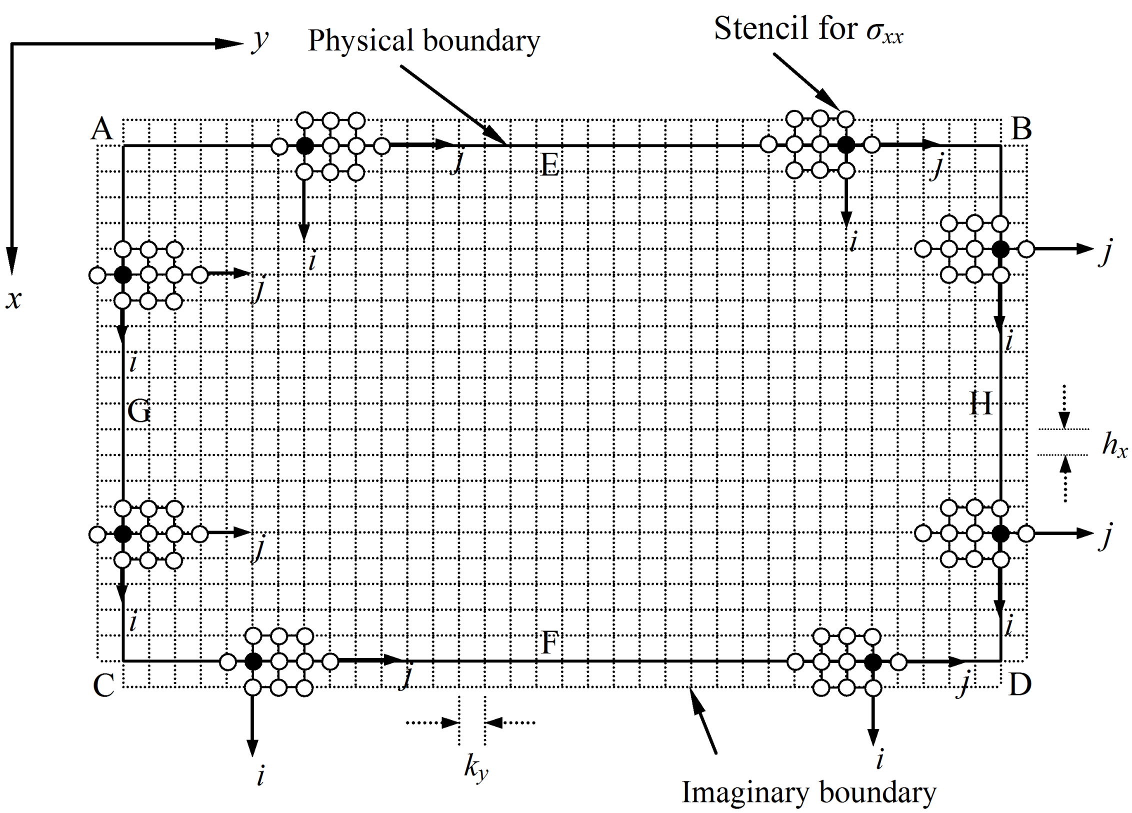

(c) Application of normal component of stress, σ_{xx} stencils on the boundaries.

Figure 4.6: Different stencils for σ_{xx} at (a) top left and bottom left corner (b) top right and bottom right corner and (e) their application on the boundaries.

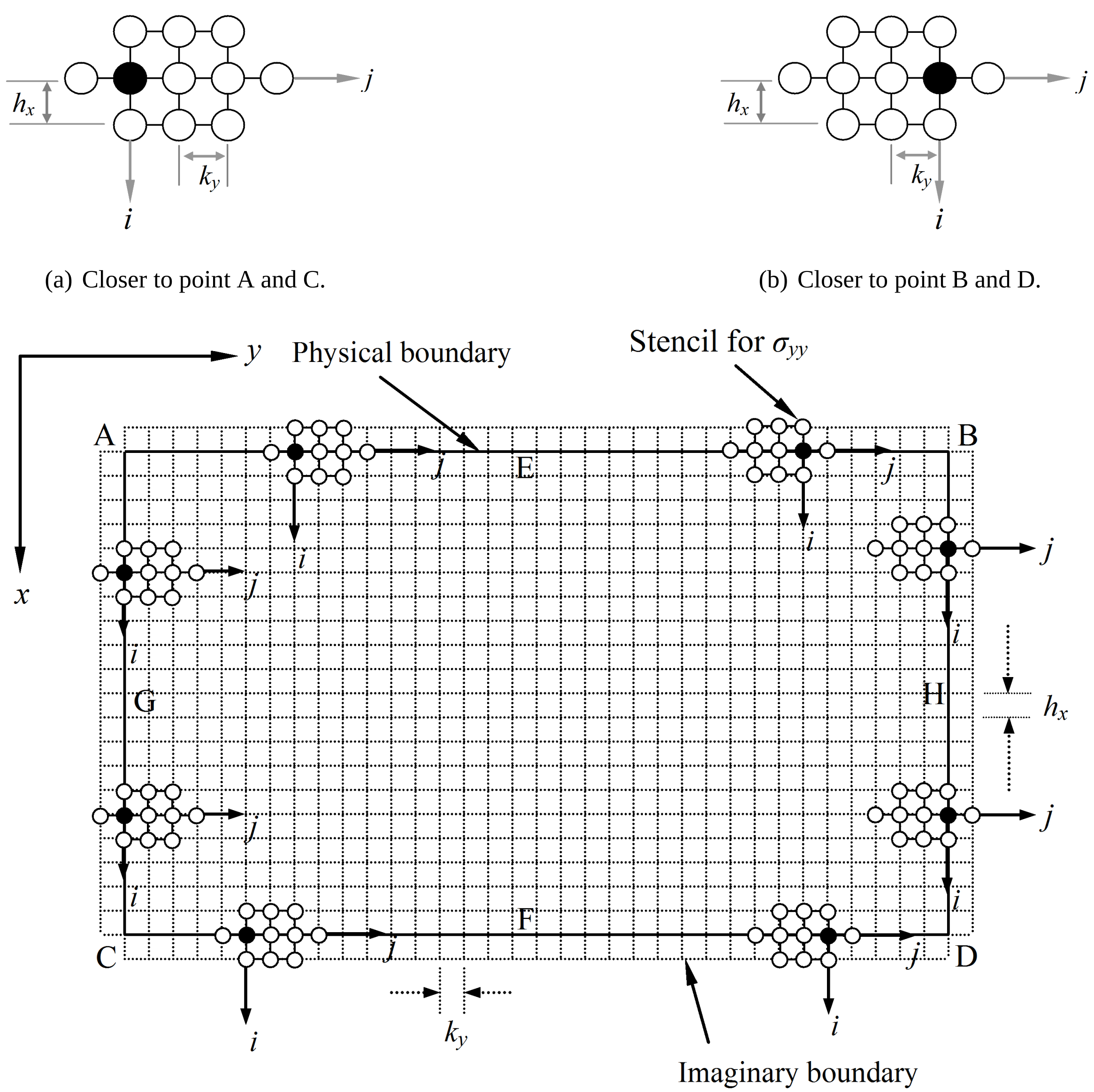

(c) Application of normal component of stress, σ_{yy} stencils on the boundaries.

Figure 4.7: Different stencils for σ_{yy} at (a) top left and bottom left corner (b) top right and bottom right corner and (e) their application on the boundaries.

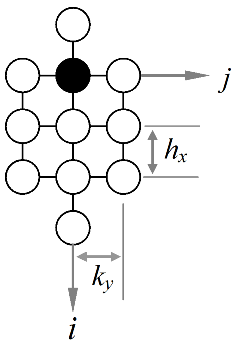

(a) Closer to point A and B.

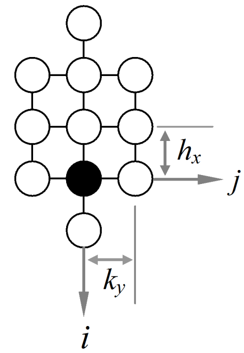

(b) Closer to point C and D.

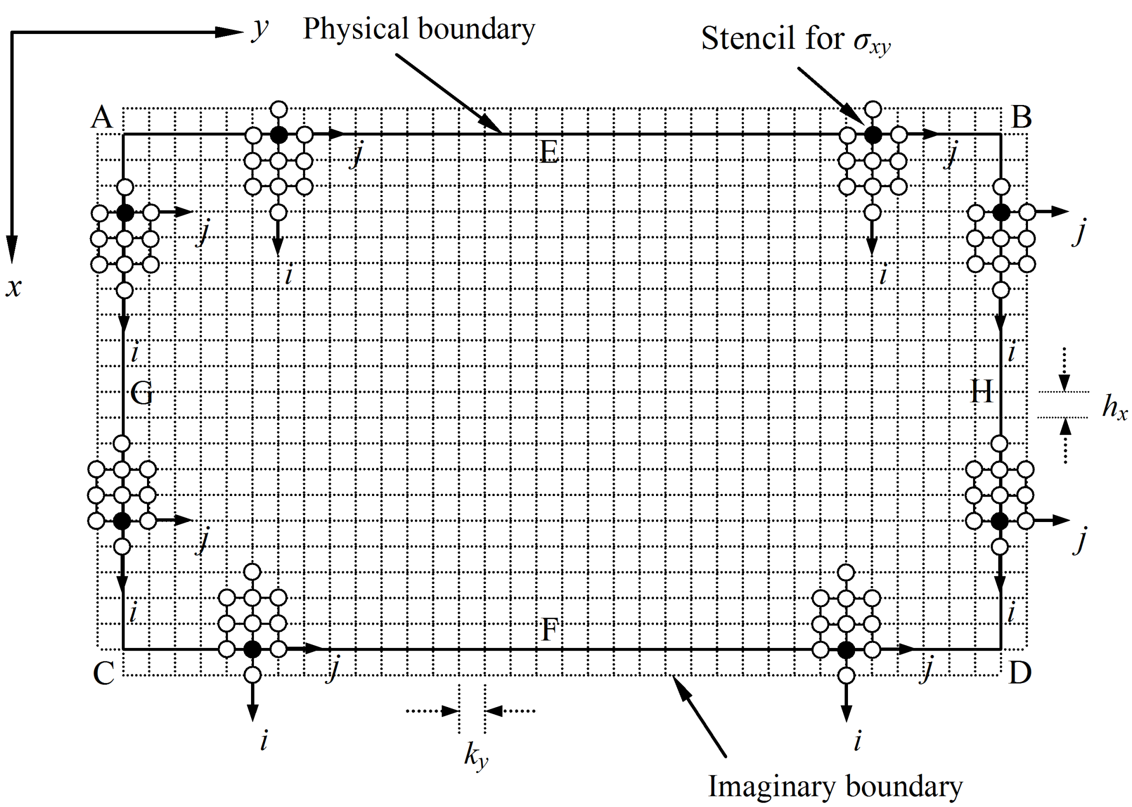

(c) Application of tangential component of stress, σ_{xy} stencils on boundaries.

Figure 4.8: Different stencils for σ_{xy} at (a) top left and top right corner (b) bottom left and bottom right corner and (e) their application on the boundaries.

Considering the edges AC and BD on the boundaries parallel to $y-$axis, the boundary conditions at any point on these edges are given in the form of any one of the following four groups:

1. (a)

$$u_x(x,y) = \frac{\partial^2\psi}{\partial x \partial y}$$

or

$$\varepsilon_{xx}(x,y) = \frac{\partial^3\psi}{\partial x^2 \partial y}$$

(b)

$$u_y(x,y) = -\frac{1}{A_{12}+A_{66}}\left[A_{11}\frac{\partial^2\psi}{\partial x^2} + A_{66}\frac{\partial^2\psi}{\partial y^2}\right]$$

or

$$\varepsilon_{yy}(x,y) = -\frac{1}{A_{12}+A_{66}}\left[A_{11}\frac{\partial^3\psi}{\partial x^2 \partial y} + A_{66}\frac{\partial^3\psi}{\partial y^3}\right]$$

2. (a)

$$u_x(x,y) = \frac{\partial^2\psi}{\partial x \partial y}$$

or

$$\varepsilon_{xx}(x,y) = \frac{\partial^3\psi}{\partial x^2 \partial y}$$

(b)

$$\sigma_{yy}(x,y) = \frac{1}{h(A_{12}+A_{66})}\left[(A_{12}^2 + A_{12}A_{16} - A_{11}A_{22})\frac{\partial^3\psi}{\partial x^2 \partial y} - A_{22}A_{66}\frac{\partial^3\psi}{\partial y^3}\right]$$

3. (a)

$$u_y(x,y) = -\frac{1}{A_{12}+A_{66}}\left[A_{11}\frac{\partial^2\psi}{\partial x^2} + A_{66}\frac{\partial^2\psi}{\partial y^2}\right]$$

or

$$\varepsilon_{yy}(x,y) = -\frac{1}{A_{12}+A_{66}}\left[A_{11}\frac{\partial^3\psi}{\partial x^2\partial y} + A_{66}\frac{\partial^3\psi}{\partial y^3}\right]$$

(b)

$$\sigma_{xy}(x,y) = \frac{A_{66}}{h(A_{12}+A_{66})}\left[-A_{11}\frac{\partial^3\psi}{\partial x^3} + A_{12}\frac{\partial^3\psi}{\partial x\partial y^2}\right]$$

4. (a)

$$\sigma_{yy}(x,y) = \frac{1}{h(A_{12}+A_{66})}\left[(A_{12}^2 + A_{12}A_{16} - A_{11}A_{22})\frac{\partial^3\psi}{\partial x^2\partial y} - A_{22}A_{66}\frac{\partial^3\psi}{\partial y^3}\right]$$

(b)

$$\sigma_{xy}(x,y) = \frac{A_{66}}{h(A_{12}+A_{66})}\left[-A_{11}\frac{\partial^3\psi}{\partial x^3} + A_{12}\frac{\partial^3\psi}{\partial x\partial y^2}\right]$$

For the case of these boundary conditions, it may be assumed that these quantities are given in numerical figures. Preceding as before and following the same arguments as for the edge AB, the difference expressions for the stress and displacement components on AC as shown Figures 4.2- 4.8, at points closer to A and applicable at region AG, are given by

$$\begin{aligned} u_x = C_1[&9\psi(i,j) - 12\{\psi(i,j+1) + \psi(i+1,j)\} + 16\psi(i+1,\\ &j+1) + 3\{\psi(i,j+2) + \psi(i+2,j)\} - 4\{\psi(i+1,j+2)\\ &+\psi(i+2,j+1)\} + \psi(i+2,j+2)] \end{aligned} \tag{4.29}$$

$$\begin{aligned} u_y = C_2&\{\psi(i+1,j) + \psi(i-1,j)\} + C_3\{\psi(i,j+1) + \psi(i,j-1)\}\\ &- 2(C_2+C_3)\psi(i,j) \end{aligned} \tag{4.30}$$

$$\begin{aligned}\varepsilon_{xx} = L_1[&-3\{\psi(i-1,j)+\psi(i+1,j)\}+4\{\psi(i-1,j+1)\\ &+\psi(i+1,j+1)\}+6\psi(i,j)-8\psi(i,j+1)+2\psi(i,j+2)\\ &-\{\psi(i-1,j+2)+\psi(i+1,j+2)\}]\end{aligned} \tag{4.31}$$

$$\begin{aligned}\varepsilon_{yy} = {} & (6L_2+10L_3)\psi(i,j)-(8L_2+12L_3)+\psi(i,j+1)+(2L_2+6L_3)\\ & \psi(i,j+2)-L_3\psi(i,j+3)-3L_3\psi(i,j-1)+L_2[-3\psi(i-1,j)\\ & -3\psi(i+1,j)+4\psi(i-1,j+1)+4\psi(i+1,j+1)\\ & -\psi(i-1,j+2)-\psi(i+1,j+2)]\end{aligned} \tag{4.32}$$

$$\begin{aligned}\sigma_{yy} = {} & (6C_6+10C_7)\psi(i,j)-(8C_6+12C_7)\psi(i,j+1)+(2C_6+6C_7)\\ & \psi(i,j+2)-C_7\psi(i,j+3)-3C_7\psi(i,j-1)+C_6[-3\psi(i-1,j)\\ & -3\psi(i+1,j)+4\psi(i-1,j+1)+4\psi(i+1,j+1)\\ & -\psi(i-1,j+2)-\psi(i+1,j+2)]\end{aligned} \tag{4.33}$$

$$\begin{aligned}\sigma_{xy} = {} & (6C_8+10C_9)\psi(i,j)-(8C_8+12C_9)\psi(i+1,j)+(2C_8+6C_9)\\ & \psi(i+2,j)+C_8[-3\psi(i,j-1)-3\psi(i,j+1)+4\psi(i+1,j-1)\\ & +4\psi(i+1,j+1)-\psi(i+2,j-1)-\psi(i+2,j+1)]\\ & -C_9[3\psi(i-1,j)+\psi(i+3,j)]\end{aligned} \tag{4.34}$$

The above difference equations (4.29) to (4.34), have been obtained by adopting i-forward, j-forward central-difference schemes for individual derivatives of the function ψ. In order to apply the above boundary conditions for points closer to B (including B) on the same boundary AC (see figures 4.2 -4.8), it requires separate versions of difference equations for most of the conditions. Similarly the corresponding finite difference expressions for the points on AC, closer to C and applicable at region CG, can be written as

$$\begin{aligned} u_x = C_1[&-9\psi(i,j) + 12\{\psi(i,j+1) + \psi(i-1,j)\} - 16\psi(i-1,\\ &j+1) - 3\{\psi(i,j+2) + \psi(i-2,j)\} + 4\{\psi(i-1,j+2)\\ &+\psi(i-2,j+1)\} - \psi(i-2,j+2)] \end{aligned} \tag{4.35}$$

$$\begin{aligned} u_y = C_2&\{\psi(i+1,j) + \psi(i-1,j)\} + C_3\{\psi(i,j+1) + \psi(i,j-1)\}\\ &- 2(C_2 + C_3)\psi(i,j) \end{aligned} \tag{4.36}$$

$$\begin{aligned} \varepsilon_{xx} = L_1[&-3\{\psi(i-1,j) + \psi(i+1,j)\} + 4\{\psi(i-1,j+1) + \psi(i+1,\\ &j+1)\} + 6\psi(i,j) - 8\psi(i,j+1) + 2\psi(i,j+2) - \{\psi(i-1,j+2)\\ &+\psi(i+1,j+2)\}] \end{aligned} \tag{4.37}$$

$$\begin{aligned} \varepsilon_{yy} = &(6L_2 + 10L_3)\psi(i,j) - (8L_2 + 12L_3)\psi(i,j+1) + (2L_2 + 6L_3)\\ &\psi(i,j+2) - L_3\psi(i,j+3) - 3L_3\psi(i,j-1) + L_2[-3\psi(i-1,j)\\ &-3\psi(i+1,j) + 4\psi(i-1,j+1) + 4\psi(i+1,j+1)\\ &-\psi(i-1,j+2) - \psi(i+1,j+2)] \end{aligned} \tag{4.38}$$

$$\sigma_{yy} = (6C_6 + 10C_7)\psi(i,j) - (8C_6 + 12C_7)\psi(i,j+1) + (2C_6 + 6C_7)$$
$$\psi(i,j+2) - C_7\psi(i,j+3) - 3C_7\psi(i,j-1) + C_6[-3\psi(i-1,j)$$
$$- 3\psi(i+1,j) + 4\psi(i-1,j+1) + 4\psi(i+1,j+1)$$
$$- \psi(i-1,j+2) - \psi(i+1,j+2)] \tag{4.39}$$

$$\sigma_{xy} = -(6C_8 + 10C_9)\psi(i,j) + (8C_8 + 12C_9)\psi(i-1,j) - (2C_8 + 6C_9)$$
$$\psi(i-2,j) + C_8[3\psi(i,j-1)3\psi(i,j+1) - 4\psi(i-1,j-1)$$
$$- 4\psi(i-1,j+1) + \psi(i-2,j+1) + \psi(i-2,j-1)]$$
$$+ C_9[3\psi(i+1,j) + \psi(i-3,j)] \tag{4.40}$$

The above difference equations (4.35) to (4.40), have been obtained by adopting i-backward, j-forward difference schemes for individual derivatives of the function ψ. The discretization scheme for normal stress, σ_{yy} of equation (4.33) closer to A and (4.39) closer to C are exactly same as shown in Figure 4.7. Similar discretization $\varepsilon_{xx}, \varepsilon_{yy}$ and σ_{yy} has been used for both corner points A and C and applicable at AGC region. Because it is symmetric with respect to $j-$ direction.

If it is assumed that the plate is divided into m number of mesh points in the $x-$direction and n number of mesh points in the $y-$direction, then the indexing in the mesh points on the edge AC and BD will be as shown in figure 4.1(c). With this indexing and preceding as before, the difference equations on BD closer to B (including point B, applicable at BH region), are given by

$$u_x = C_1[-9\psi(i,j) + 12\{\psi(i,j-1) + \psi(i+1,j)\} - 16\psi(i+1,$$
$$j-1) - 3\{\psi(i,j-2) + \psi(i+2,j)\} + 4\{\psi(i+1,j-2)$$
$$+ \psi(i+2,j-1)\} - \psi(i+2,j-2)] \tag{4.41}$$

$$u_y = C_2\{\psi(i+1,j) + \psi(i-1,j)\} + C_3\{\psi(i,j+1) + \psi(i,j-1)\}$$
$$- 2(C_2 + C_3)\psi(i,j) \tag{4.42}$$

$$\varepsilon_{xx} = L_1[3\{\psi(i-1,j) + \psi(i+1,j)\} - 4\{\psi(i-1,j-1) + \psi(i+1,$$
$$j-1)\} + 6\psi(i,j) + 8\psi(i,j-1) - 2\psi(i,j-2) - \{\psi(i-1,j-2)$$
$$+ \psi(i+1,j-2)\}] \tag{4.43}$$

$$\varepsilon_{yy} = -(6L_2 + 10L_3)\psi(i,j) + (8L_2 + 12L_3)\psi(i,j-1) - (2L_2 + 6L_3)$$
$$\psi(i,j-2) + L_3\psi(i,j-3) + 3L_3\psi(i,j+1) + L_2[3\psi(i-1,j)$$
$$+ 3\psi(i+1,j) - 4\psi(i-1,j-1) - 4\psi(i+1,j-1)$$
$$+ \psi(i-1,j-2) + \psi(i+1,j-2)] \tag{4.44}$$

$$\sigma_{yy} = -(6C_4 + 10C_5)\psi(i,j) + (8C_4 + 12C_5)\psi(i,j-1) - (2C_4 + 6C_5)$$
$$\psi(i,j-2) + C_5\psi(i,j-3) + 3C_5\psi(i,j+1) + C_4[3\psi(i-1,j)$$
$$+ 3\psi(i+1,j) - 4\psi(i-1,j-1) - 4\psi(i+1,j-1)$$
$$+ \psi(i-1,j-2) - \psi(i+1,j-2)] \tag{4.45}$$

$$\sigma_{xy} = (6C_8 + 10C_9)\psi(i,j) - (8C_8 + 12C_9)\psi(i+1,j) + (2C_8 + 6C_9)$$
$$\psi(i+2,j) + C_8[-3\psi(i,j-1) - 3\psi(i,j+1) + 4\psi(i+1,j-1)$$
$$+ 4\psi(i+1,j+1) - \psi(i+2,j-1) - \psi(i+2,j+1)]$$
$$- C_9[3\psi(i-1,j) + \psi(i+3,j)] \tag{4.46}$$

The above difference equations (4.41) to (4.46), have been obtained by adopting i-forward, j-backward difference schemes for individual derivatives of the function ψ. The another version of descritization of equations (3.43) and (3.44) on the boundary BD, closer to point D (including point D, applicable at region DH), as shown Figures 4.2- 4.8, can be written as

$$\begin{aligned} u_x = C_1[&9\psi(i,j) - 12\{\psi(i,j-1) + \psi(i-1,j)\} + 16\psi(i-1, \\ &j-1) + 3\{\psi(i,j-2) + \psi(i-2,j)\} - 4\{\psi(i-1,j-2) \\ &+ \psi(i-2,j-1)\} + \psi(i-2,j-2)] \end{aligned} \tag{4.47}$$

$$\begin{aligned} u_y = &C_2\{\psi(i+1,j) + \psi(i-1,j)\} + C_3\{\psi(i,j+1) + \psi(i,j-1)\} \\ &- 2(C_2 + C_3)\psi(i,j) \end{aligned} \tag{4.48}$$

$$\begin{aligned} \varepsilon_{xx} = L_1[&3\{\psi(i-1,j) + \psi(i+1,j)\} - 4\{\psi(i-1,j-1) + \psi(i+1, \\ &j-1)\} + 6\psi(i,j) + 8\psi(i,j-1) - 2\psi(i,j-2) - \{\psi(i-1,j-2) \\ &+ \psi(i+1,j-2)\}] \end{aligned} \tag{4.49}$$

$$\begin{aligned} \varepsilon_{yy} = &-(6L_2 + 10L_3)\psi(i,j) + (8L_2 + 12L_3)\psi(i,j-1) - (2L_2 + 6L_3) \\ &\psi(i,j-2) + L_3\psi(i,j-3) + 3L_3\psi(i,j+1) + L_2[3\psi(i-1,j) \\ &+ 3\psi(i+1,j) - 4\psi(i-1,j-1) - 4\psi(i+1,j-1) \\ &+ \psi(i-1,j-2) + \psi(i+1,j-2)] \end{aligned} \tag{4.50}$$

$$\sigma_{yy} = -(6C_4 + 10C_5)\psi(i,j) + (8C_4 + 12C_5)\psi(i,j-1) - (2C_4 + 6C_5)$$
$$\psi(i,j-2) + C_5\psi(i,j-3) + 3C_5\psi(i,j+1) + C_4[3\psi(i-1,j)$$
$$+ 3\psi(i+1,j) - 4\psi(i-1,j-1) - 4\psi(i+1,j-1)$$
$$+ \psi(i-1,j-2) - \psi(i+1,j-2)] \quad (4.51)$$

$$\sigma_{xy} = -(6C_8 + 10C_9)\psi(i,j) + (8C_8 + 12C_9)\psi(i-1,j) - (2C_8 + 6C_9)$$
$$\psi(i-2,j) + C_8[3\psi(i,j-1)3\psi(i,j+1) - 4\psi(i-1,j-1)$$
$$- 4\psi(i-1,j+1) + \psi(i-2,j+1) + \psi(i-2,j-1)]$$
$$+ C_9[3\psi(i+1,j) + \psi(i-3,j)] \quad (4.52)$$

The difference equations (4.47) to (4.52), have been obtained by adopting i-backward, j-backward-difference schemes for individual derivatives of the function ψ. The discretization scheme for normal stress, σ_{yy} of equation (4.39) closer to C and (4.51) closer to D are exactly same as shown in Figure 4.8. Similar discretization $\varepsilon_{xx}, \varepsilon_{yy}$ and σ_{yy} has been used for both corner points A and C and applicable at BHD region. Because it is symmetric with respect to $j-$direction. It is noted that the discretization scheme for u_y of equation (3.43) are similar for all boundaries and corner points as shown in Figure 4.3, because it is symmetric with respect both x and y axes.

The definition of the coefficients used in the above expressions are given below:

$$C_1 = \frac{1}{4h_x k_y} \qquad C_2 = -\frac{A_{11}}{(A_{12}+A_{66})h_x^2}$$
$$C_3 = -\frac{A_{66}}{(A_{12}+A_{66})k_y^2} \qquad C_4 = \frac{A_{11}A_{66}}{h(A_{12}+A_{66})2h_x^2k_y}$$
$$C_5 = -\frac{A_{12}A_{66}}{h(A_{12}+A_{66})2k_y^3} \qquad C_6 = \frac{A_{12}^2+A_{12}A_{66}-A_{11}A_{22}}{h(A_{12}+A_{66})2h_x^2k_y}$$
$$C_7 = -\frac{A_{22}A_{66}}{h(A_{12}+A_{66})2k_y^3} \qquad C_8 = \frac{A_{12}A_{66}}{h(A_{12}+A_{66})2h_xk_y^2}$$
$$C_9 = -\frac{A_{11}A_{66}}{h(A_{12}+A_{66})2h_x^3}$$

$$L_1 = \frac{1}{2h_x^2k_y} \qquad L_2 = -\frac{A_{11}}{(A_{12}+A_{66})}\frac{1}{2h_x^2k_y}$$
$$L_3 = -\frac{A_{66}}{(A_{12}+A_{66})2k_y^3} \qquad L_4 = \frac{A_{12}}{(A_{12}+A_{66})2h_xk_y^2}$$
$$L_5 = -\frac{A_{11}}{(A_{12}+A_{66})2h_x^3}$$

4.2.3 Management of Corner Boundary Conditions

Equations (4.29) to (4.40) and (4.41) (4.52) can be used for the mesh points on the boundary AC and BD respectively for discretizing the boundary equations. These equations are not valid for the corner points of these edges as they are treated separately. Following the arguments stated previously, the author decided to satisfy a single boundary condition out of two, for each corner points of the edges AC and BD. The choice of this single boundary conditions, which has to be satisfied, has come from the method of trial and error and listed following:

Boundary conditions	Proposed choice
u_x and u_y/ε_{yy}	u_y
u_x and σ_{yy}	σ_{yy}
σ_{xy} and u_y/ε_{yy}	u_y
σ_{yy} and σ_{xy}	σ_{yy}

Thus we need other difference equations for u_y and σ_{yy} which will be applied for the corner mesh points of the boundaries AC and BD. But difference expressions of σ_{yy} of (4.33) or (4.39) and (4.45) or (4.51) are applicable for corner points on AC and BD respectively. So, we need only difference equation for u_y for the corner mesh points of the boundaries AC and BD. The stencils of u_y of the corner points has been shown in Figures 4.9(a) and application of the stencils on corner points has been shown in Figure 4.9(c).

The difference expression for corner point A on AC can be written as

$$u_y = C_3\psi(i,j-1) + C_3\psi(i,j+1) + 2C_2\psi(i+1,j) + C_2\psi(i+2,j) \\ + (C_2 - 2C_3)\psi(i,j) \tag{4.53}$$

For corner point C on AC

$$u_y = C_3\psi(i,j-1) + C_3\psi(i,j+1) + 2C_2\psi(i-1,j) + C_2\psi(i-2,j) \\ + (C_2 - 2C_3)\psi(i,j) \tag{4.54}$$

For corner point B on BD

$$u_y = C_3\psi(i,j-1) + C_3\psi(i,j+1) + 2C_2\psi(i+1,j) + C_2\psi(i+2,j) \\ + (C_2 - 2C_3)\psi(i,j) \tag{4.55}$$

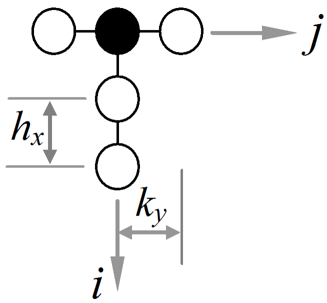

(a) At corner point A and B.

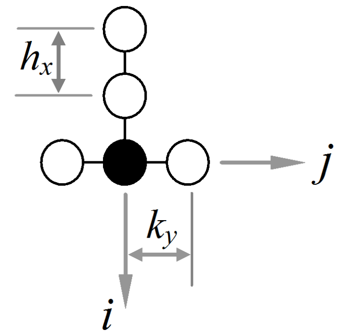

(b) At corner point C and D.

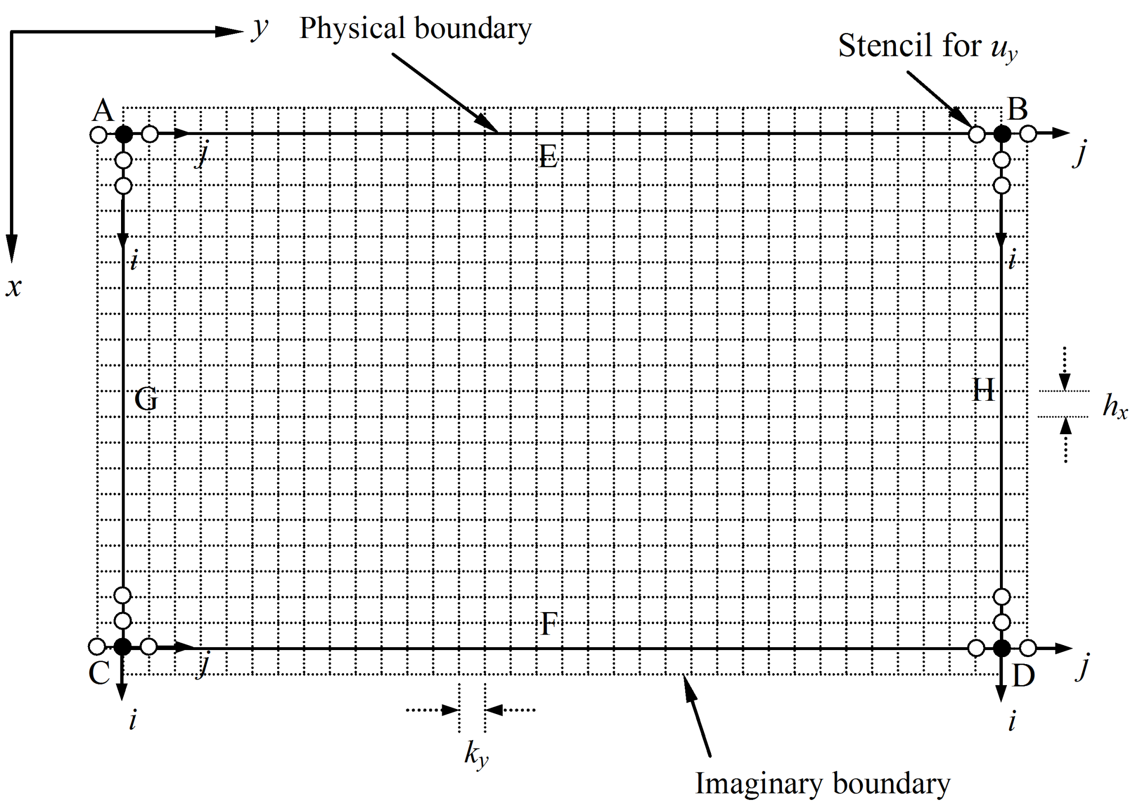

(c) Application of the displacement component, u_y on the corner points.

Figure 4.9: Different stencils for u_y at different corner points and their application on the corner points.

For corner point D on BD

$$u_y = C_3\psi(i,j-1) + C_3\psi(i,j+1) + 2C_2\psi(i-1,j) + C_2\psi(i-2,j) \\ + (C_2 - 2C_3)\psi(i,j) \tag{4.56}$$

4.2.4 Tagging of Boundary Conditions to Mesh Points, Solution and Evaluation of ψ at the Internal and Boundary Mesh Points

Since there are two conditions to be satisfied at an arbitrary point on the physical boundary of the panel, the finite difference expressions of the differential equations associated with the boundary conditions are applied to the same point on the boundary. It should be noted that two linear algebraic equations are assigned to a single point on the boundary. Out of these two equations, one is used to evaluate the function ψ at point on the physical boundary and the other one for the corresponding point on the false boundary.

Therefore, every mesh point of the domain has a single linear algebraic equation tagged to it. The discrete values of the potential function, $\psi(x,y)$, at mesh points are solved from the system of linear algebraic equations resulting from the discretization of the governing equation and the associated boundary conditions. There are numerous existing methods of solving a system of algebraic equations. $\psi(i,j)$ the discrete values of the displacement function at mesh points is to be solved by direct method of elimination from a system of linear algebraic equations resulting from the discretization of the equation (3.42) and differential equations associated with the boundary conditions. Attempt is made to organize the difference expressions in such a fashion that the concerned point, for which the equation is to be written, must be included in addition to other surrounding mesh points. Therefore, the coefficient matrix which is, of course, a square matrix, generated from the system of algebraic equations, will have all non-zero diagonal elements. This criteria must be satisfied by the coefficient matrix, otherwise the solution will be impossible.In the present problem, the number of unknowns in the system of equations is extremely large but only a few in each individual equation. Under this condition, the iterative method may be preferable. But the problem of solving the difference equations by the iterative method has certain shortcomings. Although this method works very well for certain boundary conditions, it fails to produce any solution for other complex boundary conditions. In certain cases, the rate of convergence of iteration is extremely slow, which makes it impractical. As the iterative method has the limitation of not always converging to a solution and sometimes converging but very slowly, the present problem is solved by the use of the triangular decomposition method which ensures better reliability as well as better accuracy of solution in a shorter period of time.

It is felt necessary to comment here on the corner points of the plate which are generally points os transition in the boundary condition. One way of handling the transition point is that each corner point is taken as a smooth point on the boundary and has only two boundary conditions. But, unfortunately this approach becomes unattractive as it places limitation to the style of discretization which in turn leads to the discretization error of order h_x. And finally this assumption leads to the result which is unsatisfactory as far as accuracy is concerned. As the corner mesh points processes four boundary conditions coming from both sides, It has been decided to take three conditions out of them and remaining condition was treated as redundant. The presence of excess conditions indicate that the point concerned is a *point of singularity*; finite -difference technique does not permit any spacial treatment of this point without the aid of mathematical analysis.

Once the differential equation along with the associate boundary conditions are transformed into finite-difference equations, the main problem from the computational standpoint is that of actually computing the solution of the system of difference equations. For the problem at hand we are concerned with solving a system of linear algebraic equations, expressed in matrix equation as

$$[K]\{\psi\} = \{C\} \tag{4.57}$$

Expressing explicitly, equation (4.57) becomes

$$\begin{bmatrix} K_{11} & K_{12} & K_{13} & \ldots\ldots\ldots\ldots\ldots & K_{1n} \\ K_{21} & K_{22} & K_{23} & \ldots\ldots\ldots\ldots\ldots & K_{2n} \\ K_{31} & K_{32} & K_{33} & \ldots\ldots\ldots\ldots\ldots & K_{3n} \\ . & . & . & \ldots\ldots\ldots\ldots\ldots & . \\ . & . & . & \ldots\ldots\ldots\ldots\ldots & . \\ . & . & . & \ldots\ldots\ldots\ldots\ldots & . \\ K_{n1} & K_{n2} & K_{n3} & \ldots\ldots\ldots\ldots\ldots & K_{nn} \end{bmatrix} \begin{bmatrix} \psi_1 \\ \psi_2 \\ \psi_3 \\ . \\ . \\ . \\ \psi_4 \end{bmatrix} = \begin{bmatrix} C_1 \\ C_2 \\ C_3 \\ . \\ . \\ . \\ C_n \end{bmatrix} \tag{4.58}$$

where,

K - is a known square matrix-called the co-efficient matrix.

C - is a given column matrix whose elements are zero except those which correspond to ψ on or outside the boundary.

ψ - is an unknown column matrix which we seek to determine the values.

It is obvious that the matrix [K] is non-singular and hence a unique solution exists, but the problem is how to get the solution. The iterative method is advocated for this kind of large sparse system of linear algebraic equation, but the most unfortunate part in this method is that the technique is successful to very few cases of co-efficient matrix. Considering this difficulties, the author decided to solve the system of equation by Cholesky's method which is a LU decomposition method. The requirement of the storage space in the computer and also the computer time is less in this method. Up to a large number of equations, this method can produce promising results with the minimum truncation error.

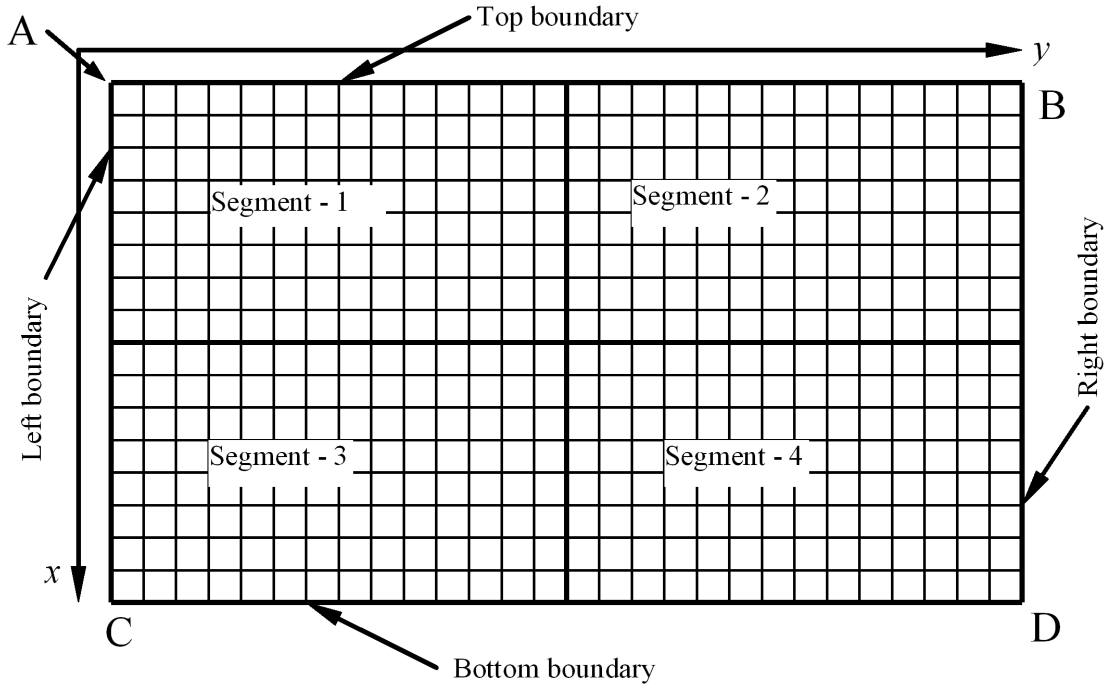

Figure 4.10: Four regions of the stressed laminated panel.

4.2.5 Evaluation of Displacement, Stress and Strain Components for Overall Laminate From the ψ Values at Mesh Points

To evaluate the stress and displacement components from the values of ψ's which are known beforehand at each grid field is divided into four region segment-1, segment-2, segment-3, segment-4 corresponding to the top-left, top-right, bottom-left and bottom-right quadrants, respectively, as shown in figure 4.10. For each of the quadrants, different forms of discretized expressions for the components of displacement, stress and strain are used. To evaluate displacement, stress and strain for segment-1 (top-left corner), equations (4.5) to (4.10) and (4.29) to (4.34) are used. Shear strain component is not used on the boundary. To evaluate shear strain for segment-1, the expression of shear strain has given below:

$$\begin{aligned}\varepsilon_{xy} = &(6L_4 + 10L_5)\psi(i,j) - (8L_4 + 12L_5) + \psi(i+1,j) + (2L_4 + 6L_5)\\ &\psi(i+2,j) - L_5\psi(i+3,j) - 3L_5\psi(i-1,j) + L_4[-3\psi(i,j-1)\\ &- 3\psi(i,j+1) + 4\psi(i+1,j-1) + 4\psi(i+1,j+1)\\ &- \psi(i+2,j-1) - \psi(i+2,j+1)]\end{aligned} \tag{4.59}$$

Similarly, to evaluate displacement, stress and strain for segment-2 (top-right corner), equations (4.11) to (4.16) and (4.41) to (4.46) are used. Shear strain component is not used on the boundary. To evaluate shear strain for segment-2, the expression of shear strain has been given below:

$$\begin{aligned}\varepsilon_{xy} = &(6L_4 + 10L_5)\psi(i,j) - (8L_4 + 12L_5) + \psi(i+1,j) + (2L_4 + 6L_5)\\ &\psi(i+2,j) - L_5\psi(i+3,j) - 3L_5\psi(i-1,j) + L_4[-3\psi(i,j-1)\\ &- 3\psi(i,j+1) + 4\psi(i+1,j-1) + 4\psi(i+1,j+1)\\ &- \psi(i+2,j-1) - \psi(i+2,j+1)]\end{aligned} \tag{4.60}$$

Similarly, to evaluate displacement, stress and strain for segment-3 (bottom-left corner), equations (4.17) to (4.22) and (4.35) to (4.40) are used. Shear strain component is not used on the boundary. To evaluate shear strain for segment-3, the expression of shear strain has been given below:

$$\begin{aligned}\varepsilon_{xy} = &- (6L_4 + 10L_5)\psi(i,j) + (8L_4 + 12L_5)\psi(i-1,j) - (2L_4 + 6L_5)\\ &\psi(i-2,j) + L_5\psi(i-3,j) + 3L_5\psi(i+1,j) + L_4[3\psi(i,j-1)\\ &+ 3\psi(i,j+1) - 4\psi(i-1,j-1) - 4\psi(i-1,j+1)\\ &+ \psi(i-2,j-1) + \psi(i-2,j+1)]\end{aligned} \tag{4.61}$$

Similarly, to evaluate displacement, stress and strain for segment-4 (bottom-right corner), equations (4.23) to (4.28) and (4.47) to (4.52) are used. Shear strain component is not used on the boundary. To evaluate shear strain for segment-4, the expression of shear strain has given below:

$$\begin{aligned}\varepsilon_{xy} = &-(6L_4+10L_5)\psi(i,j)+(8L_4+12L_5)\psi(i-1,j)-(2L_4+6L_5)\\&\psi(i-2,j)+L_5\psi(i-3,j)+3L_5\psi(i+1,j)+L_4[3\psi(i,j-1)\\&+3\psi(i,j+1)-4\psi(i-1,j-1)-4\psi(i-1,j+1)\\&+\psi(i-2,j-1)+\psi(i-2,j+1)]\end{aligned} \tag{4.62}$$

4.2.6 Evaluation of Stress Components for Individual Lamina

In previous section, displacement, sterss and strain components have been evaluated for overall laminate. Stress and displacement for lamina of the composite has been solved by the help of strain distribution. Strain distributions for overall laminate or global strain distribution has evaluated directly from the ψ values in equation (4.58) of the mesh point. The distributions of strain components are same for all plies of whole domain. These strain components are directly multiplied with the stiffness matrix of the each individual plies to evaluate the different stress components of individual plies by using equation (3.46).

CHAPTER

5

Laminated Panel Subjected to Symmetric and Antisymmetric Discrete Stiffeners

5.1 Introduction

The stress field of a laminated composite cantilever is analyzed under the influence of local stiffeners at the opposing longitudinal surfaces. The symmetric and anti-symmetric arrangements of local stiffeners are considered for the case of a symmetric cross-ply laminated cantilever subjected to a uniform shear loading. An efficient computational algorithm is developed, in which a new displacement-potential is introduced to model the problem of laminated composite materials with mixed and changeable boundary conditions. Solutions of stresses at different layers of the laminated composite are obtained, some of which, especially those around the critical regions of stiffeners are presented in a comparative fashion mainly in the form of graphs. Results are found to be accurate and reasonable when analyzed in light of comparison made with those of standard computational method (see chapter 8).

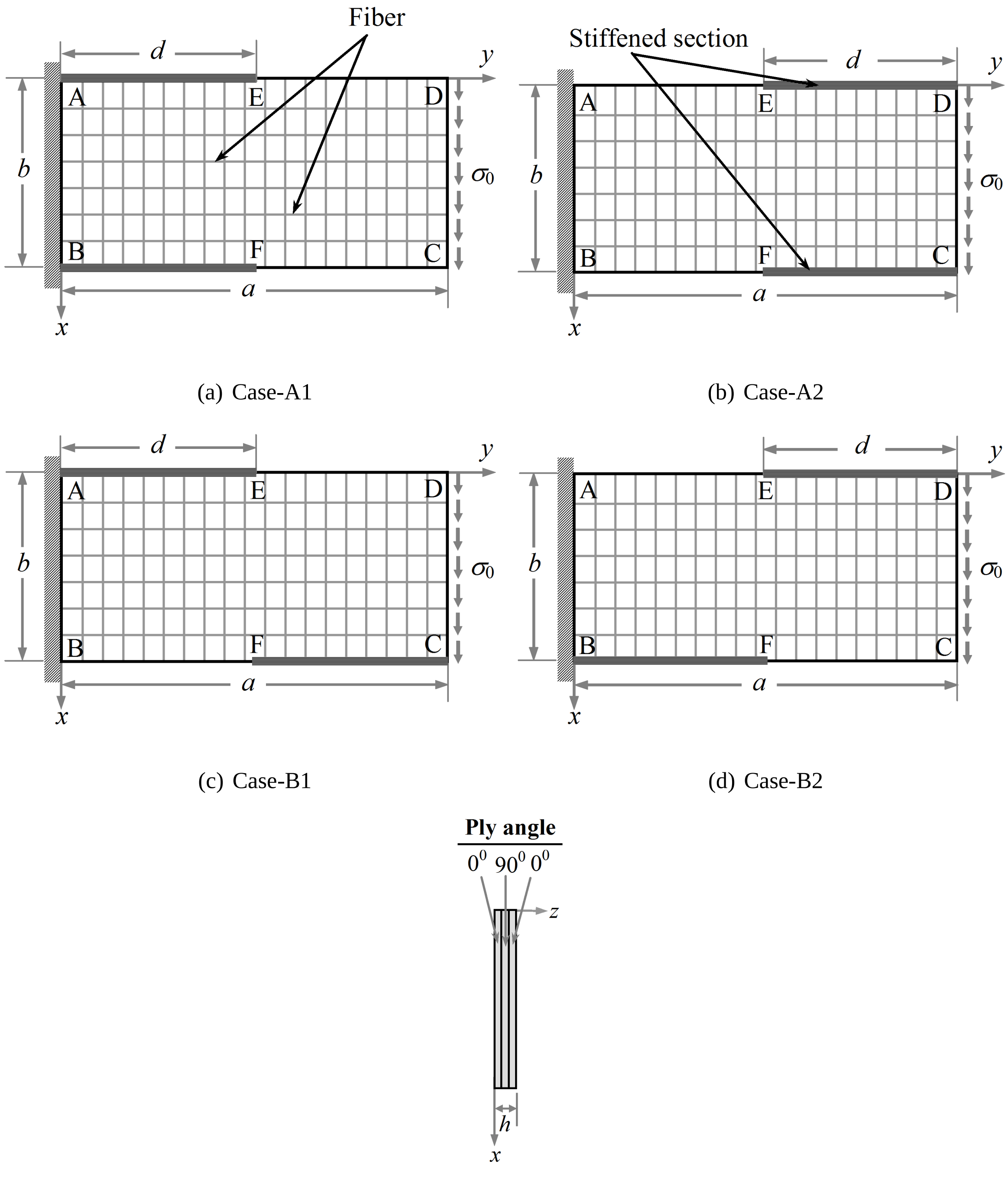

(a) Case-A1 (b) Case-A2

(c) Case-B1 (d) Case-B2

(e) End view

Figure 5.1: Loading and geometry of discretely stiffened cross-ply laminated panels: (a) Case-A1, (b) Case-A2, (c) Case-B1, (d) Case-B2 and (e) end view.

5.2 Geometry and physical conditions of the cantilever

A uniform rectangular cantilever of $[0^o/90^o/0^o]$ cross-ply laminated composite is considered for the present analysis. The length, width and thickness of the cantilever are represented by a, b and h, respectively. The laminate is assumed to be consisted of n number of plies, in which the ply thickness of individual lamina is kept constant. The left-hand lateral end of the cantilever is assumed to be rigidly fixed and the right-hand lateral end is subjected to a uniform shear loading. The two opposing longitudinal surfaces are considered to be locally stiffened by attaching rigid axial stiffeners for part of the boundary surfaces (stiffener length d). Two symmetric and two anti-symmetric arrangements of the local stiffeners are considered, which eventually lead to four different cases of the stiffened cantilever, and are identified here as Case-A1 and Case-A2, and Case-B1 and Case-B2, respectively. The geometry and loading of the four cases of the stiffened cantilevers with respect to the coordinate system are schematically illustrated in Figure 5.1. The physical conditions to be satisfied along the different boundary segments of the cantilever can be expressed mathematically as follows:

1. The supporting lateral end (boundary AB) is rigidly fixed. Both the lateral and axial components of displacement are assumed to be zero here, that is,

   $u_x(x,0) = 0$ and $u_y(x,0) = 0$ $[0 \le x \le b]$

2. The right-hand lateral end (boundary CD) of the cantilever is the loaded boundary. Here, the loading is realized through a uniform distribution of shear stress, while the associated normal stress component is assumed to be zero, that is,

   $\sigma_{yy}(x,a) = 0$ and $\sigma_{xy}(x,a) = \sigma_0$ $[0 \le x \le b]$

3. The two opposing longitudinal surfaces, AD and BC, are assumed to be stiffened locally, that is, part of the boundaries is subjected to axial stiffeners and part of them are free. In order to model the physical condition of the axial stiffeners, the tangential

strain along the stiffener is restrained, while the section is kept free from any external loading. Again along the stiffener connected with fixed end, axial strains as well as axial displacements are zero. Referring to Fig. 5.1, the mathematical modeling of the physical conditions associated with the free and stiffened sections of the boundaries AD and BC, is realized as follows:

Free region:	$\sigma_{xx}[(0,b),y]=0$	and	$\sigma_{xy}[(0,b),y]=0$
Stiffened region (near fixed boundary):	$\sigma_{xx}[(0,b),y]=0$	and	$u_y[(0,b),y]=0$
Stiffened region (near loaded boundary):	$\sigma_{xx}[(0,b),y]=0$	and	$\varepsilon_{yy}[(0,b),y]=0$

Choice of boundary conditions at the singularity points are important. With change of combination of boundary conditions at the point of singularity, accuracy may deteriorate. Table 5.1 illustrates the scheme for treating the boundary conditions of the singularity points of the cantilever, which are, in general, the points of singularity.

5.3 Results and Discussions

The results of the analysis of stresses for the laminated cantilever subjected to four different arrangements of symmetric and anti-symmetric local stiffeners along the two opposing longitudinal surfaces, as shown in Figure 5.1, are presented in this section. The results are presented mainly in the form of deformed shape as well as distribution of stress components of interest of $[0^o/90^o/0^o]$ cross-ply laminate. In all cases for distribution of stress components, stresses are normalized with respect to the maximum intensity of applied shear loading, σ_o (see Figure 5.1), the magnitude of which is arbitrarily assumed to be 3 MPa. The details of the boundary conditions as used to obtain the present FD solutions are already listed in section 5.2 and Table 5.1. Three laminae (n = 3) of unidirectional composite material with stacking sequences of $[0^o/90^o/0^o]$ and $[90^o/0^o/90^o]$ are assumed to form symmetric cross-ply laminates to find the effect of stacking sequence on stress distributions. For most of the results, the boron/epoxy composite is considered as the ply material, the effective mechanical properties of which together with those of glass/epoxy and graphite/epoxy are listed in

Table 5.1: Numerical modeling of the boundary conditions for corner and the interface boundary points of the panels for different cases (Figure 5.1).

Corner Point (Cases)	Given boundary Parameters	Used boundary Parameters	Correspondence between mesh points and given boundary conditions	
			Mesh point on the physical boundary	Mesh points on the imaginary boundary
A (Case-A1, B1)	σ_{xx}, u_y u_x, u_y	$[\sigma_{xx}, u_x, u_y]$	$\sigma_{xx}(0,0) = 0$	$u_x(0,0) = 0$ $u_y(0,0) = 0$
A (Case-A2, B2)	σ_{xx}, σ_{xy} u_x, u_y	$[\sigma_{xx}, \sigma_{xy}, u_y]$	$\sigma_{xx}(0,0) = 0$	$u_x(0,0) = 0$ $u_y(0,0) = 0$
B (Case-A1, B2)	σ_{xx}, u_y u_x, u_y	$[\sigma_{xx}, \sigma_{xy}, u_y]$	$\sigma_{xx}(b,0) = 0$	$\sigma_{xy}(b,0) = 0$ $u_y(b,0) = 0$
B (Case-A2, B1)	σ_{xx}, σ_{xy} u_x, u_y	$[\sigma_{xx}, \sigma_{xy}, u_y]$	$\sigma_{xx}(b,0) = 0$	$\sigma_{xy}(b,0) = 0$ $u_y(b,0) = 0$
C (Case-A1, B2)	σ_{xx}, σ_{xy} σ_{yy}, σ_{xy}	$[\sigma_{xx}, \sigma_{yy}, \sigma_{xy}]$	$\sigma_{xx}(b,a) = 0$	$\sigma_{yy}(b,a) = 0$ $\sigma_{xy}(b,a) = \sigma_o$
C (Case-A2, B1)	$\sigma_{xx}, \varepsilon_{yy}$ σ_{yy}, σ_{xy}	$[\sigma_{xx}, \sigma_{xy}, \varepsilon_{yy}]$	$\sigma_{xx}(b,a) = 0$	$\varepsilon_{yy}(b,a) = 0$ $\sigma_{xy}(b,a) = \sigma_o$
D (Case-A1, B1)	σ_{xx}, σ_{xy} σ_{yy}, σ_{xy}	$[\sigma_{xx}, \sigma_{yy}, \sigma_{xy}]$	$\sigma_{xx}(0,a) = 0$	$\sigma_{yy}(0,a) = 0$ $\sigma_{xy}(0,a) = \sigma_o$
D (Case-A2, B2)	$\sigma_{xx}, \varepsilon_{yy}$ σ_{yy}, σ_{xy}	$[\sigma_{xx}, \sigma_{xy}, \varepsilon_{yy}]$	$\sigma_{xx}(0,a) = 0$	$\varepsilon_{yy}(0,a) = 0$ $\sigma_{xy}(0,a) = \sigma_o$
Interface point (for all cases)				
E (Case-A1, B1)	$\sigma_{xx}, \sigma_{xy}, u_y$	$[\sigma_{xx}, u_y]$	$\sigma_{xx}(0,d) = 0$	$u_y(0,d) = 0$
E (Case-A2, B2)	$\sigma_{xx}, \sigma_{xy}, \varepsilon_{yy}$	$[\sigma_{xx}, \varepsilon_{yy}]$	$\sigma_{xx}(0,d) = 0$	$\varepsilon_{yy}(0,d) = 0$
F (Case-A1, B2)	$\sigma_{xx}, \sigma_{xy}, u_y$	$[\sigma_{xx}, u_y]$	$\sigma_{xx}(b,d) = 0$	$u_y(b,d) = 0$
F (Case-A2, B1)	$\sigma_{xx}, \sigma_{yy}, \varepsilon_{yy}$	$[\sigma_{xx}, \varepsilon_{yy}]$	$\sigma_{xx}(b,d) = 0$	$\varepsilon_{yy}(b,d) = 0$

Table 5.2. The thickness of individual plies is kept constant, which is 0.5 mm. All the results presented here correspond to a cantilever of geometrical aspect ratio, $a/b = 2.5$. For most of the results, the length of the discrete stiffener is kept constant, that is, the ratio, d/a is set equal to 0.5, although the effect of stiffening length is investigated by varying the ratio. The FD mesh-network used to model the present cantilever $(a/b = 2.5)$ contains nodal points (51×51) in the direction of x and y, respectively.

Table 5.2: Typical mechanical properties of a unidirectional lamina (SI system of units) Kaw [1]

Property	Symbol	Units	Glass/ epoxy	Boron/ epoxy	Graphite epoxy
Fiber volume fraction	v_f		0.45	0.50	0.70
Longitudinal elastic modulus	E_1	GPa	38.6	204	181
Transverse elastic modulus	E_2	GPa	8.27	18.50	10.30
Major poisson's ratio	ν_{12}		0.26	0.23	0.28
Shear modulus	G_{12}	GPa	4.14	5.59	7.17

5.3.1 Distributions of Axial Displacements

Figure 5.2 shows the distributions of normalized axial displacement of the laminated cantilever obtained with four different arrangements of local stiffeners; Case-A1, Case-A2, Case-B1 and Case-B2. It is noted that displacements are normalized with the maximum lateral displacement at the right lateral end of the same stiffener free cantilever subjected to uniform distributed loading ($\sigma_0 = 3$ MPa). At stiffening region which is attached with the fixed end, no displacement and strain has been found at top and bottom boundary that exactly matches the concept of axial stiffener. At stiffening region away from the fixed end, axial displacements are constant, i.e, laminate gives the rigid body motion at the stiffening region which satisfy the theoretical concept of the stiffener as well as boundary conditions (axial

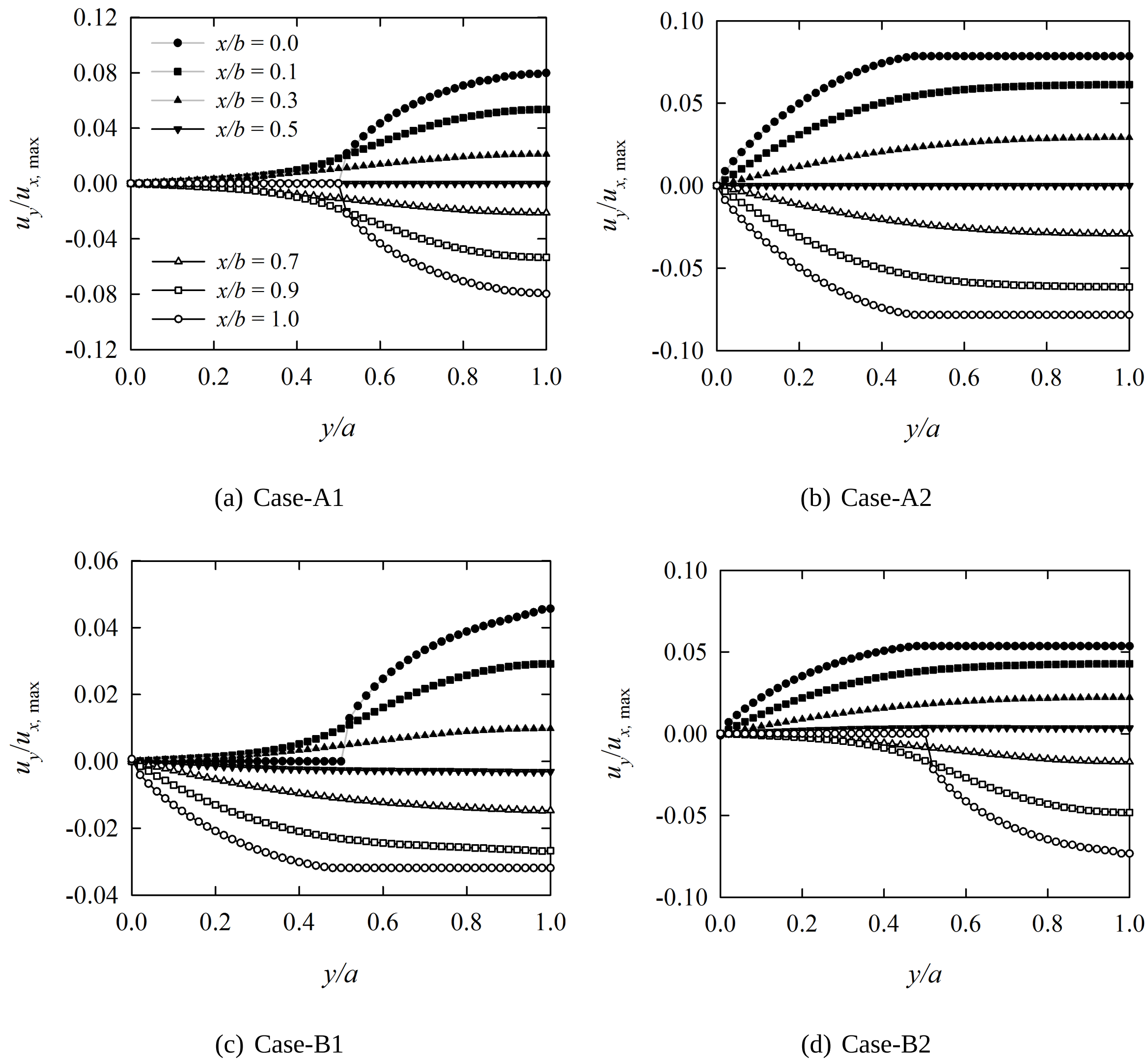

Figure 5.2: Distribution of normalized axial displacement component at different lateral sections of stiffened laminated panels: (a) Case-A1, (b) Case-A2, (c) Case-B1, (d) Case-B2

strain is zero). Overall distributions of displacement increase from left to right lateral end. Magnitude of maximum displacement has been found at the top and/ or bottom boundary at right lateral end. For symmetric cases, distributions of axial displacements are symmetric with respect to lateral section $x/b = 0.5$.

5.3.2 Deformed State of the Panel

Figure 5.3 illustrates the deformed shapes of the laminated cantilever obtained with four different arrangements of local stiffeners (namely, Case-A1, Case-A2, Case-B1 and Case-B2). The overall deformation pattern of the cantilever is found to be in good agreement with the physical model of the problem, which, in turn, verifies the appropriateness of the boundary modeling approach. As appears from the solutions, displacements in the lateral direction are much higher than those in the axial direction, thereby signifying the presence of axial stiffeners at the longitudinal surfaces of the cantilever. The presence of discrete stiffeners on the longitudinal surfaces is also reflected by the change in slopes of deflection of the top and bottom boundaries in the deformed shapes shown in Figure 5.3. As expected, maximum deflection is found to occur at the right lateral end of the cantilever. Although the displacements in all the symmetric and anti-symmetric cases are not in the same order of magnitude, differences in the magnitude caused by different arrangements of stiffeners are realized, which is even evident from Figure 5.3. A quantitative analysis of the overall deformation shows the symmetric arrangements of the local stiffeners causes the laminated cantilever to assume maximum and minimum deformation among the four cases considered. More specifically, the symmetric arrangement of stiffeners situated near the free lateral end (Case-A2) causes the maximum deflection for the cantilever. For the two anti-symmetric arrangements (Case-B1 and B2) the overall deflection is very close to each other.

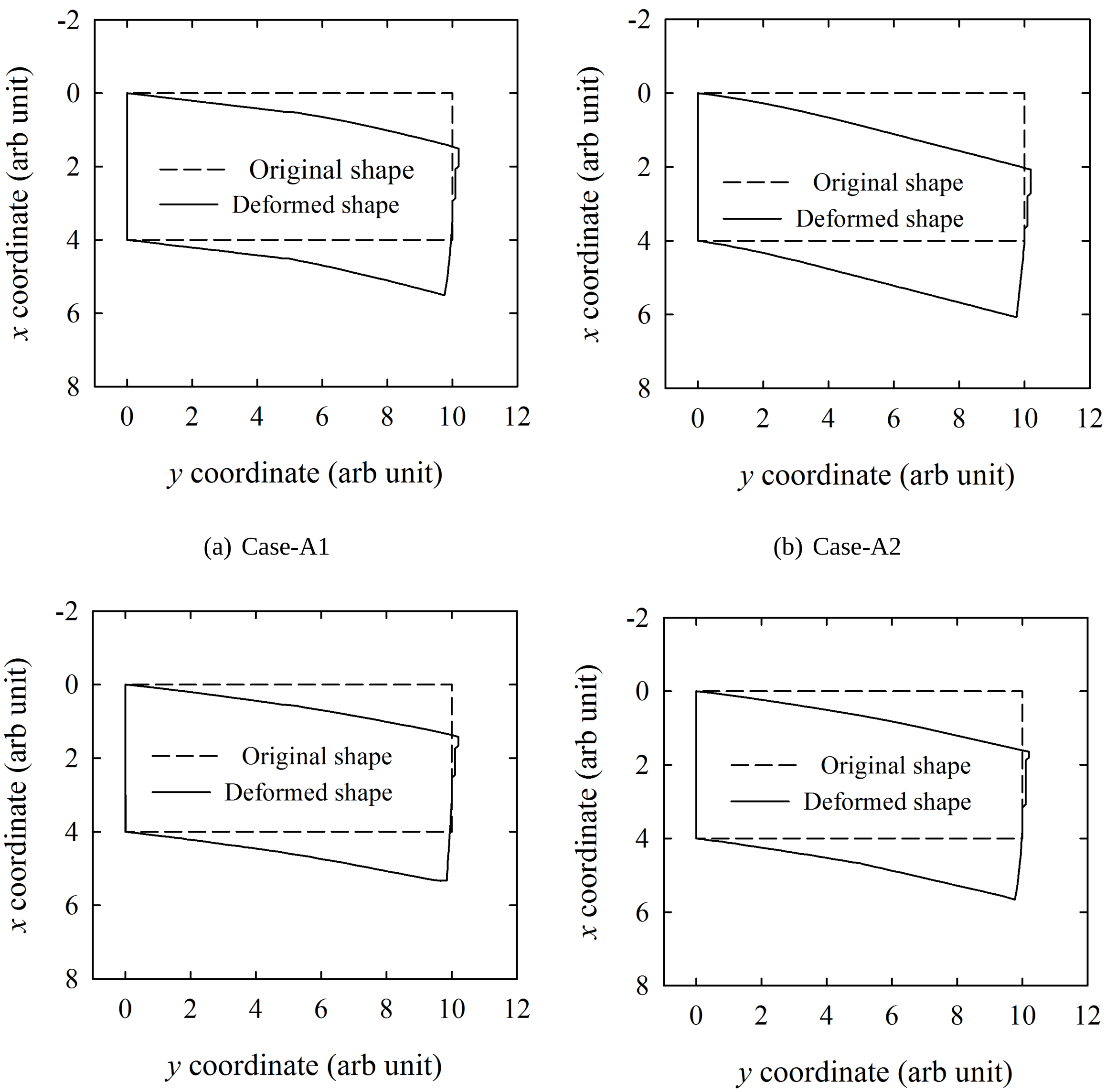

(a) Case-A1 (b) Case-A2

(c) Case-B1 (d) Case-B2

Figure 5.3: Deformed shapes of the laminated cantilever (magnification factor 300): (a) case-A1, (b) case-A2 (c) case-B1 (d) case-B2

5.3.3 Stresses at Different Plies

5.3.3.1 Distributions of the Lateral Stress Component

The stress distributions at different plies of the laminate are obtained here from the ψ-solution of the overall strains at the laminate mid-plane and the corresponding ply stiffness. The top and bottom stiffened surfaces of the laminated cantilever are found to be completely free from lateral stresses, which is in agreement with the respective physical condition of the surfaces. However, for sections immediate to the top and bottom bounding surfaces the lateral stress is found to assume its maximum value. Although the distribution of global strain components for different plies is same, the distributions of stresses at different plies are found to be different because of different stiffness of individual plies. Figure 5.4 shows the distribution of normalized lateral stress component at different lateral sections of the outer ply of the stiffened laminated cantilever for the four different symmetric and anti-symmetric arrangements of the discrete stiffeners. Here the boron-epoxy laminated composite with a stacking sequence of $(0^o - 90^o - 0^o)$ has been chosen for the demonstration of the results. The results show that the discrete stiffeners have significant influence on the distribution of lateral stresses in the individual plies, especially for the mid-span region of the cantilever, $0.4 \leq y/a \leq 0.6$. More specifically, the overall distribution of the lateral stress is found to affect by the arrangements of discrete stiffeners both in terms of magnitude as well as nature of variation. The symmetric arrangement of discrete stiffeners, Case-A1 and antisymmetric arrangement, Case-B1 has been identified to be the most critical in terms of lateral stresses, where the maximum intensity of stress is found to be more than four times the magnitude of applied loading. A comparison of the state of stresses at different plies of the laminate shows that the outer plies of the present stiffened cantilever are more critically stressed than the inner ply.

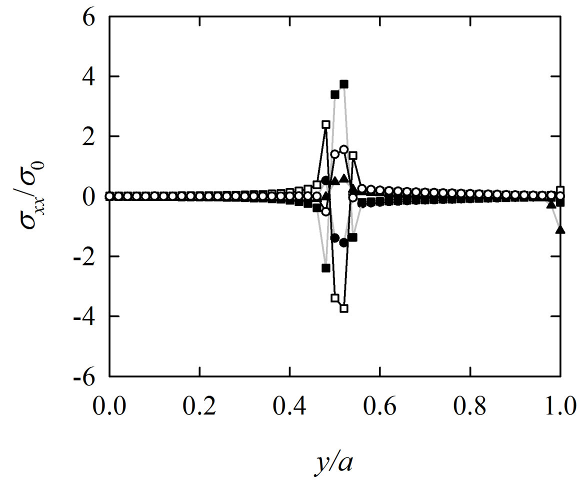

(a) Case-A1

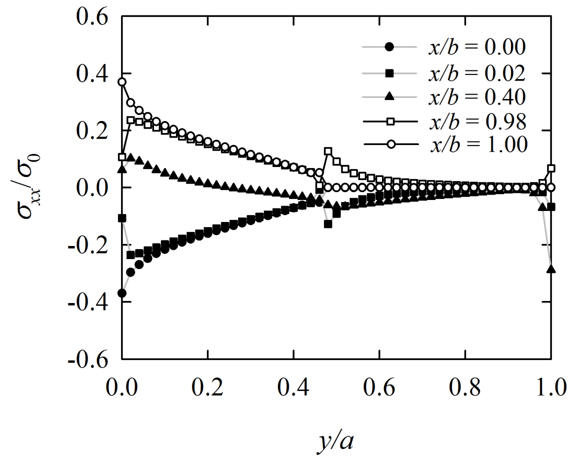

(b) Case-A2

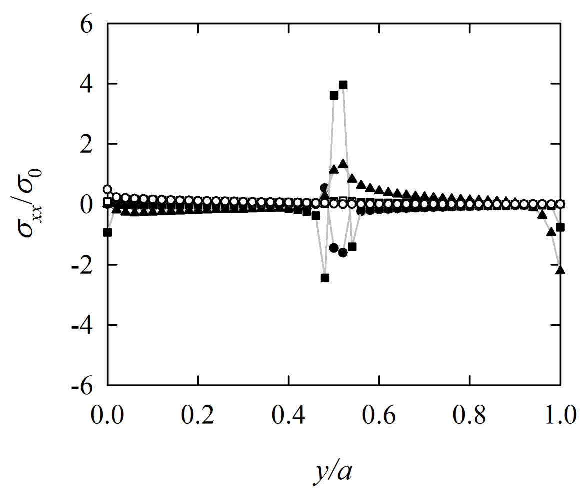

(c) Case-B1

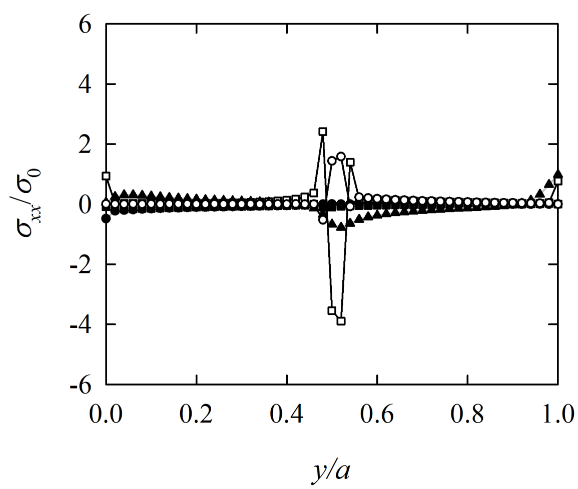

(d) Case-B2

Figure 5.4: Distribution of normalized lateral stress component at different lateral sections of the outer ply of stiffened laminated panels: (a) Case-A1, (b) Case-A2, (c) Case-B1, (d) Case-B2

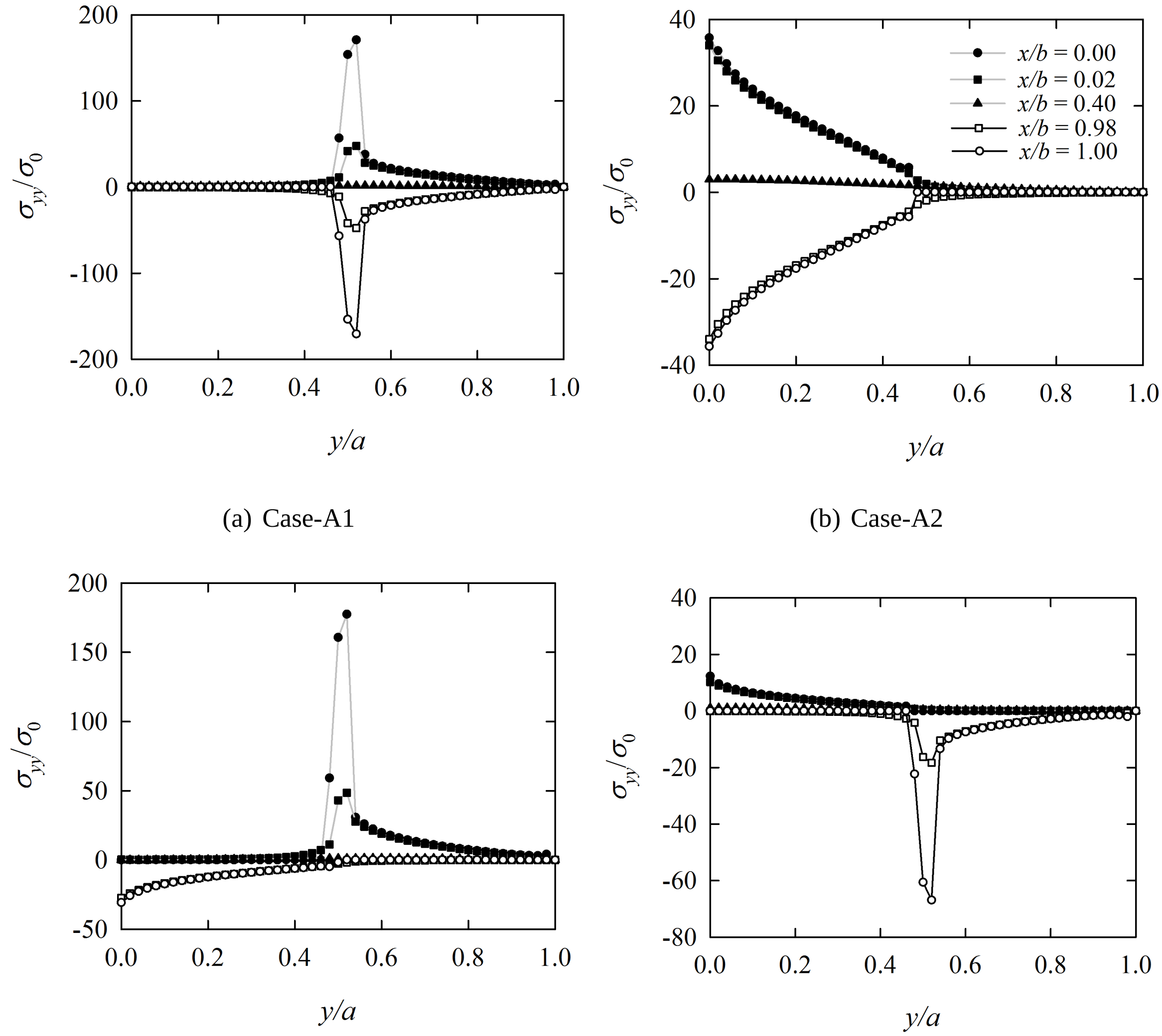

(a) Case-A1

(b) Case-A2

(c) Case-B1

(d) Case-B2

Figure 5.5: Distribution of normalized axial stress component at different lateral sections of the inner ply of stiffened laminated panels : (a) Case-A1, (b) Case-A2, (c) Case-B1, (d) Case-B2

5.3.3.2 Distributions of the Axial Stress Component

Figure 5.5 shows the distributions of axial stress component at different lateral sections of the inner ply of the same laminated cantilever as described for Figure 5.4, for different arrangements of discrete stiffeners. Likewise the case of lateral stress, the symmetric Case-A1 and antisymmetric Case-B1 has been identified to be the most critical in terms of the axial stress, among the four cases considered. Another important observation is, for the present locally stiffened cantilever under uniform shear, the axial stress component is identified to be the most dominating one compared to those of lateral and shear stress. The top and bottom longitudinal surfaces of the laminate as well as the individual plies are found to be the most critical sections in terms of this axial stress. Unlike the case of lateral stress component, the inner layer of the laminate is found to be more critically stressed in the axial direction, compared to the outer layers. Maximum stresses are found to occur around the mid-span region of the cantilever, that is, $0.4 \leq y/a \leq 0.6$. As far as the axial stress is concerned, the left supporting end is not free from the stress, except that of the symmetric Case-A1. Among the four cases considered, the left supporting end of the symmetric Case-A2, in which the discrete stiffeners are not connected with the end, is found to assume highest level of axial stress, see Figure 5.5(b).

5.3.3.3 Distributions of the Shear Stress Component

The distributions of shear stress at different transverse sections of the laminated cantilever are shown in figure 5.6 for all four cases of interest. For all the cases of stiffener arrangements, maximum shearing stress is found to occur along the stiffened surfaces of the cantilever. More specifically, when the stiffener are attached with the fixed end, the distributions of shear stress over the local stiffeners are found to assume somewhat similar to that of a quadratic variation having its peak value at $y/a = 0.5$. As expected the stiffener-free regions of the top and bottom surfaces of the cantilever are found to be completely free from shearing stresses. For the symmetric arrangements, the distribution of shear stress along the top and

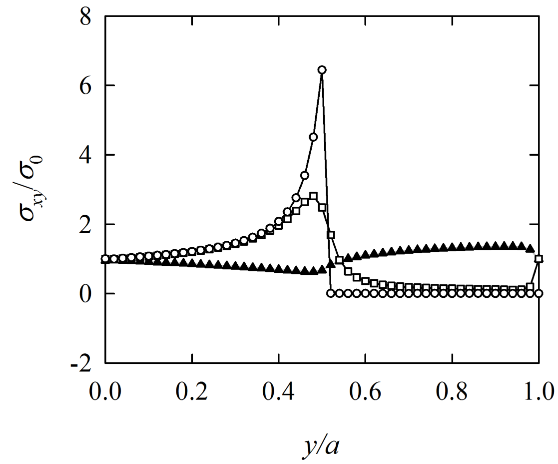

(a) Case-A1

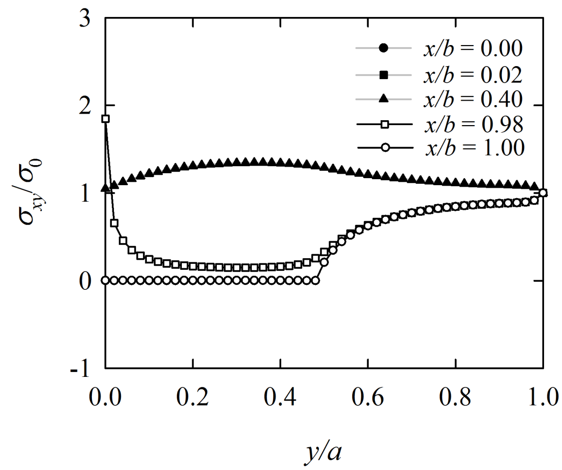

(b) Case-A2

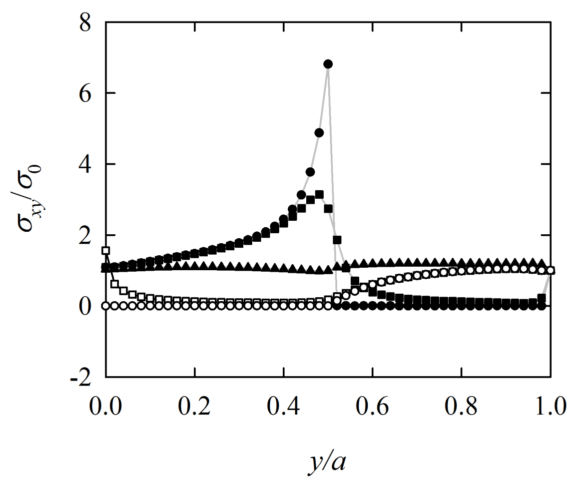

(c) Case-B1

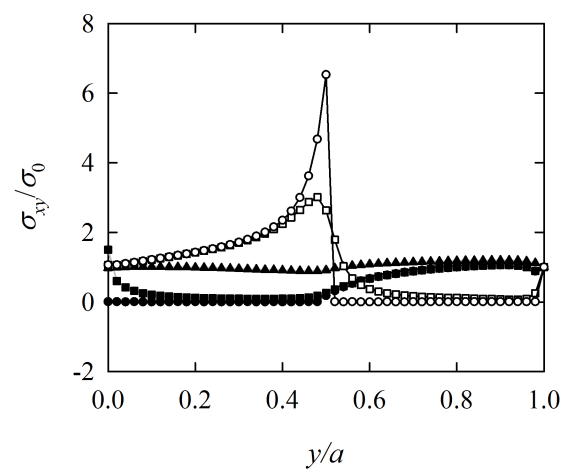

(d) Case-B2

Figure 5.6: Distribution of normalized shearing stress component at different lateral sections of the stiffened laminated panels : (a) Case A-1, (b) Case A-2, (c) Case B-1, (d) Case B-2

bottom stiffened surfaces are found to coincide with each other, which are however not the case for the anti-symmetric arrangements. For anti-symmetric arrangements of the stiffeners, stiffened sections connected to the left supporting end of the cantilever are identified to be more critical in terms of shear stresses compared to those connected with the right lateral end. Among the four cases considered, the symmetric arrangements of discrete stiffeners Case-A2 give the and lowest level of shear stress. Other arrangements of stiffener give nearly seven times higher magnitude than the applied stress.

5.3.4 Effect of Stacking Sequence

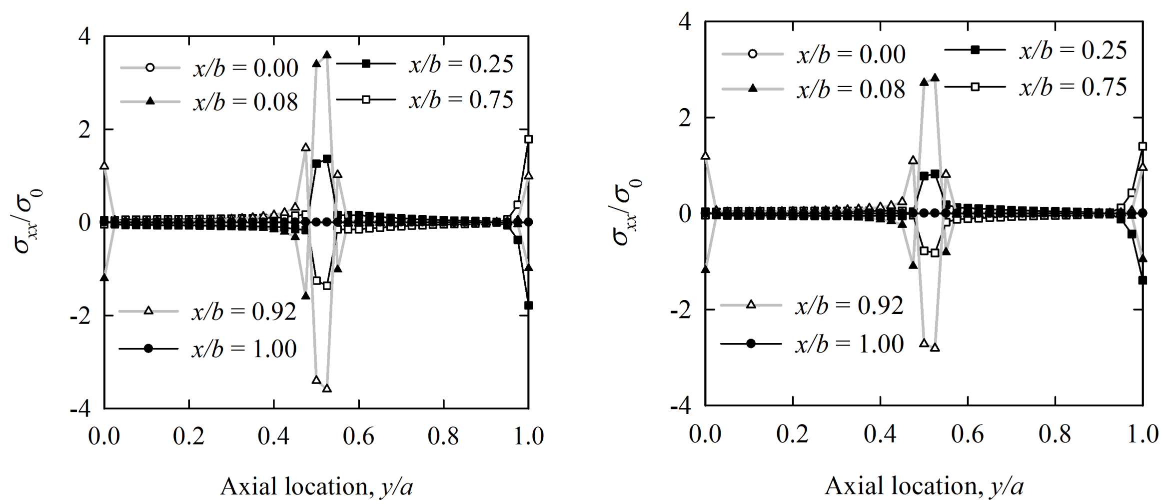

(a) $(0^o - 90^o - 0^o)$ (b) $(90^o - 0^o - 90^o)$

Figure 5.7: Effect of stacking sequence on the overall state of lateral stresses at different sections of the laminated panel (Case-A1): (a) $(0^o - 90^o - 0^o)$ and (b) $(90^o - 0^o - 90^o)$

Figures 5.7, 5.8 and 5.9 illustrates the effect of stacking sequence on the overall state of stresses at different sections of the laminated cantilever. In order to demonstrate the effect, two different stacking sequences of cross-ply laminate, namely $0^o - 90^o - 0^o$ and $90^o - 0^o - 90^o$ are considered for the symmetric case-A1. The present displacement-potential

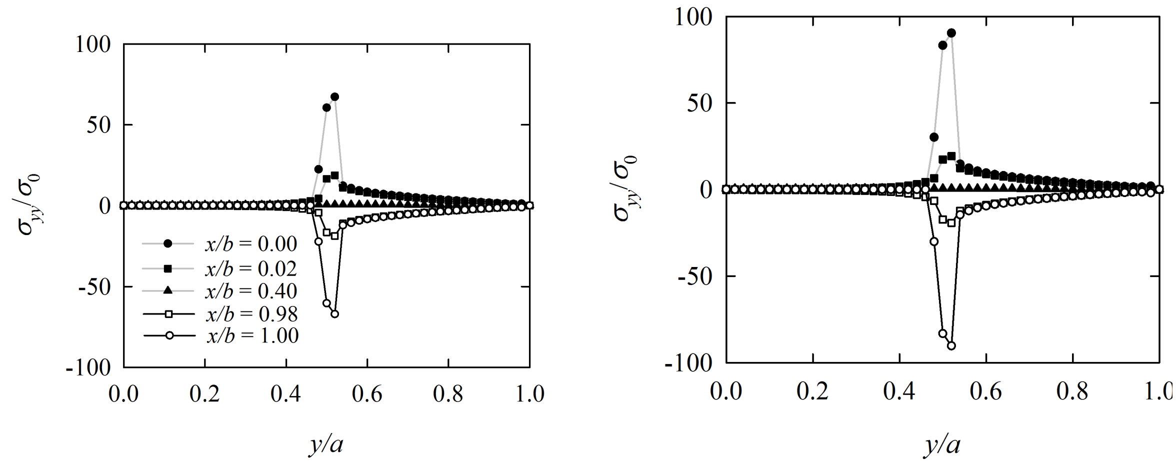

(a) $(0^o - 90^o - 0^o)$ (b) $(90^o - 0^o - 90^o)$

Figure 5.8: Effect of stacking sequence on the overall state of axial stresses at different sections of the laminated panel (Case-A1): (a) $(0^o - 90^o - 0^o)$ and (b) $(90^o - 0^o - 90^o)$

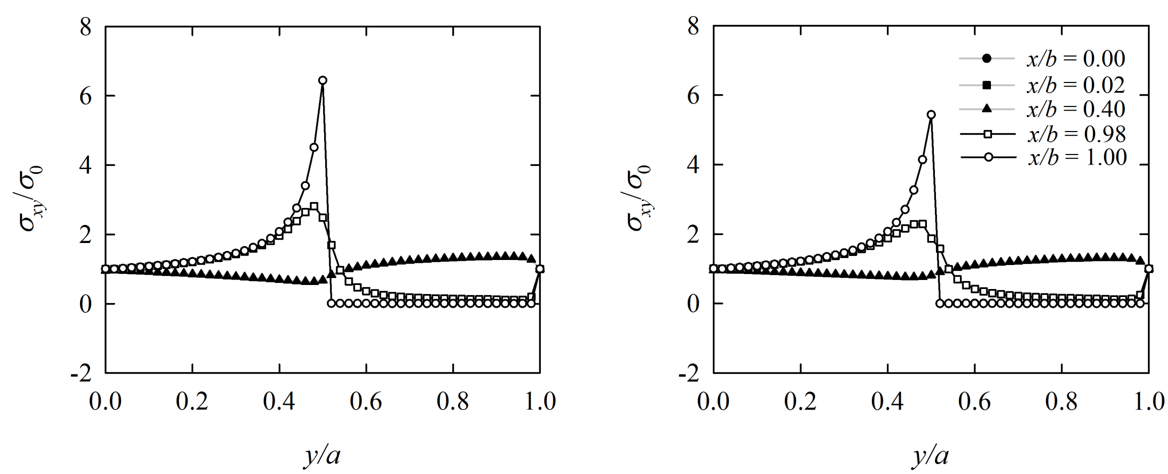

(a) $(0^o - 90^o - 0^o)$ (b) $(90^o - 0^o - 90^o)$

Figure 5.9: Effect of stacking sequence on the overall state of shear stresses at different sections of the laminated panel (Case-A1): (a) $(0^o - 90^o - 0^o)$ and (b) $(90^o - 0^o - 90^o)$

analysis (DPM) shows that the change in stacking sequence causes no change in the overall nature of variation of stresses in the laminated cantilever, even though the stiffness along the coordinate axes change with the change of stacking sequence of the relevant plies. However, the magnitude of all the stress components is found to vary quite significantly when the stacking sequence is changed from one kind to the other. Another interesting observation is that the major change in the state of stresses due to stacking sequence takes place around the mid-span position of the cantilever $(y/a = 0.5)$, which is basically the junction point of stiffener and stiffener-free regions on the top and bottom bounding surfaces. A comparative analysis of stresses shows that the axial stress component (σ_{yy}) is influenced most significantly by the change of stacking sequence, compared to the other two components of stress. The maximum lateral stress developed is found to be higher for the laminate in which the stiffness is higher in lateral direction ($0^o - 90^o - 0^o$ laminate). Likewise the case of lateral stress, the maximum axial stress is found to assume higher value when the stiffness is higher in the axial direction ($90^o - 0^o - 90^o$ laminate). The magnitude of shear stress along the stiffened surfaces is found to take higher value when the corresponding stiffness is higher along $x-$ axis, i.e., $(0^o - 90^o - 0^o)$ laminate, compared to that of $(90^o - 0^o - 90^o)$ laminate. A quantitative analysis of the stress components reveals that the maximum lateral stress in $(0^o - 90^o - 0^o)$ laminate is more than 15% higher than that of $(90^o - 0^o - 90^o)$ laminate, while the maximum axial stress associated with the $(90^o - 0^o - 90^o)$ laminate assumes a value nearly 24% higher than that of $(0^o - 90^o - 0^o)$ laminate. The maximum shear stress at the stiffened regions of the $(0^o - 90^o - 0^o)$ laminate is found to be nearly 14% higher than that associated with the $(90^o - 0^o - 90^o)$ laminate.

5.3.5 Effect of stiffening length

This section describes the effect of stiffening length on the distribution of the different stress components at a particular section of the laminated cantilever. The symmetric arrangement of stiffeners namely, Case-A1 has been chosen for the Boron-epoxy laminate $(0^o - 90^o - 0^o)$

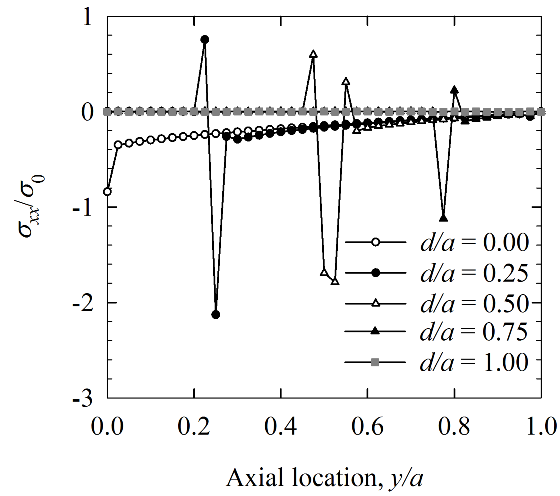

(a) Effect of stiffening length on the lateral stresses.

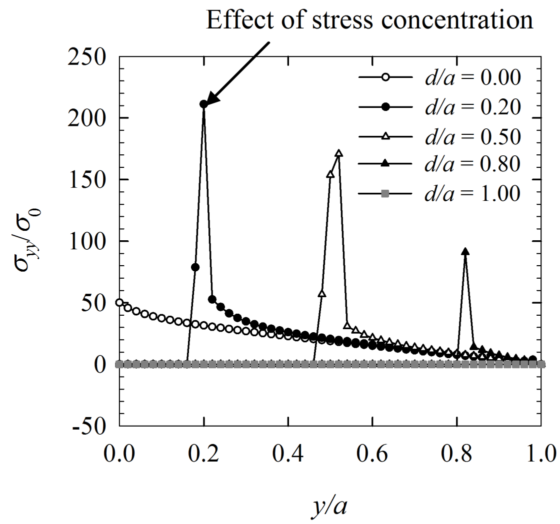

(b) Effect of stiffening length on the axial stresses.

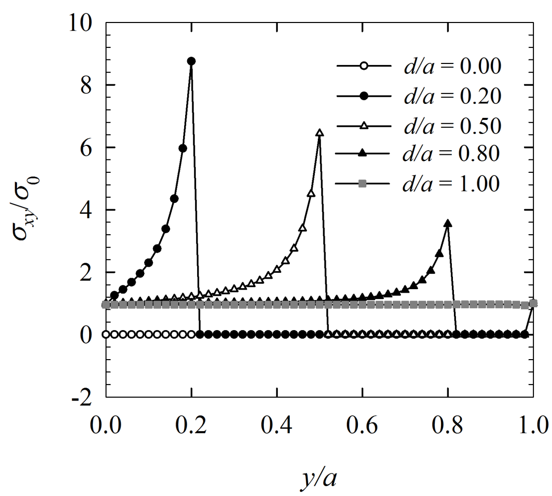

(c) Effect of stiffening length on the shear stresses.

Figure 5.10: Effect of stiffening length on the stresses along the top surface of the laminated panel (Case-A1): (a) lateral stress in outer ply, (b) bending stress in inner ply, (c) shear stress.

to investigate the above mentioned effect. Solutions are obtained for a number of normalized length of the stiffeners (d/a), which includes the case of continuous full-length stiffener as well as stiffener-free laminates. Figure 5.10(a) presents the distribution of lateral stress along the top stiffened surface of the outer layer of the laminated cantilever for different stiffening lengths. In general, the lateral stress increases with the decrease of stiffening length. For the stiffened region, the surface is free from lateral stress and for the stiffener-free regions, distribution of lateral stress coincides with corresponding distribution of stiffener-free cantilever. The increase in stress is mainly observed around the region of terminating points of the discrete stiffeners on the surfaces. Likewise the case of lateral stress, axial stress is also found to increase with the decrease of the stiffening length, which is shown in Figure 5.10(b) for the case of the inner ply of the laminate. However the increase in axial stress due to decrease of stiffener length is much more prominent in terms of magnitude, in comparison with that of lateral stress. As appears from Figure 5.10, locally stiffened cantilevers are more critical in terms of axial stress compared to the cases of full-length continuous stiffener and stiffener-free cantilevers.

The comparison of distributions of shear stress along top and bottom boundaries of the cantilever with different d/a ratio is illustrated in Figure 5.10(c). The shearing stress along the stiffened surface is also found to increase with the decrease of d/a ratio. The top and bottom boundaries of the laminated cantilever are found to be completely free from shear stresses for the case of no stiffener $(d/a = 0)$, but a uniform distribution of the stress, equal to the magnitude of the applied stress, is encountered for the case of full-length continuous stiffener. The increase in shear stress is observed to be a gradual phenomenon over the entire length of the local stiffeners, however, those associated with the normal stresses are identified to be a local phenomenon mainly around the regions of the terminating points of the discrete stiffeners.

It has seen from the figure 5.10, with the increase of stiffening length, stress concentration gradually decreases. To minimize the material cost with the effect of stress concentration, concentration of stress should not be higher. To solve the problem, stiffening length can be increased. Another way, optimized stiffening length can be used, such a way that concentration of stress would not cross the yield strength at the right end of the stiffener.

5.3.6 Effect of fiber material

Figure 5.11 presents the comparative analysis of the state of stresses set up in the cross-ply laminated cantilever due to the change of fiber material. Here a number of commonly used fiber materials, namely, boron, glass, carbon (graphite) etc. are considered for the same matrix material epoxy. In order to investigate the effect, the laminated cantilever with symmetric local stiffeners (Case-A1) with stacking sequence $(0^o - 90^o - 0^o)$ is considered. It is noted that to illustrate the effect of fiber material, (41×25) nodes have been considered. In general, the effect of fiber material on the components of stress is found to be quite substantial in terms of magnitude. An analysis of overall distributions of stress components shows that the state of stress in the three laminates differs mainly in terms of its magnitude, especially around the region of the terminating point of discrete stiffeners $(y/a = 0.5)$, while no remarkable change in the nature of variation is observed. Since all the components of stress are found to assume its maximum value around the terminating point of the stiffeners $(y/a = 0.5)$ on the top and bottom boundary surfaces, the magnitude of these critical stresses are compared in Figure 5.11 for the three laminates which differ only in terms of their fiber material. From Figure 5.11, it is evident that the lateral and shear stress components assume their highest and lowest values for Glass/epoxy and Boron/epoxy laminates, respectively, while that of Graphite/epoxy remains in between them. On the other hand, the results of axial stress component show a different picture, that is, the Boron/epoxy laminate is identified to be the most critical in terms of axial stress, while the Glass/epoxy laminate assumes lowest level of axial stress among the three. Moreover, when the results of the present comparative investigation are analyzed in the perspective of mechanical properties of the three composite materials (Table 5.2), it is observed that, lateral and shear stresses in the present stiffened

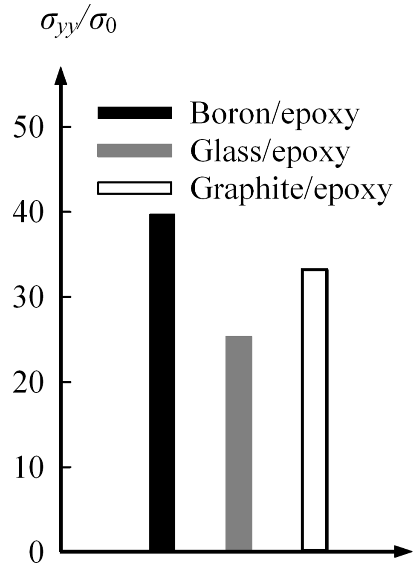

(a) Axial stress component at $x/b = 0$, $y/a = 0.5$.

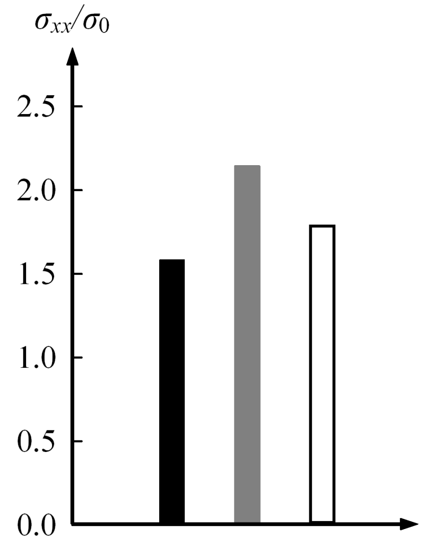

(b) Lateral stress component at $x/b = 0.04$, $y/a = 0.5$.

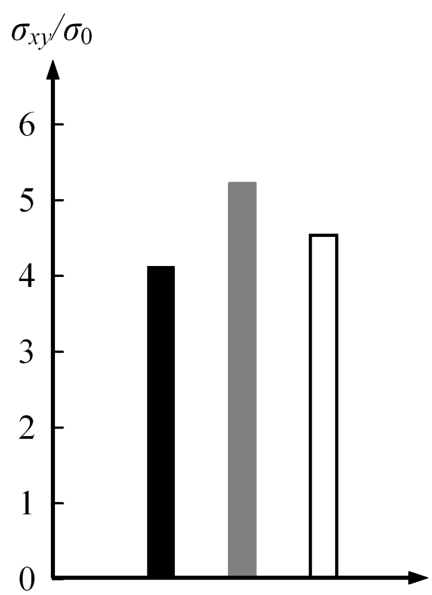

(c) Shear stress component at $x/b = 0$, $y/a = 0.5$.

Figure 5.11: Effect of fiber material on the overall state of stresses at different locations of the laminated cantilever (Case-A1).

cantilever assume higher value for the case of fiber which leads to lower overall stiffness of the laminate, and lower value for higher laminate stiffness. The corresponding maximum axial stress is however found to assume higher value for the laminate having higher stiffness and vise versa. A quantitative analysis of the results of Figure 5.11 shows that, among the three components of stress, the axial stress component is affected most seriously in the case of present stiffened cantilever due to the change of fiber material that causes a change in stiffness of the laminate.

5.4 Conclusions

The present chapter has introduced a modification to the usual approach of analyzing boundary-value stress problems of laminated composites. An investigation of the stress field of a laminated composite cantilever subjected to symmetric and anti-symmetric local stiffeners has been carried out using an efficient computational algorithm based on a new scalar potential of displacements.

No appropriate analytical approach is available in the literature that can provide explicit information about the actual stresses, especially at the critical regions of supports and local stiffeners in laminated structures. Even the standard computational approaches have been verified to be inadequate to predict the actual state of stresses accurately (see section 8.4), especially at the bounding surfaces, whether it is subjected to restraints or stiffeners or even free from external loading. The critical stresses in a discretely stiffened laminated cantilever are found to be developed around the regions of stiffeners, which have been analyzed in comparison with the corresponding standard solutions in an attempt to verify the soundness as well as superiority of the present displacement-potential based finite-difference computational scheme. The potential of the method is also utilized to investigate a number of practical issues associated with the flexural behavior of a cross-ply laminated cantilever under shear loading.

CHAPTER
6

Laminated Panel Subjected to Discrete Periodic Stiffeners

6.1 Introduction

Elastostatic response of a laminated composite panel is analyzed under the influence of discrete periodic stiffeners. The discrete axial stiffeners are considered at the opposing longitudinal edges of a cross-ply laminated panel subjected to an nonuniform axial tension and shear loading. An efficient computational scheme is developed based on a new potential function to analyze the present mixed-boundary-value stress problem of laminated composites. Results are claimed to be highly accurate and reasonable, which are however found to be in significant contrast with those of continuous as well as stiffener-free panels.

6.2 Problem Statement

A uniform rectangular cantilever of cross-ply laminated composite is considered for the present analysis. The geometry and loading of a laminated composite panel subjected to an nonuniform axial loading is shown in Fig. 6.1. The length, width and thickness of the panel are represented by a, b and h, respectively. The laminate is assumed to be consisted of n number of plies, in which the ply thickness of individual lamina is kept constant. The symmetric cross-ply laminated panel is composed of seven layers of identical thickness, the stacking sequence of which can be expressed as $[90/0/90/\bar{0}]_s$. The left-hand lateral end of the cantilever is assumed to be rigidly fixed and the right-hand lateral end is subjected to a nonuniform loading (see Fig. 6.1). Two different loading, nonuniform axial loading and nonuniform shear loading have been considered to analyze the present problem. The two opposing longitudinal surfaces are considered to be locally stiffened by attaching rigid discrete periodic axial stiffeners for part of the boundary surfaces (stiffener length d). The three-dimensional laminated panel is analyzed here considering it as a plane stress problem. The thickness of each of k-th number of ply is expressed as h_k and thus the total laminate thickness becomes $h = nh_k$.

The left lateral end of the panel is kept rigidly fixed. The discrete periodic axial stiffeners are assumed to be situated along the two opposing longitudinal edges of the panel. The right lateral end of the panel is subjected to an nonuniform axial tensile loading (parabolic distribution) of maximum intensity $\sigma_0 = 3$ MPa.

6.3 Boundary Conditions

The physical conditions to be satisfied along the different boundary segments of the cantilever can be expressed mathematically as follows:

1. The supporting lateral end (boundary AB) is rigidly fixed. Both the normal and tangential components of displacement are assumed to be zero here, that is,

$$u_x(x, 0) = 0 \quad \text{and} \quad u_y(x, 0) = 0 \quad [0 \leq x \leq b]$$

2. The right-hand lateral end (boundary CD) of the cantilever is the loaded boundary. Two different parabolic loading conditions have been considered with maximum intensity $\sigma_0 = 3$ MPa on the right lateral boundary for the same laminated composite.

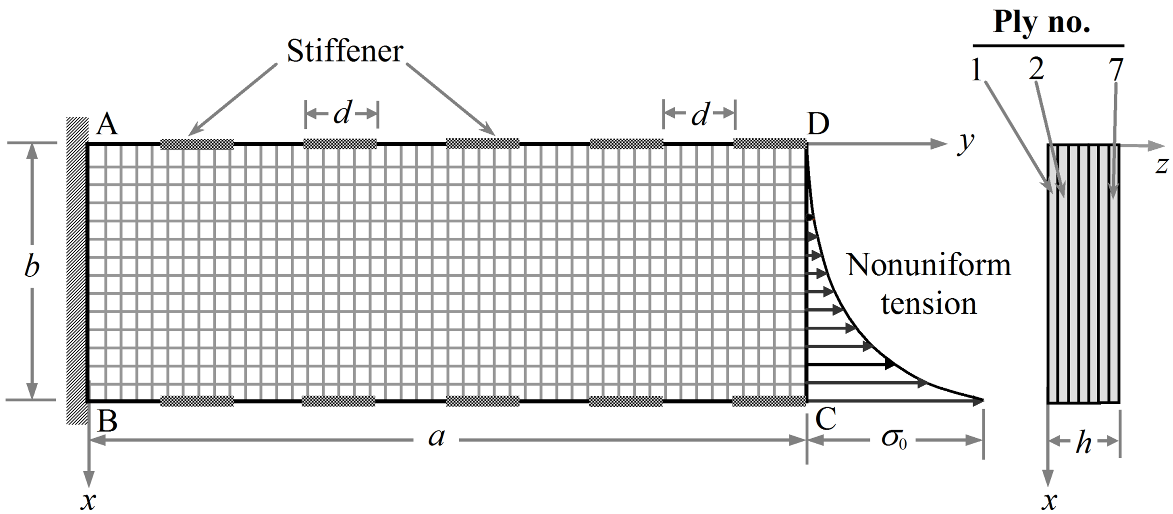

(a) Nonuniform axial loading.

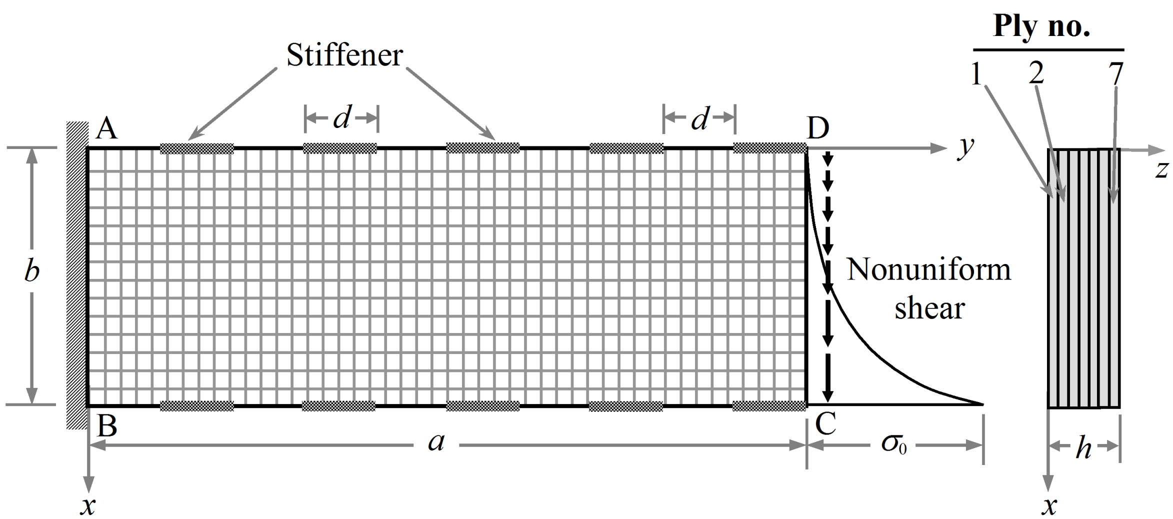

(b) Nonuniform shear loading.

Figure 6.1: Model of a laminated panel with periodic stiffeners subjected to nonuniform (a) axial loading and (b) shear loading.

(a) For the case of nonuniform axial loading, the associated shear stress component is assumed to be zero at right lateral end of the panel is simulated by

$$\sigma_{yy}(x,a) = \sigma_0(x/b)^2 \quad \text{and} \quad \sigma_{xy}(x,a) = 0 \quad [0 \leq x \leq b]$$

where, the axial loading varies following a parabolic law.

(b) For the case of nonuniform shear loading, the associated axial stress component is assumed to be zero at right lateral end of the panel is simulated by

$$\sigma_{yy}(x,a) = 0 \quad \text{and} \quad \sigma_{xy}(x,a) = \sigma_0(x/b)^2 \quad [0 \leq x \leq b]$$

where, the transverse shear loading varies following a parabolic law.

3. The two opposing longitudinal surfaces, AD and BC, are assumed to be stiffened locally, that is, part of the boundaries is subjected to axial stiffeners and part of them are free. In order to model the physical condition of the axial stiffeners, the tangential strain along the stiffener is restrained, while the section is kept free from any external loading. Referring to Fig. 6.1, the mathematical modeling of the physical conditions associated with the free and stiffened sections of the boundaries AD and BC, is realized as follows:

Free region: $\sigma_{xx}[(0,1),y] = 0 \quad \text{and} \quad \sigma_{xy}[(0,1),y] = 0$

Stiffened region: $\sigma_{xx}[(0,1),y] = 0 \quad \text{and} \quad \varepsilon_{yy}[(0,1),y] = 0$

Numerical modeling of the boundary conditions has been discussed in Table 6.1 and 6.2

Table 6.1: Numerical modeling of the boundary conditions for different boundary sections of the panels under nonuniform axial loading. (see Fig. 6.1).

Boundary edges	Boundary segments	Given and used boundary conditions	Correspondence between mesh points and given boundary conditions	
			Mesh point on the physical boundary	Mesh point on the imaginary boundary
Lateral edges	Fixed end	$u_x(x,0)=0$ $u_y(x,0)=0$	$u_x(x,0)=0$	$u_y(x,0)=0$
	Loaded end	$\sigma_{xy}(x,a)=0$ $\sigma_{yy}(x,a)=\sigma_0(x/b)^2$	$\sigma_{xy}(x,a)=0$	$\sigma_{yy}(x,a)=$ $\sigma_0(x/b)^2$
Axial edges	Stiffening region	$\varepsilon_{yy}[(0,b),y]=0$ $\sigma_{xx}[(0,b),y]=0$	$\sigma_{xx}[(0,b),y]=0$	$\varepsilon_{yy}[(0,b),y]=0$
	Free region	$\sigma_{xx}[(0,b),y]=0$ $\sigma_{xy}[(0,b),y]=0$	$\sigma_{xx}[(0,b),y]=0$	$\sigma_{xy}[(0,b),y]=0$

6.4 Results and Discussions

The results of the analysis of stresses for the laminated cantilever subjected to periodic local stiffeners along the two opposing longitudinal surfaces, as shown in Figure 6.1, are presented in this section. In this section, results of the numerical solution of the laminated panel having an aspect ratio (a/b) of 2.5 are presented. The results are presented distributions of the axial, displacements, deformed shape as well as distribution of stress components of interest. In all cases, stresses are normalized with respect to the maximum intensity of applied shear loading, σ_0 (see Fig. 6.1), the magnitude of which is arbitrarily assumed to be 3 MPa. The details of the boundary conditions as used to obtain the present FD solutions are already listed in Table 6.1 and 6.2. Seven laminae $(n = 7)$ of unidirectional composite material with stacking sequences of $[90/0/90/\bar{0}]_s$ are assumed to form symmetric cross-ply lami-

Table 6.2: Numerical modeling of the boundary conditions for different boundary sections of the panels under nonuniform shear loading. (see Fig. 6.1).

Boundary edges	Boundary segments	Given and used boundary conditions	Correspondence between mesh points and given boundary conditions	
			Mesh point on the physical boundary	Mesh point on the imaginary boundary
Lateral edges	Fixed end	$u_x(x,0)=0$ $u_y(x,0)=0$	$u_x(x,0)=0$	$u_y(x,0)=0$
	Loaded end	$\sigma_{xy}(x,a)=\sigma_0(x/b)^2$ $\sigma_{yy}(x,a)=0$	$\sigma_{xy}(x,a)=$ $\sigma_0(x/b)^2$	$\sigma_{yy}(x,a)=0$
Axial edges	Stiffening region	$\varepsilon_{yy}[(0,b),y]=0$ $\sigma_{xx}[(0,b),y]=0$	$\sigma_{xx}[(0,b),y]=0$	$\varepsilon_{yy}[(0,b),y]=0$
	Free region	$\sigma_{xx}[(0,b),y]=0$ $\sigma_{xy}[(0,b),y]=0$	$\sigma_{xx}[(0,b),y]=0$	$\sigma_{xy}[(0,b),y]=0$

nates for the cantilever. Although the method can be applied to any composite material, the boron/epoxy composite is chosen as an example in present study. The effective mechanical properties of boron/epoxy laminate are listed in Table 5.2. The thickness of individual plies is kept constant, which is 0.5 mm. All the results presented here correspond to a cantilever of geometrical aspect ratio, $a/b = 2.5$. For most of the results, the length of the discrete stiffener is kept constant and is equal to $d = a/10$, The FD mesh-network used to model the present cantilever $(a/b = 2.5)$ contains nodal points (51×51) in the direction of x and y, respectively.

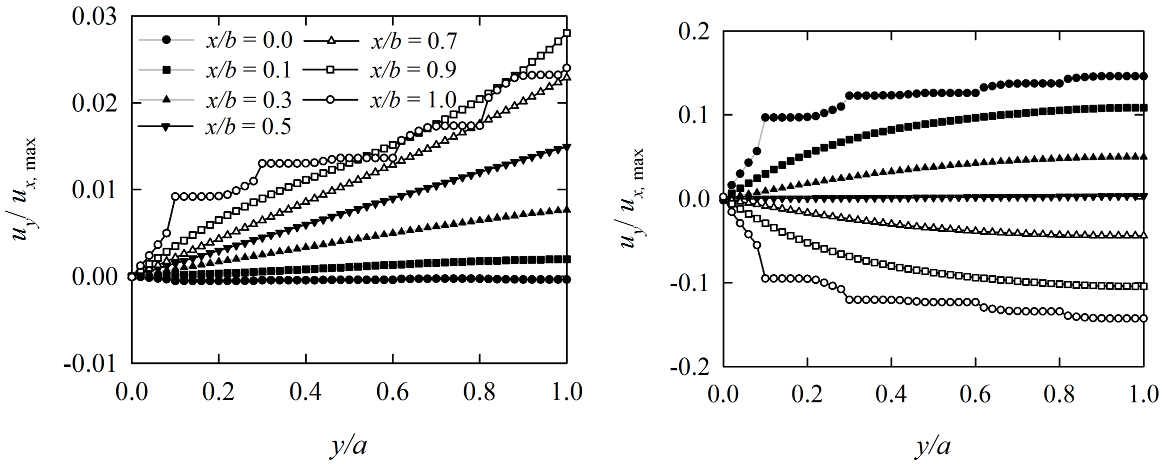

(a) Nonuniform axial loading. (b) Nonuniform shear loading.

Figure 6.2: Distributions of normalized axial displacement of laminated panel subjected to nonuniform (a) axial loading and (b) shear loading.

6.4.1 Distributions of Axial Displacements

Figure 6.2 illustrates the distributions of normalized axial displacements of the laminated panel subjected to nonuniform loading. It is noted that axial displacement is normalized with the maximum lateral displacement at the right lateral end of $[90/0/90/\bar{0}]_s$ stiffener free laminated composite subjected to same nonuniform shear loading that have been applied for the present problem. It has shown from figure that arrangement of periodic axial stiffeners have great influenced on the distributions of axial displacements. Again, distributions of axial displacements is also influenced by the change of loading as shown in Figures 6.2(a) and 6.2(b). Figure 6.2(a) shows variation of the distributions of axial stress at top boundary is very small and give negative magnitude. At top boundary, negligible fluctuation of displacements has been found by the attaching of periodic stiffener. At the bottom boundary, nonuniform load as well as stiffeners have significant influence on the distributions. The distribution of axial displacements increase from left to right lateral end, but at the stiffening region, axial displacements are constant. Figure 6.2(b) shows the almost symmetric distributions with respect to $y/a = 0.5$ of the axial displacements though the nonuniform shear has been applied at the right lateral end. At the stiffening region, axial displacements are constant at top and bottom boundary. Displacements are much higher under shear loading compare to axial loading for same laminate as shown in Figures 6.2.

6.4.2 Distributions of Axial Stresses for Laminate

To illustrate the distributions of axial stresses, two different sections have been considered: (i) under stiffened sections and (ii) Stiffener free sections along $x-$ direction. All the graphs have been presented along $x-$ axis. Figure 6.3 illustrates the distributions of normalized axial stress components at different stiffened axial sections of the laminated panel under the influence of nonuniform (a) axial loading and (b) shear loading. It is observed from Figure 6.3(a) that magnitude of the axial stress is found to increase as we go from the top to bottom longitudinal end. Highest magnitude of axial stress develops at the right stiffened region $(y/a = 0.94)$ of the laminated cantilever under axial loading. Both the two opposing longitudinal stiffened surfaces of the panel $(x/b = 0, 1)$ are found to be completely free from axial stresses. The maximum intensity of the axial stress in the laminated panel is found to assume a value as high as 0.73 times of σ_0, the location of which is at the region under stiffeners near the right lateral end (loaded end). Figure 6.3(b) shows the distributions of the axial stress components under stiffened sections of the panel under the influence of nonuniform shear stress. Though the stiffeners are present, both the two opposing longitudinal stiffened surfaces of the panel $(x/b = 0, 1)$ are found to be completely free from axial stresses. Maximum intensity of the axial stress is found to develop at section $y/a = 0.14$, which is under the stiffener near fixed end. Magnitude of distributions decrease with the increase of axial sections y/a.

Figure 6.4 illustrates the distributions of normalized axial stress components at different stiffener free axial sections of laminated panel under the influence of nonuniform (a) axial loading and (b) shear loading. It is observed from Figure 6.4(a) that magnitude of the axial

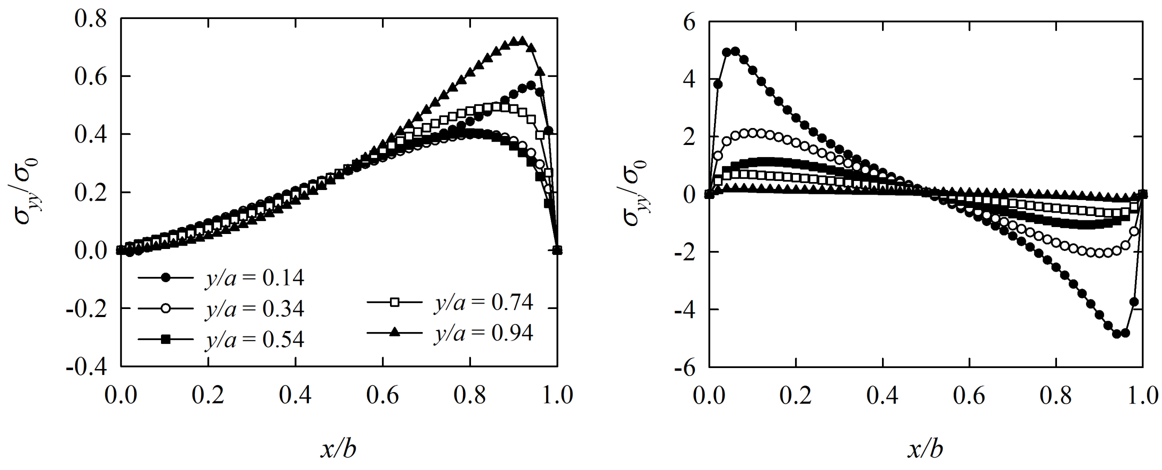

(a) Nonuniform axial loading.

(b) Nonuniform shear loading.

Figure 6.3: Distributions of axial stress components under stiffened sections of laminated panel subjected to nonuniform (a) axial loading and (b) shear loading.

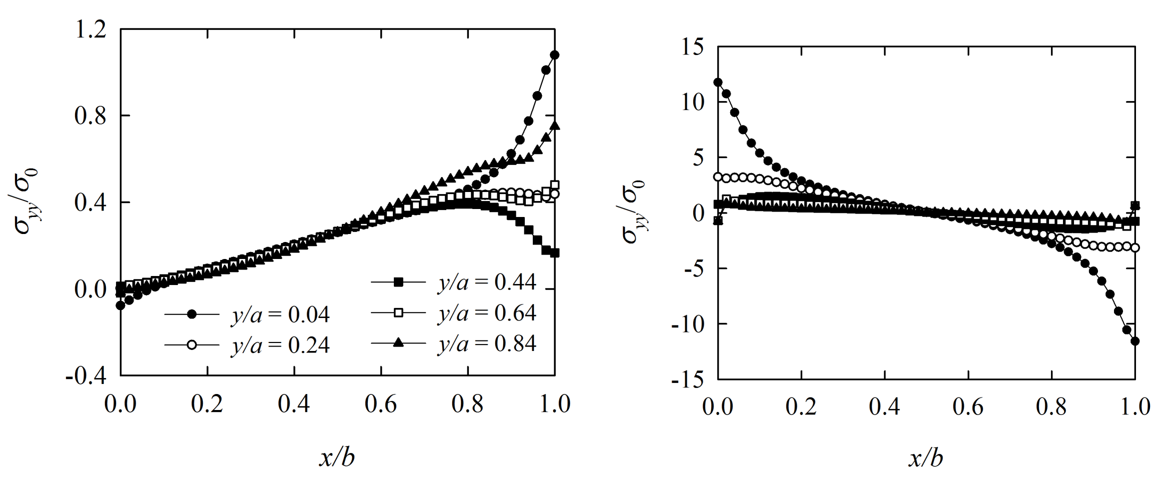

(a) Nonuniform axial loading.

(b) Nonuniform shear loading.

Figure 6.4: Distributions of axial stress components at stiffener free sections of laminated panel subjected to nonuniform (a) axial loading and (b) shear loading.

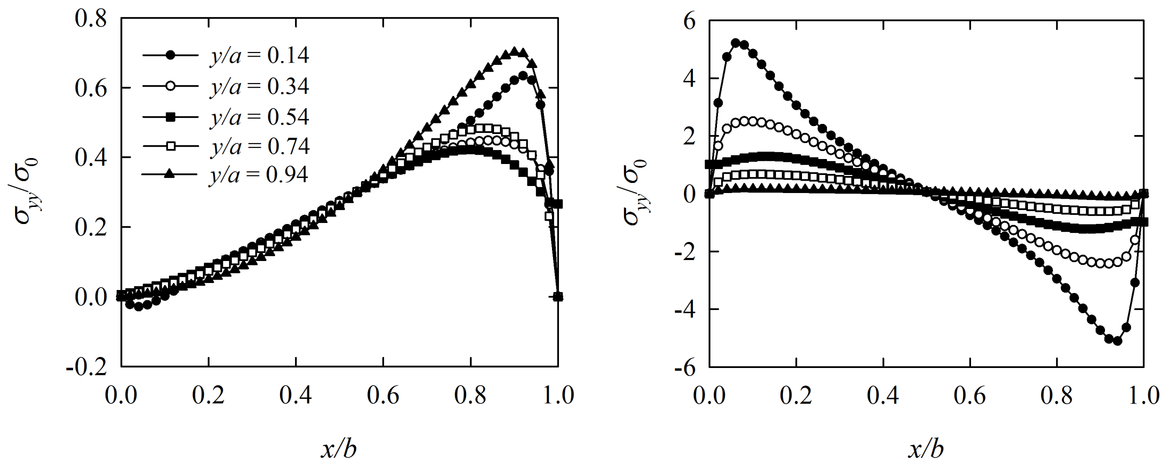

(a) Nonuniform axial loading.

(b) Nonuniform shear loading.

Figure 6.5: Distributions of axial stress components under stiffened sections of arbitrarily placed stiffened laminated panel subjected to nonuniform (a) axial loading and (b) shear loading.

stress is found to increase with the increase of distance from the top to bottom longitudinal end. Maximum magnitude of axial stresses develop at the stiffener free section $(y/a = 0.04)$, near fixed end of the laminated cantilever under axial loading. Like the stiffened sections, magnitude of axial stresses of the two opposing longitudinal free surfaces of the panel are not zero. Maximum magnitude of stress has been found at the bottom boundary. From the left and right boundary, magnitude of stress distributions decrease at bottom boundary. Figure 6.4(b) shows the distributions of the axial stress components at stiffener free sections of the panel under the influence of nonuniform shear. Magnitude of axial stresses of the two opposing longitudinal free surfaces of the panel is not zero. But maximum magnitude of all distributions have been found at top and bottom boundary. Magnitude of distributions decrease with the increase of axial sections y/a. Maximum magnitude has been found at section $y/a = 0.04$ near fixed end. Though nonuniform load has been applied, distributions are antisymmetric with respect to $x/b = 0.5$. Magnitude of distributions of the axial stresses under the nonuniform shear loading are much higher compared to nonuniform axial loading.

Figure 6.5 shows the distributions of axial stress components under stiffened sections of arbitrarily placed stiffened laminated panel subjected to nonuniform (a) axial loading and (b) shear loading. In this case, stiffeners are arbitrarily attached along the longitudinal edges of laminated cantilever. It has been seen from figures 6.3 and 6.5 shows similar distributions have been found though stiffeners have not placed at the same position.

6.4.3 Distributions of Axial Stresses for Different Plies

Figures 6.6 and 6.7 illustrate the distributions of the axial stresses under stiffener and stiffener free sections of $\theta = 90^o$ ply respectively. It has seen from Figures 6.6 and 6.7, exactly similar distributions of axial stresses for both under stiffener and stiffener free sections have been found for $\theta = 90^o$ ply compared to the distributions of laminate (see Figure 6.3), only difference is magnitude of the distributions. The similar distributions represents that distributions of strains components are similar throughout the laminate. Magnitude of stresses of $\theta = 90^o$ ply is much higher compared to the laminate stress. Because laminate stress is the average stress of the individual ply. It is noted that distributions of axial stresses of $\theta = 0^o$ ply are similar like $\theta = 90^o$ ply but the magnitudes are lower compared to $\theta = 90^o$ ply.

6.4.4 Distributions of Lateral Stresses for Laminate

To illustrate the distributions of lateral stresses two different sections have been considered : (i) under stiffener sections and (ii) stiffener free sections along $x-$ direction. Figure 6.8 illustrates the distributions of normalized lateral stress components at different axial sections under stiffener of laminated panel subjected to (a) axial loading (b) shear loading. It is observed from Figure 6.8(a) that the highest magnitude of lateral stress develops under the right axial stiffener $(y/a = 0.94)$ of the panel with axial loading conditions. Both the two opposing longitudinal stiffened surfaces of the panel $(x/b = 0, 1)$ are found to be completely free from lateral stresses which is in good agreement with the physical characteristics of

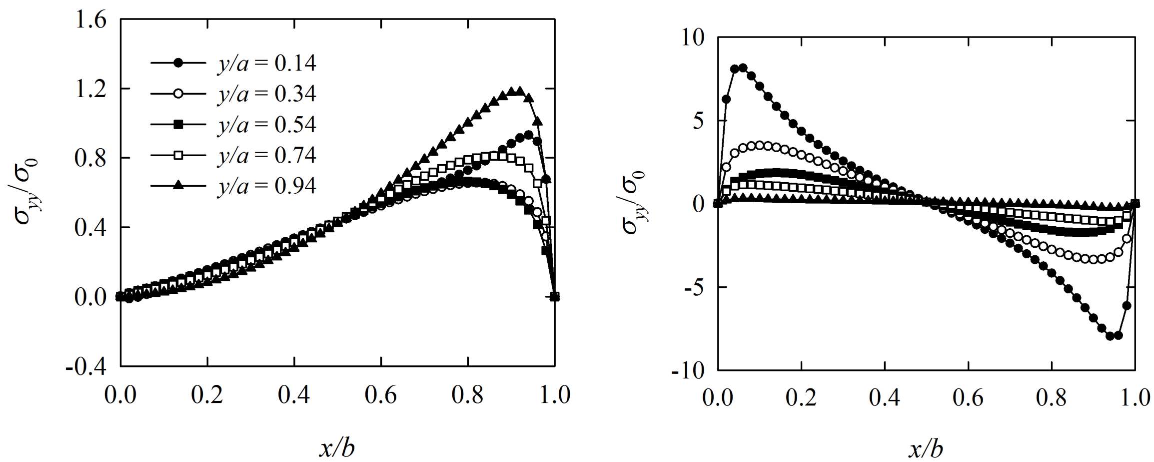

(a) Nonuniform axial loading.

(b) Nonuniform shear loading.

Figure 6.6: Distributions of axial stress components under stiffened sections of $\theta = 90^o$ ply subjected to nonuniform (a) axial loading and (b) shear loading.

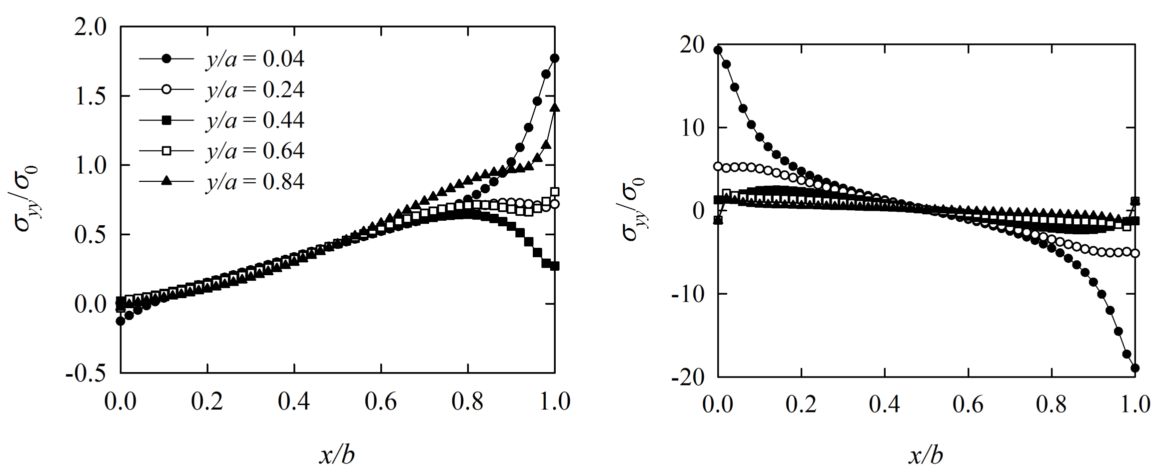

(a) Nonuniform axial loading.

(b) Nonuniform shear loading.

Figure 6.7: Distributions of axial stress components at free sections of $\theta = 90^o$ ply subjected to nonuniform (a) axial loading and (b) shear loading.

the panel. The maximum intensity of the lateral stress in the laminated panel is found to assume a value as high as 0.027 times of σ_0, the location of which is at the region of the last stiffener near the right lateral end (loaded end). Figure 6.8(b) shows the distributions of the lateral stress component under stiffened sections of the laminated cantilever under the influence of nonuniform shear. Though the stiffeners are present, no lateral stresses are developed into two opposite longitudinal surface (top and bottom boundary), which is in good agreement with the physical characteristics of the cantilever. Maximum intensity of the lateral stress is found to develop at section $x/b = 0.94$, which is under the stiffener near loaded end. Magnitude of lateral stresses are also significant at section $y/a = 0.14$. Rather than the section $y/a = 0.94$, distributions are antisymmetric with respect to section $x/b = 0.5$. Lateral stresses are found to much higher value under nonuniform shear compared to nonuniform tension.

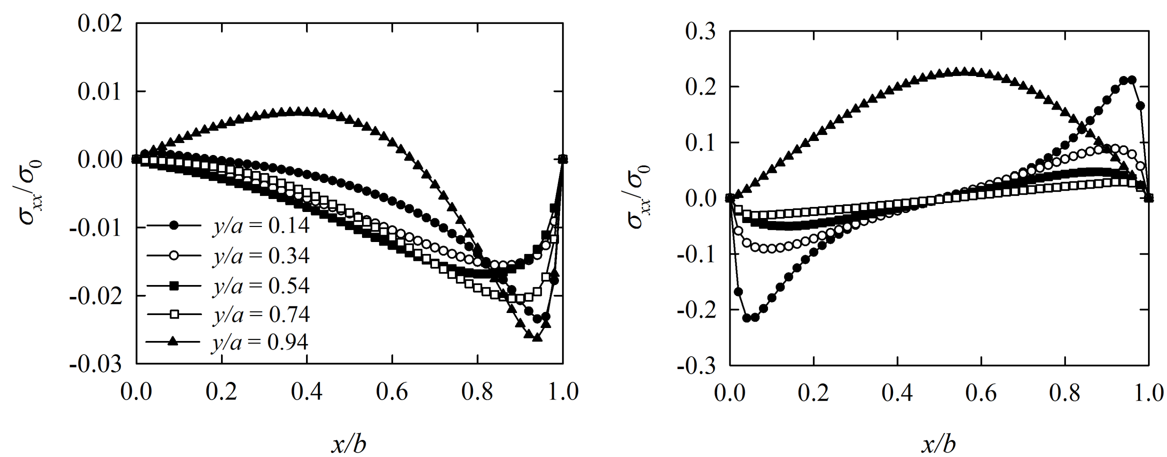

(a) Nonuniform axial loading. (b) Nonuniform shear loading.

Figure 6.8: Distributions of lateral stress components under stiffened sections of laminated panel subjected to nonuniform (a) axial loading and (b) shear loading.

Figure 6.9 illustrates the distributions of normalized lateral stress components at different stiffener free axial sections of laminated panel subjected to nonuniform (a) axial loading (b) shear loading. It is observed from Figure 6.9(a) that the highest magnitude of lateral

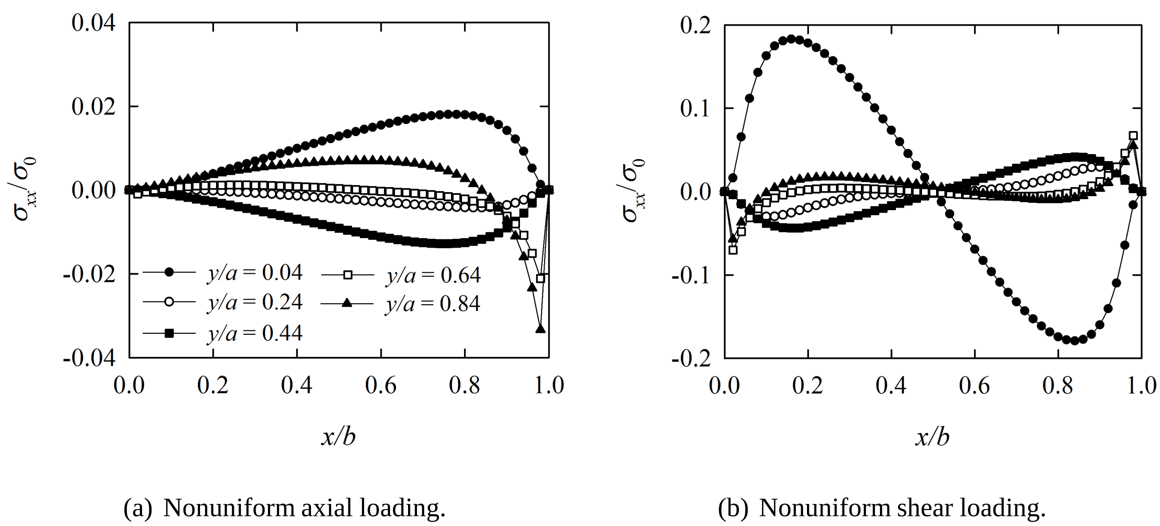

Figure 6.9: Distributions of lateral stress components at stiffener free sections of laminated panel subjected to nonuniform (a) axial loading and (b) shear loading.

stress develops at section $y/a = 0.84$, near bottom boundary of the panel. Again, significant amount of magnitude has been found at section $y/a = 0.04$ compare to other sections. Both the two opposing longitudinal surfaces of the panel $(x/b = 0, 1)$ are found to be completely free from lateral stresses which is in good agreement with the physical characteristics of the panel. Figure 6.9(b) shows the distributions of the lateral stress component at stiffener free sections of the laminated cantilever under the influence of nonuniform shear. No lateral stresses are developed both two opposite longitudinal surface (top and bottom boundary), which is in good agreement with the physical characteristics of the cantilever. Maximum intensity of the lateral stress is found to develop at section $y/a = 0.04$, which is stiffener free sections near fixed end and the distribution is sinusoidal. Distributions of the lateral stresses are antisymmetric with respect to section $x/b = 0.5$ at stiffener free sections of the laminated panel . Lateral stresses has been found much higher value for the laminate under nonuniform shear compared to nonuniform axial loading.

6.4.5 Distributions of Lateral Stresses for Different Plies

Figures 6.10 and 6.11 illustrate the distributions of the lateral stresses under stiffener and stiffener free sections of $\theta = 0^o$ ply. It has seen from Figure 6.10(a), exactly similar distributions of lateral stresses under stiffener sections have been found for $\theta = 0^o$ ply compared to the distributions of lateral stress of the laminate (see Figure 6.8), only difference is magnitude of the distributions. It also represents that distributions of strains components are similar throughout the laminate. Again, from Figure 6.11, similar distributions of lateral stresses at stiffener free sections have been found for $\theta = 0^o$ ply compared to the distributions of lateral stresses at stiffener free sections of the laminate (see Figure 6.9), only difference at the top and bottom sections, $(x/b = 0, 1)$. It should noted that the average ply stress distributions is equal to the laminate stress distributions. Though, at the top and bottom sections give much higher magnitude of stresses of $\theta = 0^o$ ply under shear stress but average stresses of all plies will be zero.

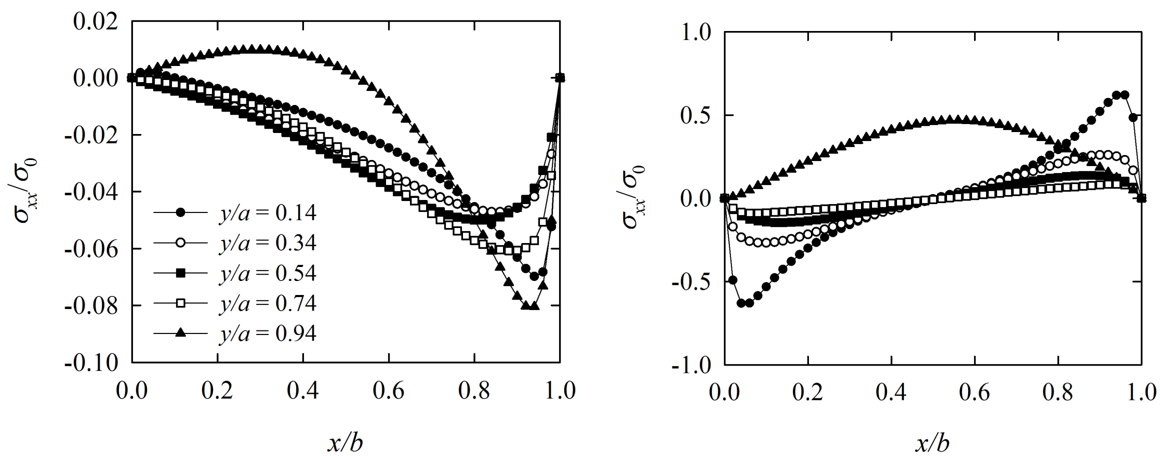

(a) Nonuniform axial loading.

(b) Nonuniform shear loading.

Figure 6.10: Distributions of lateral stress components under stiffened sections of $\theta = 0^o$ ply subjected to nonuniform (a) axial loading and (b) shear loading.

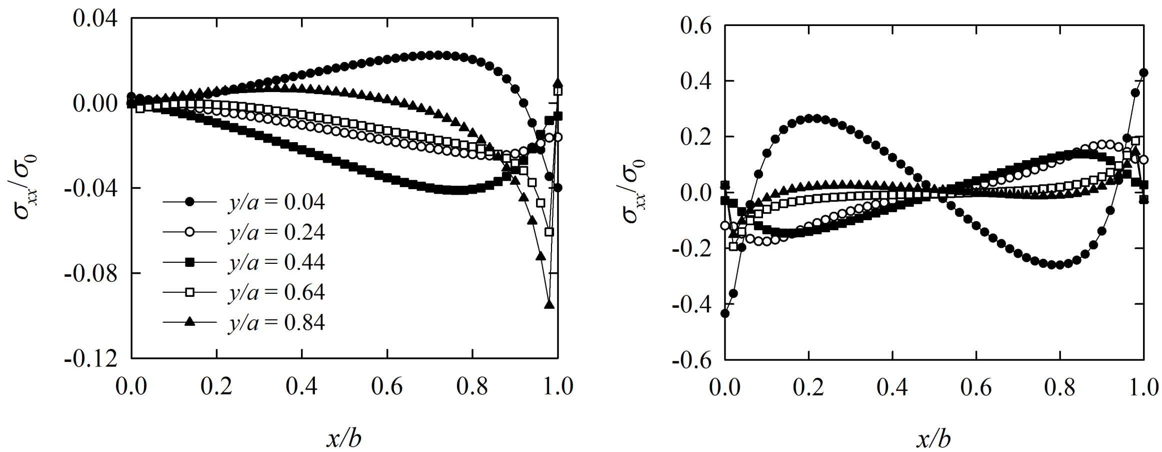

(a) Nonuniform axial loading.

(b) Nonuniform shear loading.

Figure 6.11: Distributions of lateral stress components at free sections of $\theta = 0^o$ ply subjected to nonuniform (a) axial loading and (b) shear loading.

6.4.6 Distributions of Shear Stresses

Figure 6.12 illustrates the distributions of normalized shear stress components at different lateral sections of the laminated panel subjected to (a) axial loading and (b) shear loading. The distribution of shearing stress at different sections of the panel is presented in Figure 6.12(a) for the case of nonuniform axial loading. Sawtooth like wave nature distribution has been found at the sections $x/b = 1.0$. Magnitude of distributions of other sections are very small compare to section $x/b = 1.0$. At region $0 < y/a < 0.5$, shear stress give positive magnitude, increase suddenly at certain value at start of the stiffener and decrease gradually throughout the stiffener. At region $0.5 < y/a < 1.0$, shear stress give negative magnitude and increases gradually throughout the stiffener at certain value. At stiffener free sections, top and bottom boundaries are free from shear stress which exactly matches our boundary conditions. Maximum magnitude has been found at start of stiffener near fixed end. The distribution of shearing stress at different sections of the panel under nonuniform shear is presented in Figure 6.12(b). At region $0 < y/a < 0.5$, shear stress give negative

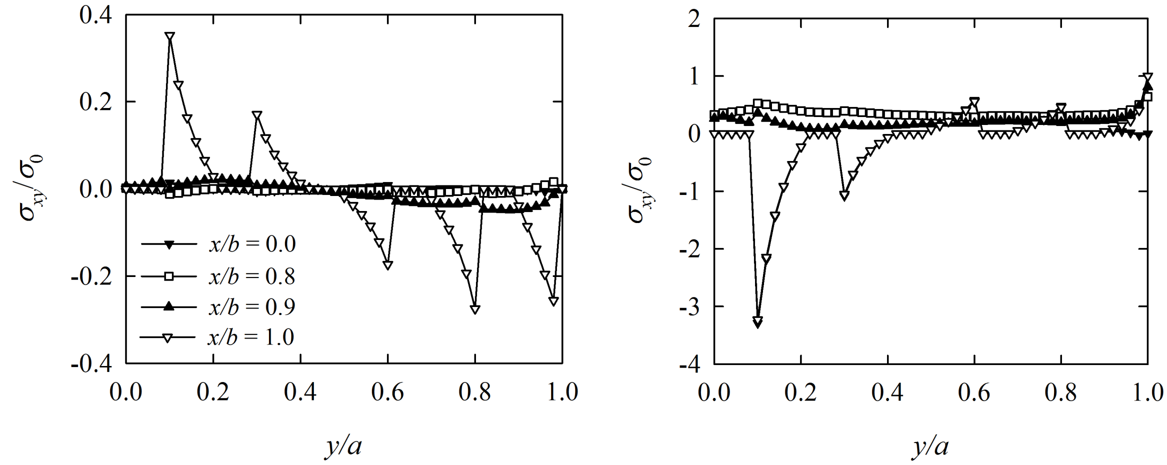

(a) Nonuniform axial loading. (b) Nonuniform shear loading.

Figure 6.12: Distributions of shear stress components at different sections of the laminated panel subjected to nonuniform (a) axial loading and (b) shear loading.

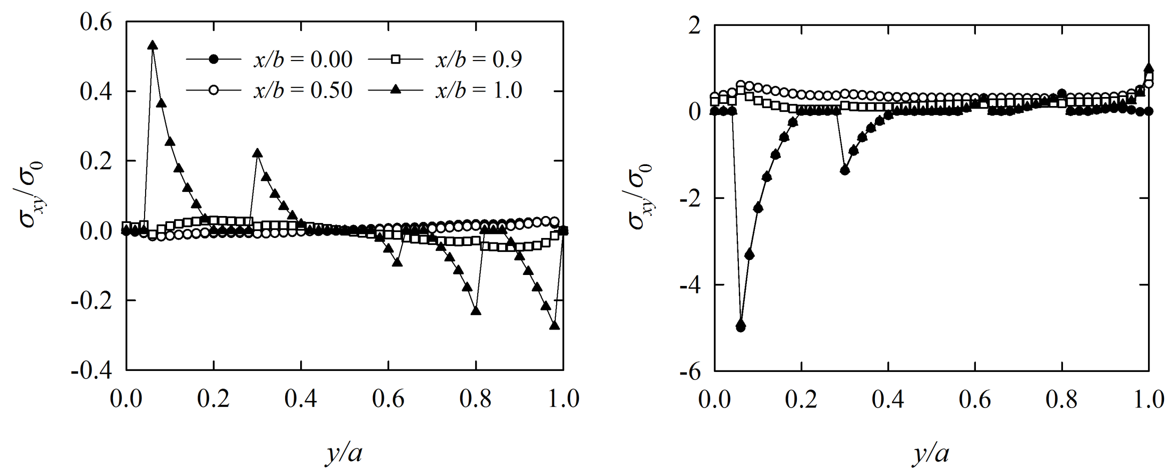

(a) Nonuniform axial loading. (b) Nonuniform shear loading.

Figure 6.13: Distributions of shear stress components under stiffened sections of arbitrarily placed stiffened laminated panel subjected to nonuniform (a) axial loading and (b) shear loading.

magnitude, increase suddenly at certain value at start of the stiffener and decrease gradually throughout the stiffener with the increase of section y/a. At region $0.5 < y/a < 1.0$, shear stress increase with positive magnitude at the stiffened section. At the stiffener free sections, both top and bottom boundary are free from shear stress which exactly satisfy the boundary conditions. Again, at stiffening region, top boundary gives slightly higher magnitude compare to the bottom boundary. Both top and bottom boundary give similar shear stress distributions. At right lateral end, shear stress approaches to zero for section $x/b = 0.0$, which exactly matches with the boundary conditions and normalized value of shear stress has been found exactly 1 at section $x/b = 1.0$ i.e., equal to applied load at the right lateral bottom end. Again, it has shown from figure 6.12, periodic stiffened laminate under nonuniform shear loading give much higher magnitude of shear stress distribution compare with laminate under nonuniform tension.

Figure 6.13 shows the distributions of axial stress components under stiffened sections of arbitrarily placed stiffened laminated panel subjected to nonuniform (a) axial loading and (b) shear loading. In this case, stiffeners are arbitrarily attached with laminated cantilever along the longitudinal edges. It has been seen from figures 6.12 and 6.13 shows similar distributions have been found though stiffeners have not placed at the same position. Again magnitude of distributions are much higher for the arbitrarily placed stiffened laminated panel compared to periodically placed stiffened laminated panel.

6.4.7 Deformed Shapes

Figure 6.14(a) and 6.14(c) illustrates the deformed shapes of the laminated panel obtained with different cases of stiffener used along the two opposing longitudinal surfaces for same $[90/0/90/\bar{0}]_s$ under nonuniform axial loading. Overall, it is revealed from the results that axial stiffeners have significant influence on the deformation pattern of the panel, particularly for the present nonuniform axial loading. The axial stiffeners at the surfaces, in general, cause the overall deformation of the panel to assume much smaller magnitude, which can

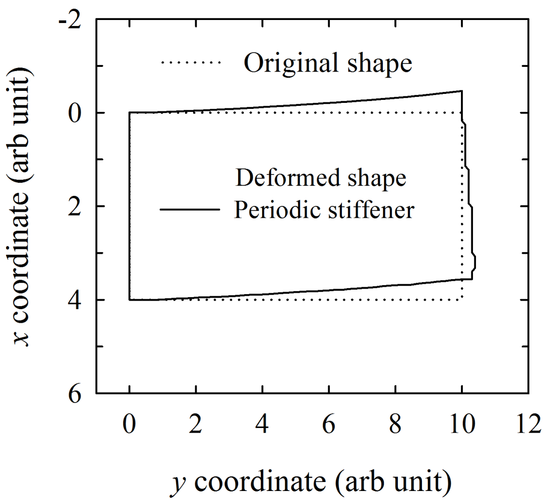

(a) Nonuniform axial loading (Magnification factor ×3000).

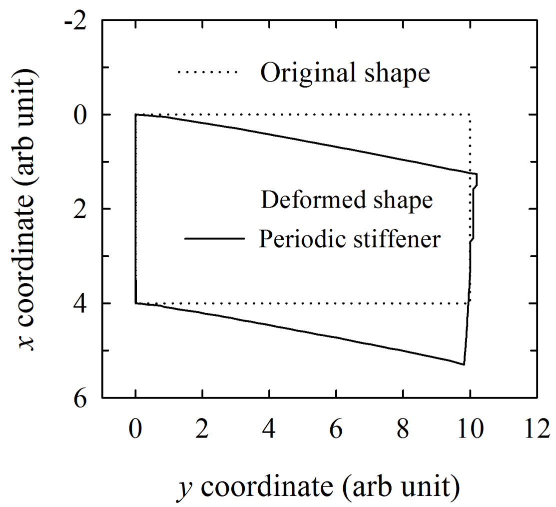

(b) Nonuniform shear loading (Magnification factor ×300).

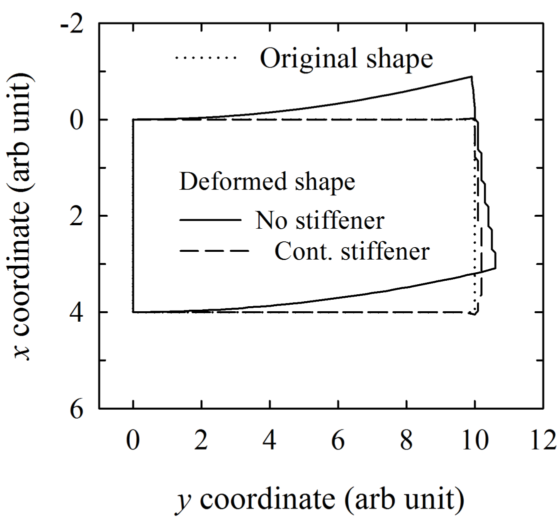

(c) Nonuniform axial loading (Magnification factor ×3000).

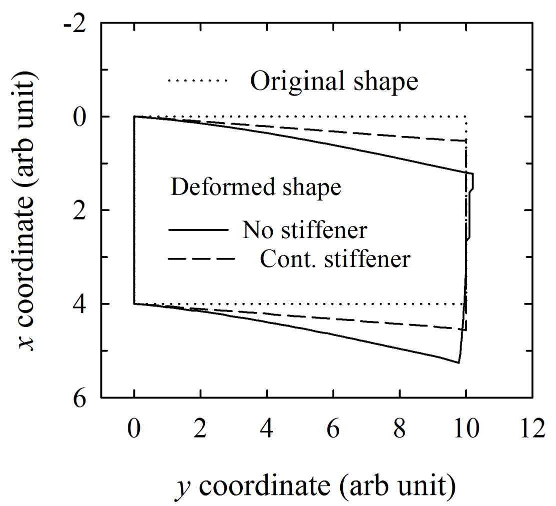

(d) Nonuniform shear loading (Magnification factor ×300).

Figure 6.14: Deformed shape of the laminated panel with different conditions of stiffener subjected to nonuniform loading.

be easily realized when compared to the case of no stiffener, as shown in Figure 6.14(a) and 6.14(c). It is interesting to note that, when the longitudinal edges of the panel are made free from stiffeners, the present nonuniform axial loading causes the deformation of the panel somewhat similar to the case of subjecting an anti-clockwise moment at the right lateral end, where the lateral component of displacement is found to be more prominent than the axial component. The above bending-like deformation pattern is also observed for the case of discrete periodic stiffeners. The deformation pattern rather conforms to the general characteristic of the model of the panel, as the axial deformation is found to be highest at the lower surface and almost zero at the upper surface of the panel (figure 6.14(a)). A critical analysis shows that the panel with periodic stiffeners experiences a bending-like deformation, somewhat similar to that of stiffener-free panel. In order to support the present nonuniform axial tension, the panel is found to follow a deformation pattern completely different from those of periodic and no stiffeners, when the two opposing longitudinal surfaces are subjected to full-length continuous stiffeners. Deformation of laminated panel with continuous stiffener is much smaller compare to stiffener free and periodic stiffener laminated panel, where the axial component of displacement is found to be more prominent than the lateral component as shown in Figure 6.14(c). Figure 6.14(b) and 6.14(d) illustrates the deformed shapes of the laminated panel obtained with different cases of stiffener used along the two opposing longitudinal surfaces under nonuniform shear loading. It has seen, the deformation pattern rather conforms to the general characteristic of the model of the panel. Contribution of lateral displacement is more prominent compared to the axial displacement. Almost similar deformation has been found for periodic, continuous and stiffener-free panel under nonuniform shear stress. Almost equal magnitude of lateral deformation for stiffener free panel and periodic stiffener has been found. Continuous stiffener give much smaller magnitude axial displacement compare to others as shown in Figure 6.14(d). The obtained deformed state of the stiffener free panel is shown in Figure 6.14(d), in which the right extreme corner of the bottom surface is found to experience the contribution of both the lateral and axial displacements. As a result, to satisfy the requirement of the applied loading as well as the given conditions on the opposing surfaces, the top-right corner of the panel is found to experience only the contribution of lateral displacement in the positive direction.

6.4.8 Effect of Periodic Stiffener

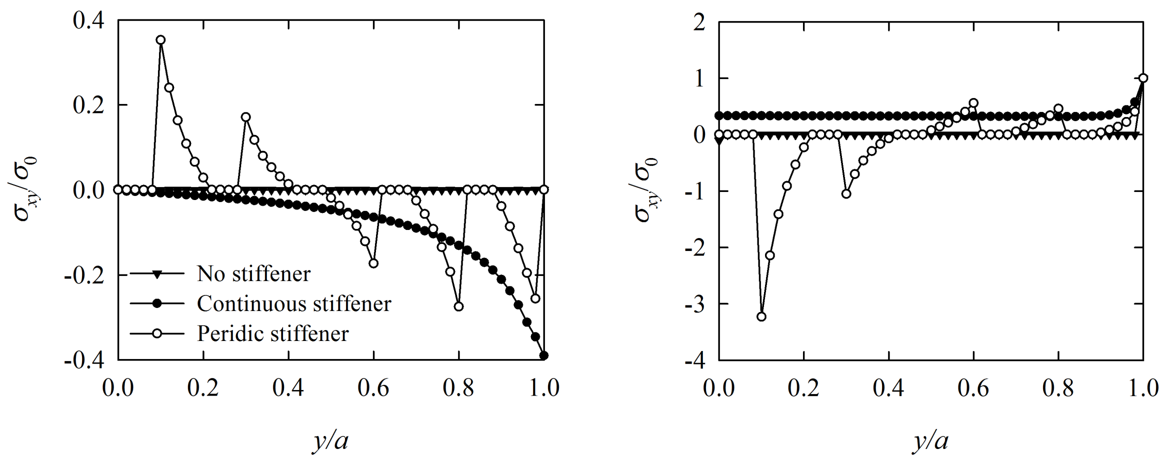

(a) Nonuniform axial loading. (b) Nonuniform shear loading.

Figure 6.15: Distributions of shear stresses along bottom edge of laminated panel with different conditions of stiffener subjected to nonuniform (a) axial loading and (b) shear loading.

Figure 6.15(a) describes the comparison of shear stress distributions along the bottom edges for the three cases of stiffeners for same $[90/0/90/\bar{0}]_s$ laminate subjected to nonuniform axial tension. For the stiffener free panel, the predicted shear stress at the bottom surface is found to be zero, which is again in good agreement with the physical characteristics of the panel. For the case of continuous stiffeners, the distribution assumes a quadratic/cubic form, which is gradually increasing from left to right with negative magnitude. Sawtooth like wave nature distribution is obtained for the case of present periodic stiffener, which give positive magnitude in region $0 < y/a < 0.5$ and negative magnitude in region $0.5 < y/a < 1$. As expected, the stiffener free regions of the boundary are found to be free from shearing stresses. The maximum shear stress developed at the bottom surface of the panel with periodic stiffener is found at start of the stiffener near fixed end. For case of continuous stiffener, maximum shear stress has been found at the right lateral end. Figure 6.15(b) describes the comparison of shear stress distributions for the three cases of stiffeners; no stiffener, continuous stiffener and periodic stiffener at the bottom section for same laminate. For the stiffener free panel, the predicted shear stress at the bottom surface is found to be zero. For the case of continuous stiffeners, the distribution is almost constant and which is gradually increasing from left to right near loaded boundary. For the case of periodic stiffener, distribution of shear stress is not constant, which is however much higher in magnitude compared to the case of continuous stiffener. Stress fluctuations have been found at start of the stiffeners (region $0 < y/a < 0.5$) and end of the stiffeners (region $0.5 < y/a < 1$). Stress distributions are almost linear along the stiffener. As expected, the stiffener free regions of the boundary are found to be free from shearing stresses. The maximum shear stress developed at the bottom surface of the panel with periodic stiffener near fixed boundary at start of the stiffener.

Figure 6.16 illustrates the comparison of distribution of normalized axial stress components for the different stiffening effect at bottom section of the laminated panel. The results basically compare the state of stresses along the bottom section of periodic stiffened laminated panel with those associated with the corresponding cases of continuous stiffener and stiffener free panels. Figure 6.16(a) describes the effect of distributions of axial stress under axial loading for the three cases of stiffeners. For the case of continuous stiffener panel, the predicted shear stress at the bottom surface is found to be zero. For the case of stiffener free laminate, the distribution assumes more or less constant which is equal to σ_0 that applied at bottom right corner. For the case of periodic stiffener, distribution of axial stress is not constant, which is however much higher in magnitude compared to the case of stiffener free laminate. Stress fluctuations have been found at start of the stiffeners (region $0 < y/a < 0.5$) and end of the stiffeners (region $0.5 < y/a < 1$). As expected, the stiffened regions of the

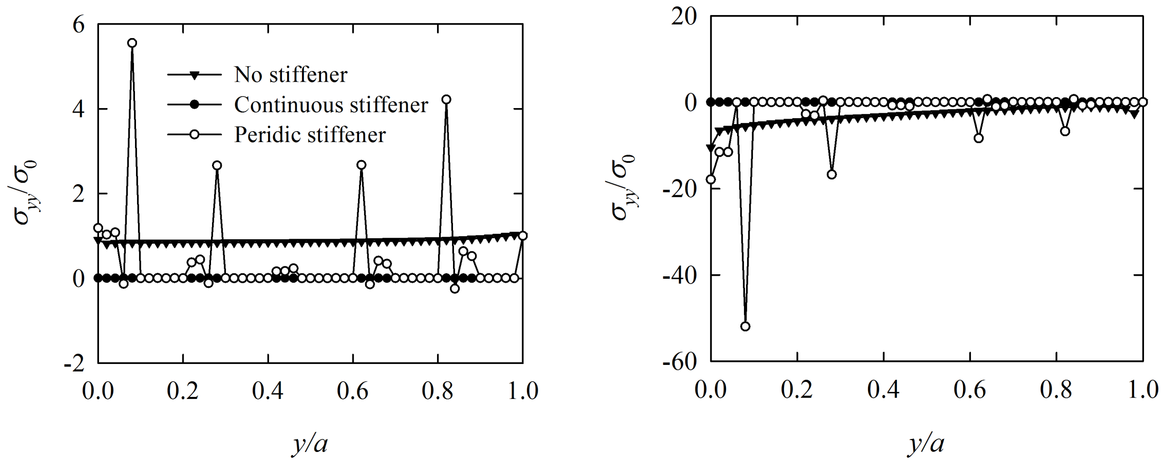

(a) Nonuniform axial loading. (b) Nonuniform shear loading.

Figure 6.16: Distributions of axial stresses along bottom edge of laminated panel with different conditions of stiffener subjected to nonuniform (a) axial loading and (b) shear loading.

boundary are found to be free from axial stresses. The maximum fluctuation of stress developed at the bottom surface of the panel with periodic stiffener near fixed boundary at start of the stiffener. Figure 6.16(b) describes the effect of distributions of axial stress of the laminated cantilever under shear loading for the three cases of stiffeners mentioned above. For the stiffener free panel, the distribution is decreasing linearly from left to right lateral end approaches to stress zero value at the right lateral end. Maximum stress has been found at the left lateral boundary. For the case of continuous stiffener panel, the predicted shear stress at the bottom surface is found to be zero. For the case of periodic stiffener, distribution of stress is not constant, which is however much higher in magnitude compared to the case of stiffener free laminate. Stress fluctuations have been found at start of the stiffeners (region $0 < y/a < 0.5$) and end of the stiffeners (region $0.5 < y/a < 1$). As expected, the stiffened regions of the boundary are found to be free from axial stresses. Fluctuations of stresses are decreasing from left to right lateral end. The maximum fluctuation of axial stress developed at the bottom surface of the panel with periodic stiffener near fixed boundary at start of the stiffener.

6.4.9 Effect of Periodic Axial Restrain

Figure 6.17 describe the comparisons of shear stress distributions for different cases of boundary conditions for same $[90/0/90/\bar{0}]_s$ laminate subjected to nonuniform loading. This comparisons are between axial stiffener (constant axial displacement at stiffened boundary, Fig 6.2) and the axial stiffener is replaced by the axial restrain (zero axial displacement). Figure 6.17(a) shows sawtooth like wave distributions of shear stresses at the stiffened region of the laminate. Positive magnitude has been found at section $0 < y/a < 0.5$ and negative magnitude has been found at section $0.5 < y/a < 1$. For the case of axial restrain, A somewhat cubic/ quadratic distributions has been found at the restrained region which is increasing from left to right lateral end. As expected stiffener free regions are free from shear stresses for both cases of the boundary restrains. Figure 6.17(b) shows the comparisons of shear stress distributions of laminated panel subjected to nonuniform shear loading. Negative magnitude has been found at section $0 < y/a < 0.5$ and positive magnitude has been found at section $0.5 < y/a < 1$. Magnitude of fluctuations of distributions decreases from left to right. Again, almost similar distributions have been found for all restraining region. As expected stiffener free regions are free from shear stresses for both cases.

Figure 6.18(a) describe the comparisons of axial stress distributions for different cases of boundary conditions for same $[90/0/90/\bar{0}]_s$ laminate subjected to nonuniform axial loading. For the case of periodic stiffener, fluctuation of stress distributions are increasing away form section $y/a = 0.5$. Stress fluctuations have been found at start of the stiffeners (region $0 < y/a < 0.5$) and end of the stiffeners (region $0.5 < y/a < 1$). For the case of periodic axial restrained, gradually increasing stresses with both positive and negative magnitudes are obtained with an alternative fashion from fixed end to loaded end. The stiffened regions of the boundary are found to be free from axial stresses for both cases. Figure 6.18(b) describe the comparisons of axial stress distributions for different cases of boundary conditions for

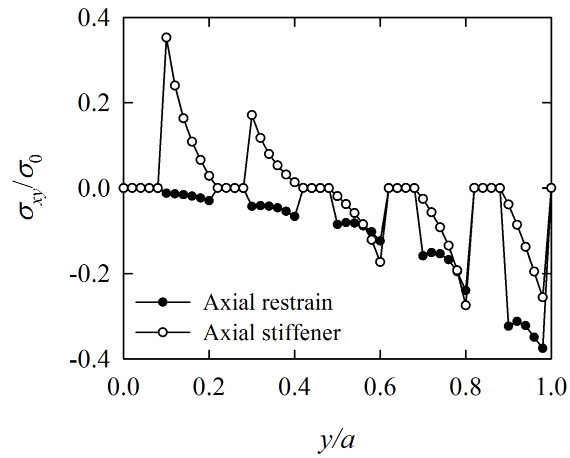

(a) Nonuniform axial loading.

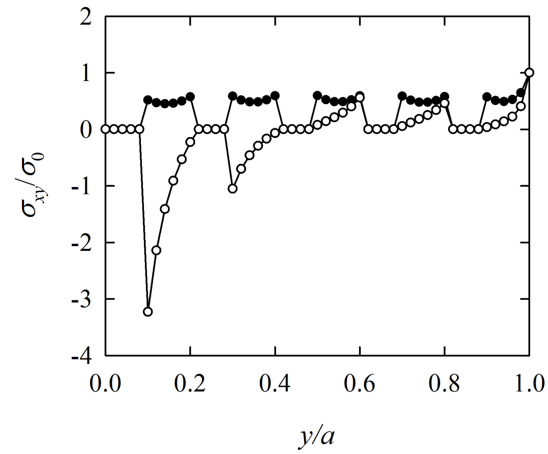

(b) Nonuniform shear loading.

Figure 6.17: Comparison of shear stress distributions of axial stiffener with axial restrain of the laminated panel subjected to nonuniform (a) axial loading and (b) shear loading.

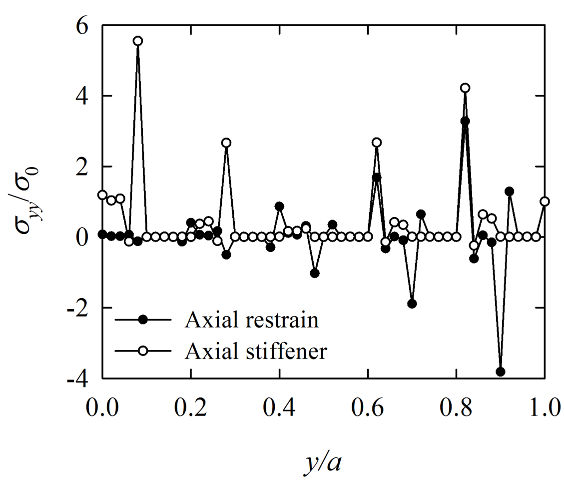

(a) Nonuniform axial loading.

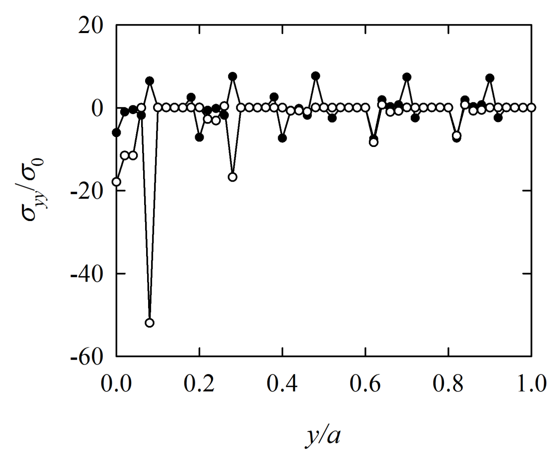

(b) Nonuniform shear loading.

Figure 6.18: Comparison of axial stress distributions of axial stiffener with axial restrain of the laminated panel subjected to nonuniform (a) axial loading and (b) shear loading.

same $[90/0/90/\bar{0}]_s$ laminate subjected to nonuniform shear loading. For the case of periodic stiffener, gradually increasing stresses with positive magnitudes are obtained from fixed end to loaded end. For the case of periodic axial restrained, stress distribution with both positive and negative magnitudes are obtained with an alternative fashion from fixed end to loaded end. Fluctuations of periodic stiffener are much higher compare to periodic axial restrained. The stiffened regions of the boundary are found to be free from axial stresses for both cases.

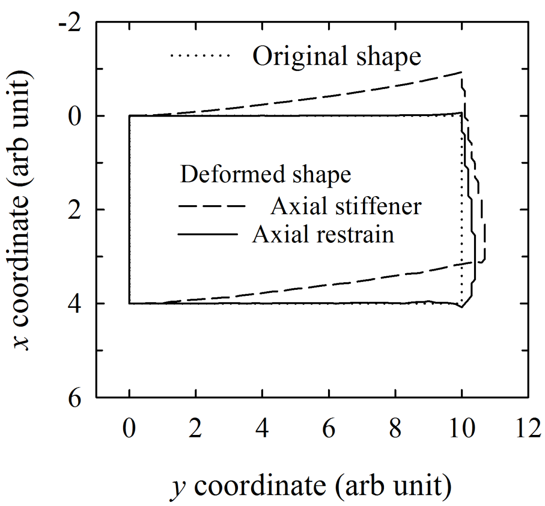

(a) Nonuniform axial loading (magnification factor $\times 6000$).

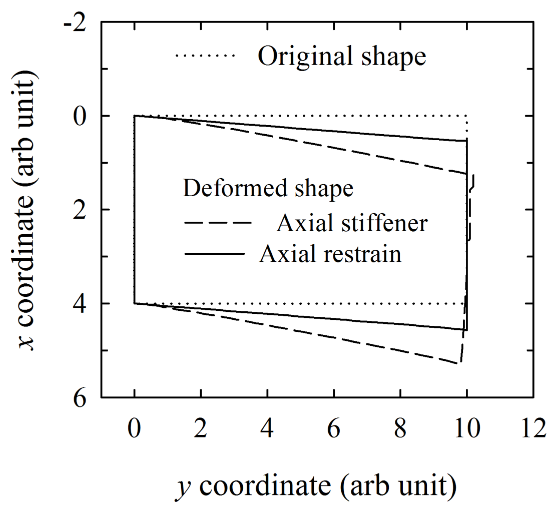

(b) Nonuniform shear loading (magnification factor $\times 300$).

Figure 6.19: Comparison of deformed shape of the periodic axial restrained and periodic stiffened laminated panel subjected to nonuniform (a) axial loading (b) shear loading.

Figure 6.19 illustrate the deformed shape of the periodic axial restrained and periodic stiffened laminated panel subjected to nonuniform axial and shear loading. In order to support the present nonuniform axial tension, the panel is found to completely different deformation for periodic stiffener from those of periodic axial strained. Deformation of the laminated panel with periodic axial restrained is much smaller compare to periodic stiffener laminated panel, where the lateral component of displacement is found to be more prominent than the axial component and the axial deformation is found to be highest at the lower surface and almost zero at the upper surface of the panel as shown in Figure 6.19(a) It is interesting to note that, when the longitudinal edges of the panel are made with periodic stiffeners, the present nonuniform axial loading causes the deformation of the panel somewhat similar to the case of subjecting an anti-clockwise moment at the right lateral end, where the lateral component of displacement is found to be more prominent than the axial component. Figure 6.19(b) illustrate the deformed shape of the periodic axial restrained and periodic stiffened laminated panel subjected to nonuniform shear loading. It has seen, the deformation pattern rather conforms to the general characteristic of the model of the panel. Contribution of lateral displacement is more prominent compared to the axial displacement. Almost similar deformation has been found for axial periodic stiffener and axial periodic restrained under nonuniform shear stress. Panel with axial restrained give much smaller magnitude of axial displacement compare to periodic stiffened panel. Overall deformation is much higher for periodic stiffened panel compare to axial restrained panel. Again deformation under axial tension is much smaller compare to shear loading.

6.5 Conclusion

A new scalar function based computational scheme has been developed to analyze the elastostatic response of laminated composite panel subjected to nonuniform loading, under the influence of discrete periodic stiffeners. No appropriate analytical approach is available in the literature, which can provide explicit information about the actual stresses, especially at the critical regions of supports and stiffeners of the laminated panel. Both the qualitative and quantitative results of the present mixed-boundary-value stress problem of laminated composites establish the soundness as well as appropriateness of the single function approach. The periodic stiffeners are found to have significant influence on the deformed shape of the panel, especially when compared with those of continuous and stiffener-free panels. Moreover, both the axial and shear stresses along the edges of the panel are found to assume much higher magnitudes from stiffener-free panels. The solutions are claiming to be highly accurate and rational for the entire region of interest, either at or away from the bounding edges of the composite panel. It is thus expected that the present data would be considered as a valuable design guide for laminated panels with discrete local stiffeners.

CHAPTER

7

Laminated Panel Subjected to Discrete Variable Stiffeners

7.1 Introduction

The elastic field of a laminated composite cantilever with discrete variable stiffeners at the two opposing longitudinal bounding surfaces is analyzed under the influence of a uniform shear loading. The variable stiffener is defined as the axial stiffener whose stiffening effectiveness is not constant, rather a function of axial location of the bounding surface. A new computational scheme is developed based on the displacement potential method for analyzing laminated panels subjected to discrete variable stiffness. First, solutions are obtained for laminated panels subjected to stiffeners having various effectiveness. The effectiveness is identified to be one of the influential factors for determining the state of stresses in the laminate. Then a laminated cantilever panel is analyzed under the influence of discrete variable stiffeners, the effectiveness of which varies linearly as a function of location over the stiffened region. The solutions of overall laminate stresses, strains and displacement are presented mainly in the form of graphs. The results appear to be quite reasonable and establish the soundness of the numerical scheme developed.

7.2 Effectiveness of Stiffener, ξ

In order to explain the concept of variable stiffener, a parameter, namely, the effectiveness of stiffener, denoted by the symbol ξ, is introduced here. The effectiveness of the stiffeners is defined in a quantitative fashion as the reduction of strain from the corresponding unstiffened strain in a normalized form. It can be expressed mathematically as

$$\xi_i = \frac{(\varepsilon_{yy}^{\text{us}})_i - (\varepsilon_{yy})_i}{(\varepsilon_{yy}^{\text{us}})_i} \tag{7.1}$$

Where, $(\varepsilon_{yy}^{\text{us}})_i$ is the nodal axial strain of unstiffened member and $(\varepsilon_{yy})_i$ is the nodal axial strain of the corresponding member subjected to variable stiffeners. For the case of rigid stiffeners, $(\varepsilon_{yy})_i$ is zero (see chapter 5) over the stiffened region. The range of variation of the parameter, ξ is from 0 to 1. When the value of ξ_i is equal to 0, it represents the case of unstiffened condition, that is the stiffener is not at all effective, and for the case of rigid stiffeners it assumes a value of unity, that is, the stiffener is 100% effective. When the effectiveness is equal to 0 or 1, it does not represent the condition of variable stiffener, rather gives the two limiting cases of the effectiveness which are uniform in nature. The value of $\xi = 0.4$ at any region or mesh point of the stiffened boundary means the stiffener is 40% effective, that is, it allows only 60% of the unstiffened strain at the region or mesh point of the stiffened boundary. When ξ varies along the stiffened region of the panel it will reflect the case of variable stiffeners, the effectiveness of which varies following a predetermined functional relationship of axial location.

In this chapter, a laminated panel with discrete variable stiffeners has been analyzed under the influence of the uniform shear loading. To solve the problem, the condition of variable stiffeners is mathematically modeled by assigning appropriate values of strain for the stiffened section. Strain at any position of the stiffened section is obtained from the corresponding stiffening effectivity, ξ by the following relation:

$$(\varepsilon_{yy})_i = (\varepsilon_{yy}^{\text{us}})_i(1 - \xi_i) \tag{7.2}$$

7.3 Computational Scheme for Solving Laminated Panels under Variable Stiffener

The variable stiffener is defined as the axial stiffeners for which stiffness is a function of the axial location. No software / analytical method has been found in the literature which can give the direct solution of the variable stiffener. This thesis is introducing a new computational algorithm to solve the laminated cantilever with variable stiffener as shown in figure 7.1. First stage: solve the stiffener free cantilever and rigid stiffened cantilever and calculate axial strains for both problems; 2nd stage: find axial strains at the stiffened region on top and bottom boundary. By default, magnitude of axial strains are zero at stiffened region for the case of rigid stiffening. 3rd stage: assume variation of effectiveness of stiffener, ξ for variable stiffener. i.e., how effectiveness of stiffener varies along the length of the stiffener. In present study, two different variations of stiffener have been considered: (a) stiffener with various effectiveness (ξ varies with magnitude) (b) stiffener with variable effectiveness (ξ varies linearly along stiffener). 4th stage: calculate the strains for variable stiffener along the length of the stiffener with corresponding variations of ξ by using equation 7.2. 5th stage: use calculated strain components $(\varepsilon_{yy})_i$ together with $\sigma_{xx} = 0$ as boundary conditions at the stiffened sections of the variable stiffened cantilever. 6th stage: Solve the cantilever problem using strain boundary conditions. 7th stage: Calculate displacement, stress and strain components for variable stiffened cantilever.

7.4 Effect of Stiffeners with Various Effectiveness

This section presents the effect of the laminated composite cantilever under the influence of discrete variable stiffener subjected to a uniform shear. To analyze the problem, discrete

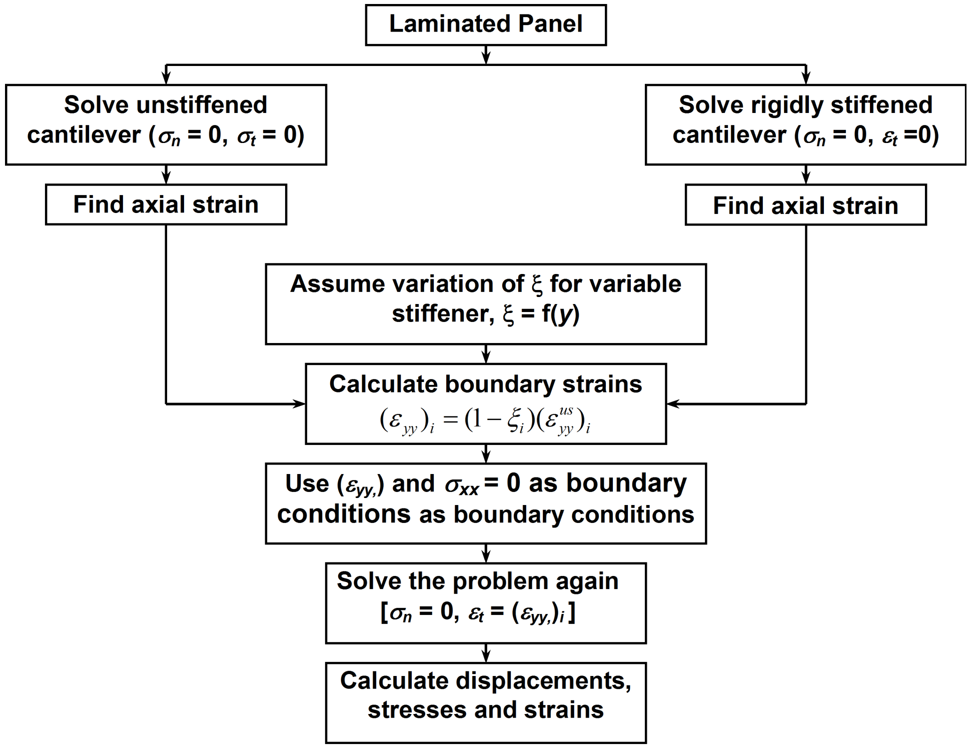

Figure 7.1: Computational scheme for solving laminated panel with variable effectiveness of the stiffener.

stiffener with different effectiveness has been considered. In this case, effectiveness of the stiffener, ξ will not vary along the length of the stiffener but varies with the magnitude. Mathematically, to analysis the rigid stiffened cantilever problem, has been solved by restraining the strain (see chapter 5). For the present variable stiffening case, strain should not be restrained rather it will be allowed that has shown in figures 7.2. Strain expression has been found from the above equation (7.2) with corresponding value of ξ. Five different cases of ξ has been considered ($\xi = 0.0, 0.25, 0.5, 0.75$ and 1.0) to solve the laminated stiffened cantilever (stiffener with various effectiveness).

7.4.1 Geometry and Physical Conditions of the Cantilever

A uniform cantilever of laminated composites is considered for the present analysis. Three plies of unidirectional boron-epoxy composite with a stacking sequence of $[0/90/0]$ are used

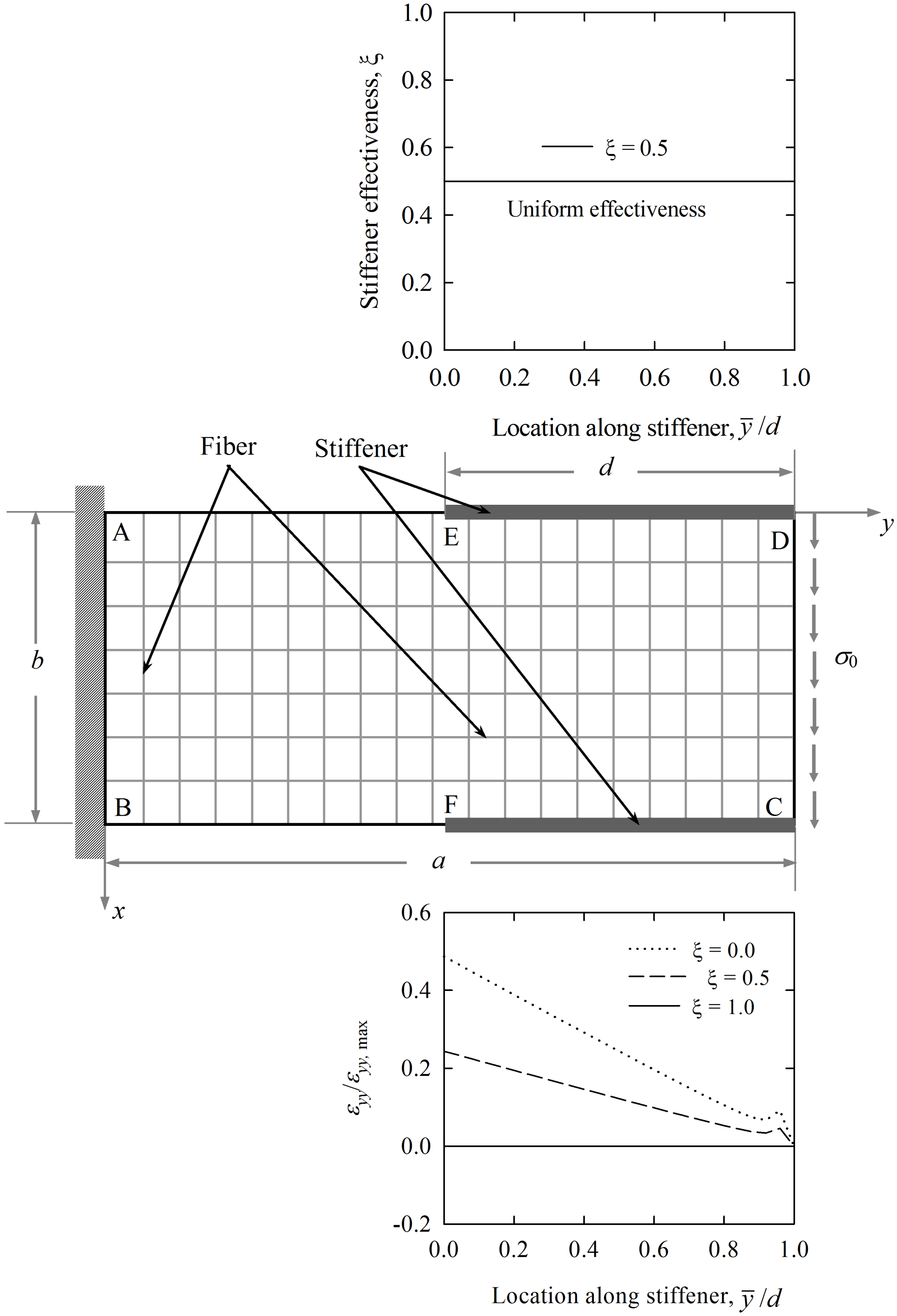

Figure 7.2: Determination of physical conditions of the stiffened section under stiffeners with uniform effectiveness $(\xi = 0.5)$.

to form the symmetric cross-ply laminate for the cantilever. Three-dimensional plates are considered into two-dimensional plane stress conditions. The length, width and thickness of the panel are represented by a, b and h respectively. Each ply has same thickness and ply thickness can be expressed as $h_k = h_k - h_{k-1}$ and total thickness $h = nh_k$. The geometry and loading of a laminated composite panels with variable stiffening subjected to uniform shear stress is shown in Figure 7.2. The left-hand lateral end of the cantilever is assumed to be rigidly fixed and the right-hand lateral end is subjected to a uniform shear loading. The two opposing longitudinal surfaces are considered to be locally stiffened by attaching variable axial stiffeners of the boundary surfaces. The length of the stiffeners is half of the total length and attached at the right side of the laminated panel.

The geometry and loading used for the solution of the cantilever problem is illustrated in Figure 7.2. The relevant boundary conditions, which have been satisfied by different segments of the boundary, are listed in table 7.1. The right lateral end of the panel is subjected to a uniform shear stress loading of intensity $\sigma_0 = 3$ MPa. Table 7.2 illustrates the scheme for treating the boundary conditions of the corner points as well as intermediate boundary transition point of the boundary section, which are, in general, the points of singularity.

7.4.2 Results and Discussions

In this section, results of the numerical solutions are presented for boron/epoxy composite cantilever problem. Here, it is worth mentioning that the formulations developed in this study can be used for any composite materials. However, the boron/epoxy composite has been chosen in this study merely as an example. The maximum value of the applied shear stress σ_0 is taken as 3 MPa. Further, all the results presented here correspond to the panel aspect ratio $a/b = 2.5$, laminate stacking sequence of $[0/90/0]$ and the number of ply $n = 3$. The thickness of each ply is considered as 0.5 mm. Although any number of plies can be used for the solution to elastic field, only three plies have been considered in this study to generate the numerical results. However, it should be ensured that the laminate is symmetric

Table 7.1: Numerical modeling of the boundary conditions for different segment of the boundary of the laminated panel (see figure 7.2)

Boundary segments	Boundary type	Parameters used to the nodal conditions	Correspondence between mesh points and given boundary conditions	
			Mesh point on the physical boundary	Mesh points on the imaginary boundary
AE	Free	σ_{xx}, σ_{xy}	$\sigma_{xx}(0, y) = 0$	$\sigma_{xy}(0, y) = 0$
BF	Free	σ_{xx}, σ_{xy}	$\sigma_{xx}(b, y) = 0$	$\sigma_{xy}(0, y) = 0$
ED	Stiffened	$\sigma_{xx}, \varepsilon_{yy}$	$\sigma_{xx}(0, y) = 0$	$(\varepsilon_{yy})_i(0, y) = (1-\xi)(\varepsilon_{yy}^{\text{us}})_i$
FC	Stiffened	$\sigma_{xx}, \varepsilon_{yy}$	$\sigma_{xx}(b, y) = 0$	$(\varepsilon_{yy})_i(b, y) = (1-\xi)(\varepsilon_{yy}^{\text{us}})_i$
CD	Loaded	σ_{yy}, σ_{xy}	$\sigma_{xy}(x, a) = \sigma_0$	$\sigma_{yy}(x, a) = 0$
AB	Fixed	u_x, u_y	$u_x(x, 0) = 0$	$u_y(x, 0) = 0$

for any number of plies as the formulations have been developed for a laminate, based on the formulation of symmetric cross-ply laminate that the bending-extension coupling stiffness matrix [B] does not come into the scenario. For most of the results, the length of the discrete stiffener is kept constant, that is, the ratio, d/a is set equal to 0.5, although the effect of stiffening length is investigated by varying the ratio. The FD mesh-network used to model the present cantilever $(a/b = 2.5)$ contains nodal points (51×51) in the direction of x and y, respectively.

7.4.2.1 Comparison of Axial Displacements and Strains

Figure 7.3(a) illustrates the comparison of the state of distributions of normalized axial displacements, u_y on the top boundary of the laminated cantilever. Distributions are normalized with the maximum lateral displacement of unstiffened panel at right lateral end. For the case of stiffener free panel, the distribution assumes a quadratic/cubic form, which is gradually increasing from left to right. For the case of rigid stiffening, distribution assumes

Table 7.2: Numerical modeling of the boundary conditions for corner and the intermediate points of the laminated panels (see figure 7.2)

Corner Point	Parameters given to the nodal conditions	Parameters used to the nodal conditions	Correspondence between mesh points and given boundary conditions	
			Mesh point on the physical boundary	Mesh points on the imaginary boundary
A	$(\sigma_{xx},\sigma_{xy})$,$(u_x,u_y)$	$[\sigma_{xx},\sigma_{xy},u_y]$	$\sigma_{xx}(0,0)=0$	$\sigma_{xy}(0,0)=0, u_y(0,0)=0$
B	$(\sigma_{xx},\sigma_{xy})$,$(u_x,u_y)$	$[\sigma_{xx},\sigma_{xy},u_y]$	$\sigma_{xx}(b,0)=0$	$\sigma_{xy}(b,0)=0, u_y(b,0)=0$
C	$(\sigma_{xx},\varepsilon_{yy})$,$(\sigma_{yy},\sigma_{xy})$	$[\sigma_{xx},\sigma_{xy},\varepsilon_{yy}]$	$\sigma_{xx}(b,a)=0$	$\varepsilon_{yy}(b,a)=0, \sigma_{xy}(b,a)=\sigma_0$
D	$(\sigma_{xx},\varepsilon_{yy})$,$(\sigma_{yy},\sigma_{xy})$	$[\sigma_{xx},\sigma_{xy},\varepsilon_{yy}]$	$\sigma_{xx}(0,a)=0$	$\varepsilon_{yy}(0,a)=0, \sigma_{xy}(0,a)=\sigma_0$
Intermediate points				
E	$(\sigma_{xx},\sigma_{xy})$,$(\sigma_{xx},\varepsilon_{yy})$	$[\sigma_{xx},\varepsilon_{yy}]$	$\sigma_{xx}(0,\frac{a}{2})=0$	$(\varepsilon_{yy})(0,\frac{a}{2})=(1-\xi)(\varepsilon_{yy}^{\text{us}})$
F	$(\sigma_{xx},\sigma_{xy})$,$(\sigma_{xx},\varepsilon_{yy})$	$[\sigma_{xx},\varepsilon_{yy}]$	$\sigma_{xx}(b,\frac{a}{2})=0$	$(\varepsilon_{yy})(b,\frac{a}{2})=(1-\xi)(\varepsilon_{yy}^{\text{us}})$

a quadratic/cubic form at free region of the boundary and axial displacements are constant at the stiffening region which give the rigid body motion at stiffened sections. With the decrease of effectiveness of stiffener, magnitude of distributions increases. Maximum magnitude of displacement has been found at the stiffener free region which is gradually increasing from left to right.

Figure 7.3(b) illustrates the comparison of the state of distributions of normalized axial strains on the top boundary of the laminated cantilever. Distributions are normalized with the maximum value of strain, $\varepsilon_{yy,\text{max}} = 0.78747E-03$ at the fixed end of the top boundary of the unstiffened laminate. For the case of stiffener free panel, the distribution gradually decreases from left to right and approaches to zero at the right lateral end. For the case of rigid stiffening, distribution decreases from left to right along the unstiffened sections and magnitude of the distribution is zero at the stiffening region which satisfy applied the

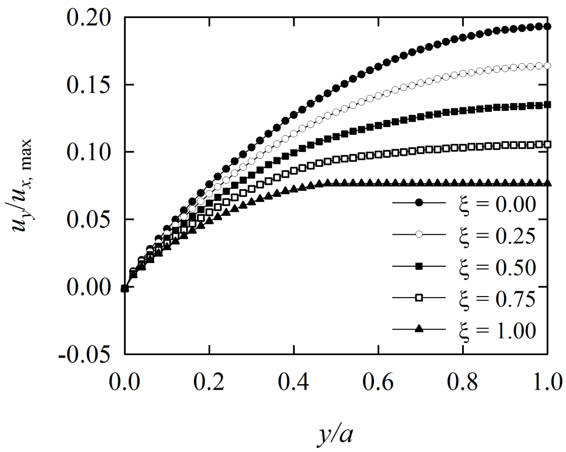

(a) Axial displacement.

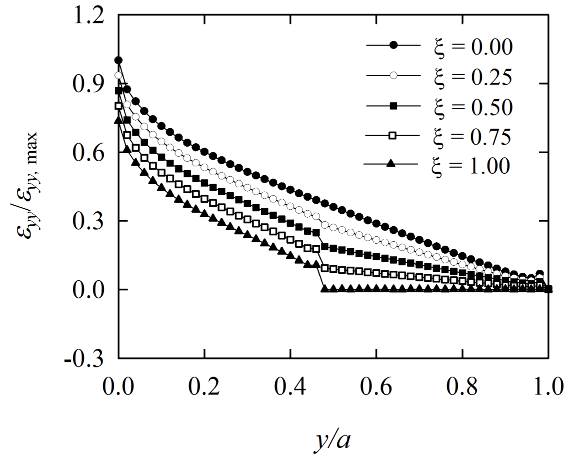

(b) Axial strain.

Figure 7.3: Distributions of axial displacements and strains along the top boundary of the laminated panel with various effectiveness of stiffeners.

boundary conditions. For all the cases of ξ, distributions decreases from left to right along the top boundary and maximum has been found at the fixed end. To satisfy the applied boundary conditions, sudden reduction of strain has been found for all ξ values at the junction point. With the decrease of effectiveness of stiffener, magnitude of distributions increases.

7.4.2.2 Deformed Shapes with Stiffeners of Various Effectiveness

Figure 7.4 illustrates the deformed shapes of the laminated panel obtained with different conditions of stiffening used along the two opposing longitudinal surfaces. It is revealed from the results that axial stiffeners have significant influence on the deformation pattern of the panel. Deformed shapes are completely different for laminate with stiffeners of various effectiveness, ξ. Deformed shape of the laminated panel with rigid stiffener is much smaller, it can be easily realized when compared to the other cases of ξ. Again deformed shape of the unstiffened cantilever is higher compared to other conditions of effectiveness of stiffener. When the two opposing longitudinal surfaces are attached with stiffeners, the obtained deformed state of the panel is shown in Figure 7.4, in which the right extreme corner of the

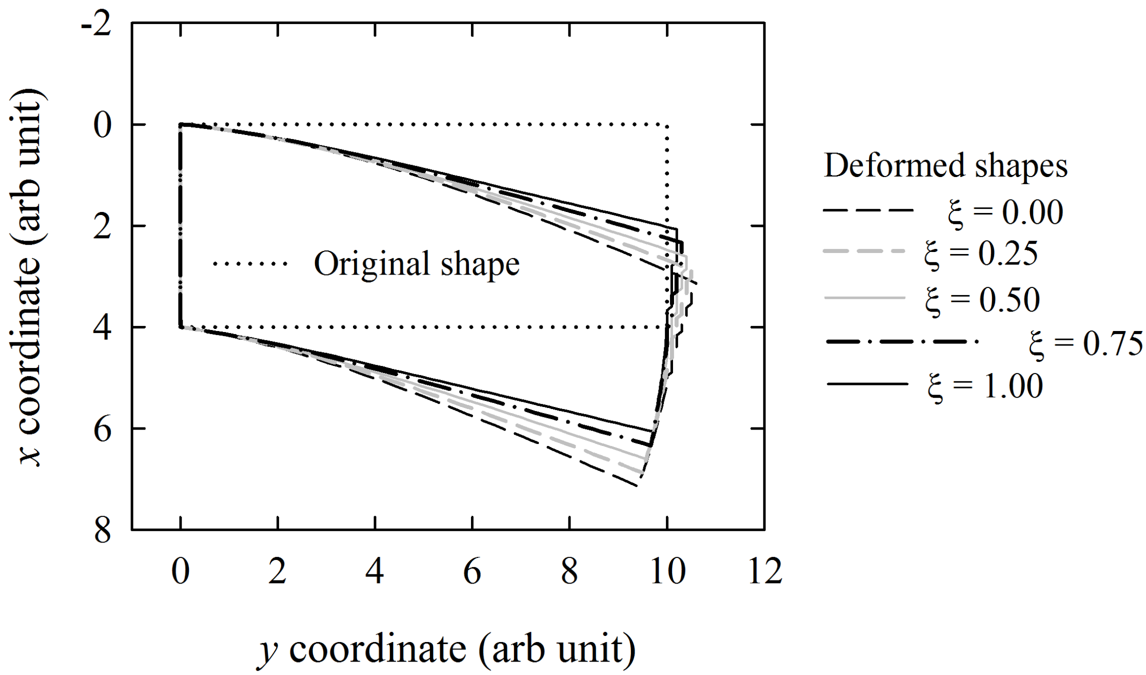

Figure 7.4: Deformed shape of the stiffened laminated cantilever with various effectiveness of the stiffener (magnification factor $\times 200$).

bottom surface is found to experience the contribution of both the lateral and axial displacements. It has noted that, with the increase of stiffening effectivity, deformations of the panel decrease.

7.4.2.3 Distributions of Different Stress Components

Figure 7.5(a) illustrates comparisons of distributions of axial stress components for different conditions of effectiveness of stiffener on top boundary of the laminated panel. It is interesting to note that distributions of axial stresses are similar compared with the distributions of axial strains. Distributions decreases from left to right along stiffener and approach to zero stress value at the right lateral end for all cases of ξ. Small fluctuation on distribution has been found at the junction point, where stiffener free and stiffened boundary are joined on top and bottom boundary. This fluctuation is lowering the magnitude of the distribution and

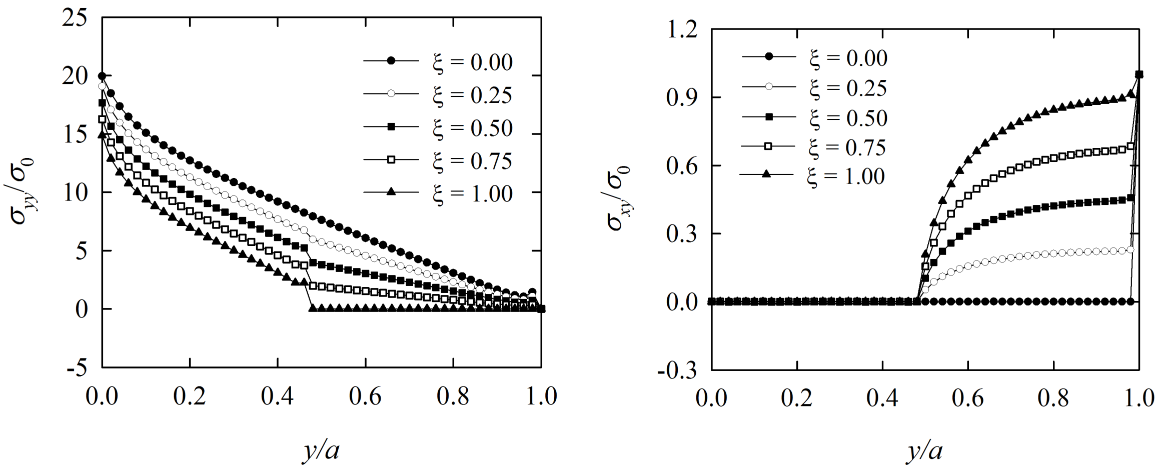

(a) Axial stresses. (b) Shear stresses.

Figure 7.5: Distributions of axial stresses and shear stresses along the top boundary of the laminated panel with various effectiveness of stiffeners.

gives linear distributions on the stiffening region. Maximum magnitude has been found at the fixed end of top boundary for all conditions of stiffness of stiffener, ξ. When rigid stiffener ($\xi = 1$) are attached with the laminated cantilever, distribution reproduce the axial stresses are zero at the stiffening region which satisfy the boundary condition. With the decrease of the magnitude of stiffness of stiffener, magnitude of the distributions of axial stresses are increases.

Comparisons of distributions of shear stress components for different conditions of effectiveness of stiffener on top boundary of the laminated panel are shown in figure 7.5(b) A somewhat parabolic distributions has been found at the stiffening region of top surfaces for all magnitude of effectiveness, ξ. Distributions are different for different magnitudes of ξ and magnitudes of distributions increase with the increase of magnitude of ξ. As expected the stiffener-free regions on the top surfaces of the cantilever are found to be completely free from shearing stresses for all ξ. Normalized value of the distributions at the right lateral end are 1 for all cases of ξ, which exactly satisfy the boundary conditions which has been applied on the right lateral end. It should be noted that magnitude of distributions of shear stresses are much lower compare to magnitude of axial stress components (see Figure 7.5(a)).

7.5 Effect of Stiffeners with Variable Effectiveness

This section presents the effect of discrete variable stiffeners in the elastic filled of the laminated composite cantilever. subjected to a uniform shear. To analyze the problem, discrete variable stiffener with varying effectiveness has been considered. i.e. effectiveness of the stiffener, ξ will vary along the length of the stiffener. To analysis the problem, linear variation of ξ has been considered as shown in Figure 7.6. Left side of the stiffened region of the cantilever is rigid $(\xi_i = 1)$ and right side of the stiffened region of the cantilever is free from stiffening $(\xi_i = 0)$. Mathematically rigid stiffening $(\xi_i = 1)$ is defined as $(\varepsilon_{yy}^{\text{vs}})_i = (\varepsilon_{yy}^{\text{rs}})_i = 0$ and unstiffened condition is defined as $(\varepsilon_{yy}^{\text{vs}})_i = (\varepsilon_{yy}^{\text{us}})_i$. To solve the present case, spatially varying strain components have been used as boundary conditions in the stiffened region on top and bottom boundary of the cantilever. Spatially varying strain components have been found from the above equation (7.2) with corresponding linear variation of ξ_i, where the strain component is equal to zero (rigidly stiffened) at the right region of the stiffened section of the cantilever is equal to unstiffened strain at the right lateral end of the stiffened section of the cantilever has been shown in figure 7.6.

Determination of physical conditions of the stiffened section under stiffeners with uniform effectiveness ($\xi = \text{f}(y)$) is shown in Figure 7.6. The geometry of the cantilever has been already discussed in section 7.4.1, only variation of ξ will be linear rather than constant.

7.5.1 Results and Discussions

The results of the analysis of stresses for the laminated cantilever subjected to local stiffeners along the two opposing longitudinal surfaces, as shown in Figure 7.6, are presented in this section. In this section, results of the numerical solution of the laminated panel having an aspect ratio (a/b) of 2.5 are presented. The results are presented, distributions of axial

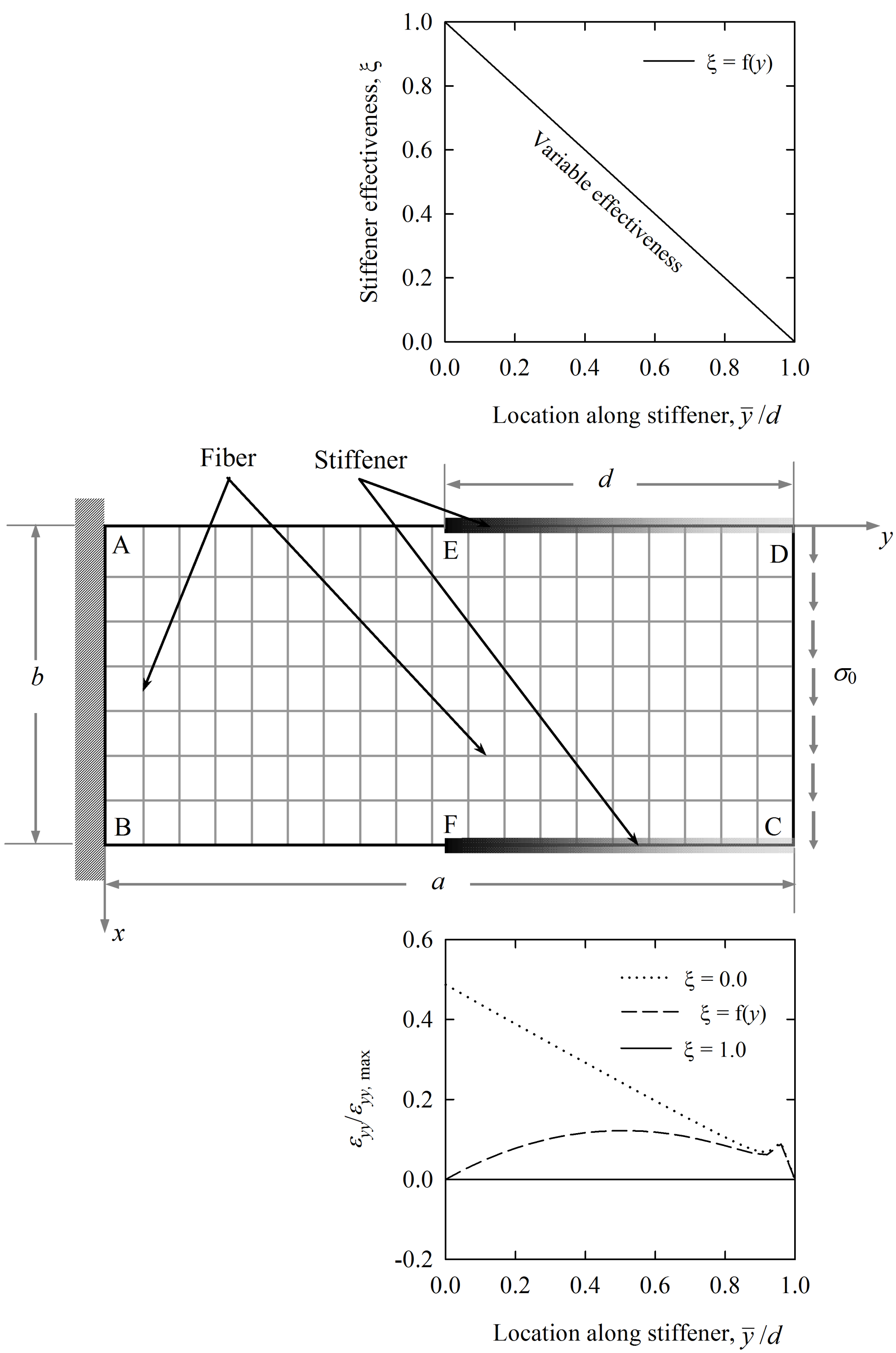

Figure 7.6: Determination of physical conditions of the stiffened section under stiffeners with uniform effectiveness ($\xi = \mathrm{f}(y)$).

displacement and strain distributions of different stress components, comparison of stress components interest as well as comparisons of deformed shape. In all cases of stress distributions, stresses are normalized with respect to the maximum intensity of applied shear loading, σ_0 (see Figure 7.6), the magnitude of which is arbitrarily assumed to be 3 MPa. The details of the boundary conditions as used to obtain the present FD solutions are already listed in Table 7.1 and 7.2. Three laminae $(n = 3)$ of unidirectional composite material with stacking sequences of $[0/90/0]$ are assumed to form symmetric cross-ply laminates for the cantilever. Although the method can be applied to any composite material, the boron/epoxy composite is chosen as an example in present study. The effective mechanical properties of boron/epoxy laminate are listed in table 5.2. The thickness of individual plies is kept constant, which is 0.5 mm. The FD mesh-network used to model the present cantilever $(a/b = 2.5)$ contains nodal points (51×51) in the direction of x and y, respectively.

7.5.1.1 Distributions of Axial Displacement and Axial Strains

Figure 7.7(a) illustrates the distributions of axial displacements for different sections of variable stiffened laminated cantilever. It is noted that distributions are normalized with the maximum lateral displacement at the right lateral boundary of the same unstiffened laminated cantilever. Distributions are symmetric with respect to the section $x/b = 0.5$ and away from the boundary, magnitude of distributions decreases. Maximum displacement has been found at top and bottom boundary. At the stiffening region, distributions are almost linear and increases from left to right hand lateral end.

Figure 7.7(b) illustrates the distributions of axial strains for different sections of variable stiffened laminated cantilever. It is noted that distributions are normalized with the maximum axial strain, $0.78747E-03$ at the fixed boundary of the unstiffened laminated cantilever. It is seen from figure, distributions decrease from left to right hand lateral end. At the start of the stiffener, axial strain is zero on top and bottom boundary which exactly satisfy the rigid conditions of the stiffener. At the end of the stiffener on top and bottom surface, axial strain

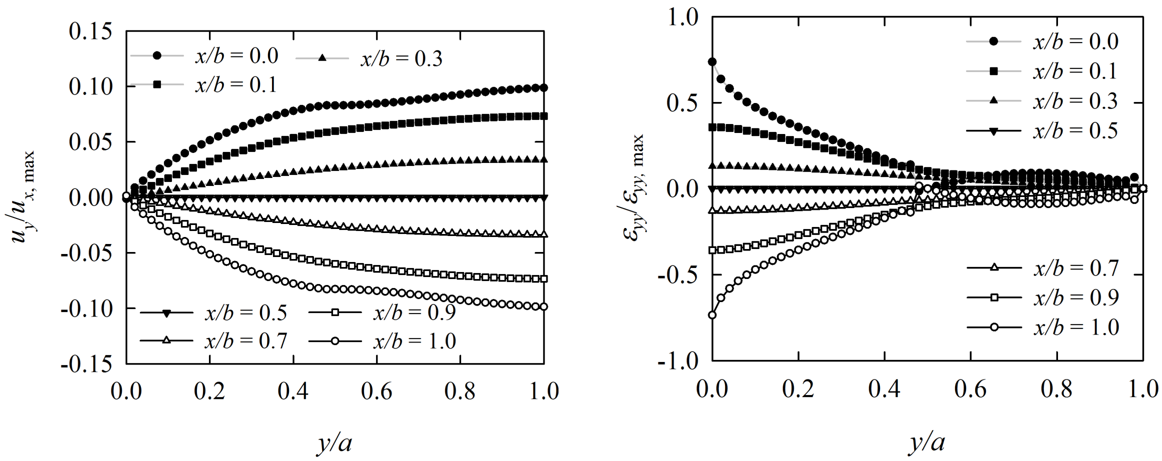

(a) Axial displacements.

(b) Axial strains.

Figure 7.7: Distributions of axial displacements and axial strains of the laminated cantilever with variable effectiveness of stiffeners.

is exactly same with the unstiffened strain. Distributions are parabolic at the stiffened region on top and bottom surface of the laminated panel. Distributions are symmetric with respect to sections $y/a = 0.5$. Magnitude of strains is higher at the fixed end for all sections.

7.5.1.2 Distributions of Stress Components

Figure 7.8(a) illustrates the distributions of the axial stress components for different lateral sections under the influence of symmetric variable stiffener (with variable effectiveness) of the stiffened laminated panel subjected to a uniform shear load. Distributions decreases from left to right at stiffener free sections and approach to zero stress value at the start of the stiffener on top and bottom boundary. Again, parabolic distributions of axial stresses have been found at top and bottom surfaces under stiffening sections. Away from the top and bottom boundary, distributions are linear under stiffener and stiffener free sections. Distributions are symmetric with respect to section $x/b = 0.5$. Maximum magnitude has been found at the fixed end on top and bottom boundary. Away from the top and bottom boundary, magnitude of distributions are decreasing.

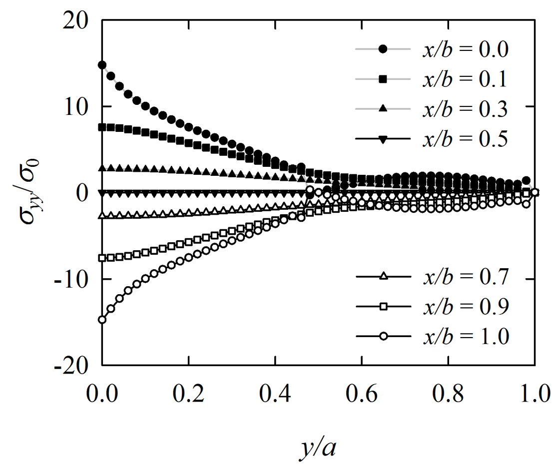

(a) Axial stresses.

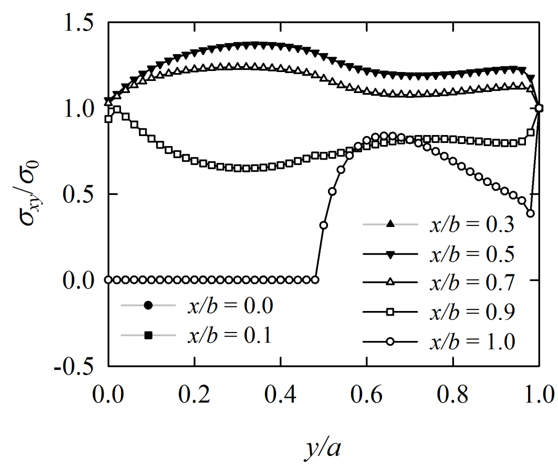

(b) Shear stresses.

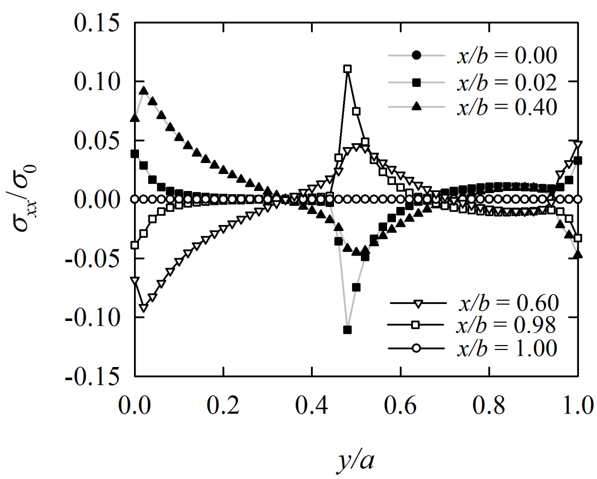

(c) Lateral stresses.

Figure 7.8: Distributions of different stress components at different sections of the stiffened laminated cantilever with variable effectiveness of stiffeners.

The distributions of shear stress at different transverse sections of the laminated cantilever are shown in figure 7.8(b) for different sections. Distributions of shear stresses are normalized with the applied load σ_0. A somewhat parabolic distributions assumes a quadratic/cubic form under the stiffening sections of top and bottom surfaces. As expected, the stiffener-free regions of the top and bottom surfaces of the cantilever are found to be completely free from shearing stresses. Distribution of shear stress are found to coincide with each other for all symmetric lateral sections. Normalized value of the distributions of all sections are equal to 1 at right hand lateral end, which exactly satisfy the boundary conditions that has been applied on the right lateral end.

Figure 7.8(c) illustrates the distributions of the normalized lateral stress components for different sections of the stiffened laminated panel. It is noted that magnitude of distributions of lateral stress components are much smaller compared to distributions of other stress components. Both stiffened and stiffener free sections of distributions are symmetric with respect to section $x/b = 0.5$. Fluctuations of distributions have been found at start and end of stiffener. As expected, top and bottom boundary are free from lateral stress which exactly satisfy the boundary conditions.

Figure 7.9(a) illustrates the distributions of the axial stress components for different axial sections under the influence of symmetric variable stiffener (with variable effectiveness) of the stiffened laminated panel subjected to a uniform shear load. Distributions are antisymmetric with respect to the section $y/a = 0.5$. Maximum magnitude has been found at the fixed end on top and bottom boundary. Magnitude of distributions decreases from left to right hand lateral end. Distributions are free from axial stresses at the right lateral boundary which exactly matches with the boundary conditions.

The distributions of shear stress at different axial sections of the laminated cantilever are shown in figure 7.9(b) for different sections. Distributions of shear stresses are normalized with the applied load σ_0.Different parabolic distributions have been found for different section. Distributions are symmetric with respect to the section $x/b = 0.5$. Distribution

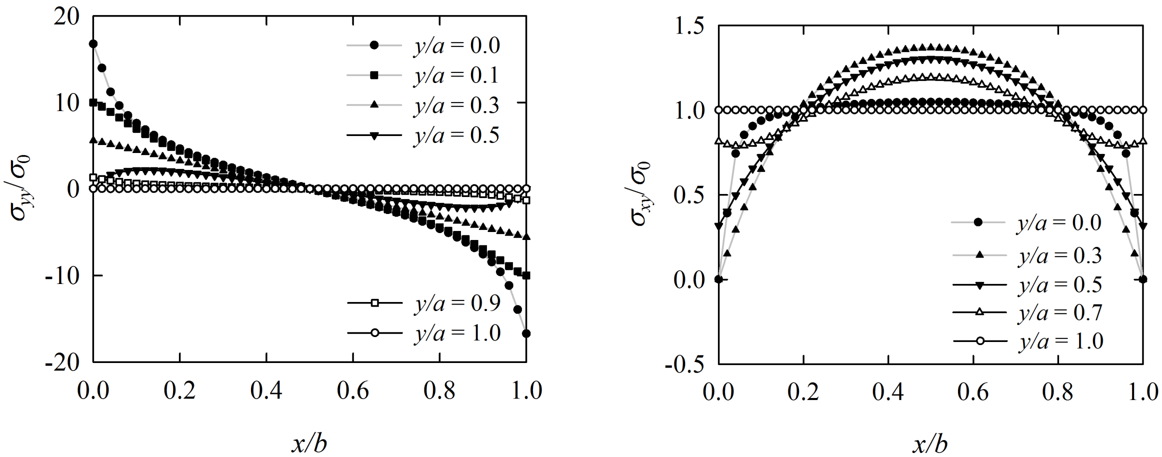

(a) Axial stresses. (b) Shear stresses.

Figure 7.9: Distributions of different stress components at different sections of the stiffened laminated cantilever with variable effectiveness of stiffener.

reproduces the exact boundary conditions at the right lateral end.

7.5.2 Comparison of Different Cases of Stiffener Effectiveness

Figure 7.10- 7.12 illustrates the comparison of distribution of normalized axial displacement, different stress components and deformed shape of the cantilever for the different stiffening effectivity on the top boundary $(x/b = 0.0)$ of the panel. The results basically compare the state of stresses and displacements along the variable stiffeners with those associated with the corresponding cases of rigid stiffener and stiffener free panels.

7.5.2.1 Comparison of Axial Displacements and Strains

Figure 7.10(a) illustrates the comparison of the state of distributions of normalized axial displacements, u_y on the top boundary of the laminated cantilever. Distributions are normalized with the maximum lateral displacement of unstiffened panel at right lateral end. For the case of stiffener free panel, the distribution assumes a quadratic/cubic form, which is gradually increasing from left to right. For the case of rigid stiffening, distribution assumes a quadratic/cubic form at free region of the boundary and axial displacements are constant at the stiffening region that give the rigid body motion at stiffened sections. For the case of present variable stiffening problem, when $\xi = \mathrm{f}(y)$, distribution has been found as a quadratic/cubic form at free region of the boundary and the distributions are linear at the stiffened region and much closer to distributions of rigid stiffened cantilever. The overall distributions of axial stresses of the panel have been found much smaller magnitude when stiffener attached with the cantilever compare to unstiffened cantilever as shown in Figure 7.10(a).

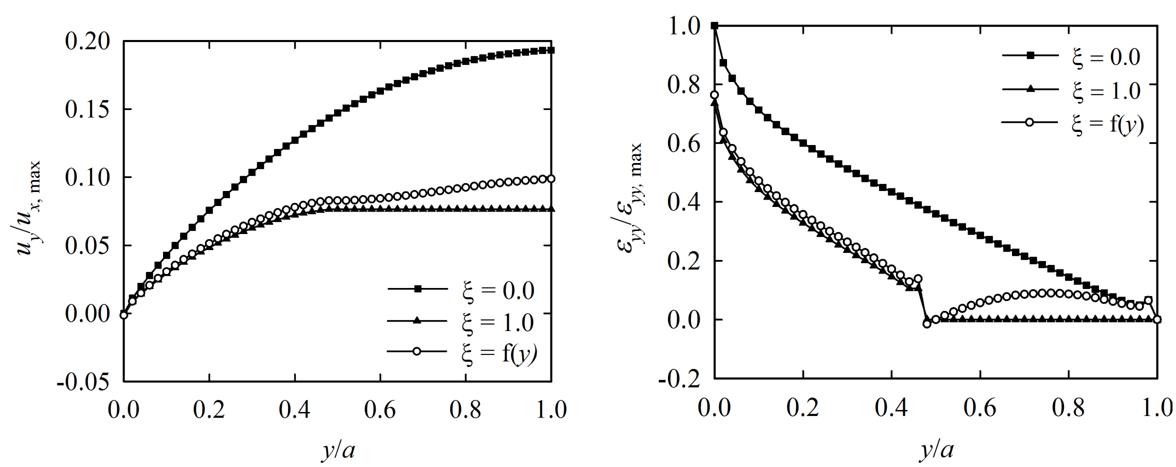

(a) Axial displacements.

(b) Axial strains.

Figure 7.10: Distributions of axial displacements and strains along the top boundary of the laminated panel with different conditions effectiveness of stiffeners.

Figure 7.10(b) illustrates the comparison of the state of distributions of normalized axial strains on the top boundary of the laminated cantilever. Distributions are normalized with the maximum value of strain, $0.78747E-03$ at the fixed end of the top boundary of the unstiffened laminate. For the case of stiffener free panel, the distribution gradually decreases from left to right and approaches to zero at the right lateral end. For the case of rigid stiffening, distribution decreases from left to right along the unstiffened sections and magnitude of the distribution is zero at the stiffened region which satisfy applied the boundary conditions. At the junction point, to satisfy the applied boundary conditions, some sudden reduction of strain has been found. Again, for the case of variable stiffened ($\xi =$ f(y)) cantilever, distribution is decreasing from left to right and very close to the distribution of rigid stiffened panel at free region of the boundary. Distribution is free from axial strain at the start of the stiffener, which is the condition of rigid stiffening. Again distribution assumes a parabolic form with maximum magnitude at the middle of the stiffener, which is exactly matches with boundary conditions that applied on the stiffened boundary. Distribution of axial strain exactly matches also with unstiffened strain at the lateral end of the top boundary. It should be noted that maximum magnitude has been found at the fixed end for all conditions of stiffener.

7.5.2.2 Comparison of Stress Components

Figure 7.11(a) illustrates the comparison of the state of distributions of normalized axial stresses on the top boundary of the laminated cantilever. Distributions are normalized with the applied loading, σ_0. For the case of stiffener free panel, the distribution gradually decreases from left to right along the top sections of the laminate and approaches to zero at the right lateral end. For the case of rigid stiffening, distribution decreases from left to right along the unstiffened sections and magnitude of the distribution is zero at the stiffened region. For the case of variable stiffening, ($\xi =$ f(y)), distribution is decreasing from left to right at free region of the boundary and give zero stress value at start of the stiffener. The distributions assumes a quadratic/cubic form and give maximum magnitude at the middle of the stiffener at the stiffening region. It should be noted that maximum magnitude has been found at the fixed end of all conditions of stiffener.

Figure 7.11(b) illustrates the comparison of the state of distributions of normalized shear stresses, on the top boundary of the laminated cantilever. Distributions are normalized

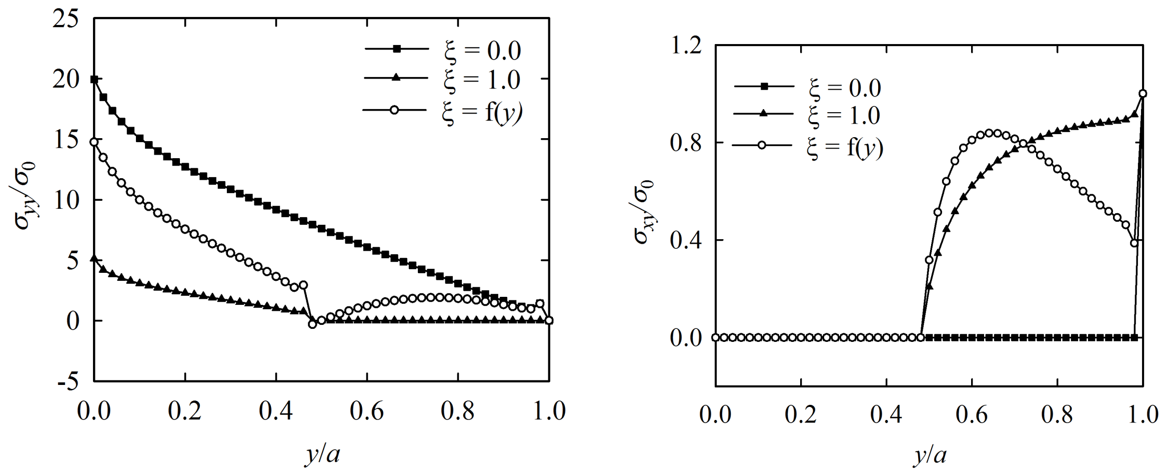

(a) Axial stresses. (b) Shear stresses.

Figure 7.11: Distributions of axial stresses and shear stresses along the top boundary of the laminated panel with different conditions of effectiveness of stiffeners.

with the applied loading, σ_0. For the case of rigid stiffening, the distribution assumes a quadratic/cubic form, which is gradually increasing from left to right along the length of the stiffener. For the case of variable stiffening, ($\xi = \mathrm{f}(y)$), a somewhat parabolic like distribution has been found at the stiffening sections but slope of the parabola is much higher compare to the distribution of shear stress of rigid stiffened cantilever. For the case of stiffener free panel, distribution are free from the shear stresses, which exactly matches with the boundary conditions.

7.5.2.3 Comparison of Deformed Shape

Figure 7.12 illustrates the deformed shapes of the laminated panel obtained with different conditions of stiffening used along the two opposing longitudinal surfaces. Overall, it is revealed from the results that axial stiffeners have significant influence on the deformation pattern of the panel, particularly for the present uniform shear loading at the right lateral end. The axial rigid stiffeners at the surfaces, in general, cause the overall deformation of the panel to assume much smaller magnitude, which can be easily realized when compared

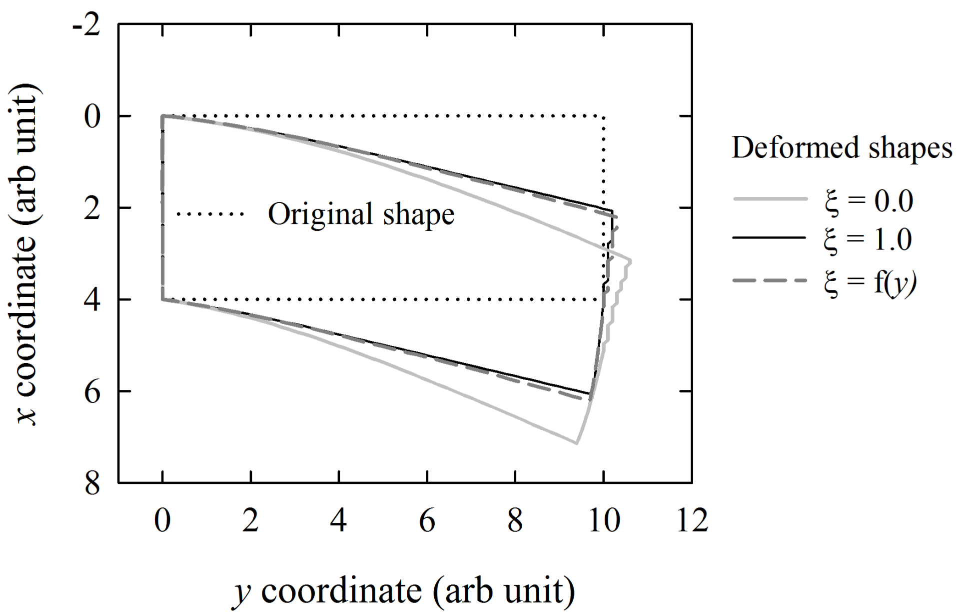

Figure 7.12: Deformed shape of the laminated cantilever with different conditions of effectiveness of stiffener (magnification factor $\times 200$).

to the case of variable stiffener and stiffener free panels as shown in figure 7.12 Deformed shape of the variable stiffened ($\xi = \text{f}(y)$) laminated cantilever, are very similar to deformed shape of rigid stiffener. When the two opposing longitudinal surfaces are free form stiffeners, the obtained deformed state of the panel is shown in Figure 7.12, in which the right extreme corner of the bottom surface is found to experience the contribution of both the lateral and axial displacements. It is interesting to note that, with the increase of stiffening effectivity, deformation of panel decrease and deformed shape becomes straight gradually at the stiffening boundary region has shown in figure 7.12.

7.6 Conclusions

A new scalar function based computational scheme has been developed to analyze of variable stiffening in a laminated composite cantilever under shear loading. No appropriate analytical and numerical approach is available in the literature, which can provide explicit information about the actual stresses, especially at the critical regions of supports and stiffeners of the laminated panel. Both the qualitative and quantitative results of the present mixed-boundary-value stress problem of laminated composites establish the soundness as well as appropriateness of the single function approach. The solutions are claimed to be highly accurate and rational for the entire region of interest, either at or away from the bounding edges of the composite panel. It is thus expected that the present data would be considered as a valuable design guide for laminated panels with variable stiffeners. Further, the solutions obtained are promising and satisfactory for the entire region of interest. Therefore, the present displacement potential formulation can be applied to obtain numerical solution to the elastic field in structural elements of laminated composites under any modes of boundary conditions.

CHAPTER
8

Validation of Displacement Potential Solution

8.1 Introduction

This chapter is intended to verify the soundness and appropriateness of the displacement potential method (DPM) developed in this study for the analysis of elastic field of structural components of laminated composites with mixed mode of boundary conditions. To achieve this goal, some of the problems discussed in previous chapters are solved by the conventional computational methods which mainly include the finite element method (FEM). An analytical solution to a stiffened laminated cantilever has also been derived based on displacement potential function in order to verify the accuracy of the finite-difference modeling of the problem. The commercial finite-element softwares SAP2000 and ANSYS have been used to obtain the corresponding finite element solutions of the problem.

8.2 Problem 1: An Unstiffened Laminated Cantilever Under Parabolic Shear

To validate of the present displacement-potential solutions, a simple unstiffened laminated cantilever as shown in figure 8.1, has been first solved using three different approaches which are completely different in terms of the solution process. First, FEM solution of the laminated cantilever problem has been obtained using the conventional commercial finite-element software, SAP2000, *Static and Dynamics Analysis of Structure, Advanced 14.1.0*. A three ply unstiffened boron-epoxy laminated cantilever under parabolic shear has been chosen for the FEM solution. The properties of the Boron-epoxy laminated composite which have been used to generate the corresponding FEM solutions are listed in Table 5.2; It can be mentioned that, in practice, FEM is considered to be the only plausible approach for analyzing such problems of discretely stiffened laminated problems. A total of $10,000(100 \times 100)$ four-noded, isoparametric layered-shell elements were used to construct the corresponding FEM mesh network for the laminate. The convergence as well as accuracy of the FEM solution has also been verified by varying the element mesh density.

A simplified finite element solution of the laminated cantilever problem has also been obtained using the conventional commercial finite-element software, ANSYS, Release 11.0 SP1. The simplified FEM solutions are obtained by converting the original laminate into an equivalent lamina. The equivalent representative material properties of the laminate which are used to obtain simplified FEM solution are known as engineering constants of the laminate The engineering constants of 3-ply the Boron-epoxy laminated composite which have been used to generate the corresponding simplified FEM solutions are listed in Table 8.1. Likewise the case of a total of (100×100) element were used to construct the corresponding simplified FEM mesh network for solution. PLANE42 is used for 2-D modeling of solid structures. The element is defined by four nodes having two degrees of freedom at each node. Again, the detailed analytical model as well as the boundary management is discussed in section 8.3.3.

8.2.1 Problem Description

A symmetric cross-ply laminated panel consisting of three plies with a stacking sequence $[90^o/0^o/90^o]$ shown in figure (8.1), has been considered. The thickness of the panel is h.

Table 8.1: Engineering constants of Boron/epoxy composite material used for simplified finite element analysis.

Material	Property	Value
Boron/epoxy	E_x (GPa)	80.59
	E_y (GPa)	142.69
	G_{xy} (GPa)	5.59
	ν_{xy}	0.3

The left end of the panel is rigidly fixed while the two longitudinal edges are free from stresses. The right lateral end is subjected to a parabolic shear load, $\sigma^o_{xy} = \frac{4\sigma_o}{b^2}(bx - x^2)$. The length of the panel is a and the width is b.

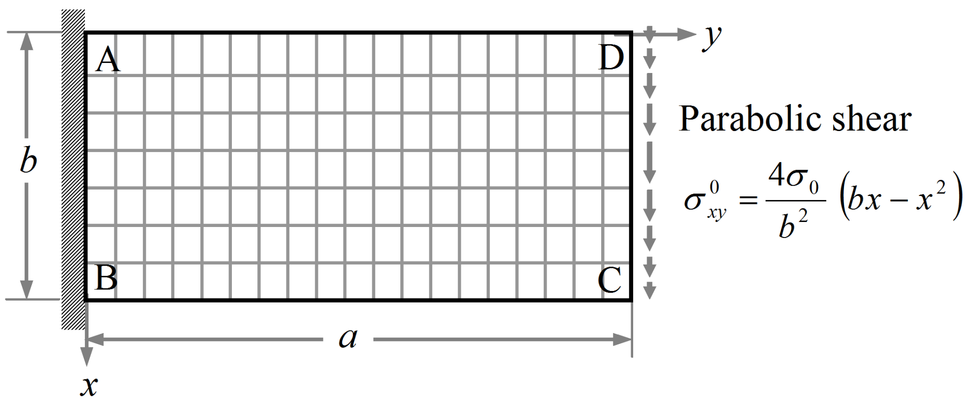

Figure 8.1: Model of an unstiffened laminated panel under parabolic shear loading.

8.2.2 Boundary Conditions

1. For longitudinal surfaces, AD:

$$\sigma_{xx}(0, y) = 0 \quad \text{and} \quad \sigma_{xy}(0, y) = 0; \qquad [0 \leq y \leq a]$$

2. For longitudinal surfaces, BC:

$$\sigma_{xx}(b, y) = 0 \quad \text{and} \quad \sigma_{xy}(b, y) = 0; \qquad [0 \leq y \leq a]$$

3. For supporting lateral boundary AB:

$$u_x(x, 0) = 0 \quad \text{and} \quad u_y(x, 0) = 0; \qquad [0 \leq x \leq b]$$

4. For right-hand lateral boundary CD:

$$\sigma_{yy}(x, a) = 0 \quad \text{and} \quad \sigma_{xy}(x, a) = \sigma^o_{xy}; \qquad [0 \leq x \leq b]$$

8.2.3 Comparisons of Results

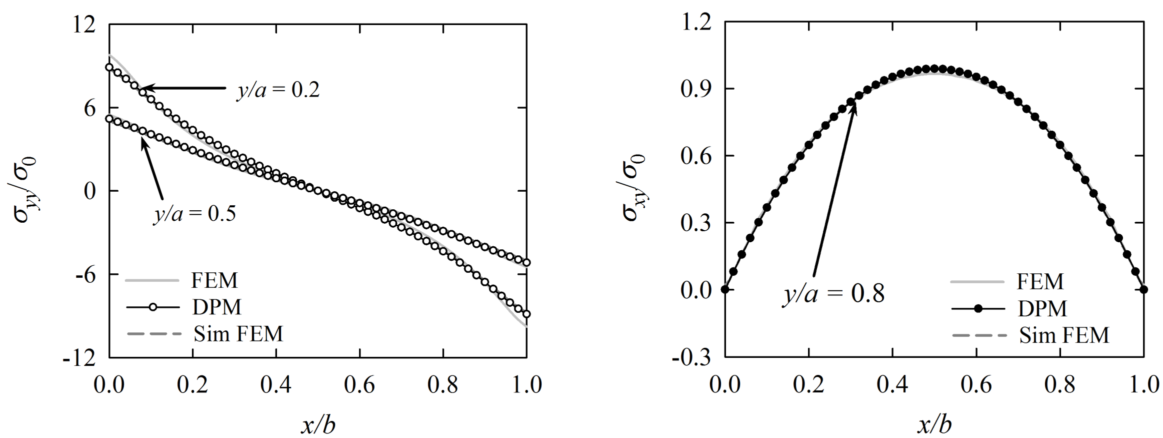

(a) Bending stress, σ_{yy}. (b) Shear stress, σ_{xy}.

Figure 8.2: Comparison of three solutions of different stress components at different sections of the unstiffened laminated cantilever, $a/b = 2.5$.

Figure 8.2 shows the comparison of FEM, simplified FEM and DPM solution of different stress components at different sections of the laminated panel. It is noted that the stresses presented in Figure 8.2 are the overall laminate stress. Three different sections have been chosen arbitrarily to compare the results. It has seen from the figure that three solutions obtained by three different approaches are in good agreement with each other for any arbitrary section of the panel. A critical analysis of the three solutions reveals that although the three solutions are nearly identical in terms of the nature of variation as well as magnitude, the simplified solutions are found to be more close to the DPM solution than the usual FEM solution and then it is very difficult to differentiate the two solutions on the graph, rather they are simply overlapping each other. Analytical solutions have not been included for the present comparison because of the fact that exact analytical solution to the fixed ended cantilever panel is not yet available in the literature. The present comparison firmly varies the reliability and accuracy of the present displacement potential method for predicting elastic behavior of laminated structures. Not only that the simplified FEM method has also been identified to be a simple but reliable finite element approach for analyzing laminated structures.

8.3 Problem 2: A Stiffened (Continuous) Laminated Cantilever Under Parabolic Shear

8.3.1 Problem Description

A symmetric cross-ply laminated panel consisting of 3 plies of $(90^o/0^o/90^o)$ as shown in figure 8.3 is considered. The thickness of the panel is h. The left end of the panel is rigidly fixed while the two opposing longitudinal edges are stiffened. The right lateral end is subjected to a parabolic shear load, $\sigma_{xy}^o = \frac{4\sigma_o}{b^2}(bx - x^2)$. The length of the panel is a and the width is b.

8.3.2 Boundary Conditions

1. The longitudinal surfaces, AD and BC are assumed to be stiffened. In order to model the physical condition of the rigid axial stiffeners, the tangential displacement along the stiffener is restrained, while the boundary section is kept free from any external loading. The mathematical modeling of the physical conditions of the stiffened bound-

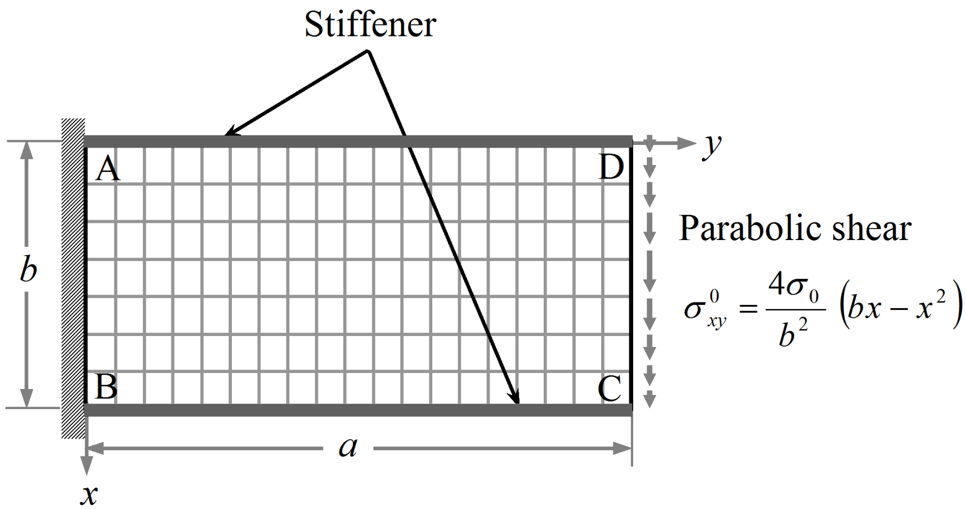

Figure 8.3: Model of a laminated panel with continuous rigid stiffener under parabolic shear loading.

aries AD and BC, are realized as follows:

$\sigma_{xx}(0, y) = 0$ and $u_y(0, y) = 0;$ $[0 \leq y \leq a]$

$\sigma_{xx}(b, y) = 0$ and $u_y(b, y) = 0;$ $[0 \leq y \leq a]$

2. The supporting lateral end (boundary AB) is rigidly fixed. Both the normal and tangential components of displacement are assumed to be zero here, that is,

   $u_x(x, 0) = 0$ and $u_y(x, 0) = 0$ $[0 \leq x \leq b]$

3. The right-hand lateral end (boundary CD) of the cantilever is the loaded boundary. Here, the loading is realized through a parallel distribution of shear stress, while the associated normal stress component is assumed to be zero, that is,

   $\sigma_{yy}(x, a) = 0$ and $\sigma_{xy}(x, a) = \sigma_{xy}^{o}$ $[0 \leq x \leq b]$

8.3.3 Analytical Solution

Based on the potential-function formulation, a new analytical scheme is developed for the analysis of the laminated cantilever as shown in Figure 8.3. It should be mentioned that a new co-ordinate system has been chosen to develop the analytical model (see Figure 8.4). In the present scheme, a trial solution to the potential function ψ is first assumed as a function of coordinate parameters (x, y) in the form of an infinite series, which has to satisfy the governing partial differential equation of equilibrium. More specifically, the solution is expressed as an infinite series of combinations of two independent functions of x and y, which assumes a form like, $\psi(x, y) = \sum_m g_m(x)h_m(y)$. A suitable form of the function is determined in a trial and error fashion so that it can automatically satisfy the prescribed physical conditions of the two opposing longitudinal stiffened edges of the cantilever. Substitution of the trial solution into the governing differential equation results in a fourth-order ordinary differential equation. A general solution to the ordinary differential equation is then assumed in terms of four arbitrary constants. These four constants are determined by satisfying the remaining four physical conditions associated with the left and right lateral surfaces of the cantilever. By knowing the values of the four arbitrary constants the trial solution assumed for the beam problem is explicitly known. Once the appropriate potential function for the beam is explicitly determined, all the parameters of interest of the elastic field can readily be obtained, as in the present potential function formulation, they are expressed as the summation of different derivatives of the function ψ.

For the present problem, as shown in figure 8.4, the potential function is assumed to be

$$\psi = \sum_{m=1}^{\infty} X_m cos\alpha y + Kx^3 \tag{8.1}$$

where, X_m is a function of x only and $\alpha = \frac{m\pi}{a}$, K is an arbitrary constant and $m = 1, 2, 3, ...\infty$. Now, substitution of equation (8.1) into equation (3.42) yields

$$\frac{d^4 X_m}{dx^4} - \left(\frac{A_{22}}{A_{66}} - \frac{A_{12}^2}{A_{11}A_{66}} - \frac{2A_{12}}{A_{11}}\right)\frac{d^2 X_m}{dx^2}\alpha^2 + \left(\frac{A_{12}}{A_{11}}\right)X_m\alpha^4 = 0 \tag{8.2}$$

The general solution of equation (8.2) is given by

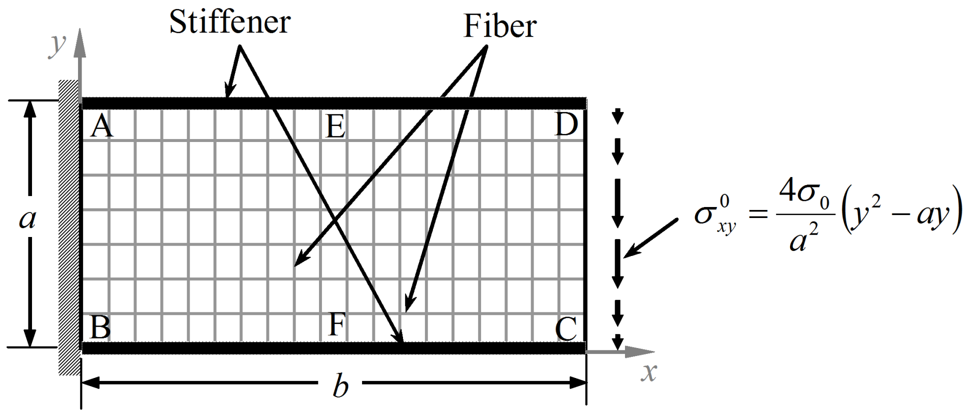

Figure 8.4: Model of a rectangular laminated panel with continuous rigid stiffener under parabolic shear loading for analytical model.

$$X_m = A_m e^{n_1 x} + B_m e^{n_2 x} + C_m e^{n_3 x} + D_m e^{n_4 x} \tag{8.3}$$

where

$$n_1, n_2 = \alpha\sqrt{\frac{B \pm \sqrt{B^2 - 4C}}{2}}$$

$$n_3, n_4 = -\alpha\sqrt{\frac{B \pm \sqrt{B^2 - 4C}}{2}}$$

and A_m, B_m, C_m, D_m are arbitrary constants.

With these expressions of displacement and stress components, the boundary conditions (1) is satisfied automatically. Therefore, only the boundary conditions (2) and (3) are remaining to be satisfied. The parabolic shear load applied at the edge $x = b$ can be expressed in terms of Fourier series as

$$\sigma_{xy}(b, y) = \sigma_{xy}^0 = E_0 + \sum_{m=1}^{\infty} E_m \cos \alpha y \tag{8.4}$$

where,

$$E_0 = \frac{4\sigma_o}{a^3}\int_0^a \left(ay - y^2\right) dy = \frac{-2\sigma_o}{3} \qquad \text{for} \quad m = 2,4,6,.......\infty \tag{8.5a}$$

$$E_m = \frac{8\sigma_o}{a^3}\int_0^a \left(ay - y^2\right) cos\alpha y dy = \frac{-16\sigma_o}{m^2\pi^2} \qquad \text{for} \quad m = 2,4,6,.......\infty \tag{8.5b}$$

Now, combining equations(3.43) and (3.44) with (8.3) and (8.4), the expressions of displacement and stress components are obtained as

$$u_x = \sum_{m=1}^{\infty}\left[n_1 A_m e^{n_1 x} + n_2 B_m e^{n_2 x} + n_3 C_m e^{n_3 x} + n_4 D_m e^{n_4 x}\right] \tag{8.6a}$$

$$\begin{aligned} u_y = \frac{1}{A_{12}+A_{66}}\sum_{m=1}^{\infty}\Big[\Big\{&A_{66}\left(A_m e^{n_1 x} + B_m e^{n_2 x} + C_m e^{n_3 x} + D_m e^{n_4 x}\right)\alpha^2 \\ &-A_{11}\left(n_1^2 A_m e^{n_1 x} + n_2^2 B_m e^{n_2 x} + n_3^2 C_m e^{n_3 x} + n_4^2 D_m e^{n_4 x}\right)\Big\}\cos\alpha y + 6KxA_{11}\Big] \end{aligned} \tag{8.6b}$$

$$\begin{aligned} \sigma_{xx} = &-\frac{1}{h(A_{12}+A_{66})}\sum_{m=1}^{\infty}\Big[\Big\{A_{12}\left(A_m e^{n_1 x} + B_m e^{n_2 x} + C_m e^{n_3 x} + D_m e^{n_4 x}\right)\alpha^3 \\ &+A_{11}\left(n_1^2 A_m e^{n_1 x} + n_2^2 B_m e^{n_2 x} + n_3^2 C_m e^{n_3 x} + n_4^2 D_m e^{n_4 x}\right)\alpha\Big\}\sin\alpha y\Big] \end{aligned} \tag{8.6c}$$

$$\begin{aligned} \sigma_{yy} = &-\frac{1}{h(A_{12}+A_{66})}\sum_{m=1}^{\infty}\Big[\Big\{A_{22}A_{66}\left(A_m e^{n_1 x} + B_m e^{n_2 x} + C_m e^{n_3 x} + D_m e^{n_4 x}\right)\alpha^3 \\ &+\left(n_1^2 A_m e^{n_1 x} + n_2^2 B_m e^{n_2 x} + n_3^2 C_m e^{n_3 x} + n_4^2 D_m e^{n_4 x}\right)\alpha \\ &+\left(A_{12}^2 + A_{12}A_{66} - A_{11}A_{22}\right)\Big\}\sin\alpha y\Big] \end{aligned} \tag{8.6d}$$

$$\begin{aligned} \sigma_{xy} = &-\frac{A_{66}}{h(A_{12}+A_{66})}\sum_{m=1}^{\infty}\Big[\Big\{A_{12}\left(n_1 A_m e^{n_1 x} + n_2 B_m e^{n_2 x} + n_3 C_m e^{n_3 x} + n_4 D_m e^{n_4 x}\right)\alpha^3 \\ &+A_{11}\left(n_1^3 A_m e^{n_1 x} + n_2^3 B_m e^{n_2 x} + n_3^3 C_m e^{n_3 x} + n_4^3 D_m e^{n_4 x}\right)\alpha\Big\}\sin\alpha y\Big] + \frac{6KA_{11}A_{66}}{h(A_{12}+A_{66})} \end{aligned} \tag{8.6e}$$

Using equations (8.4), (8.5) and (8.6e), the values of K can be obtained as

$$K = \frac{ah(A_{12} + A_{66})}{9A_{11}A_{66}}$$

Now, by applying the boundary conditions (3) and (4) in equations (8.6a) - (8.6c) and (8.6e) and making the use of relation (8.4), the following four algebraic equations can be obtained for four unknown coefficients A_m, B_m, C_m and D_m.

$$n_1 A_m + n_2 B_m + n_3 C_m + n_4 D_m = 0 \tag{8.7a}$$

$$\left(A_{11}n_1^2 - A_{66}\alpha^2\right) A_m + \left(A_{11}n_2^2 - A_{66}\alpha^2\right) B_m + \left(A_{11}n_3^2 - A_{66}\alpha^2\right) C_m$$
$$+ \left(A_{11}n_4^2 - A_{66}\alpha^2\right) D_m = 0 \tag{8.7b}$$

$$\left(A_{11}n_1^2\alpha + A_{12}\alpha^3\right) A_m e^{n_1 b} + \left(A_{11}n_2^2\alpha + A_{12}\alpha^3\right) B_m e^{n_2 b}$$
$$+ \left(A_{11}n_3^2 + A_{12}\alpha^3\right) C_m e^{n_3 b} + \left(A_{11}n_4^2 + A_{12}\alpha^3\right) D_m e^{n_4 b} = 0 \tag{8.7c}$$

$$\left(A_{11}n_1^3 + A_{12}n_1\alpha^2\right) A_m e^{n_1 b} + \left(A_{11}n_2^3 + A_{12}n_2\alpha^2\right) B_m e^{n_2 b}$$
$$+ \left(A_{11}n_3^3 + A_{12}n_3\alpha^2\right) C_m e^{n_3 b} + \left(A_{11}n_4^3 + A_{12}n_4\alpha^2\right) D_m e^{n_4 b} = \overline{E}_m \tag{8.7d}$$

$$\overline{E}_m = -\frac{E_m h(A_{12} + A_{66})}{A_{66}}$$

The solution of the above algebraic equation (8.7) yields the unknown constants, A_m, B_m, C_m and D_m. Once the values of the unknowns are determined, they are directly substituted into equation (8.6) to obtain the explicit expressions for the different parameters of interest, namely, the two displacement and the three stress components, which are valid for the entire region of the stiffened edge panel of laminated composite.

8.3.4 Comparisons of Results

Although a new co-ordinate system has been chosen to develop the analytical model but the four different solutions are presented according to original coordinate system shown in

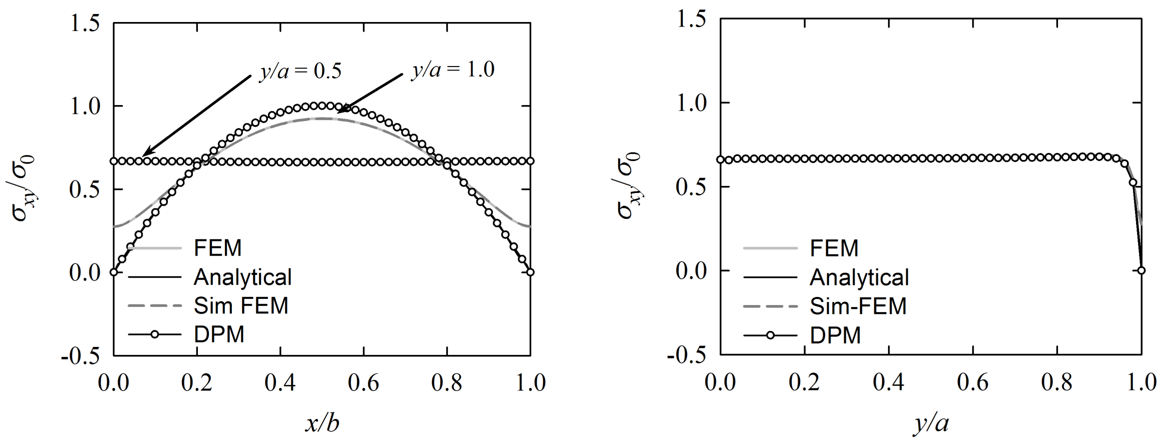

(a) At axial sections $y/a = 0.5$ and 1.0. (b) At lateral section $x/b = 0.0$.

Figure 8.5: Comparison of four different solutions of the shear stress component at different sections of the laminated cantilever $(a/b = 2.5)$.

Figure 8.3. For the present laminated cantilever supported by continuous rigid stiffeners at its both the opposing longitudinal edges, only the solutions of shear stresses at different sections are compared, as all other components of stresses as well as displacements assume extremely small values which are found to be almost negligible compared to the magnitude of applied loading. Figure 8.5 shows the comparison of FEM, Analytical, simplified FEM and DPM solutions of the shear stress component for different axial and lateral sections of the laminated panel. It has been seen from the figure that four solutions agree very well with each other for all the sections considered, but at the right lateral boundary $(y/a = 1.0)$, some discrepancy between the four solutions are noticed. More specially the solutions obtained by the four different approaches are found to be almost identical in terms of shape and magnitude except that at the right lateral end. At the right lateral end, FEM and simplified FEM solutions are found to be overlap with each other, whereas the DPM and analytical solution matches with each other. It is mentioned here that DPM and analytical solutions reproduce the boundary conditions exactly that have been applied at the right boundary. The slight discrepancy of the solutions at the right lateral end is probably due to the inherent

inaccuracy of finite element methods in reproducing the stresses at the bounding surfaces of the cantilever. This uncertainty of FEM has already been noticed by several researchers Richards [31], Smart [32], Dow and Harwood [33] in this field and a number of valuable effects has been made to remove the limitation.

8.4 Problem 3: A Discretely Stiffened Laminated Cantilever Under Uniform Shear

In this section, attempt is made to compare the solutions of symmetric discretely stiffened laminated cantilever (Case-A1) as shown in figure 5.1(a). The present displacement potential based FDM solutions are only compared with the corresponding solutions of conventional computational method, FEM. It would be worth mentioning, in practice, FEM is considered to be the only plausible approach for analyzing such problems of discretely stiffened laminated problems. Exact analytical solutions of this problem is beyond the scope of existing approaches in the literature. The convergence as well as accuracy of the FEM solution has also been verified by varying the element mesh density. The particulars of FEM modeling have been kept the same as described previous sections of 8.2 and 8.3. Figure 8.6 shows FEM modeling as well as the deformed state of the cantilever of Case-A1 as obtained by the SAP2000 FEM software.

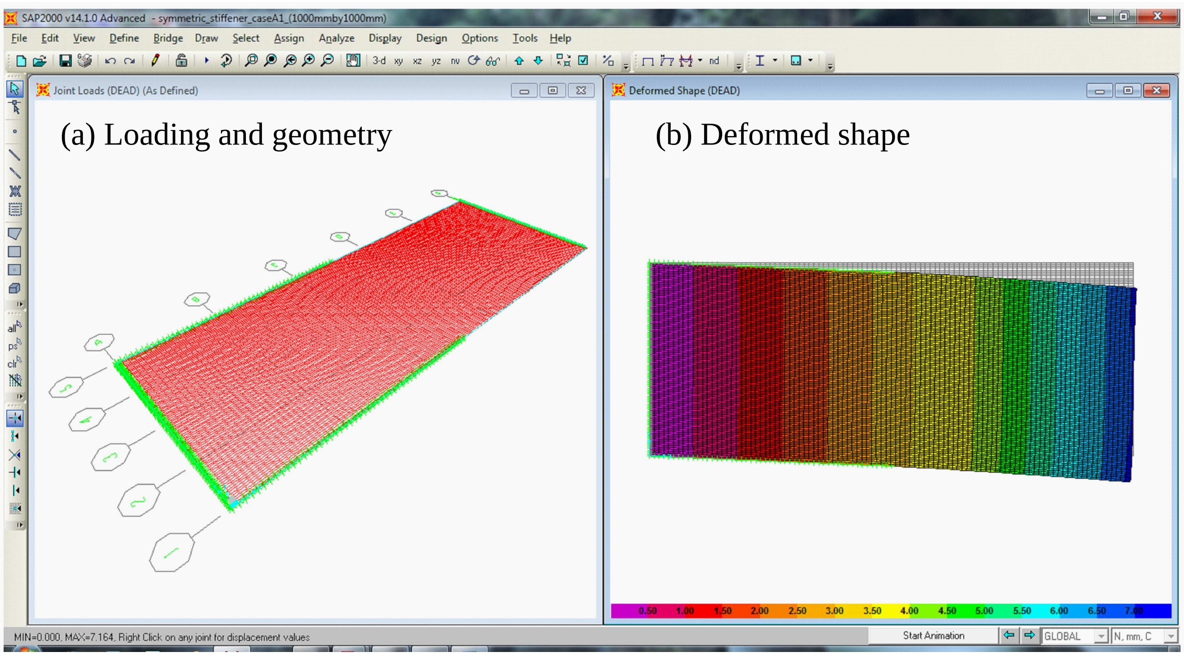

Figure 8.6: (a) Loading and geometry and (b) deformed shape of the cross-ply laminated panel (Case-A1).

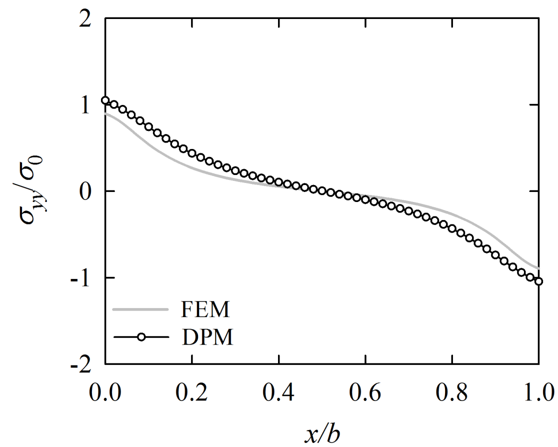

(a) At section $y/a = 0.7$ of outer ply $(\theta = 0^o)$.

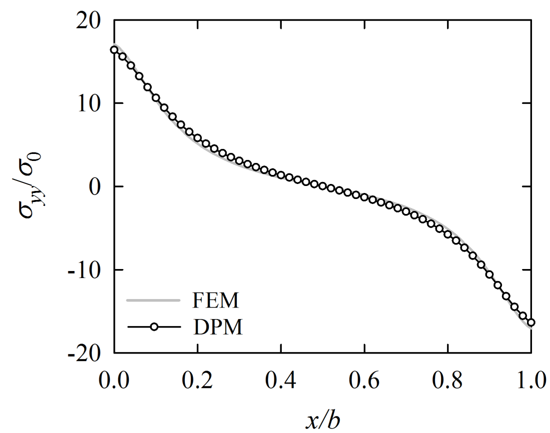

(b) At section $y/a = 0.7$ of inner ply $(\theta = 90^o)$.

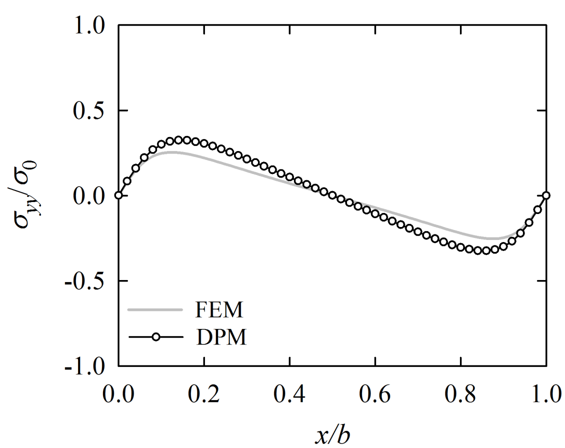

(c) At section $y/a = 0.3$ of outer ply $(\theta = 0^o)$.

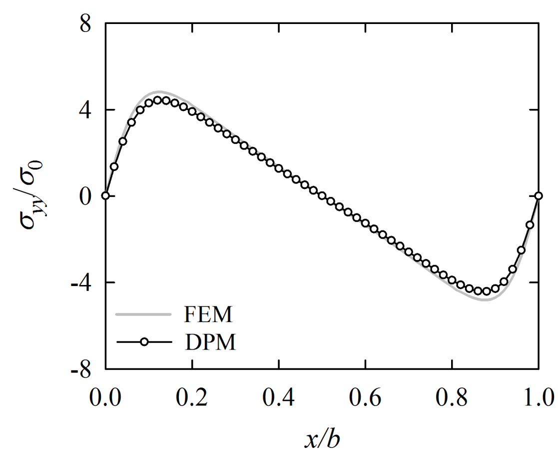

(d) At section $y/a = 0.3$ of inner ply $(\theta = 90^o)$.

Figure 8.7: Comparison of DPM and FEM solutions for the axial stresses at different axial sections of outer and inner ply of the laminate.

Figure 8.7 shows the comparison of DPM and FEM solutions of axial stresses at different axial sections of the outer and inner plies of the laminated cantilever (Case-A1). It can be noted that these two solutions are obtained from two different approaches which are completely different in terms of mathematical formulation as well as numerical modeling. In general, the distributions of the stress component are in good agreement with each other. More specifically, the agreement of solutions is found to be more close in case of the inner ply, which is more critical than the outer ply in terms of axial stresses. Another important thing is, both the magnitude and nature of variation of the both solution are found to be very similar for any sections of interest, whether it is under stiffened region or away from the stiffened region.

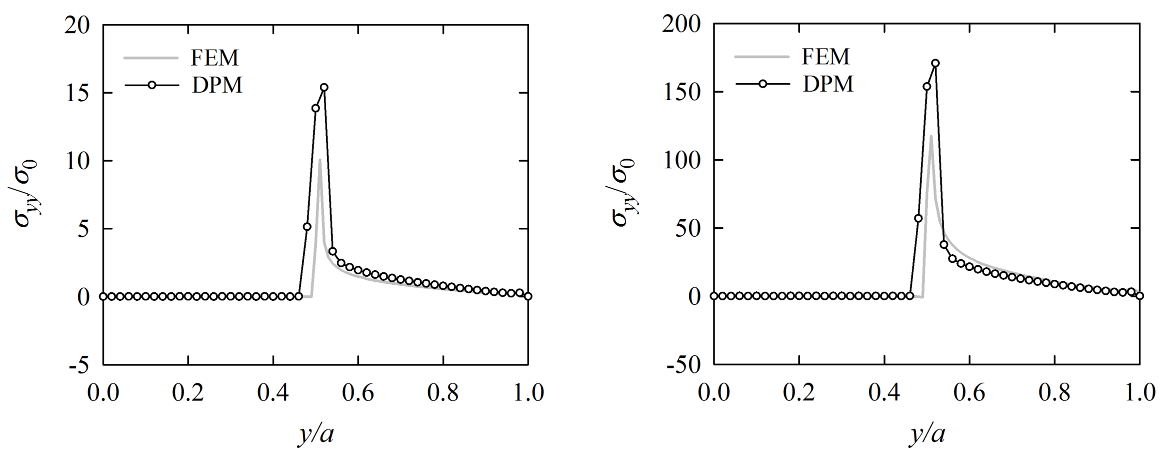

(a) At section $x/b = 0.0$ of outer ply ($\theta = 0^o$). (b) At section $x/b = 0.0$ of inner ply ($\theta = 90^o$).

Figure 8.8: Comparison of DPM and FEM solutions for the axial stresses along the stiffened surface $(x/b = 0)$ at different plies of the laminate.

Figure 8.8 presents the comparison of axial stress distributions along the upper stiffened surface of individual plies of the laminated cantilever. The two solutions are, in fact, found to be in excellent agreement for both the stiffened and stiffener-free regions of individual plies of the laminate, except at the neighborhood of the termination points of the stiffeners, $y/a = 0.5$. These termination points of discrete stiffeners are basically the points of sin-

Table 8.2: Prediction of normalized axial stresses (σ_{yy}/σ_o) for different plies of top boundary.

Mesh size	Inner layer		Outer layer	
	FDM	FEM	FDM	FEM
41×25	186.430	91.914	17.756	3.49
21×25	89.593	79.201	9.094	3.007

gularity. It is well known that reliable and accurate prediction of stresses at these points of singularities especially by numerical techniques is very difficult. Finite-difference prediction of axial stresses at these points of singularities is found to be sensitive to mesh density used to model the cantilever, which is however not the case for other regions of the cantilever. The magnitude of the stress at these points increases with the increase of mesh density. For example, in case of the inner ply, the maximum stress (σ_{yy}/σ_0) is found to increase from 89.59 to 186.43 (see Table 8.2) when the mesh-network is changed from (21×25) to (25×41) nodes, respectively. On the other hand, FEM prediction of axial stress at these points of singularities is found to be relatively less sensitive to FE mesh-density. The corresponding increase of the maximum stress due to the change of mesh-density, as predicted by FEM, is found to be from 79.20 to 91.91 (see Table 8.2). In this context, it can be mentioned that commercial FEM softwares usually apply some averaging scheme to predict these surface stresses from the stresses at neighboring Gauss points, whereas the present displacement potential solutions are obtained by direct FDM solution which is free from any kind of refining or post processing.

The comparison of predicted shear stresses at different sections of the laminated cantilever is presented in Figure 8.9. Shear stresses predicted by the two numerical approaches are, in general, found be in good agreement with each other. At the singularity point the state of shearing stress is found to be slightly under predicted by FEM compare to DPM, although both the distributions follow similar nature of variation.

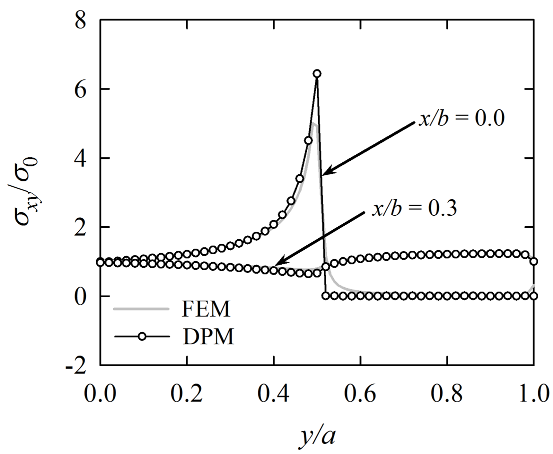

(a) At different lateral sections.

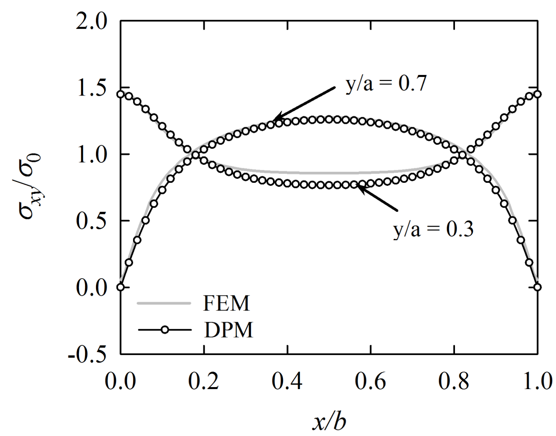

(b) At different axial sections.

Figure 8.9: Comparison of DPM and FEM solutions for the shear stresses at different sections of the laminate.

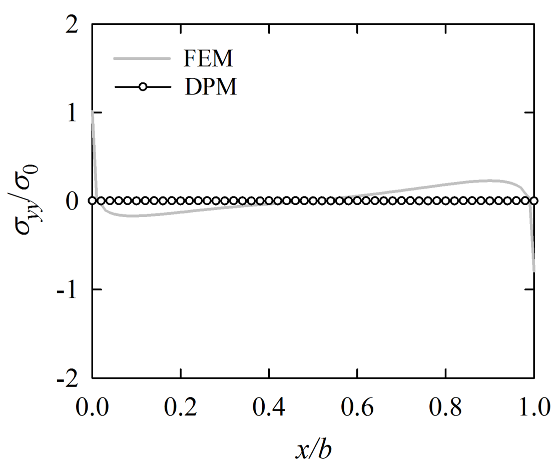

(a) Axial stress at section $y/a = 1.0$.

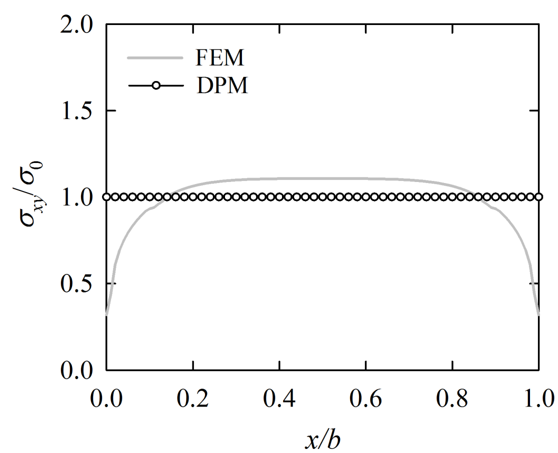

(b) Shear stress at section $y/a = 1.0$.

Figure 8.10: Comparison of DPM and FEM solutions for the axial and shear stresses at section $y/a = 1.0$ of the laminate.

Finite-difference prediction of shear stresses at the points of singularity is found to be less sensitive when compared to the corresponding case of axial stresses at these points. The corresponding values of shear stress as predicted by FEM reveal that the overall mesh dependency of the two numerical approaches is very similar in predicting shear stresses at the above point of singularities. It is known in advance from the physical conditions of the right lateral end of the present laminated cantilever that the end is free from axial stresses and is subjected to a uniform shear stress whose normalized value is unity as shown in Figure 8.10. One can easily verify the accuracy as well as appropriateness of the present computational scheme by comparing the predicted stresses with those of the known conditions at the right lateral end of the laminated cantilever. The suitability and accuracy of the present displacement-potential method in predicting stresses can be verified in a more clear fashion if one can compare the stresses at sections for which exact solutions are known in advance. Fortunately, for the right lateral end of the laminated cantilever, both the axial and shear stress distributions are known in advance, i.e., it is free from both the axial stresses.

CHAPTER
9

CONCLUSIONS

9.1 Conclusions

A suitable and effective numerical method based on potential function has been developed for the analysis of elastic field in structures of composite materials. It is a comprehensive method because it can be applied to solve problems of composite structures with any mode of boundary conditions whether they are prescribe in terms of either stresses or constraints or strains or any combination of stress, strain and constraints. Moreover, it is a very simple method because it reduces the two dimensional elastic problems of composite structures to finding a single potential function ψ, defined in terms of two displacement components, satisfying a single differential equation of equilibrium. Although the existing Airy's stress function formulation also seeks for the solution of a single function, the present method is superior to the existing stress function formulation due to the fact that the stress function formulation can deal with the problems when boundary conditions are prescribed in terms of stress only.

The finite difference scheme based on potential function is also very promising as it deals with a single unknown function-ψ. The quality of numerical solution largely depends on the number of equations i.e. the accuracy of the solution is aggravated as the number of equations increases. In any finite difference scheme, the number of equations increases with the increases of unknown functions. Since the potential based finite difference scheme has a single unknown function, the solution is improved significantly.

The method is demonstrated by solving a number of problems of composite cantilever numerically. Comparison of DPM results (using ψ-formulation) with those obtained by FEM-solution established the soundness and reliability of the present single function method. The main concluding remarks are summarized as follows:

1. A new mathematical formulation has been developed for the analysis of structural components of laminated composites, which is capable of dealing with almost all the special cases of composite material, namely orthotropic and anisotropic lamina, angle-ply and cross-ply symmetric laminates, symmetric balanced laminates, etc., with mixed and changeable physical conditions at the surfaces of the structural composites.

2. An investigation of the stress field of a laminated composite cantilever subjected to symmetric and anti-symmetric local stiffeners has been carried out based on a new scalar potential function. No appropriate analytical approach is available in the literature that can provide explicit information about the actual stresses, especially at the critical regions of supports and local stiffeners in laminated structures. The effect of stacking sequence, fiber material, stiffener length, etc. on the elastic field have been investigated for the symmetric and anti-symmetric locally stiffened cantilevers.

3. Elastostatic response of laminated composite panel subjected to an eccentric loading has been analyzed under the influence of discrete periodic stiffeners. Discrete periodic stiffened panel is revealed that the panel under eccentric shear loading is more critical compared to eccentric axial loading in terms of stresses.

4. The elastic field of a laminated composite cantilever with discrete variable stiffeners at the two opposing longitudinal bounding surfaces has been analyzed under the influence of a uniform shear loading. A new normalized parameter, effectiveness of stiffener is

identified to be one of the influential factors for determining the state of stresses in the laminate. A new computational scheme has been developed for solving laminated panels under variable stiffener. No appropriate analytical or numerical solution is available in the literature, which can provide explicit information about the actual stresses, especially at the critical regions of supports and stiffeners of the laminated panel. Both the qualitative and quantitative results of the present mixed-boundary-value stress problem of laminated composites establish the soundness as well as appropriateness of the single function approach.

5. The comparative also carried out to ascertain the reliability and credibility of the solutions obtained through displacement potential method (DPM). An analytical solution to a continuous stiffened laminated cantilever has also been derived based on displacement potential function in order to verify the accuracy of the finite-difference modeling of the problem. The commercial finite-element softwares SAP2000 and ANSYS have been used to obtain the corresponding finite element solutions of the problem. From comparison of the results of different methods, it is observed the solutions are in good agreement with each other. The uncertainties associated with the prediction of surface stresses by the standard solution (FEM) have been pointed out in this research. Displacement potential formulation of the laminated composite material has been reported that the accuracy of finite-difference method (FDM) in reproducing the state of stresses along the bounding surfaces was much higher than that of FEM analysis.

9.2 Recommendations

This is completely a new numerical method to find out the stress, strain and displacement field of the laminated composite structures. For most of the mixed boundary value problems of laminated-composites, no appropriate analytical or even numerical solution is available in the literature.

1. The present mathematical modeling can be modified to include the effect of curvature so that both the symmetric and asymmetric laminates can be analyzed.

2. The computational method is suitable for problems of stiffened, unstiffened, guided, unguided structures with uniform geometry. Like other numerical developments (FEM), the present method also needs rigorous efforts to bring it from infant stage to matured stage and make it suitable for the following cases of interest:

   - Problems having nonuniform geometry.
   - Different symmetric laminates like Cross-ply and Angle ply laminates, Hybrid and Balanced laminates, etc.

3. Structures with variable stiffeners need further investigation. The present computer code can be applied to more practical problems with different types of variable stiffeners, both at the boundary and internal sections.

Bibliography

[1] A. K. Kaw. *Mechanics of Composite Materials*. Taylor and Francis, New York, 2006.

[2] G. B. Airy. British association for the advancement of science report. Technical report, 1862.

[3] S. P. Timoshenko and J. N. Goodier. *Theory of elasticity*. McGraw-Hill Book Company, 3rd edition edition, 1988.

[4] Rankine. *Applied Mechanics*, page 344. 14 edition, 1895.

[5] Grashof. *Etastizitt festigkcit*, volume 2nd ed. 1878.

[6] M. Levy. *Compt. Rend,*, 126:1235, 1898.

[7] Abhandl Scewald, F. *Aerodynamic Ins. Tech. Hochschule, Achen*, 7:pp11, 1927.

[8] H. D. Conway, L. Chow, and G. W. Morgan. Analysis of deep beams. *Journal of Applied Mechanics, Trans ASME*, 18(2):163–172, 1951.

[9] R. E. Chapel and H. W. Smith. Finite-difference solutions for plane stresses. *AIAA Journal*, 6:1156–1157, 1968.

[10] D.F. Parker. The role of saint-venant's solutions in rod and beam theories. *Journal of Applied Mechanics, Trans ASME*, 46:861–866, 1979.

[11] C. O. Horgan and J. K. Knowels. Recent development concerning saint-venant's principle. *Advances in Applied Mechanics*, 23:179–269, 1983.

[12] C. O. Horgan and J. G. Simmonds. Saint-vennat end effects in composite structures. *Composite Engineering*, 4(3):279–286, 1994.

[13] L. Chow, H.D Conway, and G. Winter. Stresses in deep beams. *Trans ASCE*, (2557), 1952.

[14] H. D. Conway and N. Y. Ithaca. Some problems of orthotropic plane stress. *Journal of applied mechanics, Trans ASME*, 52(2557):72–76, 1953.

[15] P. Y. Tabakov and E. B. Summers. Lay-up optimization of multilayered anisotropic cylinders based on a 3-d elasticity solution. 84:374–384, 2006.

[16] M. W. Uddin. Finite difference solution of two-dimensional elastic problems with mixed boundary conditions. Master's thesis, Carleton University, Canada, 1966.

[17] S. R. Ahmed, M. R. Khan, K. M. S. Islam, and M. W. Uddin. Analysis of stresses in deep beams using displacement potential function. *J Inst Engrs (India)*, 77:141–7, 1996.

[18] A. B. M. Idris, S. R. Ahmed, and M. W. Uddin. Analytical solution of a 2-d elastic problem with mixed boundary conditions. *Inst Engrs (Singapore)*, 36(6):11–7, 1996.

[19] S. R. Ahmed, A. B. M. Idris, and M. W. Uddin. Numerical solution of both ends fixed deep beams. *Comp Struct*, 61(1):219, 1996.

[20] S. R. Ahmed, M. R. Khan, K. M. S. Islam, and M. W. Uddin. Investigation of stresses at the fixed end of deep cantilever beams. *Computers & Structures*, 69:32938, 1998.

[21] James H. S. Jr. Richard, L. B. and R. J. Eric. Nonlinear response and failure of pressurized composite curved panels. *Journal of Aerospace Engineering*, 8:129–138, 1995.

[22] J. Han and S. V. Hoa. *A three-dimensional multillayer composite finite element for stress analysis of composite laminates*, 36:3903–3914, 2005.

[23] G. Leoni and M. A. Brandford. Analysis of composite beams with partial shear interaction using avalable modeling techniques: A comparative study. *Computers and Structures*, 84:930–941, 2006.

[24] K. S. Jarmai and J. Frkas. Minimum cost design of a welded orthogonally stiffened cylindrical shell. *Computers and Structures*, 84:787–797, 2006.

[25] F. Armero and D. Ehrlish. Numerical modeling of softing hings in thin euler-bernoulli beams. *Computers and Structures*, 84:641–656, 2006.

[26] U. K. Mallela and A. Upadhyay. Buckling of laminated composite stiffened panels subjected to in-plane shear: a parametric study. *Thin-walled structures*, 44:354–361, 2006.

[27] Y. X. Zhang and C. H. Yang. Recent developments in finite element analysis for laminated composite plates. *Composite Structures*, 88:147–157, 2009.

[28] S. Shahriar, G. Zafer, and T. W. Layne. Design of variable-stiffness composite layers using cellular automata. *Computer Methods in Applied Mechanics and Engineering*, 195(9-12):836–851, 2006.

[29] Tatting B.F. Grdal, Z. and C.K. Wu. Variable stiffness composite panels: Effects of stiffness variation on the in-plane and buckling response. *Composites Part A: Applied Science and Manufacturing*, 39(5):911–922, 2008.

[30] B.F. Tatting. *Analysis and design of variable stiffness composite cylinders*. Thesis, Virginia Polytechnic Institute and State University, Blacksburg, Virginia, October 13 1998.

[31] Daniels M.J. Richards, T.H. Enhancing finite element surface stress predictions: A semi analytic technique for axisymmetric solids. *Journal of Strain Analysis*, 22(2): 75–86, 1987.

[32] J. Smart. On the determination of boundary stresses in finite elements. *J. Strain Analysis, ImechE*, 22(2):87–96, 1987.

[33] Jones M. S. Dow, J. O. and S. A. Harwood. A new approach to boundary modeling for finite difference applications in solid mechanics. *Int. J. Numerical Methods in Engineering*, (30):99–113, 1990.

[34] S. K. D. Nath and S. R. Ahmed. Displacement potential solution of stiffened composite struts subjected to eccentric loading. *Applied Mathematical Modeling*, 33(3):1761–1775, 2009.

[35] Gara F. Leoni G. Bradford M.A. Ranzi, G. Analysis of composite beams with partial shear interaction using available modeling techniques: A comparative study. *Computers & Structures*, 84:930–941, 2006.

[36] S. R. Ahmed, M. Z. Hossain, and M. W. Uddin. A general mathematical formulation for finite-difference solution of mixed-boundary-value problems of anisotropic materials. *Computers & Structures*, 83:35–51, 2005.

[37] S. K. D. Nath, A. M. Afsar, and S. R. Ahmed. Displacement potential solution of a deep stiffened cantilever beam of orthotropic composite material. *J. Strain Anal., IMechE*, 42(7):529–541, 2007.

[38] S.K. Kassegne and J.N. Reddy. Local behaviour of discretely stiffened composite plates and cylindrical shells. *Composite Structures*, 41(1):13–26, 1998.

[39] M. Tahani. Analysis of laminated composite beams using layer-wise displacement theories. *Composite Structures*, 79, 2007.

[40] S. K. D. Nath, S. R. Ahmed, and A. M. Afsar. Displacement potential solution of short stiffened flat composite bars under axial loading. *Int. J. Appl. Mech. Eng*, 11(3): 557–575, 2006.

[41] S. K. D. Nath and Ahmed S. R. Afsar, A. M. Displacement potential approach to solution of stiffened orthotropic composite panels under uniaxial tensile load. *J. Aerospace Eng., Part G, IMechE*, 221:869–881, 2007.

[42] Jones M. S. Doe, J. O. and S. A. Harwood. A new approach to booundary modeling for finite-difference applications in solid mechanics. *International Journal for Numericals Methods in Engineering*, 30:99, 1990.

[43] RM. Jones. *Mechanics of composite materials*. McGraw–Hill Book Company, 1975.

APPENDICES

APPENDIX A

ANSYS Code for Validation of Displacement Potential Solution

A.1 Problem 1: An Unstiffened Laminated Cantilever Under Parabolic Shear

```
finish
    /clear
    /title, Simple 2D Cantilever Problem
    aa=10
    bb=4
    rdiv=100
    cdiv=100
    !divsection=cdiv/5
    /prep7
    et,1,plane42
    keyopt,1,3,3
```

```
keyopt,1,5,2

mp,ey,1,8.059260987e+10

mp,ex,1,1.426255108e+11

mp,Gxy,1,5.59e+9

mp,prxy,1,0.03

!!!mp,dens,1,2.4e-9

r,1,15e-4 !thickness=100

k,1, 0, 0, 0

k,2, 0, bb, 0

k,3, aa, bb, 0

k,4, aa, 0, 0

a,1,2,3,4

lsel,s,loc,x,aa,aa

lsel,a,loc,x, 0, 0

lesize,all,,,rdiv,,1

lsel,s,loc,y, 0, 0

lsel,a,loc,y, bb, bb

lesize,all,,,cdiv,,1

!!lsel,all

!!lesize,all,125

!!allsel,all

type,1

real,1

mat,1
```

```
asel,all
amesh,all
/solu
! Applying Left Boundary Conditions
nsel,s,loc,x, 0, 0
d,all,all,0
! bottom boundary selection
nsel,s,loc,y,0,0
nsel,r,loc,x,0,aa
f,all,fx,0
f,all,fy,0
! top boundary selection
nsel,s,loc,y,bb, bb
nsel,r,loc,x,0,aa
f,all,fx,0
f,all,fy,0
!!nsel,s,loc,y,0,0
!!nsel,r,loc,x,0,aa
!!d,all,ux,0
!!f,all,fy,0
!
!!nsel,s,loc,y, bb, bb
!!nsel,r,loc,x,0,aa
!!d,all,ux,0
```

```
!!f,all,fy,0
allsel,all
*DO,ix,0, bb,(bb/rdiv)
m= 4*((3.0e+6)*(bb/rdiv)*(15e-4))*( (ix)**2 - bb*(ix) )/(bb**2)
F,NODE(aa,ix,0),Fy,m
*ENDDO
!m = -4*sigma0*( (x (j) )**2 - b*(x(j)) )/(b**2)
allsel, all
solve
/POST1
*cfopen,output.txt
!*do,i, 0,aa,(aa/cdiv)
*do,j, 0,bb,(bb/rdiv)
!j=-6*(bb/rdiv)
!j=0
!j=-bb+(bb/rdiv)
i=81*(aa/cdiv)
!i=0
!i=aa-(aa/cdiv)
!i=aa
*get,rx,node,node(i,j,0),s,xy
!*get,rff,node,node(i,j,0),rf,xy
!*get,ry,node,node(xx,0,0),rf,fy
*vwrite,rx
```

```
(f30.15)
!*enddo
*enddo
! do i=2,(m-1)
! write(11,112)(uu(j), j=((i-1)*n+2*i-2),((n+2)*i-3))
! END do
PLDISP,1
```

A.2 Problem 2: A Stiffened (Continuous) Laminated Cantilever Under Parabolic Shear

```
finish
    /clear
    /title, Simple 2D Cantilever Problem
    aa=10
    bb=4
    rdiv=100
    cdiv=100
    !divsection=cdiv/5
    /prep7
    et,1,plane42
    keyopt,1,3,3
    keyopt,1,5,2
    mp,ey,1,8.059260987e+10
    mp,ex,1,1.426255108e+11
```

```
mp,Gxy,1,5.59e+9

mp,prxy,1,0.03

!!!mp,dens,1,2.4e-9

r,1,15e-4 !thickness=100

k,1, 0, 0, 0

k,2, 0, bb, 0

k,3, aa, bb, 0

k,4, aa, 0, 0

a,1,2,3,4

lsel,s,loc,x,aa,aa

lsel,a,loc,x, 0, 0

lesize,all,,,rdiv,,1

lsel,s,loc,y, 0, 0

lsel,a,loc,y, bb, bb

lesize,all,,,cdiv,,1

!

!!lsel,all

!!lesize,all,125

!!allsel,all

type,1

real,1

mat,1

asel,all

amesh,all
```

```
/solu

! Applying Left Boundary Conditions

nsel,s,loc,x, 0, 0

d,all,all,0

! bottom boundary selection

nsel,s,loc,y,0,0

nsel,r,loc,x,0,aa

d,all,ux,0

f,all,fy,0

! top boundary selection

nsel,s,loc,y, bb, bb

nsel,r,loc,x,0,aa

d,all,ux,0

f,all,fy,0

allsel,all

*DO,ix,0, bb,(bb/rdiv)

m= 4*((3.0e+6)*(bb/rdiv)*(15e-4))*( (ix)**2 - bb*(ix) )/(bb**2)

F,NODE(aa,ix,0),Fy,m

*ENDDO

!m = -4*sigma0*( (x (j) )**2 - b*(x(j)) )/(b**2)

allsel, all

solve

/POST1

*cfopen,output.txt
```

```
*do,i, 0,aa,(aa/cdiv)

!*do,j, 0,bb,(bb/rdiv)

!j=-6*(bb/rdiv)

j=0

!j=-bb+(bb/rdiv)

!i=101*(aa/cdiv)

!i=0

!i=aa-(aa/cdiv)

!i=aa

*get,rx,node,node(i,j,0),s,xy

!*get,rff,node,node(i,j,0),rf,xy

!*get,ry,node,node(xx,0,0),rf,fy

*vwrite,rx

(f30.15)

!*enddo

*enddo

! do i=2,(m-1)

! write(11,112)(uu(j), j=((i-1)*n+2*i-2),((n+2)*i-3))

! END do

PLDISP,1
```